UNIVERSIDADE FEDERAL DO CEARÁ
CENTRO DE CIÊNCIAS
DEPARTAMENTO DE FÍSICA
PROGRAMA DE PÓS-GRADUAÇÃO EM FÍSICA

DAVI SOARES DANTAS

EMERGENT VORTEX BEHAVIOR IN SUPERCONDUCTORS AND SUPERFLUIDS WITH SINGLE AND MULTICOMPONENT QUANTUM CONDENSATES

FORTALEZA
2017

DAVI SOARES DANTAS

EMERGENT VORTEX BEHAVIOR IN SUPERCONDUCTORS AND SUPERFLUIDS WITH SINGLE AND MULTICOMPONENT QUANTUM CONDENSATES

PhD thesis presented to the Post-Graduation Course in Physics of the Federal University of Ceará as part of the requisites for obtaining the Degree of Doctor in Physics.

Advisor: Prof. Dr. Andrey Chaves.

Co-Advisor: Milorad V. Milošević.

FORTALEZA
2017

Dados Internacionais de Catalogação na Publicação
Universidade Federal do Ceará
Biblioteca Universitária
Gerada automaticamente pelo módulo Catalog, mediante os dados fornecidos pelo(a) autor(a)

D211e Dantas, Davi Soares.
Emergent vortex behavior in superconductors and superfluids with single and multicomponent quantum condensates / Davi Soares Dantas. – 2017.
156 f. : il. color.

Tese (doutorado) – Universidade Federal do Ceará, Centro de Ciências, Programa de Pós-Graduação em Física , Fortaleza, 2017.
Orientação: Prof. Dr. Andrey Chaves.
Coorientação: Prof. Dr. Milorad Milosevic.

1. Matéria de vórtice. 2. Interação vórtice-vórtice. 3. Supercondutores. 4. Condensados de Bose-Einstein. 5. Superfluidos. I. Título.

CDD 530

DAVI SOARES DANTAS

EMERGENT VORTEX BEHAVIOR IN SUPERCONDUCTORS AND SUPERFLUIDS WITH SINGLE AND MULTICOMPONENT QUANTUM CONDENSATES

Tese de Doutorado apresentada ao Programa de Pós-Graduação em Física do Departamento de Física da Universidade Federal do Ceará, como requisito parcial para obtenção do título de Doutor em Física. Área de concentração: Física da Matéria Condensada.

Aprovada em: 30/01/2017.

BANCA EXAMINADORA

_____

Prof. Dr. Andrey Chaves (Orientador)
Universidade Federal do Ceará (UFC)

_____

Prof. Dr. Raimundo Nogueira da Costa Filho
Universidade Federal do Ceará (UFC)

_____

Prof. Dr. Carlos Alberto Santos de Almeida
Universidade Federal do Ceará (UFC)

_____

Prof. Dr. Milorad Milosevic
University of Antwerp

_____

Prof. Dr. Clécio Clemente de Souza Silva
Universidade Federal de Pernambuco (UFPE)

To my wife.

Acknowledgements

Science is never made alone. In fact, there is always a lot of social work behind every studied subject. Of course this was not different for me and therefore, there is a huge list of thanks. However, among all the people who supported me along this trajectory, it is easy to point out the one that was certainly the most important for the accomplishment of this work: my advisor, Andrey Chaves, who with patience and dedication gave me the background knowledge necessary for the conclusion of this thesis. Also, I will never forget the talks with Prof. Aristeu, which I had the pleasure of working with. Beyond their wise teachings on physics, I also consider them great friends of mine for their valuable time spent with me.

Standing over the shoulders of giants of science provided a shortcut for quality improvements of the work done in this thesis. For this reason, I will always feel indebted to my co-advisor, Prof. Milorad Milošević, who, with great wisdom and dedication, supported and taught me a lot along my doctorate and specially, during my staying in Belgium. In advance, I thank other members of the jury, Professors Clécio, Carlos Alberto and Raimundo, for the time spent reviewing this work, as well as for their very important comments, corrections and suggestions that made possible to improve the quality of the final version of this thesis.

In special, I warmly thank my friends of the undergraduate course at UFC and colleagues at GTMC and CMT research groups. Last but not least, I thank to my family: my mother, Lucia, my brother, Bruno and my wife Lorrayne for always being present in difficult moments that I passed by. Finally, I thank my father, who unfortunately could not witness this moment of achievement, but who would certainly be very proud of it.

I would like to thank all the agencies that gave me financial support for carrying out my projects and also for presenting them at conferences: CAPES Foundation, CNPq, PRONEX / FUNCAP, the Flemish Science Foundation (FWO-Vl), the Bilateral programme between CNPq and FWO-Vl, and the Brazilian Program Science Without Borders (CsF).

Abstract

Using a self-devised numerical approach, we developed a powerful tool to investigate vortex properties and interactions in mean-field theories for superconductors and superfluids, based on fixing the vortex phase distribution in the energy minimization process. The method was applied to (i) multi-component Bose-Einstein condensates (BECs) and (ii) superconductors with single- or multi-component superconducting condensates. In these systems, vortex-vortex interaction and other key vortex features are analytically described only in specific regimes, that do not account for a large part of vortex behavior observed experimentally. In multi-component BECs, for example, the vortex-vortex interaction is only known for inter-vortex distances much greater than the healing length, i.e. far from the vortex core. Under our approach, by assuming multi-vortex structures, within Gross-Pitaevskii theory, we report the vortex-vortex interaction in the full range of distances, capturing the mechanism behind unusual vortex conformations previously reported in literature, such as bound clusters with two or three vortices. Usually, these clusters emerge from a competition between intra- and inter-component vortex interaction, but we demonstrate they can also emerge from the phase-frustration between the components.

In superconductors, the description of vortex-vortex interaction is usually restricted to bulk or very thin films, and most of the key vortex features, such as the spatial magnetic field and current density profiles, are known only in the limit of London theory, i.e. for coherence length ξ negligible as compared to magnetic field penetration depth λ and other system dimensions. The parametric range outside this limit is actually relevant to many materials. We fill that gap by applying our method to Ginzburg-Landau theory. The vortex structure is investigated for single- and two-gap bulk superconductors, outside the London regime. This enables us to extend analytical expressions describing the condensate and magnetic profiles around the vortex available in literature by numerical calculations and suitable fitting functions. We expand our approach to account for films with finite thickness, to connect our findings to both bulk and Pearl's description by adjusting the sample thickness. This also allowed us to describe how vortex configurations change for samples with intermediate thickness, where we observe the effective magnetic response of the superconductor changing between the textbook type-1 and type-2 behaviors, in a nontrivial manner, governed by the non-monotonic vortex interaction. As a result of a detailed analysis, we propose new critical parameters to define the crossover between different regimes and establish their relation with the superconducting critical fields.

Keywords: Vortex matter. Vortex-vortex interaction. Superconductors. Bose-Einstein condensates. Superfluids.

Resumo

Usando uma abordagem numérica própria, desenvolvemos uma ferramenta poderosa para investigar propriedades e interações de vórtices na teoria do campo médio para supercondutores e superfluidos, baseada na fixação da distribuição de fase dos vórtices no processo de minimização da energia. O método foi aplicado a (i) condensados de Bose-Einstein (BECs) com múltiplas componentes e (ii) supercondutores com um ou mais condensados que super-conduzem. Nesses sistemas, a interação vórtice-vórtice e outras características chaves são analiticamente descritas apenas em regimes específicos, que não descrevem grande parte do comportamento dos vórtices observados experimentalmente. Em condensados de Bose-Einstein com múltiplas componentes, por exemplo, a interação vórtice-vórtice é conhecida apenas para distâncias muito maiores que o comprimento de coerência, i.e. longe do centro do vórtice. Sob nossa abordagem, assumindo estruturas com múltiplos vórtices, dentro da teoria de Gross-Pitaevskii, nós reportamos a interação entre vórtices em todo o domínio de distâncias, capturando o mecanismo por trás de conformações de vórtices não usuais previamente reportadas na literatura, como aglomerados ligados com dois ou três vórtices. Sabe-se que, geralmente, esses aglomerados emergem da competição entre interações de vórtices intra-componentes com interações inter-componentes, no entanto, nós demonstramos que essas também podem emergir da frustração de fase entre as componentes.

Em supercondutores, a descrição da interação entre vórtices é geralmente restrita a materiais na forma bulk ou em filmes finos, e a maior parte das características chaves dos vórtices, tais como os perfis espaciais do campo magnético e da densidade de corrente, são conhecidos apenas no limite da teoria de London, i.e. para comprimentos de coerência ξ insignificantes quando comparados ao comprimento de penetração λ e outras dimensões do sistema. O alcance paramétrico fora desse limite é na verdade relevante para muitos materiais. Nós preenchemos essa lacuna ao aplicar nosso método à teoria de Ginzburg-Landau. A estrutura dos vórtices é investigada para supercondutores do tipo bulk com uma e duas componentes fora do regime de London. Isso nos permitiu estender expressões analíticas da literatura que descreviam os perfis do condensado e do campo magnético em torno do vórtice através de cálculos numéricos e realização de fittings com funções apropriadas. Expandimos nossa abordagem para filmes com espessura finita, a fim de conectar nossos achados a ambas as descrições do tipo bulk e de Pearl, através de ajustes da espessura da amostra. Isso também nos permitiu descrever como as configurações de vórtices mudam para amostras com espessura intermediária, onde observamos a resposta magnética efetiva alterando entre os comportamentos de tipo-1 e tipo-2 de forma não trivial, levando a uma interação não monotônica entre vórtices. Como resultado de uma análise detalhada, nós propomos novos parâmetros críticos para definir a transição entre

os diferentes regimes supercondutores e estabelecer suas relações com os campos críticos do supercondutor usual.

Palavras-chave: Matéria de vórtice. Interação vórtice-vórtice. Supercondutores. Condensados de Bose-Einstein. Superfluidos.

List of Figures

List of Tables

Contents

1 Introduction

In what follows, we present a brief introduction to both Bose-Einstein condensation and superconductivity theories in order to bridge the gap between fundamental concepts and the current research presented in this thesis. Unfortunately, summarizing over a hundred years of research in just a single chapter within the didactic purpose of teaching is certainly not a conceivable task and lies outside the scope of this thesis. Therefore, only topics directly related to the research presented in this thesis will be carefully reviewed in this thesis. In this chapter, we shall make a brief return to the past, in order to provide an historical perspective of the progress made in both fields. Starting from their prediction/discovery, some of relevant achievements which contributed substantially to the condensed state description are briefly revisited. Whenever necessary, a deeper review may be presented in subsequent chapters.

1.1 Introduction to Bose-Einstein Condensates

In the classical formalism, it is well known that the state of matter depends on a balance between temperature and the van der Waals force between the atoms. This combination aptly describes the transition between gaseous, liquid and solid states when the system is cooled down (CALLEN, 1960). However, under certain circumstances, if the atoms are cooled far down enough to extremely low temperatures, they undergo a very unusual transformation, suggesting a non-classical treatment (PATHRIA, 1995; HUANG, 1963; LANDAU; LIFSHITZ; PITAEVSKII, 1980). In fact, under these conditions, the de Broglie wave length λ associated with atoms becomes very large compared to the avarage inter-atom distances, making the quantum properties of atoms important (KETTERLE, 2007). Ruled by the laws of quantum mechanics, where the dynamical motion is governed by the Schrödinger equation, the Heisenberg uncertainity principle does not allow keeping track of particle's trajectory and, unlike in classical mechanics, particles sharing the same intrinsic properties shall be regarded as indistinguishable objects (SAKURAI; NAPOLITANO, 2011; COHEN-TANNOUDJI; DIU; LALOE, 1991). Satyendra Nath Bose was the first to consider the effects of particle indistinguishability in quantum mechanics (BOSE, 1924). In fact, under the assumption of indistinguishability of photons, he made a clean derivation of Planck's formula of black body radiation. Thereafter, expanding upon the Bose suggestion for a gas of non-interacting massive particles, Einstein pointed out that there should be a critical temperature T_c under which a large fraction of system particles collapses in the system ground state, forming a condensate which can be described by a single and uniform wavefunction (EINSTEIN, 1925). In this regime, particles lose their identity and matter stops behaving as a set of independent particles, leading inherent quantum effects of

matter to be exhibited in large scales (KETTERLE, 2007; PETHICK; SMITH, 2002). This collective behavior paved the way towards the discovery of a new state of matter usually masked by thermal motion of system particles, named Bose-Einstein condensation (BEC) in honor of its discoverers Satyendra Nath Bose and Albert Einstein. In this new state, the gas behaves as a superfluid, (FETTER, 2009a; DALFOVO et al., 1999) experiencing no flow resistance and, therefore, it no longer obeys the classical hydrodynamics description.

1.1.1 Thermal wavelength and quantum effects

Quantum effects arising from the wave nature of particles manifest themselves macroscopically only under very restricted conditions of density and temperature. To a first approximation, the critical temperature T_c might be derived as the emerging point of an identity crisis, where the spatial extension of wave packets associated with gas atoms becomes of the order of the inter-atom distances. According to the de Broglie conjecture (BROGLIE, 1924), the spatial extension of these wave-packets is governed by the de Broglie wavelength $\langle\lambda\rangle = h/\langle p\rangle$, where $\langle p\rangle$ is the average momentum of particles in the gas. The wavelength is, therefore, closely related to the thermal motion of the system. At equilibrium, the energy equipartition law holds,

$$\frac{\langle p\rangle^2}{2m} = \frac{3}{2}k_B T, \tag{1.1}$$

and the spatial extension of wave packets can be defined in terms of the gas temperature T, leading to the thermal wavelength definition $\lambda_T = h/\sqrt{3mkT}$. Because the average inter-particle distance is of the order of $n^{1/3}$, where n is the gas density, the quantum regime emerge when the phase space density, $D \equiv n\lambda_T^3$, approaches unity. A sketch of the phase transition is illustrated in Fig. 1, where quantum and classical regimes are respectively represented by the blue and red backgrounds.

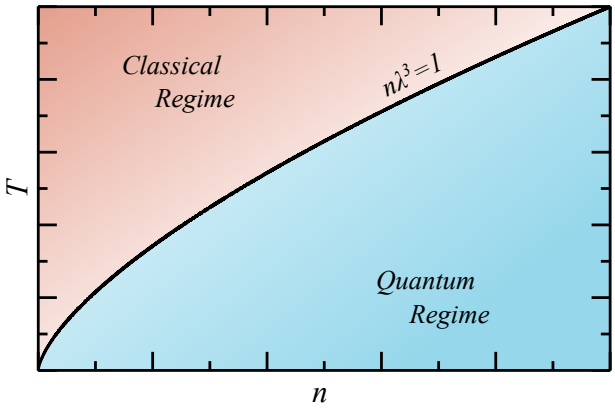

Figure 1 – Classical and quantum regimes in the temperature-density plane. The rough dividing line is $n\lambda_T^3 = 1$, where λ_T is the thermal wavelength and n stands for the density of particles.

Under usual conditions, the wave packet extension is extremely small compared to interatomic distances and the quantum mechanical distinction of particles is irrelevant.

In this regime, particles in a gas might be treated as billiard balls, obeying the Maxwell-Boltzman statistic (HUANG, 1963). On the other hand, whenever the temperature of a non-interacting gas becomes low enough and the density high enough such that the phase space density approaches unity, the quantum indistiguishability of system particles becomes relevant and must be taken into account in the theoretical description. Usually, the indistinguishability is expressed in quantum theory by imposing symmetry constraints on the state functions and on the observables, bringing consequences which deeply affect the physical nature of the system (LEINAAS; MYRHEIM, 1977). These constraints emerge from the invariance of measurable physical quantities with respect to a particle permutation. From the statistical point of view, the main difference between both regimes is the way that we count the number of different system states. Indeed, in the classical formalism, each identical system particle is treated as distinguishable, which implies that the permuting between any two identical particles of the system leads to different states. On the other hand, in the quantum mechanics description, this is no longer valid and a symmetry (anti-symmetry) between the $N!$ permutations of bosonic (fermionic) particles appears for the same physical state. This redundancy, called exchange degeneracy, violates the state vector unicity for each physical state and then must be eliminated from the theoretical formalism by limiting the state vector space to a subspace that is invariant under the permutation of labels (SAKURAI; NAPOLITANO, 2011).

1.1.2 Ideal Bose gas

To statistically address elementary effects derived from the indistinguishability of quantum particles, Einstein firstly expanded upon Bose's suggestion to a gas of N non-interacting quantum particles confined in a volume V and sharing a certain amount of energy E. Within their approach, named Bose-Einstein statistics, they predicted the novel state of matter by making no reference at all to the interaction between gas atoms. It is worth to mention that, at the time of Bose-Einstein condensation prediction, in 1924, some of the basic concepts of quantum mechanics were not yet discovered. For instance, strange as it may seem, the uncertainty principle of Heisenberg was derived only three years later. Actually, as pointed out in Ref. (DELBRUCK, 1980), the Bose-Einstein statistics may have arisen from an elementary "mistake" of Bose, which was subsequently reproduced by Einstein. The deep meaning of Bose's assumptions could only be understood after the working out of quantum mechanics (DELBRUCK, 1980). In this section, the statistical prediction of Bose-Einstein condensation is briefly reviewed, but without going into further details on the cumbersome historical path.

1.1.2.1 Bose-Einstein distribution

Rather than describing individual particle behavior, the statistical description accounts for the collective effects of entire system, by means of distribution of particles

along the system energy spectrum under macro-state constraints (N, V, E). From the principle of equal a priori probabilities, the distribution with the largest number of micro-states is more likely to occur and therefore should represent the system ground state (REIF, 1965). This requires the knowledge of the number of micro-states $\Omega(N, V, E)$, for each possible distribution. In the thermodynamic limit, where fluctuations around the average are negligible, the system total energy spectrum should be regarded as a continuum (PATHRIA, 1995; HUANG, 1963; REIF, 1965; ANNETT, 2004). Therefore, in order to to count accessible states, the energy spectrum might be divided into a large number of energy cells, indexed by $k = 1, 2, 3....$ Let ϵ_k denote the average energy of cell k and g_k the number of states inside it. Each cell contain a large, but still arbitrary, number of states, which means that $g_k >> 1$. Thus, the problem consists in finding how many different ways one can group n_1 particles in the first cell, n_2 particles in the second cell and so on, following the macro-state constraints of number of particles and total energy,

$$\sum_k n_k = N, \tag{1.2a}$$

$$\sum_k \epsilon_k n_k = E. \tag{1.2b}$$

Because exchanging of particles in different cells does not produce a new different state, the number of distinct microstates associated with each cell, $w(k)$, may be calculated separately, as the number of ways to accommodate n_k particles among g_k levels. The total number of microstates, $\Omega(N, V, E)$, associated with the set $\{n_k\}$, results from

$$\Omega(N, V, E) = \prod_k w(k), \tag{1.3}$$

where, for bosons, $w(k)$ can be achieved by counting the number of arrangements between n_k balls and $g_k - 1$ walls separating energy cells, which is given by

$$w(k) = \frac{(n_k + g_k - 1)!}{n_k!(g_k - 1)!}. \tag{1.4}$$

In the thermal equilibrium, the particles might distribute themselves such that the entropy S is maximized. Thus, the distribution of bosons may be obtained by maximizing the function $S = k_B ln\Omega$, where k_B is the Boltzmann constant. Through straightforward calculations, the result first obtained by Bose and Einstein is found

$$n_k = \frac{g_k}{e^{(\epsilon_k - \mu)/k_B T} - 1}, \tag{1.5}$$

where μ is the chemical potential and T the temperature (HUANG, 1963; PATHRIA, 1995; ANNETT, 2004). Roughly, the Bose-Einstein distribution is the most random way to distribute particles among system's micro-states under the constraints of fixed number of particles N and total energy E (INGUSCIO et al., 1999). The average number of particles occupying any single quantum state is given by the ratio n_i/g_i,

$$\langle n_k \rangle = \frac{1}{e^{(\epsilon_k - \mu)/k_B T} - 1}. \tag{1.6}$$

1.1.2.2 BEC in an ideal gas

Unlike the classical ideal gas, or the Fermi-Dirac gas, the Bose-Einstein gas presents a very peculiar regime. In fact, as illustrated in Fig. 2, if the chemical potential μ becomes equal to the energy level ϵ_k, the average number of particles of the k-th states becomes infinitely high. The condensation of particles in a single state, however, can only occur for the lowest energy level, otherwise the occupation number of some states would assume negative values, which has no physical meaning. This macroscopic occupation of the lower energy state is reflected in the abrupt changes on thermodynamical properties, signed by a change of behavior in specific heat that closely resembles the λ-point transition observed in liquid helium (FEYNMAN, 1957).

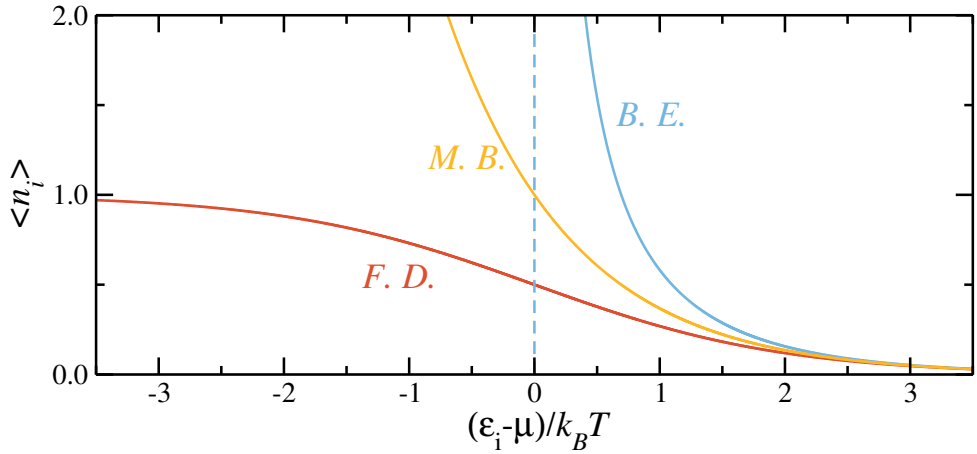

Figure 2 – The mean occupation number $\langle n_\epsilon \rangle$ of a single-particle energy state ϵ in a system of non-interacting particles for Fermions (red line), Bosons (blue line) and classical particles (yellow line). Acronyms $F.D.$, $M.B.$ and $B.E.$ respectively account for the Fermi-Dirac, Maxwell-Boltzmann and Bose-Einstein distributions governing particle's statistics.

Making the chemical potential approach the ground state energy is probably the simplest way to observe the origin of Bose-Einstein condensation phenomenon. However, it is by no means something rigorous, since it provides no clue on the fraction of condensed particles or even the critical temperature required to define this new state of matter. The comprehensiveness of phase transition's thresholds lies somehow on the total number of particles constraint and emerges as a pathology derived from the inability to count for ground-state particles in thermodynamic limit. In the thermodynamic limit, the sum over discrete quantum states of Eq. (1.2a) might be replaced by an integral over the continuum energy spectrum and the density of particles may be written

$$n = \int_0^\infty \frac{g(\epsilon)}{e^{(\epsilon-\mu)/k_B T} - 1} d\epsilon, \tag{1.7}$$

where $g(\epsilon)$ stands for the density of states per unit of volume and accounts for the number of available states inside an energy element $d\epsilon$ per unit of volume. For spin-0 particles, the

density of states becomes

$$g(\epsilon) = \frac{m^{3/2}}{\sqrt{2}\pi^2\hbar^3}\epsilon^{1/2}. \tag{1.8}$$

Here, it is worth mentioning that, symmetry properties of particles are not included in the density of states. In fact, their quantum nature is completely contained on Bose-Einstein distribution, that governs allocation of particles among micro-states. The outcome of Eq. (1.7) enables writing down the particle density as a function of the temperature T and the gas fugacity, defined by $z = \exp(\mu/k_BT)$,

$$n\left(\frac{2\pi\hbar^2}{mk_BT}\right)^{3/2} = g_{3/2}(e^{\mu/k_BT}), \quad \text{or} \quad n\lambda^3 = g_{3/2}(z). \tag{1.9}$$

where λ is the redefined de Broglie wavelength and the function $g_{3/2}(z)$ stands for the sum series

$$g_{3/2}(z) = \sum_{n=1}^{\infty}\frac{z^\alpha}{\alpha^{3/2}}. \tag{1.10}$$

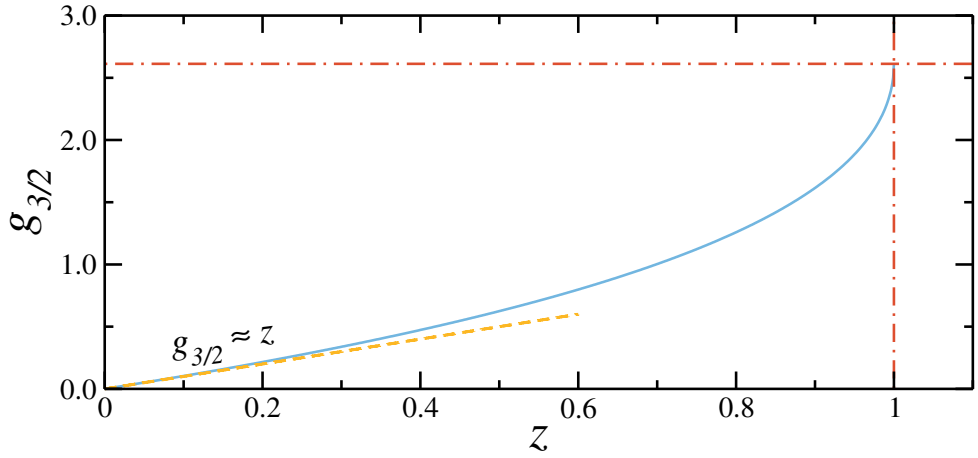

Figure 3 – Function $g_{3/2}$ as a function of the gas fugacity represented by the blue line. The yellow line show that $g_{3/2}$ can be approximated by a linear function for low values of z.

In Fig. 3, the $g_{3/2}(z)$ sum is plotted as a function of the gas fugacity and is represented by the blue solid line. For low values of z, which corresponds to the high temperature and low density limits, the $g_{3/2}$ function presents an almost linear behavior and can be well approximated by $g_{3/2} \approx z$, as illustrated by the linear function designed by the yellow dashed line. As a consequence, in the classical regime, the chemical potential may be well described by

$$\mu \approx -\frac{3}{2}k_BTln\left(\frac{mk_BT}{2\pi\hbar^2n^{2/3}}\right). \tag{1.11}$$

In contrast, the other limit is bounded by the convergence of the sum of (Eq. 1.10) , which diverges when the fugacity becomes greater than unity. Exactly at $z = 1$, the function $g_{3/2}$ presents a diverging derivative and assumes the value $\zeta(3/2) = 2.612$, which

is represented by the interception of the red dashed-dotted lines in Fig 3. Although the right side of the Eq. (1.9) presents this bounding condition, the left side does not and thus, the limiting condition $n\lambda^3 \leq \zeta(3/2)$ is not physical. This comes from the fact that the density of states $g(\epsilon)$ assigns zero weight to the ground state energy level and thus, n should be taken as the density of particles with non-zero momentum. Therefore, as the temperature (density) is decreased (increased) the left side of the former equation becomes higher, until it reaches its maximum value, $g_{3/2}(1) = 2.612$. At this point, the chemical potential energy equates to the ground-state energy of an ideal gas, characterized by zero momentum $\vec{k} = 0$. Beyond this limit, any excess of particles goes into the ground-state energy states macroscopically occupying it and therefore, giving rise to the BEC phase. The critical temperature follows from Eq. (1.9) for $z = 1$, where the right-hand side of Eq. (1.9) becomes equal to $\zeta(3/2) = 2.612$,

$$T_c = \frac{2\pi\hbar^2}{k_B m}\left(\frac{n}{2.612}\right)^{2/3}. \tag{1.12}$$

Below the critical temperature T_c, the condensed fraction of particles can be achieved by the particle conservation principle, where the total number of particles N is a sum between all particles with zero momentum $N_{k=0}$ and those with non-zero momentum, which obeys expression $N_{k\neq 0} = V g_{3/2}/\lambda^3$. The condensed fraction of particles of the system naturally follows from conservation of the total number of particles,

$$\frac{n_0}{n} = \left[1 - \frac{g_{3/2}}{\lambda^3}\right] = \left[1 - \left(\frac{T}{T_c}\right)^{3/2}\right], \tag{1.13}$$

where n_0 and n accounts for the condensed and uncondensed densities. A sketch of density-temperature phase diagram is shown in Fig. 4, where the blue background represents the condensed state and the red one stands for the gas phase. The origin of the Bose-Einstein

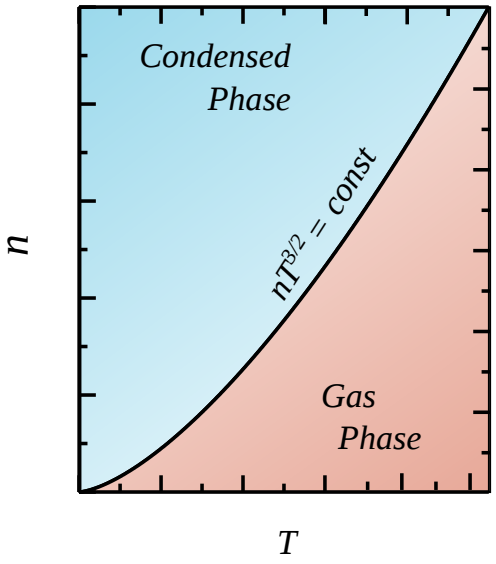

Figure 4 – Phase diagram of Bose-Einstein condensation in the density-temperature plane.

phase transition lies in the particles nature and therefore, it is driven only by its statistics

and not by their inter-atomic interactions. Actually, one should expect interactions to spoil such phase transition, since under required temperature and density conditions, any set of particles would condense into solid state. Fortunately, current set of experiments has proved that such phase transition is robust enough so that, even in the presence of interactions and external confining potentials a gas can Bose condense (BURNETT MARK EDWARDS, 2008). However, a price has to be paid: in order to avoid the solid state of matter, the condensed phase must be achieved under the metastable phase of a very dilute gas, limiting, therefore, the visualization lifetime.

1.1.3 Path towards BECs

Because this was a theory without an experimental example at the time of its prediction, the BEC phenomenon did not received the proper and deserved attention. In fact, most physicists of that time, including Albert Einstein, took such idea as a mathematical pathology of non- interacting systems, which has nothing to do with the physical reality and, therefore, could never be realized experimentally. Moreover, except for ^4He, at required densities and temperatures, all materials resides in its solid state and atoms are not delocalized as required by BEC theory. The closest evidence of Bose-Einstein condensation in nature was in the superfluid phase of helium isotope ^4He (for $T \leq 2.17$), found only later in 1937, which London tried to explain as a condensation phenomenon distorted by the presence of strong interactions between helium atoms (LONDON, 1938). London's assumption was supported by a similar λ- point transition of the specific heat at an acceptable close critical temperature of 3.13 K, strengthening the link between BEC and superfluidity, (FEYNMAN, 1957; KAPITSZA, 1938; ALLEN, 1938). Further, more precisely in 1957, the BEC assumption was, again, taken as the main mechanism behind the microscopic explanation of superconductivity phenomena provided by Bardeen, Cooper and Schrieffer theory (BCS theory) (BARDEEN; COOPER; SCHRIEFFER, 1957). In BCS model, mediated by electron-phonon interactions, a weak effective attraction between electrons inside the superconducting material correlates electrons in pairs leading to the instability of Fermi sea. Because these pairs behave as bosonic particles, they could also Bose condense, exhibiting an electronic superfluidity (superconductivity) when subjected to sufficiently low temperatures. Subsequently, the BCS mechanism was used to explain the superfluid phase of the fermionic isotope of helium, ^3He, which, despite presenting a half-integer spin, could also undergo through a Bose-Einstein phase transition by the same pairing mechanism (OSHEROFF; RICHARDSON; LEE, 1972; OSHEROFF et al., 1972; LEGGETT, 1972).

Despite many evidences of condensation provided by nature, the rush towards BEC experimental achievement only attained notorious dimension in beginning of 80's, after development of laser and evaporative cooling techniques (CHU, 1998; PHILLIPS, 1998; COHEN-TANNOUDJI, 1998; KETTERLE; DRUTEN, 1996). Firstly, the average

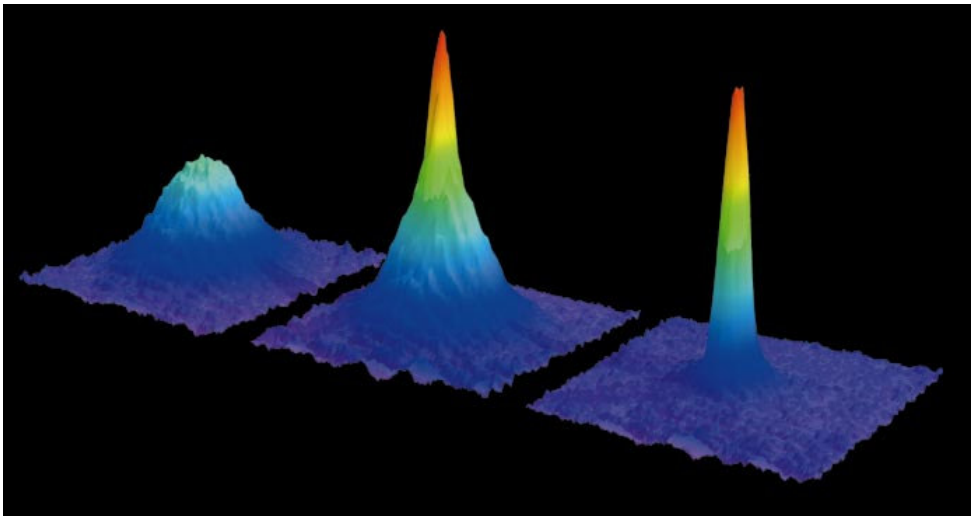

Figure 5 – Observation of Bose-Einstein condensation by means of absorption imaging technique, where the absorption is illustrated as a function two spatial directions for temperatures above, just below and well below the critical temperature, respectively illustrated in pictures from the left- to right-hand side. Figure retrieved from Ref. (DURFEE; KETTERLE, 1998).

kinetic energy of atoms is reduced by shining counter-propagating laser beams. In a complex process, the scattered light carries more energy than the absorbed one, cooling the gas to a few hundred of microkelvins. The gas is then deposited in a magnetic trap and then subjected to the evaporative cooling process, where only the most energetic particles are allowed to escape from the local minimum magnetic trap, making remaining atoms cooler on average. These cooling techniques allowed to reach temperatures of the order of few μK and therefore, could pay the price of diluteness requirements, necessary to avoid solidification before BEC could be visualized. In fact, within the advent of these cooling schemes, BEC phase transition was independently obtained in metastable states of a very dilute gas of Rubidium ^{87}Rb(ANDERSON et al., 1995) and Sodium ^{23}Na(DAVIS et al., 1995). At the ground state, condensed particles might exhibit no net velocity when barriers of trapping potential are removed, whereas non-condensed particles might spread out, maximizing the entropy. Indeed, measurements of velocity distribution provided the first evidence of Bose-Einstein condensation. In Fig. 5, the macroscopic occupation of the ground-state in a dilute gas of Sodium ^{23}Na was obtained by means of absorption imaging technique (DURFEE; KETTERLE, 1998). This outstanding experimental achievement pushed further theoretical and experimental researches in the field. As a consequence, BEC was one of the most investigated topics of the end of the past century and still remains as a field of high-interest nowadays (KETTERLE, 2002). Meanwhile, subsequent condensation experiments for different types of atoms were realized (BRADLEY et al., 1995; BRADLEY; SACKETT; HULET, 1997; CORNISH et al., 2000; ROBERT et al., 2001; TAKASU et al., 2003; WEBER et al., 2003; GRIESMAIER et al., 2005; STELLMER et al., 2009; ESCOBAR et al., 2009; STELLMER et al., 2010; MICKELSON et al., 2010; KRAFT et

al., 2009; LU et al., 2011), comprising different inter-particle interaction schemes, such as the contact, dipolar (LU et al., 2011) and even the spin-orbit coupling interactions(LIN; JIMENEZ-GARCIA; SPIELMAN, 2011). In fact, differently from the ideal Bose gas, alkali atoms in a magnetic trap do interact with each other, repelling (attracting) at short (large) interatomic distances. Usually, due to the gas diluteness, interactions are well described by a Lennard-Jones potential and theoretically modeled by a short-range contact interaction (HUANG; YANG, 1957; LEE; HUANG; YANG, 1957), governed by the s-wave scattering length a (PETHICK; SMITH, 2002),

$$V_i(\vec{r} - \vec{r}') = \frac{4\pi\hbar^2 a}{m}\delta(\vec{r} - \vec{r}'). \tag{1.14}$$

The interaction strength can be experimentally tunned by means of an externally applied magnetic field, in a Feshbach resonance process, where quasibound molecular states share the same energy as an unbound state and thus couples resonantly to the free state of the colliding atoms (INOUYE et al., 1998; CHIN et al., 2010). The closer this molecular level lies with respect to the energy of two free atoms, the stronger the interaction between them. In fact, this resonance mechanism has strong influence on elastic collisions and because incoming atoms and quasibound states have different spin arrangements, the magnetic field becomes a powerful tool in order to control such interactions.

Recently, ^{52}Cr atoms with high magnetic moment were also observed to exhibit a different type of interaction that could no longer be described only by the simple hard-wall interacting model. Despite still sharing the short-range contact interaction, these atoms also interact with each other via the long-range and anisotropic dipole-dipole interaction (LU et al., 2011), whose properties strongly contrast with those observed in standard condensed gases described exclusively by contact interaction (SABARI et al., 2015). Indeed, theses gases exhibit a completely different collective excitation spectrum, with the presence of rotons quasiparticles, also observed in liquid helium superfluid phase. Due to the anisotropic character of the dipolar interaction, different patterns of equilibrium states and new quantum phases were also observed. Actually, although not depicted in the original theory, particle-particle interactions play an important role in BEC theory. Not surprisingly, experimental realization of different interacting regimes, such as the dipolar and the recently engineered spin-orbit coupling (LIN; JIMENEZ-GARCIA; SPIELMAN, 2011), where particle's momentum couples with their magnetic moment, had opened up subbranches in ultra-cold atoms physics. Moreover, the recent improvement in trapping techniques allowed different confinement geometries, such as the effectively two-dimensional and one-dimension confining potentials where the condensate dynamic is suppressed in one or in two directions due to a strong confinement. Usually, external potentials are well described by an anisotropic parabolic potential, however, it is worth to mention that different geometries, such as the toroidal confinement, have already been experimentally realized. In special, the development of optical trapping techniques, which has no effect

on the hyperfine spin states structure, have allowed the realization of multi-component BECs, where the macroscopic occupation occur in multiple spin substates (MYATT et al., 1997; HALL et al., 1998). Further, multi-component BEC was also observed to occur in mixtures of different isotopes of the same(PAPP; PINO; WIEMAN, 2008) and different atomic species (FERRARI et al., 2002; MODUGNO et al., 2002; THALHAMMER et al., 2008). As we shall see further in this thesis, multi-component BECs have a much richer physics and are far from being just a trivial extension of the single-component case.

1.1.4 Theoretical description of an interacting Bose gas

The collective behavior of particles lies in the heart of condensation phenomenon. In fact, for inherent quantum effects to be observed in a macroscopic scale, a large number (usually between $10^4 - 10^6$ atoms) of particles is required (ANNETT, 2004). Therefore, a complete description of physical properties of realistic BECs would then require the solution of, at least, thousands coupled Schrödinger's equations, which is numerically challeging nowadays. Then we must be satisfied with only an approximate understanding of how the Schrödinger equation could lead to solutions that would indicate a similar behavior to those observed experimentally. Fortunately, an approximate understanding might be achieved under the assumption of mean-field theory for weakly interacting systems, which yields to a Schrödinger-like equation, known as the Gross-Pitaevskii equation.

1.1.4.1 Second quantization and the many-body Hamiltonian

In the single-particle wave mechanics, the quantum mechanical formalism is usually developed over the eigenstates of position $\hat{x}$ and momentum $\hat{p}$ operators. However, expanding up the formalism in order to account for many-body quantum objects leads to an ambiguity of eigenstates as a result of the exchanging degeneracy. Because it violates the state vector unicity, restrictions might be imposed on vector space, limiting it to a subspace that is invariant under the permutation of labels (SAKURAI; NAPOLITANO, 2011). At the end, the resulting basis might not contain individual information of each system particle, since, even in theory, this information is lost during the time evolution of the system (MERZBACHER, 1998).

One of the most elegant ways to avoid ambiguity on many-body quantum space proceeds by means of the introduction of a linear operator $\hat{\psi}(\vec{r})$, which resembles the annihilation operator $\hat{a}$ commonly used in quantum harmonic oscillator formalism (ROBERTSON, 1973). The quantum field ψ depends on vector position $\vec{r}$ and obeys, as the only requirement, the symmetry properties of particles, which is done by imposing the following (anti-) commutation relation that $\hat{\psi}(\vec{r})$ and its hermitian conjugate $\hat{\psi}^\dagger(\vec{r})$ must obey,

$$\hat{\psi}(\vec{r})\hat{\psi}(\vec{r}') \mp \hat{\psi}(\vec{r}')\hat{\psi}(\vec{r}) = 0, \tag{1.15a}$$

$$\hat{\psi}^\dagger(\vec{r})\hat{\psi}^\dagger(\vec{r}') \mp \hat{\psi}^\dagger(\vec{r}')\hat{\psi}^\dagger(\vec{r}) = 0, \tag{1.15b}$$

$$\hat{\psi}(\vec{r})\hat{\psi}^\dagger(\vec{r}') \mp \hat{\psi}^\dagger(\vec{r}')\hat{\psi}(\vec{r}) = \delta(\vec{r} - \vec{r}'), \tag{1.15c}$$

where $\delta(\vec{r} - \vec{r}')$ is the Dirac delta function and the upper (lower) signal stands for bosonic (fermionic) particles. Operators $\hat{\psi}(\vec{r})$ and $\hat{\psi}^\dagger(\vec{r})$ provide a convenient and useful basis for representing many-particle states and many-body operators. In fact, it leads to a less superfluous notation than symmetrized and anti-symmetrized wave functions. The analogy between $\hat{\psi}$ and $\hat{a}$ becomes clear by defining an hermitian operator

$$\hat{N} \equiv \int d^3r \hat{\psi}^\dagger(\vec{r})\hat{\psi}(\vec{r}), \tag{1.16}$$

where, the employment of $\hat{\psi}$ must guarantee the existence of at least one non-trivial eigenstate $|\phi\rangle$, with a corresponding eigenvalue n_ϕ defined by $\hat{N}|\phi\rangle = n_\phi|\phi\rangle$. Through the application of commutation relations $[N, \hat{\psi}(r)] = -\hat{\psi}(\vec{r})$ and $[N, \hat{\psi}^\dagger(r)] = \hat{\psi}^\dagger(\vec{r})$ on state $|\phi\rangle$, one may derive

$$\hat{N}\hat{\psi}(\vec{r})|\phi\rangle = (n_\phi - 1)\,\hat{\psi}(\vec{r})|\phi\rangle, \tag{1.17a}$$

$$\hat{N}\hat{\psi}^\dagger(\vec{r})|\phi\rangle = (n_\phi + 1)\,\hat{\psi}^\dagger(\vec{r})|\phi\rangle. \tag{1.17b}$$

States $\hat{\psi}(\vec{r})|\phi\rangle$ and $\hat{\psi}^\dagger(\vec{r})|\phi\rangle$ are, therefore, identically zero or new nontrivial eigenstates of operator $\hat{N}$ with eigenvalues $n_\phi - 1$ and $n_\phi + 1$ respectively. The expected value of operator $\hat{N}$ in the state $|\phi\rangle$ establish a lower bound for eigenvalues, $n_\phi \geq 0$, and then, from the existence of an arbitrary nontrivial eigenstate $|\phi\rangle$ of N, a nontrivial eigenstate $|0\rangle$ of $\hat{N}$ must exist, satisfying the equation

$$\hat{\psi}(\vec{r})|0\rangle = 0. \tag{1.18}$$

The decreasing sequence of eigenvalues has integral spacing and must have zero as the lower bound value, making non-negative integers the only accessible numbers: $n_\phi = 0, 1, 2, 3....$ In turn, the creation operator $\psi^\dagger(\vec{r})$ may be used to remove almost completely the need of state vector, allowing to retain only the special state $|0\rangle$. In fact, any other eigenstate of $\hat{N}$ can be achieved by successive applications of $\psi^\dagger$ on $|0\rangle$: $|0\rangle$, $\hat{\psi}^\dagger(\vec{r}_1)|0\rangle$, $\hat{\psi}^\dagger(\vec{r}_2)\hat{\psi}^\dagger(\vec{r}_1)|0\rangle$, etc. This enable to use operators rather than vector states to describe the physics, which is advantageous since operators $\psi^\dagger$ and ψ carry the symmetry properties of particles. In fact, one could anticipate that operator $\hat{N}$ must have the same properties of the number operator widely used for harmonic oscillators and therefore conclude that n_ϕ actually represents the number of particles in the state ϕ. However, in order to preserve the mathematical rigor, these statements shall arise naturally in the present formalism. Before expressing the Hamiltonian and state vectors in terms of eigenstates of $\hat{N}$, it is noteworthy that

eigenfunctions are highly degenerate, indeed, states $\psi^\dagger(\vec{r})|0\rangle$ and $\psi^\dagger(\vec{r}')|0\rangle$ are, for example, associated with the same eigenvalue $n = 1$, even if $\vec{r} \neq \vec{r}'$. The orthogonality of these states is satisfied under two circumstances:(i) If their corresponding eigenvalue of N are different or (ii) if their corresponding eigenvalues are the same, but their arguments $\vec{r}_1, \vec{r}_2, ..., \vec{r}_n$ are not all the same. The last condition can be expressed mathematically, in the two-particle context, as

$$\langle 0|\hat{\psi}(\vec{r}_1)\hat{\psi}(\vec{r}_2)...\hat{\psi}^\dagger(\vec{r}_2')\hat{\psi}^\dagger(\vec{r}_1')|0\rangle = \delta(\vec{r}_1 - \vec{r}_1')\delta(\vec{r}_2 - \vec{r}_2') \pm \delta(\vec{r}_1 - \vec{r}_2')\delta(\vec{r}_2 - \vec{r}_1'). \tag{1.19}$$

Except for state $|0\rangle$, eigenstates of $\hat{N}$ can not be normalized, since Dirac delta function diverge at the origin. Still, following a similar procedure of free-particles in the standard wave mechanics formalism, normalized states might be achieved. For instance, through an educated guess, the single-particle non-normalized state may be written as

$$|\Psi_1\rangle = \hat{\psi}^\dagger(\vec{r}_1)|0\rangle. \tag{1.20}$$

Actually, this is exactly the same process of adding one quantum of energy in the case of a harmonic oscillator. However, as we shall see further, it now means an addition of one particle in space at position $\vec{r}_1$. The norm, $\langle\Psi_1|\Psi_1\rangle$ is not well defined, since

$$\begin{aligned}\langle\Psi_1'|\Psi_1\rangle = \langle 0|\hat{\psi}(\vec{r}_1')\hat{\psi}^\dagger(\vec{r}_1)|0\rangle = \\ = \delta(\vec{r}_1 - \vec{r}_1'),\end{aligned} \tag{1.21}$$

diverges when $\Psi = \Psi'$. However, with the experience provided by the standard formalism, a general single-particle state may be contructed as a linear spatial superposition of position eigenfunctions

$$|\Psi_1\rangle = \int d^3r_1 \Psi(\vec{r}_1)\hat{\psi}^\dagger(\vec{r}_1)|0\rangle, \tag{1.22}$$

where $\Psi(\vec{r}_1)$ is a weight factor. Substituing last equation in the time-dependent Schrödinger equation, it turns out that $\Psi(\vec{r}_1)$ is actually the wave function of a free particle in the wave conjecture of quantum mechanics. Similarly, the N-particle state may be defined as

$$|\Psi_n\rangle = \frac{1}{\sqrt{n!}} \int d^3r_1 ... \int d^3r_n \Psi(\vec{r}_1, ..., \vec{r}_n)\hat{\psi}^\dagger(\vec{r}_n)...\hat{\psi}^\dagger(\vec{r}_1)|0\rangle. \tag{1.23}$$

The meaning of such assumption becomes clear when the state $|\Psi_N\rangle$ is subjected to the application of operator $\hat{N}$. In fact, recalling the commutation that $[\hat{N}, \hat{\psi}^\dagger(\vec{r})] = \hat{\psi}^\dagger(\vec{r})$, or similarly $\hat{N}\hat{\psi}^\dagger(\vec{r}) = \hat{\psi}^\dagger(\vec{r})(\hat{N} + 1)$, it is possible to derive from direct application of $\hat{N}$ on $|\Psi_n\rangle$ the eigenvalue equation

$$\hat{N}|\Psi_n\rangle = n|\Psi_n\rangle, \tag{1.24}$$

This matches with the previous definition of $|\Psi_n\rangle$ as a proper n-particle state, since it is indeed an eigenstate of $\hat{N}$ with eigenvalue n and strengthens the interpretation of operator

$\hat{N}$ as a number operator, where the special state $|0\rangle$ plays the role of a vacuum state, characterized by the absence of particles. It also turns out, through direct application on $|\Psi_n\rangle$, that operators $\hat{\psi}^\dagger(\vec{r})$ and $\hat{\psi}(\vec{r})$ may create a particle or destroy a partice at $\vec{r}$, leading to a new eigenstate of $\hat{N}$ and justifying the educated guess for the n-particle state. Because the application of $\hat{\psi}(\vec{r})$ and $\hat{\psi}^\dagger(\vec{r})$ to any linear combitation of eigenstates of $\hat{N}$ always generate a vector inside this same subspace, the closure condition is satisfied and subspace vectors $|0\rangle$, $\hat{\psi}^\dagger(\vec{r}_1)|0\rangle$, $\hat{\psi}^\dagger(\vec{r}_2)\hat{\psi}^\dagger(\vec{r}_1)|0\rangle$, ..., $\hat{\psi}^\dagger(\vec{r}_N)...\hat{\psi}^\dagger(\vec{r}_2)\hat{\psi}^\dagger(\vec{r}_1)|0\rangle$ indeed form a basis in Fock space.

By repeated applications of the annihilation operator in the state $|\Psi_n\rangle$ and using the normalization rule for the vacuum state, it is possible to derive the state in the wavefunction formalism $\Psi_n(\vec{r}_1, ..., \vec{r}_2)$ in terms of Fock state $|\Psi_n\rangle$

$$\Psi_n(\vec{r}_1, ..., \vec{r}_n) = \frac{1}{\sqrt{n!}}\langle 0|\hat{\psi}(\vec{r}_1)...\hat{\psi}(\vec{r}_n)|\Psi_n\rangle, \tag{1.25}$$

which carries permutation (anti-)symmetry in (anti-)commutation relations obeyed by creation and annihilation operators. Despite we are avoiding to work with $\Psi_n(\vec{r}_1, ..., \vec{r}_n)$, due to the ambiguity of the wavefunction description, the former equation allows one to prove the equivalence between the field operator and wavefunction formalisms (ROBERTSON, 1973). This means that the transformation that takes a Hamiltonian from wavefunction space to the Fock space preserves the physical result. In a many particle system, where particles are subjected to an external potential $V_e(\vec{r})$ and interact with each other through the potential $V_i(\vec{r}, \vec{r}')$, the Fock-space Hamiltonian may be defined by (ROBERTSON, 1973)

$$\hat{H} = \int d^3r\hat{\psi}^\dagger(\vec{r})\left[-\frac{\hbar^2}{2m}\nabla^2 + V_e(\vec{r})\right]\hat{\psi}(\vec{r}) + \frac{1}{2}\int d^3r d^3r'\hat{\psi}^\dagger(\vec{r})\hat{\psi}^\dagger(\vec{r}')V_i(\vec{r}, \vec{r}')\hat{\psi}(\vec{r})\hat{\psi}(\vec{r}'). \tag{1.26}$$

The first and second terms account for all single-particle processes that might occur and operate on a many particle state. In fact, both operators represent a sum over all spatially avaiable process in which a particles is removed from position $\vec{r}$, submitted to the single-particle matrix element and then replaced at position $\vec{r}$. In turn, the last term represents the energy associated with the atom-atom interaction, where the coefficient $1/2$ avoid double counting pairwise interactions. The equivalence between theses operators and operators in wave mechanics formalism may be derived from their direct application on the n-particle state $|\Psi_n\rangle$. As previously pointed out, for evaporatively cooled gases, like in mixtures of rubidium and caesium, the de Broglie wavelength of atoms is very large compared with length scales of interatomic forces and are mainly described by two-body scattering, which, under low-energy condition, may be modeled by contact interactions, $V_i = g\delta(\vec{r} - \vec{r}')$, where g is proportional to the s-wave scattering length a_s and is defined by

$$g = \frac{4\pi\hbar^2}{m}a. \tag{1.27}$$

In fact, this is a good approach for the most cases of BECs and it is of the main interest for the work presented in this thesis.

1.1.4.2 Bogoliubov approach

Because, the condensation occur in a single state of momentum space, it is advantageous to perform a change of basis and write operators $\hat{\psi}(\vec{r})$ and $\hat{\psi}^{\dagger}(\vec{r})$ in terms of operators which annihilate and create particles in momentum space, designed by $\hat{a}_{\vec{k}}$ and $\hat{a}^{\dagger}_{\vec{k}}$ (LANCASTER; BLUNDELL; BLUNDELL, 2014). The basis change can be performed under a Fourier transform of momentum space operators, which leads to

$$\hat{\psi}(\vec{r}) = \frac{1}{\sqrt{V}} \sum_{\vec{k}} e^{i\vec{k}\cdot\vec{r}} a_{\vec{k}}, \tag{1.28}$$

$$\hat{\psi}^{\dagger}(\vec{r}) = \frac{1}{\sqrt{V}} \sum_{\vec{k}} e^{-i\vec{k}\cdot\vec{r}} a^{\dagger}_{\vec{k}}. \tag{1.29}$$

After straightfoward calculations, the $\vec{k}$-space hamiltonian describing Bose particles in absence of external potential and interacting with each other through contact mechanism becomes,

$$\hat{H} = \sum_{p} \frac{\hat{p}^2}{2m} \hat{a}^{\dagger}_{p} \hat{a}_{p} + \frac{g}{2V} \sum_{kpq} \hat{a}^{\dagger}_{p-q} \hat{a}^{\dagger}_{k+q} \hat{a}_{k} \hat{a}_{p}, \tag{1.30}$$

where the sum goes over all momentum states. Despite it provides a general way to discuss many-body systems in a much more simplified picture than in usual wave mechanics formalism, solving Eq. (1.30) for macroscopic samples is still an impossible task and then requires subsequent approximations. In fact, diagonalizing the interaction contribution term is still very tricky when a large amount of particles is considered. To overcome difficulties provided by the Hamiltonian interaction term, Bogoliubov proposed to explore the consequences of the macroscopic occupation of the ground state. Instead of using exact properties obeyed by $\hat{a}^{\dagger}$ and $\hat{a}$ when applied to the ground-state $|\Omega\rangle$,

$$\hat{a}_{\vec{k}=0} |\Omega_{N_0}\rangle = \sqrt{N_0} |\Omega_{N_0-1}\rangle, \tag{1.31}$$

$$\hat{a}^{\dagger}_{\vec{k}=0} |\Omega_{N_0}\rangle = \sqrt{N_0+1} |\Omega_{N_0+1}\rangle. \tag{1.32}$$

Bogoliubov replaced creation and annihilation operators by numbers, by assuming that adding or removing a particle from the macroscopically occupied ground-state does not promote significant changes in the resulting eigenstate (BOGOLIUBOV, 1947). This approximation is valid when (i) the temperature is much less than the transition temperature for the onset of condensation, and (ii) when the condensate is sufficiently weakly-interacting. In fact, for strongly interacting systems, like the liquid ^4He in its superfluid phase, the

condensate fraction represents only 8% of the total number of particles (PENROSE; ONSAGER, 1956), which explains nonconformities between experimental observations and the present microscopic theory. Therefore, under sufficiently low temperatures, it would be reasonable to state that

$$\hat{a}_{\vec{k}=0}|\Omega_{N_0}\rangle = \sqrt{N_0}|\Omega_{N_0}\rangle, \tag{1.33}$$

$$\hat{a}^{\dagger}_{\vec{k}=0}|\Omega_{N_0}\rangle = \sqrt{N_0}|\Omega_{N_0}\rangle. \tag{1.34}$$

The error associated with Bogoliubov's prescription is of the order of the commutator $[\hat{a}_0, \hat{a}_0^{\dagger}] = 1$ and is much smaller than the avarage values of creation and annihilation in macroscopically occupied ground-state and therefore, may be neglected. Within this approach, a spontaneous global symmetry break occur. In fact, the $U(1)$ symmetry is lost and consequently the particle number is not conserved. However, the hamiltonian could be reduced to its simplest form

$$\begin{aligned}\hat{H} &\approx \frac{gN_0^2}{2V} + \sum_{p\neq 0}\left(\frac{p^2}{2m} + \frac{2gN_0}{V}\right)\hat{a}_p^{\dagger}\hat{a}_p + \frac{gN_0}{2V}\sum_{p\neq 0}\left(\hat{a}_p^{\dagger}\hat{a}_{-p}^{\dagger} + \hat{a}_p\hat{a}_{-p}\right) \\ &= \frac{1}{2}gn^2 + \sum_{p\neq 0}\left(\frac{p^2}{2m} + ng\right)\hat{a}_p^{\dagger}\hat{a}_p + \frac{1}{2}\sum_{p\neq 0} ng\left(\hat{a}_p^{\dagger}\hat{a}_{-p}^{\dagger} + \hat{a}_p\hat{a}_{-p}\right).\end{aligned} \tag{1.35}$$

Here, $n = N/V$ stands for the total density of particles and the total number of particles N was taken as the sum of ground state particles N_0 and all the rest occupying excited states,

$$N = N_0 + \sum_{p\neq 0}\hat{a}_p^{\dagger}\hat{a}_p. \tag{1.36}$$

The Hamiltonian of Eq. (1.35) may be exactly diagonalized by means of a canonical transformation, where creation and annihilation particle operators are replaced by Bogoliubov quasiparticle operators $\hat{\alpha}_k^{\dagger}$ and $\hat{\alpha}_k$, defined by

$$\hat{\alpha}_k = f_k\hat{a}_k + g_k a_{-k}^{\dagger} \quad \text{and} \quad \hat{\alpha}_{-k}^{\dagger} = g_k\hat{a}_k + f_k a_{-k}^{\dagger}. \tag{1.37}$$

where f_k and g_k are real functions and must be such that preserve commutation relations originally obeyed by creation and annihilation operators, $[\hat{\alpha}_k, \hat{\alpha}_{-k}^{\dagger}] = f_k^2 - g_k^2 = 1$. $\hat{\alpha}_k$ and $\hat{\alpha}_{-k}^{\dagger}$ actually account for exchanging particles with the system ground-state and provide, under an unitary transformation, a proper basis where the Hamiltonian may be exactly diagonalized. The ground-state of such approximated Hamiltonian enabled Bogoliubov to describe the energy dispersion of quasi-particle excitations for weakly interacting set of bosonic particles, named Bogolons. The energy dispersion may be expressed as following

$$\epsilon(\vec{p}) = \sqrt{\frac{p^2}{2m}\left(\frac{p^2}{2m} + 2ng\right)}, \tag{1.38}$$

where, for small values of momentum $\vec{p}$, resembles the linear phonon dispersion spectrum, $\epsilon(\vec{p}) \approx \sqrt{ng/m}|\vec{p}|$. While failing in explaining excitations in superfluid phase of ^4He,

since it does not account for roton excitations expected for larger values of momentum $\vec{p}$ (FEYNMAN, 1998), the Bogoliubov approach still enabled to understand the superfluidity effects as well as its requirements from dispersion energy spectrum. Moreover, it is also rigorous enough to account for most part of BECs realized experimentally.

1.1.4.3 Landau superfluidity criterion

The linear phonon dispersion $\epsilon(\vec{p}) \approx \sqrt{ng/m}||\vec{p}||$ behavior derived in last section is crucial for the appearance of superfluidity phenomena in Bose-Einstein condensates (LANDAU, 1941). In fact, because a quantum system does not exchange energy continuously, excitations must be created in order to absorb any dissipated energy. The circumstances under which theses excitations become energetically favorable to emerge can be derived from energetic analysis of an amount of superfluid mass M flowing with velocity $\vec{v}$. The momentum and the energy carried out by the fluid is therefore, respectively given by $\vec{P} = M\vec{v}$ and $E = Mv^2/2$. However, if an excitation with momentum $\vec{p}$ and energy $\epsilon(\vec{p})$ is created, the updated quantities are $\vec{P'} = \vec{p} + M\vec{v}$ and $E' = \epsilon(\vec{p}) + \vec{p}\cdot\vec{v} + Mv^2/2$. Whether or not excitations become energetically propitious depends basically on the energy difference sign. In fact, excited states must have lower energy than the unexcited one, since there is no external energy source. Mathematically, it means that $E' - E < 0$, or

$$\epsilon(\vec{p}) + \vec{p}\cdot\vec{v} < 0. \tag{1.39}$$

In order to be satisfied, this condition requires that excitations must oppose to the fluid flow, $\vec{p}\cdot v < 0$, and then, the excited phase condition may be expressed as $||\vec{v}|| > \epsilon(\vec{p})/||\vec{p}||$. It is therefore natural to define a critical velocity, $v_c = (\epsilon(\vec{p})/||\vec{p}||)_{min}$, under which no excitation may be created and the fluid remains frictionless. Within Bogoliubov dispersion, a gas of weakly interacting bosons must remain in its superfluid phase only if

$$v_c \leq \sqrt{ng/m}. \tag{1.40}$$

Notice that, interaction plays a crucial role in superfluidity phenomena. In fact, despite the macroscopic occupation of zero momentum state, the ideal Bose gas, defined by $g = 0$, does not behave as a superfluid even at the absolute zero temperature, since the critical velocity vanishes for $g = 0$. Actually, despite the close relation in nature, Bose-Einstein condensation and superfluidity are distinct phenomena. Indeed, BEC accounts for macroscopic occupation of the ground-state, whereas superfluidity may be considered a pathology of the explicit form of excitation energy spectrum, which does not allow dissipations below a certain critical velocity. In fact, Landau explained superfluidity of liquid helium isotope ^4He without making any reference to BEC phenomenon. Therefore, despite both phenomena are closely related, there is no cause-effect relation between them.

1.1.4.4 Vortex states

Viscous free fluids respond to rotations in quite different ways when compared to conventional fluids (YARMCHUK; GORDON; PACKARD, 1979; MADISON et al., 2000a; ABO-SHAEER et al., 2001). In fact, a normal fluid in a rotating vessel rotates by means of friction between the vessel and fluid particles. The friction enables transferring the angular momentum to fluid, which rotates as a rigid body with velocity $v_s = \Omega r$. However, because superfluids experience no friction, it should not be possible, at least below v_c, to set it into rotation. In order to glimpse the irrotational superfluid property, it is handy to take a similar, but distinct way of following the Bogoliubov approach, by replacing the field operator $\hat{\psi}$ by a wave function ψ. This is supported by splitting the ground-state from the sum in Eq. (1.28) ,

$$\hat{\psi}(\vec{r}) = \psi(\vec{r}) + \delta\hat{\psi}(\vec{r}) = \sqrt{n_0}e^{i\theta} + \frac{1}{\sqrt{V}}\sum_{\vec{k}\neq 0} e^{\vec{k}\cdot\vec{r}}a_{\vec{k}}, \tag{1.41}$$

and then, neglecting lower order terms involving the fluctuation operator $\delta\hat{\psi}$ by means of mean field theory, that assigns a null contribution to these fluctuations $\delta\psi(\vec{r})$. Under this condition, the function $\psi(\vec{r}) = \sqrt{n(\vec{r})}e^{i\theta(\vec{r})}$ works as the system order parameter and shall vanish for $T > T_c$. Here, the modulus $\sqrt{n(\vec{r})}$ determines the condensate density, whereas the phase $\theta(\vec{r})$ may account for the superfluid dynamical properties. In fact, from the quantum mechanical expression for the current density, the superfluid velocity field is given by

$$\vec{v}_s = \frac{\hbar}{m}\vec{\nabla}\theta, \tag{1.42}$$

characterizing an irrotational potential flow, since $\vec{\nabla} \times \vec{v} = 0$ should always hold, independent of the specific form of the phase θ. This can also be expressed in terms of the null circulation Γ,

$$\Gamma = \oint_C \vec{v}_s \cdot d\vec{l} = \int \vec{\nabla} \times \vec{v}_s \cdot d\vec{S} = 0 \tag{1.43}$$

which holds as long as the surface enclosed by the path C is singly connected. Under stability velocity criteria, superfluids indeed do not experience rotations like normal fluid. However, out of stability conditions, as first pointed out by Onsager (ONSAGER, 1949; FEYNMAN, 1955), excitations in the form of quantized vortex might appear if the rotating vessel exceeds the critical velocity, fulfilling the quantization rule requirements of rotating quantum particles which must assign an integer number of wavelengths over the circular path. In this regime, particles described by a macroscopic wavefunction do not satisfy Eq. (1.43), which means that enclosed surfaces are not singly connected anymore and superfluidity is locally broken down by the emergence of singular regions. The difference between a rotating normal fluid and superfluid is illustrated in the sketch presented in Fig. 6

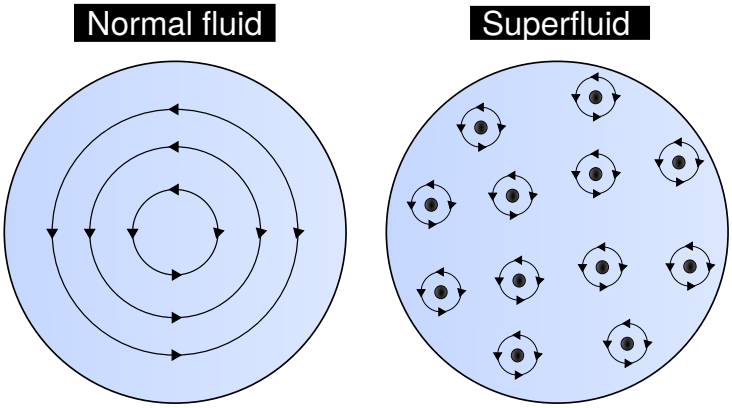

Figure 6 – Sketch of a normal fluid and a superfluid in a rotating vessel. Whereas normal fluids experiment a rigid-body rotation, superfluids rotate by forming arrays of quantized vortices.

Any rotational motion of superfluid is sustained by the emergence of quantized vortices, characterized by zero density at its center and circulation Γ described by

$$\Gamma = \oint_C \vec{v}_s \cdot d\vec{l} = \int \vec{\nabla} \times \vec{v}_s \cdot d\vec{S} = \frac{\hbar}{m} 2\pi l. \tag{1.44}$$

Quantized vortices are an unambiguous signature of superfluidity and therefore are crucial for its understanding. Due to its superfluid nature, Bose-Einstein condensates also respond to rotation by forming quantized vortices (MADISON et al., 2000a; ABO-SHAEER et al., 2001; MATTHEWS et al., 1999a). In general, these vortices have much larger dimensions than those observed in liquid helium and in superconductors, making Bose-Einstein condensates one of the best environments for their observation. There are several ways to set a condensate in a rotating frame. For instance, as long as the critical angular velocity is reached, angular momentum might be transfered to BEC by stiring it with laser beams or even by inducing slightly asymmetric external confining potentials into rotation. Within required conditions, multiple vortices may emerge absorbing the provided rotating energy. In the simplest single-component case, where particles interact via contact interaction, vortex might interact with each other repulsively, forming a triangular Abrikosov vortex lattice. The study of vortex states in weakly interacting bosons was one of the main motivations for the Gross-Pitaevskii equation development(GROSS, 1961; GROSS, 1963; PITAEVSKII, 1961). Since then, many efforts have been made to understand the vortex dynamics in different types of condensates. Among them, it is worth mentioning the asymptotic calculation of vortex-vortex interaction (ETO et al., 2011; AFTALION; MASON; WEI, 2012), as well as the achievement of Abrikosov and exotic vortex lattices in single and multi-component condensates(ABO-SHAEER et al., 2001; MATTHEWS et al., 1999a; KASAMATSU; TSUBOTA; UEDA, 2004; KUOPANPORTTI; HUHTAMÄKI; MÖTTÖNEN, 2012; ETO; NITTA, 2012; CIPRIANI; NITTA, 2013; LIU et al., 2014), respectively. The understanding of vortex lattices conformation represents

the main motivation for the work presented in this thesis and therefore shall be revisited carefully in the subsequent chapter.

1.1.4.5 The Gross-Pitaevskii equation

Under the mean-field theory approach, the Bogoliubov approximation enabled to investigate the dynamics of condensed system of particles. In fact, following the Heisenberg picture, where the dynamics of the operator $\hat{\psi}(\vec{r},t) = \exp(i\hat{H}t/\hbar)\hat{\psi}(\vec{r})\exp(-i\hat{H}t/\hbar)$ is governed by the equation

$$i\hbar\frac{\partial}{\partial t}\hat{\psi}(\vec{r},t) = \left[\hat{\psi}(\vec{r},t), \hat{H}\right], \tag{1.45}$$

and then, using the many-body Hamiltonian in Eq. (1.26), one may obtain the equation governing the time evolution of the annihilation operator.

$$i\hbar\frac{\partial}{\partial t}\hat{\psi}(\vec{r},t) = \left[\frac{\hbar^2}{2m}\nabla^2 + V_e(\vec{r}) + \int d^3r\hat{\psi}^\dagger(\vec{r}',t)V_i(\vec{r}-\vec{r}')\hat{\psi}(\vec{r},t)\right]\hat{\psi}(\vec{r},t). \tag{1.46}$$

Within the Bogoliubov approach limits, the assignment $\hat{\psi}(\vec{r},t) = \psi(\vec{r},t)$ and $\hat{\psi}^\dagger(\vec{r},t) = \psi^*(\vec{r},t)$ leads to the well-known time-dependent Gross-Pitaevskii equation (GPE), which was independently derived by E. P. Gross and L. P. Pitaevskii in 1961,

$$i\hbar\frac{\partial}{\partial t}\psi(\vec{r},t) = \left[\frac{\hbar^2}{2m}\nabla^2 + V_e(\vec{r}) + \int d^3r\psi^\dagger(\vec{r}',t)V_i(\vec{r}-\vec{r}')\psi(\vec{r},t)\right]\psi(\vec{r},t). \tag{1.47}$$

Because of the mean field approximation, this equation has a restricted range of validity. In fact, the GPE works properly for condensates at temperatures well below the critical temperature and with weak interactions between particles. Its first attribution was exploring emerging vortices in rotating weakly interacting Bose gases, where interactions were assumed to be essentially provided by the elastic, hard-sphere collisions between two atoms. Elastic colisions has short-range and isotropic character and may be described by

$$V_i(\vec{r}-\vec{r}') = g\delta(\vec{r}-\vec{r}'). \tag{1.48}$$

This greatly simplifies the GPE to a nonlinear time-dependent Schrodinger-like equation, which, in the rest frame becomes,

$$i\hbar\frac{\partial}{\partial t}\psi(\vec{r},t) = \left[\frac{\hbar^2}{2m}\nabla^2 + V_e(\vec{r}) + g|\psi(\vec{r},t)|^2\right]\psi(\vec{r},t). \tag{1.49}$$

This equation describes BECs in the dilute limit, where each atom feels the effect of its surrounding atoms via an effective potential energy proportional to the local density of the condensate. The s-wave scattering length should then be much smaller than the average distance between atoms and the number of atoms much larger than unity. As long as these two conditions are satisfied, Eq. (1.49) properly describes the condensed gas.

1.1.4.6 Time-independent GPE

Under the constraint of fixed number of particles, stationary solutions describing ground-state of BECs might also be achieved by variationally minimizing the expectation value of the free energy for non-isolated systems, $F = E - \mu N$, where $E(\Psi) = \langle \Psi_N | \hat{H} | \Psi_N \rangle$ is the system energy and μ stands for the chemical potential and might vary in order to keep the number of ground-state particles constant. Evaluating all Hamiltonian terms in Eq. (1.26) and then differentiating with respect to Ψ^*, the equilibrium configuration is provided by

$$\frac{\delta}{\delta \Psi^*} \langle \Psi_N | \hat{H} - \mu \hat{N} | \Psi_N \rangle = 0. \tag{1.50}$$

This procedure is similar to minimize the thermodynamic free energy

$$F[\Psi] = \int d\vec{r} \left[\frac{\hbar^2}{2m} |\nabla \Psi|^2 + (V_e(\vec{r}) - \mu) |\Psi|^2 + \frac{g}{2} |\Psi|^4 \right], \tag{1.51}$$

with respect to Ψ^* by means of Euler-Lagrange equation and yields to the GPE in its time-independent form,

$$\left[-\frac{\hbar^2}{2m} \nabla^2 + V_e(\vec{r}) - \mu + g |\psi(\vec{r})|^2 \right] \Psi(\vec{r}) = 0. \tag{1.52}$$

The time-independent GPE can also be achieved by directly substituing the Ansatz $\Psi(\vec{r}, t) = e^{-i\mu t} \Psi(\vec{r})$ into the time-dependent GPE, where $e^{-i\mu t}$ accounts for oscillations of the off-diagonal matrix elements $\langle N-1 | \hat{\psi}(\vec{r}, t) | N \rangle$ with frequencies of the order of $\mu \approx E(N) - E(N-1)$. In the thermodynamic limit, $N \to \infty$, the chemical potential thermodynamical definition, as the amount of energy to add a particle into the condensate is recovered, $\mu = \partial E / \partial N$. If the interaction is weakly enough, so that the non-linear quadratic term may be neglected, the Schrödinger equation is recovered and its solution depends only on the confining potential shape, V_e. In general, trapping potentials produced in BEC experiments are well approximated by harmonic potentials and, therefore, in the weakly interacting regime, the expected density distribution for an isotropic harmonic potential might be given by

$$n(\vec{r}) = N \left(\frac{m\omega}{\pi \hbar} \right)^{3/4} \exp \left(-\frac{m\omega}{2\hbar} r^2 \right). \tag{1.53}$$

This result, however, is not in good agreement with most observations done experimentally, where the atomic cloud is much larger than the predicted one. Actually, despite the diluteness, the interaction plays an important role in the atomic cloud shape and can not be neglected. In fact, under typical laboratory conditions, only the kinetic term associated with the curvature of particle density might be neglected. This regime is covered by the Thomas-Fermi approximation and express an opposite behavior of weakly interacting regime, where the kinetic term is an important contribution. In Thomas-Fermi regime, after straightfoward calculations, the density becomes

$$n(\vec{r}) = |\Psi|^2 = \frac{\mu - V_e(\vec{r})}{g}, \tag{1.54}$$

for $\mu > V_e$, otherwise it vanishes, where μ is obtained by normalizing $n(\vec{r})$ to the total number of particles N. Differently of the weakly interacting case, extension of the atomic cloud is well defined as long as the chemical potential is determined. In fact, spatial limits of the condensate are described by $V_e = \mu$, where, for isotropic harmonic traps, leads to

$$R^2 = \frac{2\mu}{m\omega^2}, \tag{1.55}$$

with

$$N = \frac{8\pi}{15}\left(\frac{2\mu}{m\omega^2}\right)^{3/2}\frac{\mu}{g}. \tag{1.56}$$

As we shall see further, the time-independent GPE provide a complete description of the vortex-vortex interaction and it turns out to be the main tool used in the present work. Usually, Eq. (1.52) is presented with the angular momentum contribution, which induce vortex formations. This may be achieved by expressing the functional $F[\Psi]$ in a rotating frame,

$$F[\Psi] = \int d\vec{r}\left[\frac{\hbar^2}{2m}|\nabla\Psi|^2 + \left(V_e(\vec{r}) - \mu\right)|\Psi|^2 + \frac{g}{2}|\Psi|^4 - \Omega\Psi^* L_z\Psi\right], \tag{1.57}$$

where Ω denotes the angular velocity and $L_z = (\vec{r}\times\vec{p})_z = -i\hbar(\vec{r}\times\vec{\nabla})$ represent the angular momentum operator in its spatial representation. However, in our approach, for reasons that we shall see later, this term is not considered.

1.1.4.7 GPE for two-component BECs

The Gross-Pitaevskii formalism can be straightforwardly extended in order to cover multi-component BECs by assuming the existence of multiple order parameters as well as their respective energetic contributions in the energy density functional. The extension, however, also depends on the interplay between particles of different condensates and, therefore, there is no general form of proceeding with it. Here, we are going to restrict ourselves to only two different types of inter-species interaction: the contact and internal coherent coupling, implemented by inducing an external driving field, which allows particles to move from one hyperfine spin state to another. Therefore, particles from different component may interact with each other either by contact interaction or by Rabi oscillations, which accounts for the interplay of atoms between different components (MATTHEWS et al., 1999b). Under these conditions, the extended formalism ends up with

$$\begin{aligned}\mathcal{E} = &\sum_{\alpha=1}^{N_c}\left\{\frac{\hbar^2}{2m_\alpha}|\nabla\Psi_\alpha|^2 + \frac{g_\alpha}{2}|\Psi_\alpha|^4 + V_\alpha^e|\Psi_\alpha|^2\right\} + \\ &\sum_{i}^{N_c}\sum_{j>i}^{N_c} g_{ij}|\Psi_i|^2|\Psi_j|^2 - w_{ij}\left(\Psi_i\Psi_j^* + \Psi_j\Psi_i^*\right).\end{aligned} \tag{1.58}$$

First and second terms of multi-component energy density functional account for intra-component contributions, which respectively includes the kinetic and contact interaction

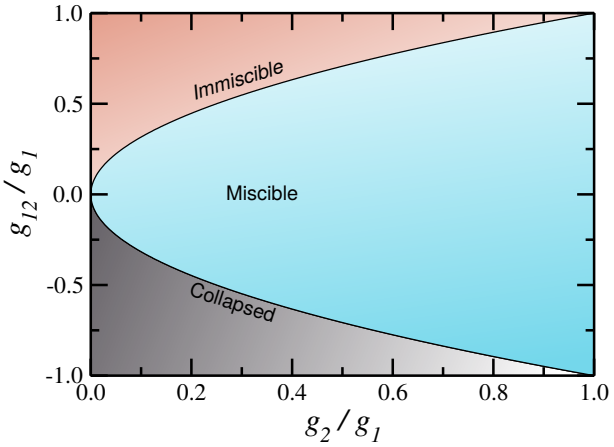

Figure 7 – Miscible and Imiscible conditions in the inter-particle interactions phase diagram.

energy. On the other hand, the remaining terms of the former functional stand for the inter-component couplings. In special, the last term can be easily understood as the sum of every possible contribution of removing a particle from one component and replace it in another one. Eventually, the condensate nature is fully defined by the set of parameters m_i, g_α, g_{ij} and w_{ij} and it is governed by (in the two-component case)

$$\begin{aligned}\mu_1\Psi_1(\vec{r}) = &\left[-\frac{\hbar^2}{2m_1}\nabla^2 + V_1(\vec{r}) + g_1|\Psi_1(\vec{r})|^2 + g_{12}|\Psi_2(\vec{r})|^2\right]\Psi_1(\vec{r}) \\ &- \omega_{12}\Psi_2(\vec{r}),\end{aligned} \tag{1.59a}$$

$$\begin{aligned}\mu_2\Psi_2(\vec{r}) = &\left[-\frac{\hbar^2}{2m_2}\nabla^2 + V_2(\vec{r}) + g_2|\Psi_2(\vec{r})|^2 + g_{12}|\Psi_1(\vec{r})|^2\right]\Psi_2(\vec{r}) \\ &- \omega_{12}\Psi_1(\vec{r}).\end{aligned} \tag{1.59b}$$

In absence of coherent coupling and considering an homogenous system confined by hard wall barriers, $V_\alpha(\vec{r}) = 0$ ($\alpha = 1, 2$), the immiscibility criterion can be annalitically derived for two-component BECs in the Thomas-Fermi regime. Under these circunstances, the governing equations become

$$g_1|\Psi_1(\vec{r})|^2 + g_{12}|\Psi_2(\vec{r})| = \mu_1, \tag{1.60a}$$

$$g_2|\Psi_2(\vec{r})|^2 + g_{12}|\Psi_1(\vec{r})| = \mu_2, \tag{1.60b}$$

Whether the condensates prefer to occupy the same region in space or not depends on the energy difference of both situations. Straightforward calculations show that such difference is given by

$$\Delta U = U_{mi} - U_{im} \propto g_{12} - \sqrt{g_1 g_2} \tag{1.61}$$

and, therefore the miscibility condition may be summarized in terms of coupling forces: $-\sqrt{g_1 g_2} < g_{12} < \sqrt{g_1 g_2}$. Otherwise, if $g_{12} > \sqrt{g_1 g_2}$, components remain segregated due

to the overcoming of mutual repulsion whereas, for $g_{12} < -\sqrt{g_1 g_2}$, the system becomes unstable and collapses as a consequence of the strong attraction between particles of different condensates. These three dinstinct situations are illustrated in Fig. 7

1.2 Introduction to superconductivity

Because the wavelike nature of matter is very difficult to be demonstrated outside the microscopic limit, whenever a quantum property is observed on a macroscopic scale, a great effort is made to explain it (COHEN-TANNOUDJI; DIU; LALOE, 1991). This was not different for the resistanceless state of matter discovered by Kamerlingh Onnes in 1908 (KAMERLINGH-ONNES, 1911), where charge carriers were found to flow through some materials without experiencing any electrical resistance. In fact, the non-triviality of quantum effects exhibited by the so-called superconducting materials has puzzled the greatest minds of the past century and still does nowadays. No wonder, superconductivity is also one of the topics of physics with the highest number of Nobel prizes winners and still remains as one of the most promising research subjects of science. Despite superconductivity discovery has preceded the wave formalism description of matter, promising applications boosted early researches in the field. In fact, in a society extremely dependent on electricity, applications were easily devised by the scientists of that time.

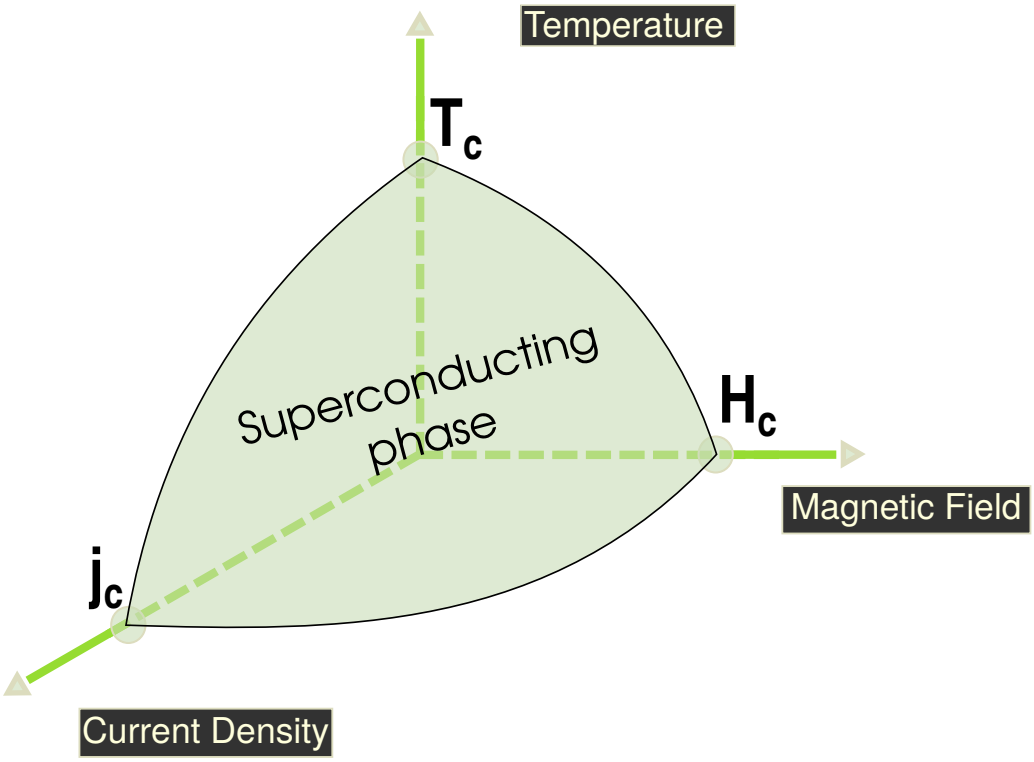

Figure 8 – Sketch of the phase diagram of an arbitrary superconducting material. The superconducting phase is delimited by the critical values of current $\vec{j}$, magnetic field $\vec{H}$ and temperature T. From a practical point of view, these critical values are in general very small, making it difficult for commercial applications.

Unfortunately, over a hundred years have passed and the vast majority of idealized applications still remains at the horizon of superconductivity field. Such applications are, nowadays, commercially unfeasible, mainly due to the high manufacturing costs associated with the fragility of superconducting state, which requires extremely low temperatures and can be easily destroyed when currents or magnetic fields exceed their respective critical values, see Fig. 8. Hopefully, this scenario has been changing with the vast knowledge acquired over all those years, where great improvements on critical parameters have been reported and new materials with higher critical temperatures have been discovered. Yet so far, despite the longstanding discovery and immeasurable efforts, the superconducting state is not fully characterized nor understood. Indeed, the original microscopic theory of superconductivity (BARDEEN; COOPER; SCHRIEFFER, 1957), which proposes an electronic condensation as the main mechanism behind this novel and strange phenomenon, was developed to model an isotropic single superconducting energy band, accounting only for the most basic properties of homogeneous bulk superconducting materials (TANAKA, 2015) and, despite having undergone several refinements (TANAKA, 2015; SUHL; MATTHIAS; WALKER, 1959; ORLOVA et al., 2013), it was not able to explain the high critical temperature exhibited in the recent discovered class of superconducting materials, denominated High-T_c superconductors (BEDNORZ; MÜLLER, 1986).

Moreover, the discovery of multi-band superconducting materials (BOUQUET et al., 2001; SZABÓ et al., 2001; SEYFARTH et al., 2005; TEAGUE et al., 2011; KIM et al., 2011) has opened up even more the superconductivity field, making bigger the gap between experimental achievements and the current theoretical knowledge. In fact, such superconductors are far from being just a trivial extension of a single band superconductor case and even when the extensibility of the microscopic formalism covers the superconducting phase of the multi-band superconducting materials, there are still many relevant theoretical details to be addressed concerning macroscopic features of these superconductors. No wonder, multiband superconductor properties have been widely investigated in the last few years (CHAVES et al., 2011a; YANAGISAWA et al., 2012; SILVA et al., 2015; VAGOV et al., 2016). Actually, even in the simplest homogeneous single-band bulk superconductor case, there are several features not well described yet, such as vortex inner structure and their role in vortex-vortex interaction. In fact, vortex profiles and their magnetic distribution are only asymptotically known under the very restricted regime of London's approach(TINKHAM, 1975). For instance, it has been recently realized that it is possible to extract, from the inner structure of vortices, signatures of phase transition between different single-gap superconducting types (WANG, 2015) and, despite it may seem fundamental enough to be presented in textbooks, experimental techniques with higher resolutions capable to describe the inner structure of such vortices have been constantly reported until nowadays (SUDEROW et al., 2014).

Current efforts also involve many other facets, in particular, the handling of the quantum confinement through the sample size reduction have proven to be of great commercial and technological relevance, leading to appreciable increases of critical currents and fields (TOXEN, 1962; TINKHAM, 1963; CHAUDHARI, 1966; FETTER; HOHENBERG, 1967; ONORI; ROGANI, 1980; SCOTTO; PESCH, 1991; BRANDT; INDENBOM; FORKL, 1993; POZA et al., 1998; BERDIYOROV; MILOŠEVIĆ; PEETERS, 2006; SILHANEK et al., 2007; POSEN et al., 2015). This boosted recent researches on superconducting nanostructures and films. In special, superconducting films are observed to exhibit a much more rich phase diagram of vortex lattice conformations than in bulk samples and therefore, because it lies in the heart of current dissipation, a great effort has been made to characterize and control these vortex states (TINKHAM, 1963; FETTER; HOHENBERG, 1967; LASHER, 1967; KREMEN et al., 2016) as well as understand their dynamics (PEARL, 1964; LUNDQVIST et al., 1999; HILLMER et al., 1996; SENAPATI et al., 2006; GUTIERREZ et al., 2009; CUCOLO et al., 2012; SILVA et al., 2016).

1.2.1 Experimental background

Before the pioneering refrigeration techniques developed by Kamerlingh Onnes in 1908, the ideas concerning the properties of matter under extremely low temperatures were only speculative. At that time, physicists already knew that resistance generally dropped as a sample was cooled, but the mechanism behind electric conduction was poorly understood and very little was known about the behavior of conductors near the absolute zero (BUCKEL; KLEINER, 2008). After the unsuccessful attempt to find the solidification point of helium, the usage of liquid helium as a cryogenic fluid became quite convenient to investigate properties of matter near the absolute zero. Onnes devoted subsequent years of research developing techniques for storage and manipulation of liquid helium. These techniques would enable him to answer one of the still opened questions at that time concerning the electrical resistance of matter at 0 K. First experiments were carried out with gold and platinum and indicated the existence of a residual resistance, as proposed by Matthiesen in 1864 (BUCKEL; KLEINER, 2008). However, the residual resistance was then proved to be only a consequence of material impurities and not an intrinsic property of the matter, suggesting that extremely pure materials would present a measurably negligible resistance close to 0 K. In order to test this hypothesis, Onnes used mercury samples, the purest metal that he could obtain at that time. Surprisingly, the experiment outcome was quite different from the expected. In fact, instead of decreasing smoothly, the resistance dropped abruptly to zero just below the temperature of 4.2 K, as illustrated in Fig. 9 (KAMERLINGH-ONNES, 1911). Soon after the discovery of the resistanceless state of matter, other metals and compounds were found to share this same properties with mercury, however, for different temperatures, which led to the definition of a critical temperature T_c, characteristic of the material.

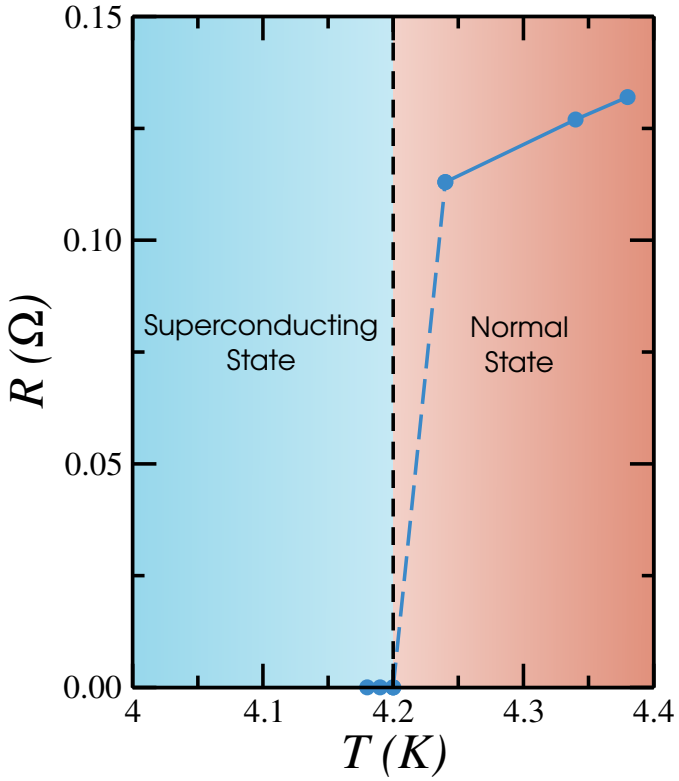

Figure 9 – The electrical resistance of mercury as a function of temperature. Here, the white circles represent the experimental measurements of the mercury resistance, whereas the red and blue backgrounds denote the normal and superconducting states respectively. This figure was made by the author, based on the result presented in Ref. (KAMERLINGH-ONNES, 1911).

The sudden disappearance of electrical resistance is a signature and the first hallmark of a transformation into a novel state, called superconductivity. In this state, an electric current could flow through the sample without experiencing any energy dissipation. In fact, all attempts to find at least small signals of electric resistance were frustrated, even with the high-resolution equipments present nowadays (ONNES; TUYN, 1923; SCHMIDT; MÜLLER; USTINOV, 1997). Unfortunately, the resistanceless state can also be destroyed by the application of a sufficiently strong magnetic field, as reported by Onnes soon after his discovery (LONDON, 1950). The upper field value where superconductivity remains sustained also depends on the material and is called the critical field H_c of the material. It was empirically found a parabolic dependence between the critical field and the corresponding critical temperature (TINKHAM, 1975; LONDON, 1950),

$$H_c(T) \approx H_c(0)\left[1 - \left(\frac{T}{T_c}\right)^2\right]. \tag{1.62}$$

A scheme of $H \times T$ phase diagram is illustrated in Fig. 10. The blue background represents the superconducting regime, whereas the red one stands for the normal state.

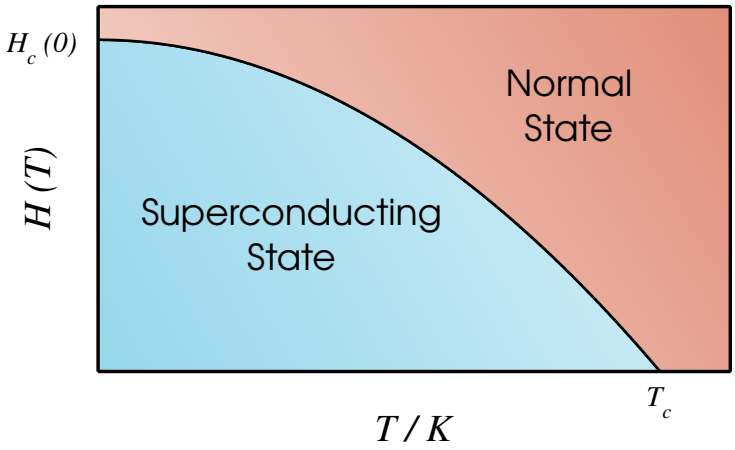

Figure 10 – A sketch of $H \times T$ diagram. The blue background represents the superconducting regime, wheres the red stands for the normal state.

1.2.1.1 Meissner Effect

At the time of superconductivity discovery, the basic concepts of quantum mechanics were not still developed nor understood. Therefore, it was not surprising that the first description have been based on the classical electromagnetism formalism (DEAVER; RUVALDS; DIVISION, 1983). In fact, the first natural proposal was to treat superconductors as perfect conductors, by assuming an infinite conductivity, $\sigma \to \infty$, which by Ohm's law would lead to a vanishing electric field inside the superconductor, $\vec{E} \to 0$. As a consequence of Maxwell's induction law, temporal variations of the magnetic field could also not occur inside a superconducting sample, $\dot{\vec{B}} = 0$, and the state of a superconductor should depend on its pre-history, as illustrated in Fig 11.

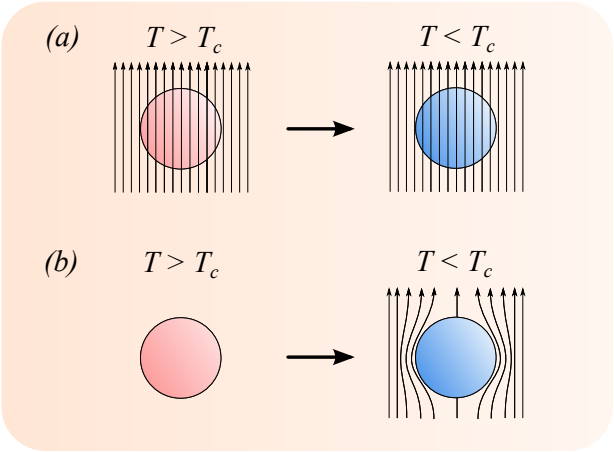

Figure 11 – The expected experimental outcome from the perfect conductance theory: (a) The superconducting material is firstly subjected to an external magnetic field and then cooled down below its critical temperature, "freezing" the magnetic field inside the sample; and (b) The material is first cooled down below T_c and then, an external magnetic field is applied. Since $\dot{\vec{B}} = 0$, the magnetic field inside the sample should remains null.

With the support of some experimental evidences (LONDON, 1950), the theory of perfect conductance was well accepted for a long time, however, from the thermodynamical point of view, it was always doubtful. In fact, the existence of multiple states for the same imposed external conditions characterizes a non-equilibrium state that could hardly be sustained by electrons even in the absence of electrical resistance. Moreover, the perfect conductor theory was not able to explain the existence of the critical magnetic field H_c. Even so, the need of a new theory emerged only in 1933, after the Meissner and Oschsenfeld milestone experiment (MEISSNER; OCHSENFELD, 1933), which showed that, regardless of the pre-existing state, the field inside the sample is always null whenever the superconducting state is achieved, exhibiting also perfect diamagnetism properties. Because perfect conductivity and diamagnetism could not coexist simultaneously, the Meissner effect uniquely characterizes superconductors and for this reason it was considered the second hallmark of superconductivity theory.

Differently from zero resistivity effect, Meissner's effect led to the recognition of superconducting state as an equilibrium state and allowed the development of its thermodynamical description, where the normal/superconductor transition was classified as a transition of the second kind (GORTER; CASIMIR, 1934). Within such description, the annihilation of superconductivity due to an external applied field $H = H_c$ could be understood in terms of the free energy difference between the normal and superconducting phases at zero field, also called condensation energy $f_{n0} - f_{s0}$. The energy cost of holding the field outside the sample should be equal to the condensation energy

$$f_{n0} - f_{s0} = \frac{H_c^2}{8\pi}. \tag{1.63}$$

In fact, at the critical field, normal and superconducting phases share equal thermodynamical potentials and therefore are allowed to coexist.

The Meissner's effect was soon found out to emerge from the appearance of screening currents flowing around the edges of a superconducting sample. These screening currents would suppress the applied field from inner region of superconductors by producing a field with equal intensity and opposite direction and could be well described by Maxwell's equation in a magnetic medium, where the Meissner's effect could be characterized by a magnetic material with magnetic susceptibility $\chi = -1$ and magnetization $\vec{M} = -\vec{H}$. However, the origin of such currents remained unexplained until London's description of superconductivity, which we shall see further.

1.2.1.2 Type-I and Type-II superconductivity

Subsequent experiments carried out by Rjabinin and Schubnikow revealed that superconductors should be distinguished into two different classes according to its response to an applied magnetic field (RJABININ; SHUBNIKOW, 1935). If fact, all

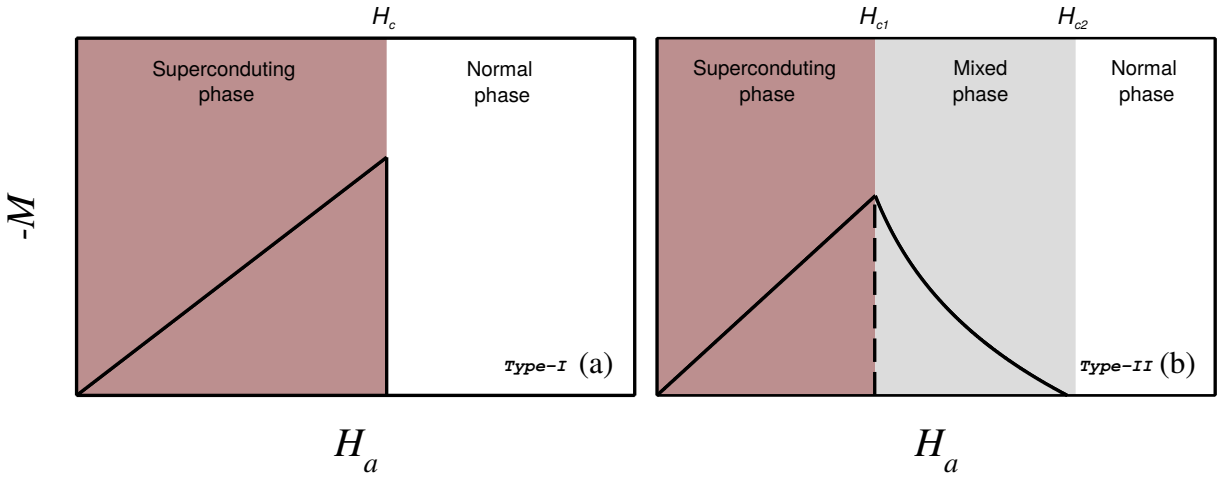

Figure 12 – Magnetization as a function of the applied field for: (a) a type-I superconductor and (b) a type-II superconductor.

superconducting materials share perfect diamagnetism effect as long as the applied field does not exceed a certain critical value, however, the superconducting phase may be suppressed in two different ways, depending on the material. In type-I materials, Fig. 12 (a), the magnetization falls to zero abruptly whenever the thermodynamical critical field H_c is achieved, (ii) whereas in type-II materials, Fig. 12 (b), the Meissner effect is suppressed gradually until the normal phase is recovered. This result led to the definition of two new critical fields, named the lower and the upper critical fields, respectively denoted by H_{c1} and H_{c2}. Below H_{c1}, a type-II superconductor exhibits perfect diamagnetism, fully expelling the magnetic field from its inner region. However, as the applied field H_a increases, the magnetization decays gradually until vanish at the upper critical field $H_a = H_{c2}$. At this point, superconductivity effects are fully suppressed and the normal phase is recovered. This behavior clearly contrast with type-I superconductors, where the ability to expel field lines is lost abruptly at the thermodynamical critical field. Nevertheless, the mechanism behind the nature of this segregation remained misunderstood for many years, until Abrikosov's remarkable work, which, within the Ginzburg-Landau formalism, predicted the existence of a mixed phase characterized by the emergence of quantized vortices in type-II superconductors.

1.2.2 London's description

A new theory encompassing both perfect conductivity and diamagnetism phenomena was then required. After repeated frustrations in attempting to explain it through the classical formalism, the quantum nature of the phenomenon became evident. Based on Bose-Einstein condensation theory and ignoring the fermionic nature of electrons, Fritz London assumed a condensation of charge carriers inside the superconducting material, describing them with a single uniform wave-function (LONDON, 1938; LONDON, 1950; LONDON; LONDON, 1935; LONDON, 1937; LONDON, 1948). Without the magnetic

field, electrons in a bulk superconductor should then be represented by the free-particle wave-function $\Psi(\vec{r}) = e^{i\vec{k}\cdot\vec{r}}$, where the wave vector $\vec{k}$ is defined by $\hbar\vec{k} = \vec{p} = m\vec{v_s}$. On the other hand, if an external magnetic field is applied, the wave-function phase $\phi(\vec{r})$ is a much more complex function of $\vec{r}$ and obeys

$$\hbar\vec{\nabla}\phi(\vec{r}) = \vec{p} = m\vec{v_s} + q\vec{A}. \tag{1.64}$$

Integrating through an arbitrary closed path C inside the superconducting sample, the left side of Eq. (1.64) vanishes and the Schorödinger equation becomes

$$\oint_C \left(m\vec{v_s} + q\vec{A}\right) d\vec{l} = 0. \tag{1.65}$$

Using Stokes theorem, the magnetic contribution can be transformed into a surface integral of vector potential curl $\vec{H} = \vec{\nabla} \times \vec{A}$, whereas the velocity $\vec{v_s}$ can be written in terms of the density current, $\vec{v_s} = \vec{j_s}/qn_s$. Here, n_s is the density of charge carriers and $q = -e$ the electric charge. The consequences of electric condensation are then summarized by the following equation,

$$q\int_S \vec{H}\cdot d\vec{S} = -\frac{m}{qn_s}\oint_C \vec{j_s}\cdot d\vec{l}, \tag{1.66}$$

or, by its local form,

$$\vec{\nabla}\times\vec{j_s} = -\frac{q^2 n_s}{m}\vec{H}. \tag{1.67}$$

In contrast to the classical electrodynamic theory, Eq. (1.67) predicts a circulating and superficial supercurrent flow as a result of an external magnetic field application, shielding the inner region of the superconducting sample as predicted by Meissner's effect. Together with Maxwell's equation $\vec{\nabla}\times\vec{H} = 4\pi\vec{j_s}/c$ and the Gauss's law for magnetism $\vec{\nabla}\cdot\vec{H} = 0$, the magnetic field and the density current might be fully determined under stationary conditions,

$$\nabla^2\vec{H} - \frac{1}{\lambda_L^2}\vec{H} = 0, \quad \text{where} \quad \lambda_L = \sqrt{\frac{mc^2}{4\pi e^2 n_s}}. \tag{1.68}$$

Although expelled, the applied magnetic field might penetrate a superconducting sample of arbitrary shape to a depth of the order of λ_L, a characteristic length scale of the superconducting material named London penetration depth. In fact, the solution of Eq. (1.68) for a slab is an exponentially decaying function, $\vec{H} \propto \exp(-x/\lambda_L)$, which means that the magnetic field is screened only from the inner region of the sample. However, at least from qualitative point of view, this result is still in agreement with the Meissner's effect, since the penetration depth of metallic compounds is of the order of 10^{-5} cm. On the other hand, the perfect conductivity effect would be explained by the second London's equation, which describes the superconductor response to an external electric field $\vec{E}$. Without rigor, this equation could be derived from the free electron-gas model, where $\vec{v_s} = \vec{j_s}/qn_s$. In this approach, the 2^{nd} Newton's law states that

$$\frac{\partial\vec{j_s}}{\partial t} = \frac{n_s e^2}{m}\vec{E} = \frac{1}{\lambda_L^2}\vec{E}. \tag{1.69}$$

The presence of an external electric field induce temporal variations on current density, accelerating the superconducting electrons instead of only sustaining their velocities, as expected in a standard conductor. The London approach may also be summarized into the superconductor energy, expressed as the sum of superconducting electrons kinetic energy with the energetic cost of sustaining the magnetic field outside the sample

$$E = \frac{1}{8\pi}\int_V \left[\lambda^2\left(\vec{\nabla}\times\vec{H}\right) + H^2\right]. \tag{1.70}$$

Because those superconducting effects should disappear for $T > T_c$, a dependence between the penetration depth and temperature is expected. In fact, it was empirically estimated that,

$$\lambda_L(T) \approx \frac{\lambda_L(0)}{\sqrt{1-(T/T_c)^4}}. \tag{1.71}$$

Therefore, reducing the temperature leads to a shorter penetration depth, enhancing the superconducting properties from the experimental point of view. Exactly for $T = T_c$, the penetration depth diverges and the normal properties of the material would be recovered. Despite the successful explanation of Meissner's effect, the London theory was still considered incomplete and unsatisfactory. Supported by a dubious postulate that would break the well accepted Pauli's exclusion principle, the London theory was not able to estimate the surface tension between normal and superconducting interfaces or even predict the existence of a critical field H_c. Moreover, as we shall see further, it is also supposed to be inaccurate in describing the internal structure of vortex states in non-extreme Type-2 superconductors, since vortices are treated as point-like objects.

1.2.2.1 Flux quantization

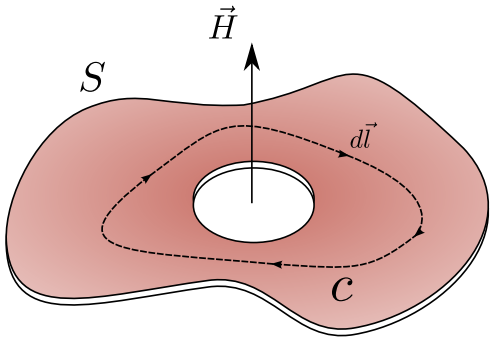

Figure 13 – A singly connected surface S under and externally applied magnetic field $\vec{H}$.

Still, stressing the quantum nature of superconductivity, London took another important step towards the understanding of superconductivity. Within his theory, he was able to predict the flux quantization of magnetic field almost fifteen years after the first formulation of his theory (LONDON, 1950). In fact, because superconducting electrons should be described by a single uniform quantum mechanical wave function, they also

should obey Bohr-Sommerfeld quantization rule. Therefore, for a multiply connected superconductor, illustrated in Fig. 13 , Eq. 1.66 should be rewritten as

$$\oint \oint_S \vec{H} \cdot d\vec{S} + c\Lambda \oint_C \vec{j_s} \cdot d\vec{l} = \frac{nhc}{e}, \tag{1.72}$$

where the left side, named fluxoid, is quantized in units of $\phi_{0L} = hc/e$. However, to better explore the consequences of Bohr-Sommerfeld rule on superconductors, it is worth to apply Eq. 1.72 to a specific geometry, where the path and surface integrals might be evaluated under symmetry arguments. For instance, one may consider a hollow cylinder sheet with radius R subjected to an externally applied H parallel to its axial direction and obtain according to London's prediction,

$$j_s = \frac{\phi_{0L}}{c\Lambda 2\pi R}\left(n - \frac{\pi R^2 H}{\phi_{0L}}\right) \tag{1.73}$$

From the angular current density j_s, the kinetic energy associated to superconducting electrons can be extracted and the magnetic flux quantization derived,

$$K_s = \frac{1}{2}\Lambda j_s^2 = \frac{\phi_{0L}^2}{8c^2\Lambda\pi^2 R^2}\left(n - \frac{\pi R^2 H}{\phi_{0L}}\right)^2 \tag{1.74}$$

In fact, from Fig. 14, where the energy is plotted as a function of magnetic flux $\phi = \pi R^2 H$, the system is indeed expected to find its equilibrium state for discrete values of magnetic flux, ϕ/ϕ_{0L}=n. As a consequence, in multiply connected superconductors, quantities such as critical temperature and resistivity are also expected to oscillate with the applied field H. This enabled experimental confirmations of superconductivity as a macroscopic quantum phenomenon (DEAVER; FAIRBANK, 1961; DOLL; NÄBAUER, 1961; PARKS, 1964). Indeed, almost fifteen years after London's prediction, oscillations in resistivity of a hollow cylinder near the superconducting transition point were measured as a function of the applied field (PARKS, 1964). However, these oscillations were found to exhibit a period $\phi_0 = hc/2e$ instead of the predicted by London $\phi_{0L} = hc/e$. As we shall see further, this is a consequence of the pairing mechanism behind the electronic condensation proposed in the microscopic theory of superconductivity.

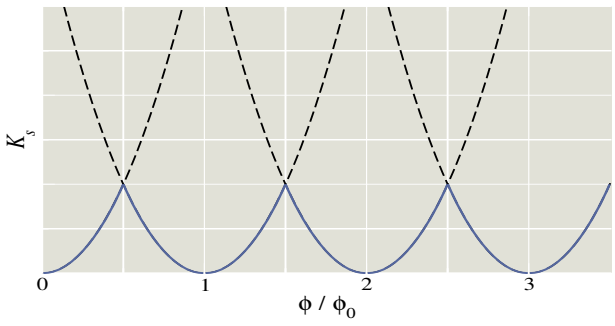

Figure 14 – Kinetic energy of superconducting electrons in a hollow cylinder as a function of magnetic flux.

1.2.3 The Ginzburg-Landau theory

The weaknesses of London's theory and the recognition of the superconductor transition as a transition of the second kind led the physicists Ginzburg and Landau to extend the pre-existing Landau's theory of phase transitions to superconductors, combining it with a Schrödinger-like wave function $\Psi(\vec{r},t)$ (GINZBURG; LANDAU, 1950; GINZBURG, 1955). In this thermodinamical approach, a complex pseudowave-function Ψ describing the superconducting electrons was proposed as the system order parameter, assuming non-zero values for $T < T_c$ (ordered or superconducting phase) and vanishing at $T > T_c$(disordered or normal phase). The order parameter Ψ is uniquely defined except for a phase factor, which might preserve the invariance of physical properties. This suggested a correlation with the quantum nature of superconductivity, where the order parameter could be associated with the local density of superconducting electrons by $|\Psi|^2 \propto n_s$. At that time, despite the belief of an electronic condensation behind the superconductivity phenomena, the quantum mechanical connection between the order parameter Ψ and the observable quantities was not well established, so an arbitrary normalization equalizing $|\Psi|^2$ to n_s was proposed (GINZBURG, 2008).

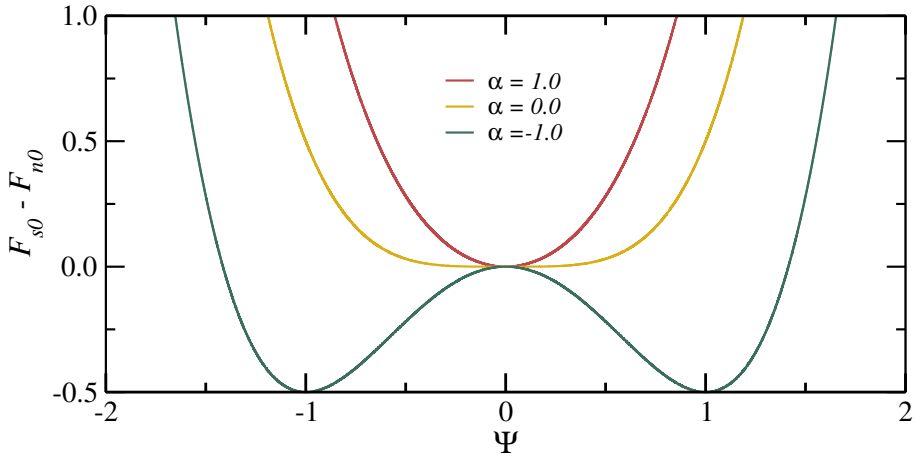

Figure 15 – The free energy density difference between superconducting and normal states $F_{s0} - F_{n0}$ as a function of Ψ for $\beta = 1.0$ and three different values of α: -1.0 (blue triangles), 0.0 (yellow squares) and 1.0 (red circles).

According to Landau's picture, near the transition point T_c, the energy difference between the normal and superconducting phases could be expanded in powers of the order parameter $n_s = |\Psi(\vec{r},t)|^2$. Therefore, in the absence of an external magnetic field and neglecting spatial variations of the order parameter, the free energy density of a superconductor could be expressed as

$$F_{s0} = F_{n0} + \alpha|\Psi|^2 + \frac{\beta}{2}|\Psi|^4. \tag{1.75}$$

The free energy density difference between the superconducting and normal states might be distinguished in three different manners depending on the signal of the coefficient

α. In Fig. 15, regardless of the phase factor, these forms are illustrated by assuming $\beta = 1.0$ and different values of α: -1.0 (blue triangles), 0.0 (yellow squares) and 1.0 (red circles). For $\alpha > 0$, the energy density difference function has only one minimum at the equilibrium value $|\Psi| = 0$, characterizing the higher energy disordered state, where $T > T_c$. For $\alpha < 0$, there exists two minima, where the superconducting phase become energetically favorable, and that corresponds for the low temperature case $T < T_c$. Theses two regimes are separated by the case $\alpha = 0$, which corresponds to the transition point $T = Tc$. At this point, the energy difference become flat around the minimum, allowing thermal oscillations to become evident. It is worth mentioning that, these profiles are valid whenever the phase of the superconductor is zero, which is the case for, for example, one dimension superconductors. However, whenever the phase becomes important, the free energy density becomes a surface that may be achieved under the rotation of former profiles, so that negative values of α are, in fact, described by the Mexican Hat surface. Even so, these minimum conditions can be mathematically achieved by differentiating the free energy density F_{s0} with respect to the order parameter $|\Psi|^2$. In fact, in equilibrium, the following conditions must be satisfied

$$\frac{\partial F_{s0}}{\partial |\Psi|^2} = 0, \qquad \frac{\partial^2 F_{s0}}{\partial^2 |\Psi|^2} > 0. \tag{1.76}$$

The last condition constrains β to be positive, whereas the first condition determines the equilibrium values of the order parameter $\psi_0 = \sqrt{-\alpha/\beta}$. Within the original assumption of Landau's picture of phase transtions, it becomes natural to assume α to be temperature-dependent in order to achieve the ordered ($|\Psi|^2$=1) and disordered ($|\Psi|^2$=0) conditions for the order parameter. Assuming a linear dependence, $\alpha \propto (T - T_c)$, in the neighbourhood of T_c, the equilibrium point could then be characterized by

$$|\Psi|^2 = -\frac{\alpha}{\beta} = -\frac{T - T_c}{\beta_c}\left(\frac{d\alpha}{dT}\right)_c \tag{1.77}$$

and

$$F_{s0} - F_{n0} = -\frac{\alpha^2}{2\beta} = -\frac{(T - T_c)^2}{2\beta_c}\left(\frac{d\alpha}{dT}\right)_c^2. \tag{1.78}$$

In fact, the linear choice for the temperature dependence of α is in agreement with the thermodynamic description of the critical field, $f_{s0} - f_{n0} = -H_c^2/8\pi$, since it recovers the empirically found expression for H_c as a function of the temperature T. It also suggested a correlation between the order parameter $|\Psi|^2$ and the density of superconducting electrons n_s, since the temperature dependence of the order parameter, $|\Psi|^2 \propto (1 - T/T_c)$, resembles the n_s dependence on temperature empirically found through London's theory. Therefore, the expansion in powers of $|\Psi|^2$ provides the theory background to describe the normal/superconducting phase transition with respect to the system temperature T. However, it accounts only for the most ideal situation, where the

superconducting phase is uniform and no applied fields are considered, being not able to explain by itself the odd electrodynamic properties exhibited by superconductors.

In order to fullfill the theory, Ginzburg extended the formalism in order to account for possible fluctuations in the complex order parameter $\Psi(\vec{r})$. At least for small fluctuations, the energetic contribution would be well described by the lowest order term in $|\nabla\Psi|^2$ allowed by symmetry of series expansion: $\epsilon_s^k|\nabla\Psi|^2$. An anallogy with the quantum mechanical definition of the kinetic energy, suggested fluctuations to be a consequence of the superconducting electrons flow. Therefore, according to Ginzburg, the energetic contribution associated with these local variations of the order parameter could be well described by,

$$\epsilon_s^k|\vec{\nabla}\Psi|^2 = \frac{1}{2m}|-i\hbar\vec{\nabla}\Psi|^2 = \frac{\hbar^2}{2m}|\vec{\nabla}\Psi|^2, \tag{1.79}$$

where $\hbar = 1.05 \times 10^{-27}\ erg\ s$ and m represents the effective mass of superconducting electrons. In the presence of a magnetic field, however, this term has to be corrected in order to account for the interaction between the magnetic field and the current induced by the spatial variance of Ψ. This was provided by considering the gauge invariant quantum mechanical expression for the momentum operator $\hat{P} = -i\hbar\vec{\nabla} - e\vec{A}/c$, where $\vec{A}$ is the vector potential, defined by $\vec{H} = \vec{\nabla} \times \vec{A}$, and e stands for the effective superconducting electric charge. Hence, in the Ginzburg-Landau picture of superconductivity, the general expression of free energy density near T_c may be expressed as following

$$F_{sH} - F_{nH} = \frac{1}{2m}\left|\left(-i\hbar\vec{\nabla} - \frac{e}{c}\vec{A}\right)\Psi\right|^2 + \alpha|\Psi|^2 + \frac{\beta}{2}|\Psi|^4 + \frac{H^2}{8\pi}, \tag{1.80}$$

where the last term stands for the energetic cost of sustaining the magnetic field $\vec{H}$, as previously proposed in Gorter and Casimir's thermodynamical description. Again, the problem is reduced to find the minimum energy condition, where the system should find its equilibrium state. Therefore, the stationary conformations of the order parameter and magnetic field might be extracted by minimizing the total energy with respect to Ψ^* and $\vec{A}$, which leads to the set of well known coupled Ginzburg-Landau equations (see the Appendix for a detailed derivation)

$$\alpha\Psi + \beta|\Psi|^2\Psi + \frac{1}{2m}\left(-i\hbar\vec{\nabla} - \frac{e}{c}\vec{A}\right)^2\Psi = 0, \tag{1.81a}$$

$$\frac{c}{4\pi}\vec{\nabla}\times\vec{\nabla}\times\vec{A} = \frac{i\hbar e}{2m}\left(\Psi^*\vec{\nabla}\Psi - \Psi\vec{\nabla}\Psi^*\right) - \frac{e^2}{mc}|\Psi|^2\vec{A}. \tag{1.81b}$$

Except for a nonlinear term, Eq. (1.81a) has the same form of the Schrödinger equation for a free-particle under an externally applied field $\vec{H} = \vec{\nabla} \times \vec{A}$, highlighting the quantum character of the Ginzburg-Landau description. In turn, the second Ginzburg-Landau equation, Eq. (1.81b), is nothing less than the quantum form of the circuital Ampere's law, where the right-hand side of the equality contains the expression for the

superconducting current density j_s. Indeed, the supercurrent has exactly the same form of the quantum mechanical Noether's current expression for particles with mass m and charge $q = -e$. This set of coupled equations, within the proper boundary conditions, would then be able to describe the electrodynamic properties of superconductors and, despite they were meant to describe only the transition regime, near $T \approx Tc$, the Ginzburg-Landau equations have proven to be valid even deep in the superconducting phase, for instance, see Ref. (DEO et al., 1997). In fact, over the years, extra energetic contributions have been suggested in order to promote a better description far from the transition point. However, the obtained corrections are, in general, very small and might be disregarded in most of the cases. This makes the Ginzburg-Landau formalism a powerful tool to investigate the macroscopic features of superconductors. However, before going into further details concerning the descriptive advantages and limitations of the theory, let us first address some aspects obeyed by scalar Ψ and vectorial $\vec{A}$ fields near the system boundaries, restricting them to the set of the physical solutions.

1.2.3.1 Boundary conditions

The first constraint lies in the argument that there should be no electronic exchange between the superconductor and vacuum or insulator medium, so the normal component of current density should vanish at system's interfaces. This boundary condition is also achieved from the variational principle. In fact, taking the variation with respect to Ψ^*, besides the Ginzburg-Landau equations, the following equality must be satisfied (GINZBURG, 2008)

$$\oint_S \delta\Psi^* \left(-i\hbar\vec{\nabla} - \frac{e}{c}\vec{A}\right) \Psi \cdot \hat{n} dS = 0, \tag{1.82}$$

where $\hat{n}$ is a unit vector normal to the interface and S is a surface which encloses the sample. Because of the arbitrariness of both the variational element $\delta\Psi^*$ and surface S, the last equation may be satisfied under two different conditions: (i) for an infinite system, where integrand contributions of opposite sides of unity cell cancels out each other vanishing the total surface integral, or (ii) when the normal component of the supercurrent is null at the boundaries, which leads to the standard boundary condition

$$\left(-i\hbar\vec{\nabla} - \frac{e}{c}\vec{A}\right) \Psi \cdot \hat{n} = 0. \tag{1.83}$$

Despite derived from the variational principle (see Appendix), this Neumann boundary condition may not be reasonable from the first sight, since, as a possible system wave function, one would expect Ψ to obey continuity requirement and impose a Dirichlet boundary conditions, $\Psi = 0$. This apparent contradiction was further explained by Ginzburg, whose argument lies in the fact the Ψ may not be regarded as a real wave function, but just an average quantity. Still, Eq. (1.83) represents just an ideal situation where the spatially confined sample do not interact with its surroundings. Therefore,

it should then be regarded as a limiting case of a most general one, where the leakage of superconducting electrons are taken into account. In fact, a most general boundary condition was later proposed by de Gennes in 1966 (GENNES, 1966),

$$\left(-i\hbar\vec{\nabla} - \frac{e}{c}\vec{A}\right)\Psi \cdot \hat{n} = \frac{i}{b}\Psi, \tag{1.84}$$

where b is a positive constant and defines the distance outside the boundary where the order parameter would vanish if extrapolated to outside region of the superconducting sample, as illustrated in Fig 16.

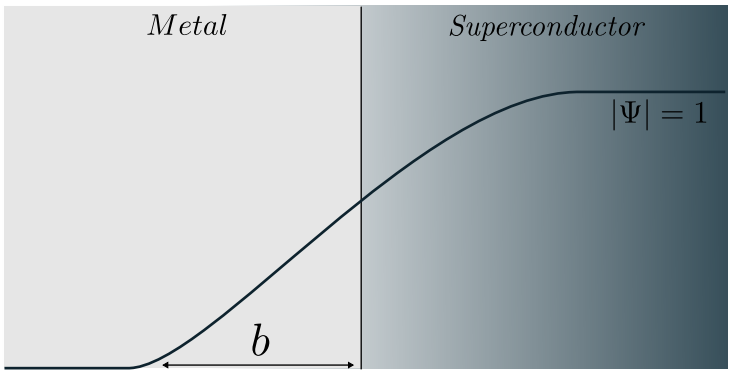

Figure 16 – The superconducting/normal metal interface: the illustration of the spatial dependence of the superconducting order parameter $|\Psi|$ where b denotes the extrapolation length.

Actually, b is closely related to the interaction between the superconductor and its environment and could then be distinguished in three different ways: (i) $b \to \infty$, where the environment strongly interacts with superconducting electrons, forming an infinity energetic wall which prevents the electronic leakage and recovers the insulating or vacuum boundary condition predicted by Ginzburg-Landau theory, (ii) $b > 0$, where the surrounding material provides an energetic barrier that might be tunneled by the superconducting electrons, featuring a superconductor/metal interface, and (iii) $b \to 0$, where, despite the absence of energetic confinement, the order parameter shall vanish at the edges, prohibiting the existence of superconducting electrons beyond the sample frontiers. This last condition is very unusual and must be valid only for ferromagnetic surroundings. Its understanding requires the knowledge of the microscopic electronic pairing mechanisms behind the superconductivity phenomena, where electrons with opposite spins are grouped in pairs as a consequence of the electron-phonon interaction. The bosonic nature of these electronic pairs enable the condensation, leading to the superconductivity phenomena. However, due to the magnetic nature of ferromagnetic materials, which induces spins alignments, this condensation is forbidden beyond the frontiers of the sample, so that, Dirichilet boundary condition, where the order parameter must satisfy $\Psi = 0$, must be satisfied.

1.2.3.2 Characteristic length scales

The theory of Ginzburg and Landau, in its comprehensiveness, contains the London formalism as a limiting case, where the fields do not significantly affect the superconducting state. Naturally, the Meissner effect also must elapse from the set of Ginzburg-Landau equations. In order to attest it, let us start from a quite general situation by assuming a polar decomposition of the order parameter

$$\Psi(\vec{r}) = e^{i\phi(\vec{r})}\sqrt{n_s(\vec{r})}, \tag{1.85}$$

where $\sqrt{n_s}$ represents the order parameter modulus, assuming values between 0 and $\sqrt{-\alpha/\beta}$, and $\phi(\vec{r})$ stands for the superconductor's phase. Within this decomposition, the supercurrent density becomes

$$\vec{j}_s = n_s(\vec{r})\left[\frac{e^*\hbar}{m^*}\vec{\nabla}\phi(\vec{r}) - \frac{e^{*2}}{m^*c}\vec{A}(\vec{r})\right]. \tag{1.86}$$

Under sufficiently weak fields, the London's limit is recovered and, according to Eq. (1.81a), the modulus $\sqrt{n_s}$ may be regarded to be invariant over space and approximately equals to $\sqrt{-\alpha/\beta}$. Thus, by taking the curl of the current density $\vec{j}_s$, the original London's equation, which explains the Meissner's effect, is recovered

$$\vec{\nabla} \times \vec{j}_s(\vec{r}) = -\frac{e^{*2}}{m^*c}\frac{|\alpha(T)|}{\beta}\vec{H}(\vec{r}). \tag{1.87}$$

Together with the Maxwell's equation, the former equation allows to determine, under London's gauge, the temperature-dependent effective penetration depth, which scales changes in magnetic field profiles and current densities

$$\lambda(T) = \sqrt{\frac{m^*c^2\beta}{4\pi e^{*2}|\alpha(T)|}}. \tag{1.88}$$

Specially, for a superconductor defined in the half-space region $x > 0$ and surrounded by vacuum at $x < 0$, it might be found that both magnetic field and current density decays exponentially with x inside the sample, $B \propto j_s \propto e^{-x/\lambda(T)}$. Besides the expression of the penetration depth, the Giznburg-Landau theory also accounts for another meaningful length scale, which provides the stiffness of the order parameter in a zero field conformation. It follows from the first Ginzburg-Landau equation, which, in absence of magnetic field, becomes

$$-\frac{\hbar^2}{2m^*}\nabla^2\Psi + \alpha\Psi + \beta\Psi^3 = 0. \tag{1.89}$$

Here, the order parameter Ψ was assumed to be a real quantity. This choice is supported by the gauge invariance of Ginzburg-Landau equations. In fact, despite Ψ and $\vec{A}$ are not uniquely defined, the equations have their form preserved if a gauge transformation, $\Psi = \exp(i\phi)\Psi'$ and $\vec{A} = \vec{A} + \vec{\nabla}\phi$, is performed. Therefore, physical properties are invariant

under the phase choice and a proper ansatz for the order parameter is $\Psi(\vec{r}) = \sqrt{-\alpha/\beta} f(\vec{r})$, where f is a real function that assume values between 0 and 1. This leads to a second length scale ξ appearing as a prefactor of the gradient term in Eq. (1.89),

$$-\xi^2 \nabla^2 f - f + f^3 = 0, \quad \text{where} \quad \xi = \sqrt{\frac{\hbar^2}{2m^*|\alpha(T)|}}. \tag{1.90}$$

Therefore, if the order parameter is somehow changed from its equilibrium value, ξ specifies the length scale over which the bulk homogeneous value of $|\Psi|^2$ is recovered. The healing character may be analytically derived for small fluctuations of f. In one-dimensional case, where these small fluctuations are described by the ansatz $f(x) = 1 - \epsilon(x)$ with $\epsilon(x) << 1$, non-linear terms remnants of Eq. (1.89) might be disregarded and the final outcome solution for the resulting differential equation is the exponential function,

$$\epsilon(x) \propto e^{\sqrt{2}x/\xi(T)}. \tag{1.91}$$

The definition of ξ as the superconductor healing or coherence length proves to be quite convenient, since disturbances in the order parameter occur in a scale of the order of ξ. In special, for a half-space superconductor, defined in the region $x > 0$ and delimited by an ferromagnetic material at $x < 0$, the solution of Eq. (1.89) is the rapidly increasing function of x

$$f(x) = \tanh\left(\frac{x}{\xi\sqrt{2}}\right), \tag{1.92}$$

which clearly satisfies the boundary conditions $\Psi = 0$ at $x = 0$ and $\Psi = 1$ when $x \to \infty$. Sudden variations of the order parameter results from the existence of a non-linear term in the first Ginzburg-Landau equation, which acts as a repulsive potential on Ψ itself, energetically favoring the spreading of superconducting phase and contributes to more uniform conformations of the order parameter.

1.2.3.3 Superconducting types according to GL theory

Within Ginzburg-Landau formalism, the classification between different superconducting types could then be understood as a stability problem of the normal state in a superconducting sample and might be distinguished from the energy cost of sustaining a normal-superconducting interface at the critical field H_c, under which the energy of superconducting and normal states are the same. The presence of critical field parallel to the NS interface removes the energy contribution from pure phases and capture only the energetic contribution provided by the domain wall, which is the relevant quantity to determine whether sustaining the normal-superconducting interface is favorable or not. The domain-wall energy σ_{ns}, for an interface defined at $x = 0$, where the superconducting

(normal) phase occupy the half-space region $x > 0$ ($x < 0$), may be written, according to the Gibbs free-energy, as

$$\begin{aligned}\sigma_{ns} &= \int_{-\infty}^{\infty}\left[\alpha|\Psi|^2 + \frac{1}{2}\beta|\Psi|^4 + \frac{1}{2m^*}\left|\left(-i\hbar\vec{\nabla} - \frac{2e}{c}\vec{A}\right)\Psi\right|^2 + \left(\frac{h-H_c}{8\pi}\right)^2\right] \\ &= \int_{-\infty}^{\infty}\left[-\frac{1}{2}\beta|\Psi|^4 + \left(\frac{h-H_c}{8\pi}\right)^2\right] \propto (\xi - \lambda).\end{aligned} \tag{1.93}$$

Under an externally applied magnetic field, the thermodynamic Gibbs potential proves to be the appropriate choice for the free energy, since it presumes constant external field and temperature, instead of magnetization and temperature, as in the case of Helmoltz free energy. Moreover, it naturally removes energetic contributions provided by the external field that, indeed, should not be taken into account for the domain wall energy calculation. Because, Ψ is expected to be a solution of the Ginzburg-Landau equations, the thermodynamic equilibrium state may be reduced to a balance between two terms: a negative condensation energy and the positive energy cost of screening the magnetic field. If the domain wall energy is positive, sustaining such surface is not energetically favorable and the superconductivity might be destroyed abruptly, characterizing the type-I behavior. On the other hand, the negative surface energy was considered, at that time, only an evidence of type-II behavior, which would explain the soft decaying of magnetization by the coexistence of normal and superconducting phases. In fact, the knowledge of type-II phases was only understood after Abrikosov remarkable work. Roughly, one may presume that superconductors with larger (lower) values of ξ might exhibit a slower (faster) recovery of pure superconducting phase, reducing (increasing) the negative condensation energy contribution. In contrast, superconductors with lower (large) values of λ might spend less (more) energy for sustaining the field outside, reducing (increasing) the positive contribution. Therefore, it is possible to anticipate that positive (negative) surface energies may occur whenever $\xi >> \lambda$ ($\xi << \lambda$), characterizing type-I (type-II) superconductors. A sketch of both superconducting regimes is presented in Fig. 17.

In fact, the boundary between type-I and type-II behaviors depends exclusively on the temperature independent ratio $\kappa = \lambda(T)/\xi(T)$, named Giznburg-Landau parameter. Numerical calculations shows that $\kappa = 1/\sqrt{2}$ is the dividing value of both phases (OSBORN; DORSEY, 1994). However, such a treatment is valid for bulk superconductors only. In fact, whether applied field may be depicted by the critical field depends on the sample geometry. In the former picture, the magnetic field at the surface of a superconductor was assumed to be homogeneous and equal to the applied field. However, whenever demagnetization effects are considered, the magnetic field might exceed the critical field at certain points, so that even type-I superconductors might exhibit a mixed phase, formed by macroscopic normal domains (PROZOROV, 2007; BRANDT; DAS, 2011). These states, however, were

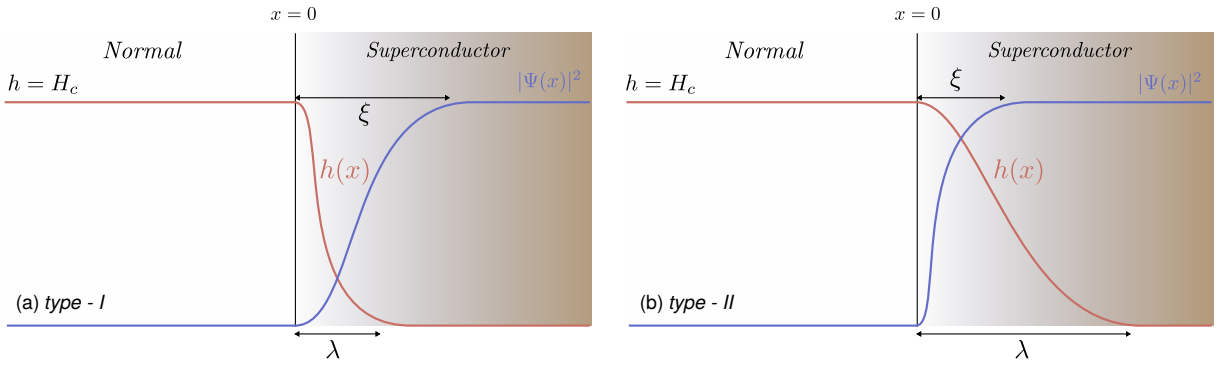

Figure 17 – Magnetization as a function of the applied field for: (a) a type-I superconductor and (b) a type-II superconductor.

experimentally found to depend on sample pre-history and therefore, do not characterize a thermodynamical equilibrium phase.

At this point, it worths to recall the impossibility of making distinction between different superconducting types following London's theory, since the transition threshold and the nature of each type strongly depend on the ratio between both superconducting length scale. Rather, London model presume an abrupt change from normal to superconducting phase and therefore, it should only works for extremely type-II superconductors, where coherence length becomes negligible ($\xi \to 0$).

1.2.4 Vortex states and Abrikosov flux lattice

Even within longstanding experimental evidences obtained by Rjabinin and Schubnikow, in the very beginning after Ginzburg and Landau predictions, type-II regime was believed to be unphysical. In fact, there was a lack of experimental proof, since neither Niobium nor most of type-II compounds superconducting phases known up to date were explored at that time. So, it is not surprising that only in 1952, two years after the first formulation of GL theory, the question about the existence of a second superconducting type turned out to be relevant, exactly when it has been experimentally reported by Zavaritskii (ZAVARITSKII, 1952) that, superconducting phases of pure metals thin films does not obey type-I theory regime.

Still, the exact mechanism behind type-II annomalous magnetization remained unexplained until 1957, when Abrikosov explored type-II regime theory within the Ginzburg-Landau formalism (ABRIKOSOV, 1957). Actually, it was already expected the soft decay of magnetization to be a consequence of a mixed conformation of normal and superconducting domains. However, the exact form of such domains as well as its appearance mechanism was still a mystery. In order to fill this lack of knowledge, Abrikosov considered a superconducting cylinder in a longitudinal magnetic field. Restricting himself to external fields very close to the upper critical field H_{c2}, where GL equation could be linearized by neglecting the quadratic term, he made a parallel with quantum mechanical oscillator

and obtained the upper critical field H_{c2} in terms of the coherence length and penetration depth without making any mention to the specific form of the order parameter

$$H_{c2} = \frac{\Phi_0}{2\pi\xi(T)^2} = \sqrt{2}\kappa H_c. \tag{1.94}$$

When compared with the thermodynamical critical field, the distinction between first and second order phase transitions as a classifying criterion of superconducting types emerged. In fact, differently from type-I materials, type-II superconductors shall experiment a second order phase transition, since for $\kappa > 1/\sqrt{2}$ the upper critical field suppress the thermodynamical critical field $H_{c2} > H_c$. Interestingly, at H_{c2}, there should exist exactly one quantum flux per unit area $2\pi\xi^2$. Within the appropriate guess for the order parameter, Abrikosov realized that vortices would carry these quantized flux lines, which would interact with each other forming a periodic lattice. However, instead of square lattices investigated in Abrikosov's paper, triangular arrangement of vortices were soon realized to have lower energy. Even so, these lattices received the name of Abrikosov's lattice. A sketch of Abrikosov's vortex lattice is presented in Fig. 18 (MOSHCHALKOV; FRITZSCHE, 2011).

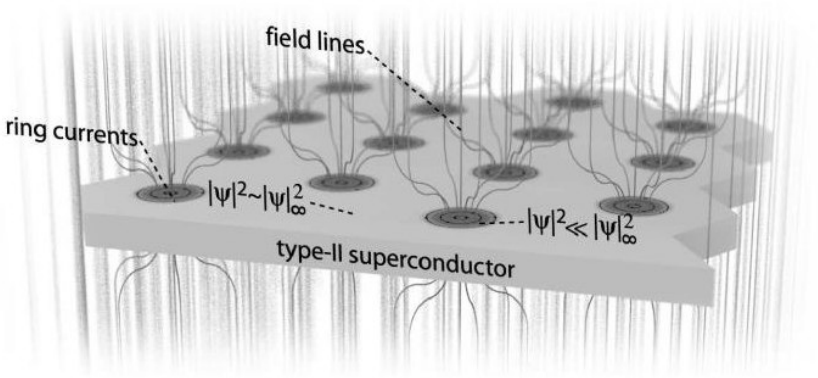

Figure 18 – Sketch of quantized vortices in a type-II superconducting sample. Figure retrieved from Ref. (MOSHCHALKOV; FRITZSCHE, 2011).

Abrikosov's results proved to be in a good agreement with Zavaritskii experimental data and soon the existence of vortex lattices was exhaustively confirmed with different experimental techniques (ESSMANN; TRÄUBLE, 1967; GAMMEL et al., 1987; HESS et al., 1989; BOLLE et al., 1991; HARADA et al., 1992; MOSER et al., 1995; KIRTLEY et al., 1996). Remarkably, it is worth to mention the first experimental visualization by Bitter decoration technique, illustrated in Fig. 19 (ESSMANN; TRÄUBLE, 1967), where a paramagnetic powder was deposited above a dopped Pb superconducting rod. Due to its magnetic nature, the powder particles prefer to sit on top of vortex core, where the magnetic field penetrates the sample.

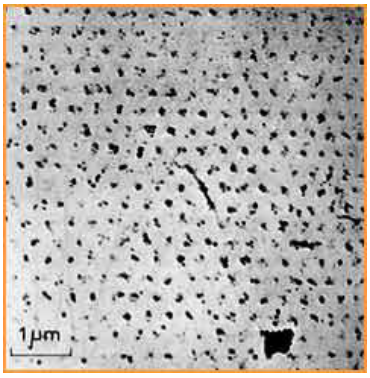

Figure 19 – First image of Abrikosov vortex lattice in a dopped Pb sample using Bitter decoration. Figure retrieved from Ref. (ESSMANN; TRÄUBLE, 1967).

1.2.5 BCS theory

Despite strong evidences of an electronic condensation behind superconductivity phenomenon, the idea of breaking particle symmetry properties remained cumbersome for many years. Still, a microscopic theory was required. Only in 1957, a mechanism of electronic coupling proposed by Bardeen, Cooper and Schriffer was able to model single-gap bulk superconductors as a condensation of bosonic electronic pairs. The coupling of the so-called Cooper pairs was supported by previous works that suggested the existence of an electronic attraction mediated by the presence of phonons in the superconducting crystal (FRÖHLICH, 1950). According to the electron-phonon interaction model, the lattice of positively charged atoms is deformed due to the presence of electronic charges in Fermi levels, producing positively charged quasiparticles which are dragged behind the electric charges, as illustrated by in Fig 20. In fact, the time-scale of lattice deformation, $\tau_D = 1/\omega_D$, governed by Debye frequency ω_D, is much larger than the time-scale of electrons moving at the Fermi velocity $\hbar/E_F$, which means that the electric charge is no longer there when the distortion takes place.

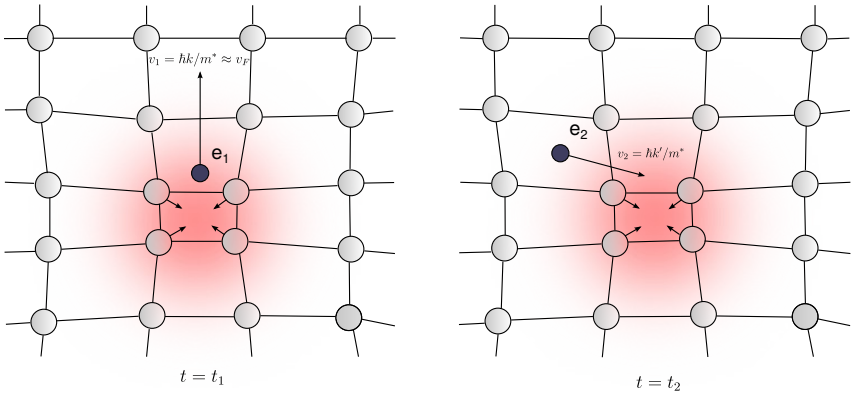

Figure 20 – Mechanism behind electronic attraction in an ion lattice. Due to the polarization cloud left by an electron traveling through the ion lattice, a second electron may experience a net attractive interaction. Figure made by the author, based on a Wikipedia image.

1.2.5.1 Revisiting the non-interacting Fermi-gas at $T = 0$

In the absence of lattice deformations, the problem is reduced to the non-interacting electron model, where the ground state is a filled Fermi sea with each state being occupied by only one electron. With electron-electron interactions ignored due to the Pauli's exclusion principle, the non-interacting Fermi gas may be described by the single-particle Hamiltonian

$$\hat{H} = \frac{\hat{P}^2}{2m} + V(\vec{r}), \tag{1.95}$$

where $V(\vec{r})$ is an infinitely periodic potential produced by lattice ions. The eigenstates of such a periodic Hamiltonian are given by

$$\phi_k(\vec{r}) = \frac{1}{\sqrt{V}} e^{i\vec{k}\cdot\vec{r}}, \tag{1.96}$$

where $V = L_x L_y L_z = L^3$ is the box volume and $\vec{k}$ is the wave vector. Because the wave function must be periodic, it follows that $k_{x,y,z} = 2\pi n_{x,y,z}/L$ in order to obey the periodic boundary conditions, where $n_{x,y,z}$ are integers. The allowed energy levels are, therefore, of the form

$$\epsilon_{n_x,n_y,n_z} = \frac{\hbar^2\pi^2}{2mL^2}(n_x^2 + n_y^2 + n_z^2). \tag{1.97}$$

Each state is therefore, completely determined by their corresponding wave-vectors and has an average volume in phase space given by $\Delta k = (2\pi/L)^3$. In the thermodynamical limit, where $V \to \infty$ and $N \to \infty$, $\Delta k \to 0$ and considering the electron spin S the density of states becomes

$$D(E) = \frac{2S+1}{2\pi^2}\left(\frac{2m}{\hbar^2}\right)^{3/2} E^{1/2}. \tag{1.98}$$

Within the constraint of fixed number of particles N, the Fermi energy E_F of the non-interacting electron gas at $T = 0$ is provided by

$$\begin{aligned} n = \frac{N}{V} &= \int_0^\infty f(E)D(E)dE \\ &= \int_0^{E_F} D(E)dE \\ &= \left(\frac{2m}{\hbar^2}\right)^{3/2} \frac{1}{2\pi^2}\frac{2}{3}E_F^{2/3}, \end{aligned} \tag{1.99}$$

where $f(E)$ is the occupation probability of the space orbital which is equal to unity for energies E lower than the chemical potential μ and zero otherwise.

1.2.5.2 Cooper pairs

At finite temperatures, however, excitations might emerge with energies of the order of $k_B T$. In general, these excitations may be described by means of two process: (i) First, a particle in a filled state below the Fermi surface is annihilated and, subsequently, (ii) the creation of a particle in an unfilled state above the Fermi level. Their origin lies on

a continuous process of absorption and emission of phonons. In a first approach, lattice deformations may thus be understood as a superposition of these process, where the net effect is transferring momentum $\hbar\vec{q}$ from one electron to the other. In fact, through scattering theory, it can be shown that an electron in a state $\vec{k}$ can undergo into a quantum transition to $\vec{k}'$ state mediated by the absorption (emission) of a phonon with momentum $\vec{q} = \vec{k} - \vec{k}'$. As pointed out by Fröhlich (FRÖHLICH, 1950), this phonon exchange between electrons may produce an effective attractive interaction between electrons near the Fermi surface.

The mechanism behind lattice deformation can thus be well understood through the electron-hole model within the Fermi sea background. In such model, the removed particle with momentum $||\vec{p}'|| < ||\vec{p}_F||$ and energy $E' < E_F$ creates an excitation, named a hole, with momentum $-\vec{p}'$ and energy $\epsilon_{-\vec{p}'} = E_F - E'$. On the other hand, the energy involved when an extra electron with momentum $\vec{p} > \vec{p_F}$ and energy $E > E_F$ is added, is given by $\epsilon_{\vec{p}} = E - E_F$. Using the free-particle spectrum, this can be summarized as following

$$e_{\vec{p}} = \begin{cases} p^2/2m - E_F & \text{if } p > p_F \\ E_F - p^2/2m & \text{if } p < p_F \end{cases}, \tag{1.100}$$

Instead of electron-hole model, however, Cooper's approach deals with two extra electrons added slightly above the Fermi surface, with momenta $\hbar k_1$ and $\hbar k_2$. Regardless of the nature of an attractive interaction between these extra electrons, its consequence should be understood by the two-body Hamiltonian

$$\left[\frac{p_1^2}{2m} + \frac{p_2^2}{2m} + V(\vec{r}_1 - \vec{r}_2) - (\epsilon + 2E_F)\right]\Psi(\vec{r}_1\sigma_1, \vec{r}_2\sigma_2) = 0, \tag{1.101}$$

where $\vec{r}_1$, $\vec{r}_2$, σ_1, σ_2 are the space and spin coordinates, ϵ is the energy of the paired electrons relative to the Fermi level $E_F = \hbar^2 k_F^2/2m$ and $V(\vec{r}_1 - \vec{r}_2)$ accounts for the effective interaction between the extra electrons. In contrast, electrons at the Fermi sea shall interact only via Pauli exclusion principle and, in the end, one can always express the two-particle wave-function of extra electron as

$$\Psi(\vec{r}_1\sigma_1, \vec{r}_2\sigma_2) = e^{i\vec{k}_{cm}\cdot\vec{R}_{cm}}\varphi(\vec{r}_1 - \vec{r}_2)\phi^{spin}_{\sigma_1,\sigma_2}, \tag{1.102}$$

where $\vec{R}_{cm}$ is the center of mass and $\hbar\vec{k}_c$ its total momentum. Due to phonon exchange, both extra electrons are continuously scattered, changing their wave vectors, which, according to the momentum conservation law can be mathematically expressed by

$$\vec{k_1} + \vec{k_2} = \vec{k_1}' + \vec{k_2}' = \vec{K}, \tag{1.103}$$

where $\vec{k}_{cm} = \vec{K}$ is the conserved quantity during the scattering process. Because we are interested in the lowest energy state, motion of the center of mass must be neglected $\hbar\vec{K} = 0$, so that $\vec{k}_{cm} = 0$ and $\vec{k}_1 = -\vec{k}_2$. The two-electron model proposed by Cooper

becomes then equivalent to an electron-hole system. On the other hand, the spin wave function can be either singlet, with $S = 0$, or, triplet, where, $S = 1$. However, apart from some exception, most of known superconductors exhibit singlet cooper pairs, so we shall assume that

$$\phi^{spin}_{\sigma_1,\sigma_2} = \frac{1}{\sqrt{2}} \left(|\uparrow\downarrow\rangle - |\downarrow\uparrow\rangle \right). \tag{1.104}$$

To obey the anti-symmetry character of a fermionic wave-function, for a singlet state, the relative coordinate wave-function must be even, $\varphi(\vec{r}_1 - \vec{r}_2) = \varphi(\vec{r}_2 - \vec{r}_1)$. Expanding it in Bloch waves, the wave-function can be expressed as

$$\Psi(\vec{r}_1, \vec{r_2}) = \frac{1}{V} \sum_{\vec{k}} g(\vec{k}) e^{i\vec{k}\cdot(\vec{r}_1 - \vec{r}_2)}, \tag{1.105}$$

where the sum is restricted to pairs with $\vec{k} = \vec{k}_1 = -\vec{k}_2$ and $g(\vec{k})$ are expansion coefficients that provide the probability of finding one electron in state $\vec{k}$ and the other in $-\vec{k}$. Because the momentum transfered by phonons is limited by Debye frequencies ω_D, it follows, from energy conservation, that $g(\vec{k}) = 0$ for $E_{\vec{k}} > E_F + \hbar\omega_D$, where $E_{\vec{k}}$ is the unperturbed free electron energy. Also, due to Pauli's exclusion principle, the extra electron may not occupy a state below the Fermi energy and, therefore, $g(\vec{k}) = 0$ for $E_{\vec{k}} < E_F$. It turns out, from Schrödinger equation, that

$$\left(2E_{\vec{k}} - \epsilon - 2E_F\right) g(\vec{k}) + \sum_{\vec{k}'} V_{\vec{k}\vec{k}'} g(\vec{k}') = 0, \tag{1.106}$$

which holds for $E_F < E_{\vec{k}}, E_{\vec{k}'} < E_F + \hbar\omega_D$. Here, $V_{\vec{k}\vec{k}'}$ is the effective interaction in momentum representation. Instead of using the true interaction potential, however, the problem is better reduced by assuming the simple picture where the interaction is attractive and independent of $\vec{k}$ in the small energy shell around the Fermi level, $V_{\vec{k}\vec{k}'} = -V_0$, with $V_0 > 0$. In order to determine whether electron pairs may form a bound state, with $E < 2E_F$, one may sum Eq. (1.106) over all $\vec{k}$ states and apply the thermodynamic limit, where the sum is then replaced by an integral. The result may be summarized as

$$1 = V_0 \int_{E_F}^{E_F + \hbar\omega_D} \frac{D(E)}{2E - \epsilon - 2E_F} dE, \tag{1.107}$$

where $D(E)$ is the electronic density of states for one spin direction. Because the integral extends only over a narrow spheric shell defined between the limits E_F and $E_F + \hbar\omega_D$, the density of states $D(E)$ may be taken as a constant and therefore, Eq. (1.107) becomes

$$1 = V_0 D(E) ln \left(\frac{\epsilon - 2\hbar\omega_D}{\epsilon} \right) \tag{1.108}$$

or

$$\epsilon = \frac{2\hbar\omega_D}{1 - e^{2/V_0 D(E)}}. \tag{1.109}$$

The bound state becomes energetically available when the energy contribution of paired electrons is lower than that of a fully occupied Fermi sea or, mathematically, when

$\epsilon = E - 2E_F < 0$. The bound state condition is achieved when $V_0 D(E) << 1$, which accounts for the weak coupling limit. In fact, in this regime, Eq. (1.109) may be reduced to

$$\epsilon \approx -2\hbar\omega_D e^{-2/V_0 D(E)}, \tag{1.110}$$

which is negative and, therefore, favors the Cooper pairs formation. This result may also be achieved under the second quantized formalism, with the Cooper-pair added to the Fermi sea represented by the state vector

$$|\Psi_{CP}\rangle = \sum_{\vec{k}} g(\vec{k}) c^{\dagger}_{\vec{k}\uparrow} c^{\dagger}_{\vec{k}\downarrow} |\Psi_N\rangle \tag{1.111}$$

and the second quantized Hamiltonian governing eigenstates of paired system given by

$$\hat{H} = \sum_{\vec{k}} E_{\vec{k}} \left(c^{\dagger}_{\vec{k}\uparrow} c_{\vec{k}\uparrow} + c^{\dagger}_{-\vec{k}\downarrow} c_{-\vec{k}\downarrow} \right) + \sum_{\vec{k}} \sum_{\vec{k}'} V_{\vec{k}\vec{k}'} c^{\dagger}_{\vec{k}\uparrow} c^{\dagger}_{-\vec{k}\downarrow} c_{-\vec{k}'\downarrow} c_{\vec{k}'\uparrow}, \tag{1.112}$$

where $c^{\dagger}_{\vec{k}\uparrow}$ ($c_{\vec{k}\uparrow}$) and $c^{\dagger}_{\vec{k}\downarrow}$ ($c_{\vec{k}\downarrow}$) respectively create (annihilate) electrons with spin up and down in the state $\vec{k}$ and $|\Psi_N\rangle$ denotes the normal ground-state of a free-electron metal, which, in turn, may be expressed as

$$|\Psi_N\rangle = \prod_{\vec{k}}^{k<k_F} (c^{\dagger}_{\vec{k}\uparrow} c^{\dagger}_{\vec{k}\downarrow}) |0\rangle. \tag{1.113}$$

1.2.5.3 The BCS theory

The instability of the Fermi sea under the attractive electronic interaction mediated by phonons is the background theory behind superconductivity. However, effects of the Cooper pairs prediction could only be understood by the many-body theory. In fact, once the energy is reduced by a Cooper pair formation, more electrons near the new Fermi energy may be expected to group in pairs, requiring a many-particle description. Because these pairs behave as particles with zero total spin, it would then be possible to write down a coherent state of theses electronic pairs. Within this purpose, because $\vec{k}$ state can be either occupied or unoccupied by a Cooper pair, Schrieffer suggested a variational ground-state wavefunction made of a linear combination between the vacuum state $|0\rangle$ and the state $c^{\dagger}_{\vec{k}\uparrow} c^{\dagger}_{\vec{k}\downarrow} |0\rangle$, occupied by a Cooper pair

$$|\Psi_S\rangle = \prod_{\vec{k}} \left(u_{\vec{k}} + v_{\vec{k}} c^{\dagger}_{\vec{k}\uparrow} c^{\dagger}_{\vec{k}\downarrow} \right) |0\rangle, \tag{1.114}$$

where $u_{\vec{k}}$ and $v_{\vec{k}}$ are variational parameters representing the probability amplitude of both states and must be determined under the energy minimization process, within the normalization constraint $u^2_{\vec{k}} + v^2_{\vec{k}} = 1$. Still, it is worth to mention that the state proposed by Schrieffer recovers the normal metal state in the particular case where $u_{\vec{k}} = 0$, $v_{\vec{k}} = 1$ for $k < k_F$ and $u_{\vec{k}} = 1$, $v_{\vec{k}} = 0$ for $k > k_F$. Finally, with the proper variational ground-state,

the problem was reduced to minimize the Hamiltonian $\hat{H}$ within the constraint of fixed number of particles,

$$E_S(\Psi_S) = \frac{\langle \Psi_S | \hat{H}_{BCS} | \Psi_S \rangle}{\langle \Psi_S | \Psi_S \rangle} \tag{1.115}$$

where $\hat{H}_{BCS}$ is the Bardee-Cooper-Schrieffer many-body Hamiltonian for Cooper pairs and is given by

$$\hat{H}_{BCS} = \sum_{\vec{k}} \epsilon_{\vec{k}} \left(c^{\dagger}_{\vec{k}\uparrow} c_{\vec{k}\uparrow} + c^{\dagger}_{-\vec{k}\downarrow} c_{-\vec{k}\downarrow} \right) + \sum_{\vec{k}} \sum_{\vec{k}'} V_{\vec{k}\vec{k}'} c^{\dagger}_{\vec{k}\uparrow} c^{\dagger}_{-\vec{k}\downarrow} c_{-\vec{k}'\downarrow} c_{\vec{k}'\uparrow} \tag{1.116}$$

and $\epsilon_{\vec{k}} = E_{\vec{k}} - \mu$ accounts for the single particle energy with respect to the Fermi level. Using variational ground-state function, after some straightforward calculations, one may find

$$E_S(\Psi_S) = 2 \sum_{\vec{k}} \epsilon_{\vec{k}} v^2_{\vec{k}} + \sum_{\vec{k}} \sum_{\vec{k}'} V_{\vec{k}\vec{k}'} u_{\vec{k}} v_{\vec{k}} u_{\vec{k}'} v_{\vec{k}'} \tag{1.117}$$

Because $u_{\vec{k}}$ and $v_{\vec{k}}$ must obey the constraint $u^2_{\vec{k}} + v^2_{\vec{k}} = 1$, there must be only one independent variable in the system. Under a polar transformation: $u_{\vec{k}} = \cos\theta_{\vec{k}}$ and $v_{\vec{k}} = \sin\theta_{\vec{k}}$, an independent variational parameter $\theta_{\vec{k}}$ is obtained and the Euler-Lagrange equation of motion can be achieved for every $\vec{k}$,

$$2\epsilon_{\vec{k}} \sin 2\theta_{\vec{k}} + \sum_{\vec{k}'} V_{\vec{k}\vec{k}'} \cos 2\theta_{\vec{k}} \sin 2\theta_{\vec{k}'} = 0 \tag{1.118}$$

Replacing back $u_{\vec{k}}$ and $v_{\vec{k}}$ parameters, the Euler-Lagrange equation becomes

$$2\epsilon_{\vec{k}} u_{\vec{k}} v_{\vec{k}} - \Delta_{\vec{k}} (u^2_{\vec{k}} - v^2_{\vec{k}}) = 0 \tag{1.119}$$

where $\Delta_{\vec{k}}$ is given by

$$\Delta_{\vec{k}} = -\sum_{\vec{k}'} V_{\vec{k}\vec{k}'} u_{\vec{k}'} v_{\vec{k}'} \tag{1.120}$$

Under the constraint condition, $u^2_{\vec{k}} + v^2_{\vec{k}} = 1$, the solution of Eq. (1.119) is found to be

$$\begin{aligned} u^2_{\vec{k}} &= \frac{1}{2} \left[1 + \frac{\epsilon_{\vec{k}}}{\sqrt{\epsilon^2_{\vec{k}} + \Delta^2_{\vec{k}}}} \right] \\ v^2_{\vec{k}} &= \frac{1}{2} \left[1 - \frac{\epsilon_{\vec{k}}}{\sqrt{\epsilon^2_{\vec{k}} + \Delta^2_{\vec{k}}}} \right] \end{aligned} \tag{1.121}$$

Because they follow from the minimization process, these parameters enable us, at least in the weak interacting limit, to evaluate the condensation energy, defined as the energy difference between superconducting and normal states. In fact, under the energetic limits $-\hbar\omega_D < \epsilon_{\vec{k}} < \hbar\omega_D$, where $V_{\vec{k}\vec{k}'}$ is reduced to a constant averaged potential

$-V_0$, with $V_0 > 0$, the condensation energy becomes

$$\begin{aligned} E_S - E_N &= 2 \sum_{\vec{k}}^{|\epsilon_{\vec{k}}|<\hbar\omega_D} \epsilon_{\vec{k}} v_{\vec{k}}^2 + \sum_{\vec{k},\vec{k}'}^{|\epsilon_{\vec{k},\vec{k}'}|<\hbar\omega_D} V_{\vec{k}\vec{k}'} u_{\vec{k}} v_{\vec{k}} u_{\vec{k}'} v_{\vec{k}'} - 2 \sum_{\vec{k}}^{-\hbar\omega_D<\epsilon_k<0} \epsilon_{\vec{k}} \\ &= \sum_{\vec{k}}^{|\epsilon_{\vec{k}}|<\hbar\omega_D} \left[2\epsilon_{\vec{k}} v_{\vec{k}}^2 - \Delta_0 u_{\vec{k}} v_{\vec{k}} \right] - \sum_{\vec{k}}^{-\hbar\omega_D<\epsilon_k<0} 2\epsilon_{\vec{k}} \\ &= \sum_{\vec{k}}^{|\epsilon_{\vec{k}}|<\hbar\omega_D} \left[\epsilon_{\vec{k}} - \frac{2\epsilon_{\vec{k}}^2 + \Delta_0^2}{2\sqrt{\epsilon_{\vec{k}}^2 + \Delta_0^2}} \right] - \sum_{\vec{k}}^{-\hbar\omega_D<\epsilon_k<0} 2\epsilon_{\vec{k}}. \end{aligned} \tag{1.122}$$

where $\Delta_{\vec{k}}$ was also taken as a constant, Δ_0, inside the energetic spherical shell $-\hbar\omega_D < \epsilon_{\vec{k}} < \hbar\omega_D$ and 0 outside. Finally, in the thermodynamic limit, where sums may be replaced by integrals, the energetic difference is reduced to

$$E_S - E_N = D(E) \left[\hbar^2\omega_D^2 - \hbar\omega_D \sqrt{\hbar^2\omega_D^2 + \Delta_0^2} \right] \tag{1.123}$$

or, for $\Delta \ll \hbar\omega_D$,

$$E_S - E_N = -\frac{1}{2} D(E) \Delta_0^2 \tag{1.124}$$

One may therefore conclude that, there exist an energy gap Δ_0 separating superconducting and normal states and, because the superconducting state has lower energy electrons indeed may prefer to group in pairs forming a bound state. In 1959, extending up the BCS theory in order to account for externally applied magnetic fields, Gor'kov has shown that the Ginzburg-Landau theory is just a limiting case of the BCS theory near the critical field, where the order parameter was found to be proportional to the band gap Δ_0 (GOR'KOV, 1959).

1.3 Our goals

For a long time, theories of superconductors and Bose-Einstein condensates were investigated separately. However, a very close link can be observed between the Gross-Pitaevskii theory of Bose-Einstein condensation and the Ginzburg-Landau theory of superconductivity. In fact, in both cases, the main equation governing the particles density is a non-linear Schrödinger-like equation. More than this, both subjects are indeed a condensation phenomena, differing only in the kind of particle which is condensed. In this thesis, we took advantage from the similarity of both subjects, to investigate, using similar models, emergent vortex behavior in superconducting and superfluid systems with single and multiple quantum condensates. In special, we attempt to explain, through the vortex-vortex interaction, recently obtained vortex states in both superconducting thin films and multi-component BECs which are not covered by current theory, as they suggest non-monotonic behavior. Also, we provide further information about vortex inner structures with suggested approximated behavior.

Part I

Bose-Einstein condensates

2 Bound vortex states and exotic vortex lattices in multi-component BECs: the role of the vortex-vortex interaction

We numerically study the vortex-vortex interaction in multi-component homogeneous Bose-Einstein condensates within the realm of the Gross-Pitaevskii theory. We provide strong evidences that pairwise vortex interaction captures the underlying mechanisms which determine the geometric configuration of the vortices, such as different lattices in many-vortex states, as well as the bound vortex states with two (dimer) or three (trimer) vortices. Specifically, we discuss and apply our theoretical approach to investigate intra- and inter-component vortex-vortex interactions in two- and three-component Bose-Einstein condensates, thereby shedding light on the formation of the exotic vortex configurations. These results correlate with current experimental efforts in multi-component Bose-Einstein condensates, and the understanding of the role of vortex interactions in multiband superconductors.

2.1 Introduction

The realization of Bose-Einstein condensates (BECs) has brought about a suitable research environment for investigating general properties of superfluidity and superconductivity with a high degree of control and versatility (ANDERSON et al., 1995; BRADLEY et al., 1995; DAVIS et al., 1995). This has led vortex states and their dynamics, key concepts for both superfluidity and superconductivity, to the rank of some of the most investigated topics in low temperature physics (YARMCHUK; GORDON; PACKARD, 1979; FETTER, 2009b; COOPER, 2008). Remarkably, since the first observation of vortices (MADISON et al., 2000a; MADISON et al., 2000b) and, subsequently, the formation of highly-ordered vortex lattices in BECs (ABO-SHAEER et al., 2001), much theoretical and experimental effort has been made to push further the understanding of these systems. Specially, recent advances in experimental techniques have led to the realization of condensates with several different types of particle-particle interaction, making this research field even broader. In the spotlight, theoretical results on dipolar (COOPER; REZAYI; SIMON, 2005; ZHANG; ZHAI, 2005) and spin-orbit-coupled (RADIĆ et al., 2011) BECs exhibit rich ground-state phases, with bubbles, density stripes and various vortex lattice geometries. Besides the already mentioned possibilities, further remarkable physical phenomena to be addressed with ultracold atomic systems include, for example, quantum-fluid turbulence in BECs (HENN et al., 2009), multicharged vortices (TELES et

al., 2013) and vortex-antivortex lattices in superfluid fermionic gases (BOTELHO; MELO, 2006).

With the recent prospects of producing condensates with a large number of components and different types of interaction (LU et al., 2011; AIKAWA et al., 2012), vortex-states in multi-component condensates become even more important. Indeed, recent theoretical results on vortex lattice conformations have shown that multi-component Bose-Einstein condensates are far from being just a trivial extension of the single component case. In fact, adding a component brings a diversity of possible configurations never found in a one-component system, such as amorphous conformations, square lattices and bound states, including overlapped vortices, vortex dimers and molecules (KASAMATSU; TSUBOTA; UEDA, 2004; ETO; NITTA, 2012; CIPRIANI; NITTA, 2013; LIU et al., 2014; KUOPANPORTTI; HUHTAMÄKI; MÖTTÖNEN, 2012). Some of these conformations suggest that the interaction between vortices can be nonmonotonic with respect to the inter-vortex distance. Unfortunately, to date, the interaction between vortices in the simplest multi-component BEC is known only in specific limits of scale, by either assuming inter-vortex distances much greater than the healing length (ETO et al., 2011) or considering the interaction energy near the vortex peak in the Thomas-Fermi regime (AFTALION; MASON; WEI, 2012). As it turns out, the asymptotic behavior does not account for all conformations found (KUOPANPORTTI; HUHTAMÄKI; MÖTTÖNEN, 2012; ETO; NITTA, 2012; CIPRIANI; NITTA, 2013; LIU et al., 2014). Furthermore, the generalization of these analytical approaches to more complex cases with more components or even with a different kind of inter-component particle-particle interaction seems to be highly non-trivial.

Within this context, we investigate in the present paper the origin of these unusual quantized vortex states by focusing on the pairwise vortex-vortex interaction (CHAVES et al., 2011b; CHAVES et al., 2011a; DANTAS et al., 2015). We consider homogeneous BECs, which possess translation invariance. On the one hand, this is important in itself, since the key properties of the experimentally more relevant harmonically trapped BECs in the large particle number regime bear close resemblance to those of their homogeneous counterparts (LIMA; PELSTER, 2012). On the other hand, the recent achievement of a condensate in a uniform potential (GAUNT et al., 2013) enables the experimental verification of our predictions. The experimental progress has already led to the detection of extended phase coherence in a uniform quasi-two-dimensional Bose gas (CHOMAZ et al., 2015). In our approach, constraints are imposed on the Gross-Pitaevskii (GP) formalism, allowing for fixing the vortices in desired positions for further analysis. In other words, vortices no longer arise naturally from the GP equation itself, but are instead placed manually in the position of interest. This brings about the possibility of calculating the interaction energy between vortices as a function of their distance. Then, by investigating conformations which minimize the corresponding energy, we are able to

present a simple physical picture of the underlying phenomena which lead to elsewhere observed vortex states.

2.2 Vortex states in BECs

The existence of a macroscopic wave function associating the superfluid flow with its phase gradient provides an unique environment to glimpse the macroscopic manifestation of quantum mechanics in fluid dynamics. The contrast between classical and quantum hydrodynamics emerges from Bohr-Sommerfeld quantization rule, imposed by the single-valued character of the wave-function. Its consequences may be easily seen in a rotating frame, where the phase around a closed loop must return on itself if the surface is singly connected, or be increased by a multiple of 2π for multiply-connected surfaces. The later represents the only way of a superfluid to rotate: by forming topological defects, named vortices. These topological defects represents an unambiguous signature of quantum character of superfluidity and therefore, with the advent of BECs, became the target of a huge portion of theoretical and experimental researches in ultra-cold atomic gases.

2.2.1 Single-component BECs

The first experimental observation was made in a stirred Bose-Einstein condensate of ^{87}Rb confined in a magnetic trap (MADISON et al., 2000a; MADISON et al., 2000b) (see Fig.21), where laser beams were used to engineer the condensate phase and set/control the superfluid velocity.

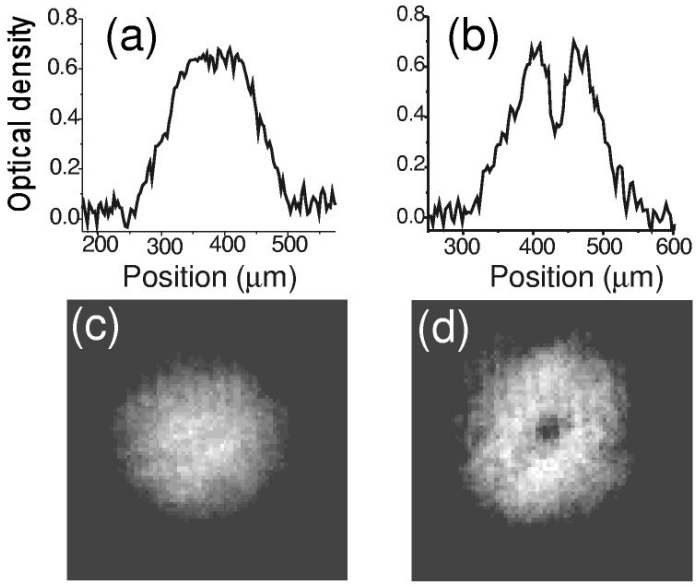

Figure 21 – Stirred Bose-Einstein condensation before vortex entry in panels (a) and (c). First vortex observation image after exceed the critical rotation frequency in (b) and (d). This figure was retrieved from Ref. (MADISON et al., 2000a).

In the absence of external confining potentials, the single vortex structure may be modeled analytically under the Gross-Pitaevskii formalism, with order parameter

$$\Psi(\vec{r}) = e^{il\phi} f(\rho, z), \tag{2.1}$$

and total free-energy,

$$E = \int d\vec{r} \left\{ \frac{\hbar^2}{2m} \left[\left(\frac{\partial f}{\partial \rho} \right)^2 + \left(\frac{\partial f}{\partial z} \right)^2 \right] + \frac{l^2 \hbar^2 f^2}{2m\rho^2} + \frac{g}{2} f^4 \right\}. \tag{2.2}$$

Here, the phase ϕ is identified as the polar angle around the vortex. Notice that, whenever flux quantization is taken into account, $l \neq 0$, singularities on superfluid particle density may appear at $\rho = 0$, otherwise the second term derived from kinetic energy contribution would diverge at the origin. Around this singularity, there should be an azimuthal superfluid flow, with velocity $v_\phi = l\hbar/m\rho$. Because the irrotational flow character is lost, the curl of the velocity field should be redefined to

$$\vec{\nabla} \times \vec{v} = \frac{lh}{m} \delta(\rho) \hat{z}, \tag{2.3}$$

in order to account for vortex entry. The energy barrier that a vortex needs to overcome in order to step into the system may be derived from the Ginzburg-Landau equation for the amplitude f of the order parameter,

$$-\frac{\hbar^2}{2m} \left[\frac{1}{\rho} \frac{\partial}{\partial \rho} \left(\rho \frac{\partial f}{\partial \rho} \right) + \frac{\partial^2 f}{\partial z^2} \right] + \frac{\hbar^2}{2m\rho^2} l^2 f + g f^3 = \mu f. \tag{2.4}$$

Far from the vortex core, where the order parameter becomes uniform and the third term may be neglected, the wavefunction amplitude is given by $f_\infty = (\mu/g)^{1/2}$. On the other hand, outside the long-range limit, the solution is only achieved numerically. Still, the energy associated to a singly quantized vortex can be estimated from the the energy difference between E and the energy associated to an uniform gas, which yields

$$E_v \approx \frac{\pi n_s \hbar^2}{m} \ln \left(\frac{R}{\xi} \right), \tag{2.5}$$

where n_s is the density of superfluid particles, $\xi = \sqrt{\hbar/2mng}$ is the length scale over which order paramenter variations may occur and R is an upper integration limit of the free-energy expression, included to avoid divergence of the angular kinetic energy term. The former result may also be generelized in order to account for vortices with more than one flux quanta (giant-vortices), which can be roughly approximated to

$$E_v^l = \frac{\pi n_s \hbar^2 l^2}{m} \ln \left(\frac{R}{l\xi} \right). \tag{2.6}$$

Whether vortices might stick together to form giant-vortices depends only on the energy difference $E_v^l - lE_v$. Because giant-vortices have higher energy than the collection

of singly quantized states, vortices should repel each other in order to avoid overlapping. Using a double-vortex structure ansatz $\Psi = e^{il_1\phi}e^{il_2\phi}f$ and assuming inter-vortex distances much larger than the coherence length $d >> \xi$, the long-range vortex-vortex interaction energy is found to be well approximated by

$$E_{int} = \frac{2\pi l_1 l_2 \hbar^2 n}{m} \ln\left(\frac{R}{d}\right), \tag{2.7}$$

where $R >> d >> \xi$. Due to the repulsive nature of interaction, highly ordered lattices might be formed with the emergence of multiple vortices in the condensate. Its first observation was made by Abo-Shaeer et al. (ABO-SHAEER et al., 2001), where Abrikosov lattices were found for different vortex densities (see Figure 22)

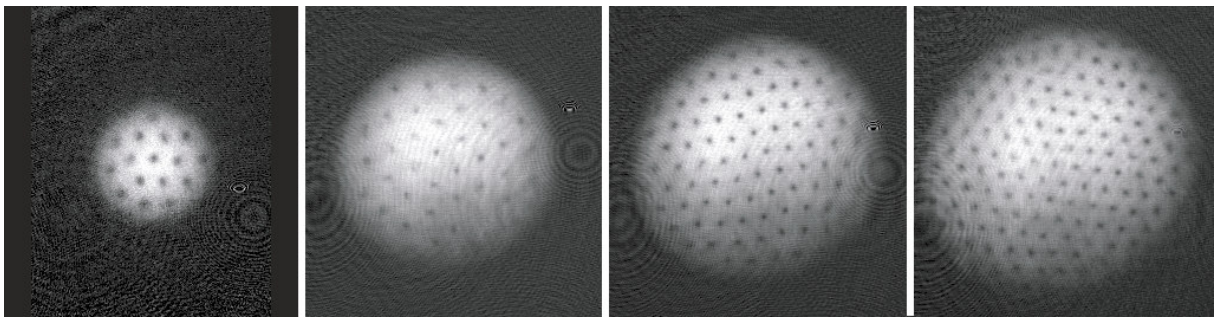

Figure 22 – Observation of Abrikosov vortex lattices in a stirred Bose-Einstein condensation for (a) 16, (b) 32, (c) 80 and (d) 130 vortices. This figure was retrieved from Ref. (ABO-SHAEER et al., 2001).

2.2.2 Multi-component BECs

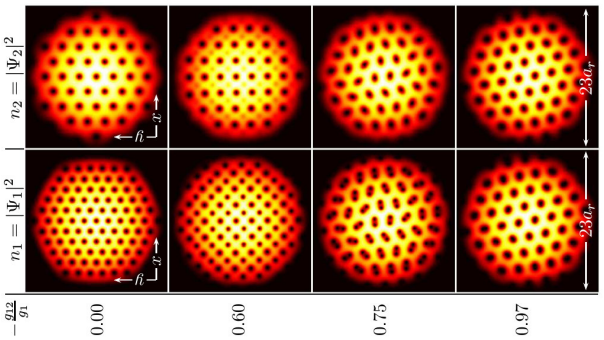

Figure 23 – Vortex states obtained for different values of inter-component coupling in a two-component Bose-Einstein condensate. Figure retrieved from Ref. (KUOPANPORTTI; HUHTAMÄKI; MÖTTÖNEN, 2012)

Vortex structure and their dynamics in single-component BECs are nowadays considered to be well understood. However, there is still a lack of knowledge concerning vortex properties in multiple-component condensed systems. In fact, they exhibit a much more rich phase diagram and the mechanism behind most of vortex states remains misunderstood. For instance, it is worth to revisit the remarkable theoretical work of

Kuopanportti (KUOPANPORTTI; HUHTAMÄKI; MÖTTÖNEN, 2012), where triangular and square vortex lattices were found and new states such as intra-component vortex dimers and giant-vortex states were predicted in a two-component Bose-Einstein condensate with contact interaction between condensed particles. Such results are presented in Fig.23. Here, we try to understand the crossover between these vortex states through the vortex-vortex interaction calculation.

As we shall see further, differently from single component BECs, the exact form of the vortex lattice does not depend only on the nature of the interaction played between vortices of different and same components. Rather, it may also depend on the mass distribution between different components, as it has strong influence on the number of vortices in each condensate. Subsequently, by including a third-component and considering an internal coherent coupling between the components we reproduce vortex molecules found in Ref. (ETO; NITTA, 2012) (see Fig. 24).

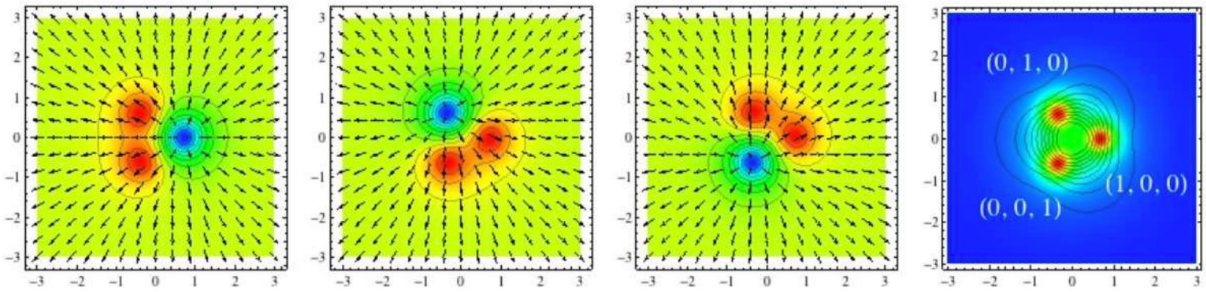

Figure 24 – Triangular conformation of vortex molecules obtained in coherently coupled three-component Bose-Einstein condensate. Figure retrieved from Ref. (ETO; NITTA, 2012)

2.3 Our theoretical approach

We begin our consideration from the Gross-Pitaevskii energy functional for an N_c-component homogeneous BEC. When set into rotation above a given critical angular velocity, superfluids acquire angular momentum in the form of vortices (BUTTS; ROKHSAR, 1999; LINN; FETTER, 1999). In turn, these can be represented by nodes in the wave-function Ψ (FEYNMAN, 1955). Here we adopt a different approach and include vortices directly in the form of a node, disregarding rotation. Therefore, only contributions from the kinetic and interaction energies should enter in the energy functional. Moreover, since vortices will be placed manually in fixed positions, we also do not need to account for the energy provided by the angular momentum of the system, L_z, which is only necessary to allow the vortex formation in the Gross-Pitaevskii theory for a rotating BEC. Then, in the present case, the energy density functional reads

$$\mathcal{E} = \sum_{\alpha=1}^{N_c} \left\{ \frac{\hbar^2}{2m_\alpha} |\nabla \Psi_\alpha|^2 + \frac{g_\alpha}{2} |\Psi_\alpha|^4 \right\} + V_{ij}, \tag{2.8}$$

where the components are labeled by the index α. Here, the first and second terms, respectively, account for the usual kinetic and contact interaction energies within each component. In addition, the term V_{ij} stands for the inter-component coupling energy density.

In what follows, we will be interested in cases where V_{ij} can be written as

$$V_{ij} = \sum_{i}^{N_c}\sum_{j>i}^{N_c} g_{ij}|\Psi_i|^2|\Psi_j|^2 - w_{ij}\left(\Psi_i\Psi_j^* + \Psi_j\Psi_i^*\right), \tag{2.9}$$

where the first term stands for the contact interaction and the last one represents the Rabi term. The latter characterizes the internal coherent coupling between the components and has been already experimentally implemented by inducing an external driving field, which allows particles to move from one hyperfine spin state to another (MATTHEWS et al., 1999b). These interaction terms are controlled by the parameters g_α, g_{ij} and w_{ij}, respectively. However, it is convenient to redefine them in order to have dimensionless units of energy and length. Therefore, for a two-dimensional system, we introduce the units $\mathcal{E}_1 = \hbar^2\bar{\rho}_1^2/2m_1$ for energy density and $\xi = 1/\sqrt{\bar{\rho}_1}$ for distances. Here, $\bar{\rho}_1$ is the average particle density of the first species. With $E = \mathcal{E}/\mathcal{E}_1$ and $\vec{r} = \vec{r}'/\xi$, the energy density can be written in its dimensionless form as

$$\begin{aligned} E = &\sum_{\alpha=1}^{N_c}\left[M_{1\alpha}|\nabla\psi_\alpha|^2 + \frac{\gamma_\alpha}{2}|\psi_\alpha|^4\right] \\ &+ \sum_{i}^{N_c}\sum_{j>i}^{N_c}\left[\gamma_{ij}|\psi_i|^2|\psi_j|^2 - \omega_{ij}\left(\psi_i\psi_j^* + \psi_j\psi_i^*\right)\right], \end{aligned} \tag{2.10}$$

where $\psi_\alpha = \xi\Psi_\alpha$ is the dimensionless order parameter. This procedure leads to the definition of the mass ratio $M_{1\alpha} = m_1/m_\alpha$, the dimensionless contact interaction strengths $\gamma_\alpha = g_\alpha\bar{\rho}_1^2/\mathcal{E}_1$ and $\gamma_{ij} = g_{ij}\bar{\rho}_1^2/\mathcal{E}_1$, and the dimensionless Rabi frequencies $\omega_{ij} = w_{ij}\bar{\rho}_1/\mathcal{E}_1$. The contact parameters can be well controlled in experiments by means of Feshbach resonances and appropriate values should enable the visualization of properties of interest.

In order to measure the interaction potential between two vortices, we consider the total energy as a function of the inter-vortex distance. This is justified because the system is free from external contributions, so that the vortex position only affects the vortex-vortex interaction. Moreover, calculating the system energy as a function of the distance between vortex pairs requires the vortex fixing, which is achieved by fixing the 2π whirl of the phase of the condensate wave function, thereby introducing a node in it. For one vortex in the α-component, for example, the wave function is given as $\psi_\alpha(x,y) = \sqrt{N_\alpha}e^{in_k\theta_k}f_\alpha(x,y)$, with N_α the number of particles in the α-component and n_k the corresponding winding number, i.e., the quanta of circulation carried by the vortex. In addition, the angle θ_k is defined around the locus of the k-th vortex. Correspondingly, for two vortices, we have $\psi_\alpha(x,y) = \sqrt{N_\alpha}e^{in_{1,\alpha}\theta_{1,\alpha}}e^{in_{2,\alpha}\theta_{2,\alpha}}f_\alpha(x,y)$. Since the two-vortex

structure is not circularly symmetric, Cartesian coordinates are an appropriate choice, with $e^{in_{k,\alpha}\theta_{k,\alpha}}$ is written as

$$e^{in_{k,\alpha}\theta_{k,\alpha}} = \left(\frac{x_{k,\alpha} + iy_{k,\alpha}}{x_{k,\alpha} - iy_{k,\alpha}}\right)^{n_{k,\alpha}/2}, \tag{2.11}$$

where $\vec{r}_{k,\alpha} = (x_{k,\alpha}, y_{k,\alpha}, 0)$ stands for the in-plane position vector with origin at the center of the vortex k. As a consequence of the fixed circular phase around the vortex, singularities in the amplitudes appear naturally from the energy functional minimization.

We remark that the present ansatz is general enough to allow for considering components whose vortices might differ both in position and winding number. This is important in order to obtain the total energy of the system in the presence of the inter-component coupling as a function of the relative distance of the vortices and then verify whether one has found the lowest energy configuration or not. Indeed, in the absence of inter-component coupling $\gamma_{ij} = \omega_{ij} = 0$, we have found that the single-vortex state is infinitely degenerate and the respective position of vortices in different components is irrelevant. This supports our statement above that the total energy depends only on the inter-vortex distance. In the presence of an inter-component coupling, however, vortices in different components will rather stay on top of each other (separate away) for attractive (repulsive) effective vortex-vortex interaction potentials.

With the adequate ansatz for the condensate wave function at hand, we minimize the total energy, which is obtained by integrating in space the quantity $E - \sum \mu_\alpha |\psi_\alpha|^2$, with respect to f_α. Here, μ_α stands for the chemical potential of the the α-component and is introduced to keep the corresponding number of particles constant, which means that we are not taking population transfer between different hyperfine spin states into account. The minimization process is implemented by numerically solving the set of N_c Euler-Lagrange equations

$$\begin{aligned} &M_{1\alpha}K_\alpha f_\alpha + \mu_\alpha f_\alpha - \gamma_\alpha N f_\alpha^2 f_\alpha \\ &+ \sum_{i}^{N_c}\sum_{j>i}^{N_c} \omega_{ij}\Theta_{ij}\left(f_i\delta_{\alpha,j} + f_j\delta_{\alpha,i}\right) \\ &-N\gamma_{ij}\left(f_j^2 f_i\delta_{i,\alpha} + f_i^2 f_j\delta_{j,\alpha}\right) = 0, \end{aligned} \tag{2.12}$$

where

$$\Theta_{ij} = \cos\left[(n_{1i}\theta_{1i} - n_{1j}\theta_{1j}) + (n_{2i}\theta_{2i} - n_{2j}\theta_{2j})\right]. \tag{2.13}$$

At this point, we have chosen the same number of particles for all components by setting $N_\alpha = N$. Notice that Eq. (2.12) has the same form of the Gross-Pitaevskii equation and we shall call it constrained GP equation (CGP). One important difference, however, should be emphasized: the term

$$K_\alpha = \nabla^2 - \left(\overline{X_\alpha}^2 + \overline{Y_\alpha}^2\right), \tag{2.14}$$

which arises from the kinetic contribution of the energy density functional, carries two extra terms $\overline{X_\alpha}$ and $\overline{Y_\alpha}$, allowing us to manually set the coordinates of fixed vortices as well as their winding numbers. These terms are given by

$$\overline{X_\alpha} = \frac{n_{1,\alpha}x_{1,\alpha}}{r_{1,\alpha}^2} + \frac{n_{2,\alpha}x_{2,\alpha}}{r_{2,\alpha}^2}, \qquad \overline{Y_\alpha} = \frac{n_{1,\alpha}y_{1,\alpha}}{r_{1,\alpha}^2} + \frac{n_{2,\alpha}y_{2,\alpha}}{r_{2,\alpha}^2}.$$

Finally, we remark that a similar procedure has already been successfully applied to superconductors in the framework of the Ginzburg-Landau theory (CHAVES et al., 2011a; CHAVES et al., 2011b).

2.4 Numerical Results

The numerical solution of the CGP equations is obtained considering a two-dimensional rectangular system divided in a uniform square grid 4000×2000 with total dimension $1000\xi \times 500\xi$, by using the finite-difference technique and a relaxation method suitable for non-linear differential equations. This leads us to the lowest-energy vortex structure that satisfies the constraint that vortices are placed in the fixed positions. The obtained condensate amplitudes are then substituted back in the energy density, which is numerically integrated, yielding the total energy $U = \int E(\psi_\alpha)dxdy$ (dimensionless in units of $E_1 = \mathcal{E}_1\xi^2$) of the corresponding vortex configuration. With the total energy as a function of the vortex-vortex distance at hand, our theoretical approach will then be used to investigate vortex-state solutions of the Gross-Pitaevskii equation in the presence of rotation, reflecting the real experimental conditions under which vortices are generated.

In what follows, we present the results first for BECs with contact interaction only, where we focus on the two-component case, and then also for coherently coupled two- and three-component BECs. For simplicity, we took the same number of particles per component for all situations, $N = 5 \times 10^4$, as well as the intra-component couplings ($\gamma_1 = \gamma_2 = \gamma_3 = 1$). Since the investigation of the vortex-vortex interaction is performed within the miscibility condition: $\gamma_1\gamma_2 - \gamma_{12}^2 > 0$, the used inter-component coupling parameters are within the upper and lower limits $|\gamma_{12}| < 1$. We denote by $U_{i,j,k}$ the total energy for the case of i vortices placed in the first component, j vortices placed in the second, and k vortices placed in the third (if considered).

2.4.1 Two-component BEC with contact interaction

Let us first consider the case of a two-component condensate, with two vortices placed at $(x, y) = (\pm d/2, 0)$ so that the distance between them is d. We shall consider components with different masses, as this has been found to lead to unusual lattice conformations in Ref. (KUOPANPORTTI; HUHTAMÄKI; MÖTTÖNEN, 2012). By assuming a mass ratio of $M_{12} = 2.0$ between the different components, we plot in Fig. 25 the vortex-vortex interaction for different values of the inter-component coupling strength:

$\gamma_{12} = -0.20$ (circles); $\gamma_{12} = -0.45$ (squares); $\gamma_{12} = -0.75$ (triangles); and $\gamma_{12} = -0.98$ (downward triangles). Fig. 25 (a) and (b) represent the intra-component vortex-vortex interaction for the first and second component respectively, whereas Fig. 25(c) depicts the inter-component vortex-vortex interaction.

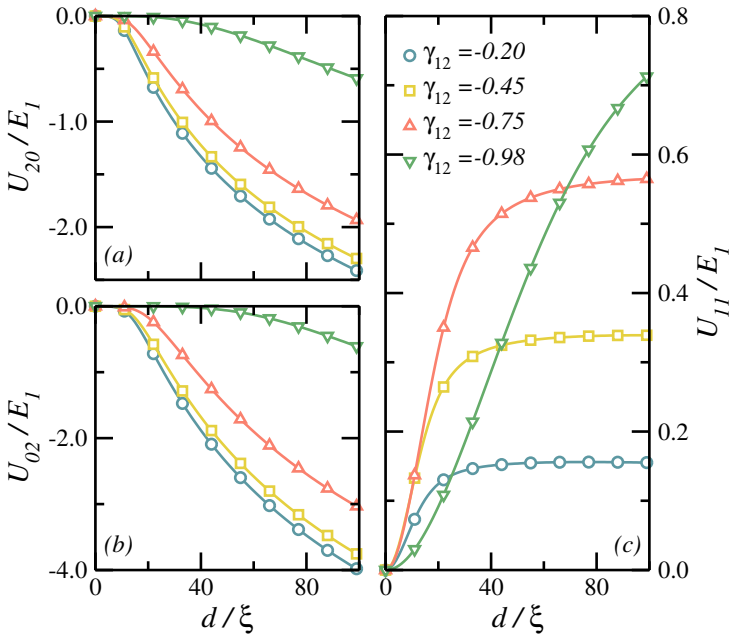

Figure 25 – Vortex-vortex interaction potentials, considering $M_{12} = 2.0$, for (a-b) two vortices in the same component and (c) vortices in different components. Colours and symbols denote different inter-component coupling strength: $\gamma_{12} = -0.20$ (blue circles); $\gamma_{12} = -0.45$ (yellow squares); $\gamma_{12} = -0.75$ (red triangles); and $\gamma_{12} = -0.98$ (green downward triangles).

It turns out that for a two-vortex configuration, the interaction potential is always a monotonic function of the distance, where the attractive or the repulsive behavior is determined by the properties of the particle-particle interaction. Nonetheless, one interesting feature can already be identified at this level: for *inter*-component attraction, increasing the corresponding interaction strength $|\gamma_{12}|$ weakens the *intra*-component vortex-vortex repulsion. This can be understood in terms of the form of the amplitudes $f(x, y)$. Indeed, as the attractive *inter*-component interaction becomes stronger, the energy is lowest for the largest possible superposition of the amplitudes, leading to a decrease in the density of one component in the spatial region where the other one has a vortex. Consequently, as $|\gamma_{12}|$ increases, these depletions should become more akin to vortices and the repulsive nature of the intra-component vortex-vortex interaction is softened by the depletion-vortex attractive interaction.

Before we explore the consequences of the depletion induced in one component due to the presence of vortices in the other one, let us turn our attention to the mass ratio M_{12}. According to the Feynman relation of the vortex density in a rotating superfluid

(FEYNMAN, 1955), the vortex density is proportional to the particle mass, according to

$$n_{v,\alpha} = \frac{m_\alpha \Omega_R}{\pi\hbar}, \tag{2.15}$$

where Ω_R is the angular rotation frequency of the condensate. Thus, for a mass ratio of $M_{12} = 2.0$, it is natural to investigate situations where two vortices (one vortex) are placed in the heavier (lighter) component. To this end, we have pinned a vortex in the second component in the center of the mesh and have placed two further vortices in the first component, separated by a distance d, as illustrated in Fig. 26 by a contour plot of both components. In Fig. 26, colors represent the density occupation number for both order parameters, and vortices coordinates are explicited as a function of the inter-vortex distance d. In this case, the system energy is no longer a vortex-vortex interaction potential. However, this conformation should enable the identification of possible bound states provided by the competition between the inter-component and intra-component interactions, such as dimers and giant vortices (SCHWEIGERT; PEETERS; DEO, 1998; XU et al., 2011; CREN et al., 2011; AFTALION; DANAILA, 2004; DANAILA, 2005; FETTER; JACKSON; STRINGARI, 2005; KASAMATSU; TSUBOTA, 2006; GEURTS; MILOŠEVIĆ; PEETERS, 2008) in the same component. Notice the weaker density in one component in the positions where the other component features a vortex, characterizing the depletion effect discussed before.

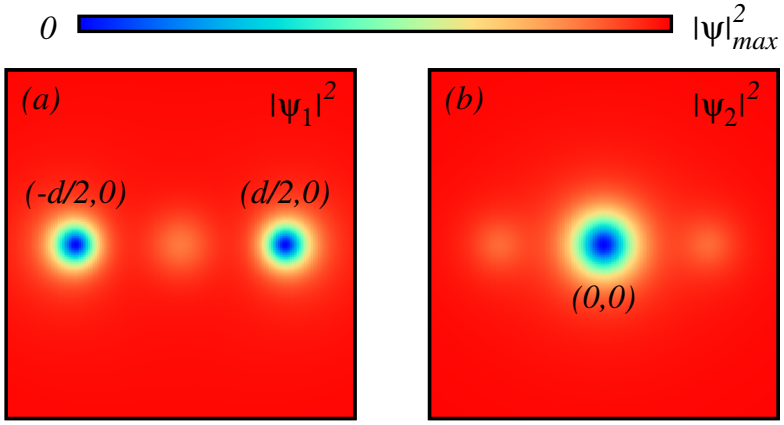

Figure 26 – The occupation number density contour plots for: (a) first component with two vortices positioned at $(-d/2, 0)$ and $(d/2, 0)$ and (b) second component with a single vortex in the center of the mesh. Notice the depleted density in one component in the positions where the other component features a vortex. The investigation of the system energy with respect to d for this conformation enables us to identify possible bound states in a two-component Bose-Einstein condensate with mass ratio $M_{12} = 2.0$.

The total energy of this three-vortex configuration is plotted in Fig. 27 (a) and (b), whereas Fig. 27(c-f) demonstrates the previously discussed density depletion for several values of the relative interaction strength.

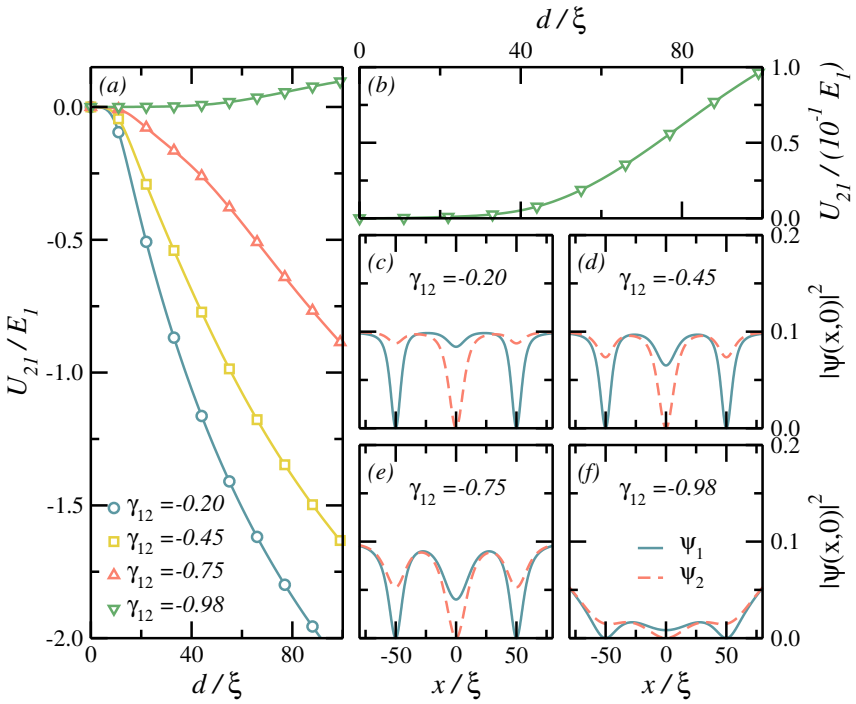

Figure 27 – (a) Total energy for three vortices configuration U_{21}, characterizing a binary system with $M_{12} = 2$. The vortex in the second component is fixed in the center of the mesh, whereas vortices in the first component are placed at symmetric positions separated by distance d. (b) A magnification of the particular case γ_{12}=-0.98 shows that in the favored configuration, the two vortices in the first component are located on top of each other, and on top of the vortex in the second component. (c-f) Occupation number density of both components, considering vortices separated by 100 ξ, for all cases considered in (a), where the solid (dashed) line stands for the first (second) component.

From Fig. 27(a), one sees that for low values of $|\gamma_{12}|$ the energy is a monotonically decreasing function with the distance d, indicating repulsion between the vortices in the same component. However, this behavior is completely changed for $\gamma_{12} = -0.98$, where the total energy turns into a monotonically increasing function, allowing vortices of the same component to occupy the same position, thus, forming a giant vortex. Indeed, as one can see in the magnification of this result in Fig. 27(b), the energy minimum corresponds to a vanishing distance between the vortices in the same component. At this point, it is evident that the depletion effect is the main cause for the behavioral change of the effective interaction. In fact, the strong coupling between the components makes the intra-component repulsive contribution less relevant than the inter-component vortex-vortex interaction, and the attractive effective interaction is achieved for every distance d. In Fig. 27(c-f), the occupation number density for vortices separated by 100 ξ shows the depletion

effect, where depletions become more akin to vortices for higher values of inter-component particle coupling $|\gamma_{12}|$. It is noticed that vortices become larger when γ_{12} is increased, causing the vortex strong overlap illustrated in Fig 27(f). This effect depends on the inter-component particle coupling and vortex density.

Before going into further details concerning vortex core, let us first analyze how the effective interaction between vortices changes from repulsive to attractive, by considering intermediate values of γ_{12} between $\gamma_{12} = -0.75$ and $\gamma_{12} = -0.98$. We have found that, for $\gamma_{12} = -0.90$ and $\gamma_{12} = -0.92$, as illustrated in Fig. 28(a), the energy curves still have repulsive characters, but they exhibit shoulders at finite distances, which could indicate the formation of non-triangular lattices in these minima of the interaction potential, despite the overall repulsive behavior. In Fig. 28(b), by setting $\gamma_{12} = -0.95$, we have obtained a total energy which exhibits a non-monotonic behavior and acquires a clear minimum at finite inter-vortex distance. This strongly indicates that the presence of a vortex in one component can cause the formation of a bound state of two vortices (dimer) in the heavier component, illustrated in Fig. 28(c). This results corroborates the states obtained in numerical experiments of Ref. (KUOPANPORTTI; HUHTAMÄKI; MÖTTÖNEN, 2012), where the Abrikosov lattice of vortex dimers in one component, sitting on single vortices in the other, was found in a binary mixture.

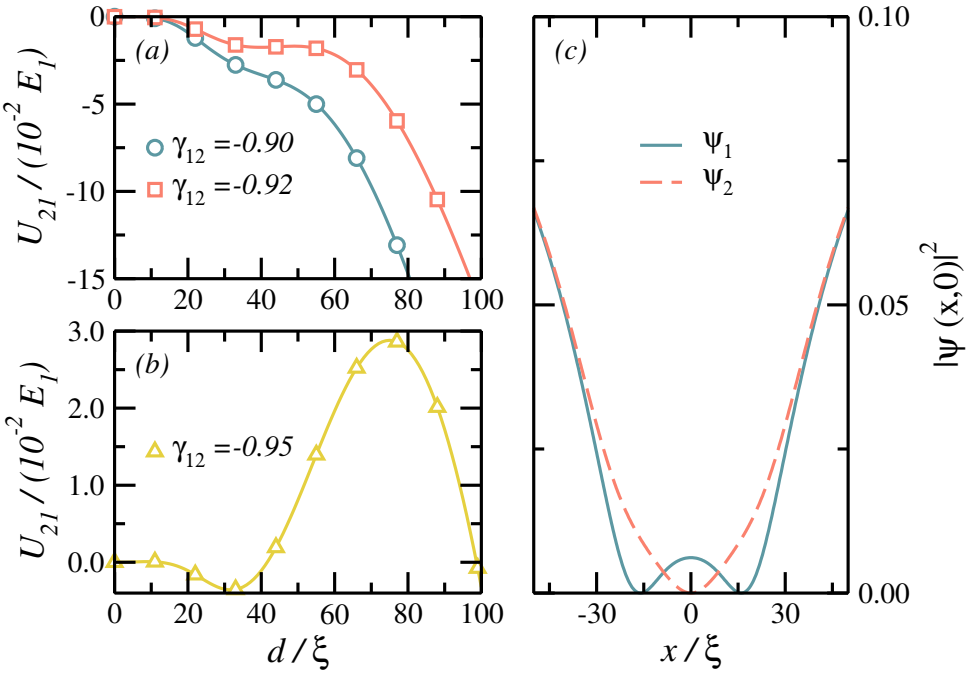

Figure 28 – (a) Total energy of a three vortex structure in a two-component BEC, for $\gamma_{12} = -0.90$ (blue circles) and -0.92 (red squares). The curve bumps may lead to non-triangular lattices, despite the overall repulsive behavior. (b) Particular case of a triple-vortex structure with $\gamma_{12} = -0.95$. The minimum far from the origin allows for the formation of dimers for specific vortex densities. (c) Dimer configuration profile for $\gamma_{12} = -0.95$.

In addition to effects caused in the vortex-vortex interactions, leading to different lattice conformations, the depletion effect also leads to formation of vortices with different core sizes according to the choice of the γ_{12} parameter. Actually, this was pointed out before in Fig. 27(c-f), where more negative values of γ_{12} result in vortices with larger core sizes. To investigate this dependence, in Fig. 29, by setting a vortex in only one of the two components, the vortex core radius was measured for different values of inter-component coupling, between $\gamma_{12} = -0.90$ and $\gamma_{12} = 0.90$. This was done by measuring the distance between the center of the vortex and the point at which the order parameter decreases by half of its long-range convergence value.

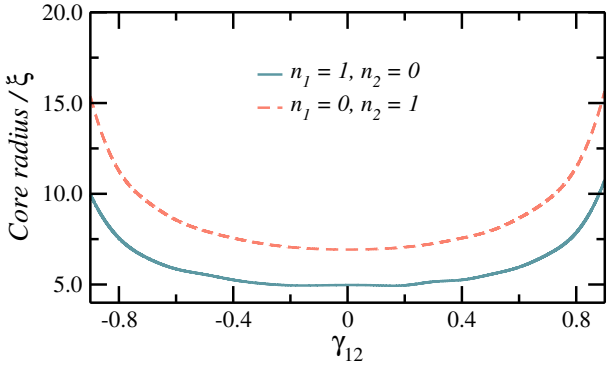

Figure 29 – Vortex core size as a function of the inter-component coupling, for $M_{12} = 2.0$. The blue solid line (red dashed line) represents the core radius of a vortex in the first (second) component.

Since the components have different mass, in Fig. 29 we investigated this effect for vortices in both components, where the core size for a first(second)-component vortex is presented by the solid (dashed) line. It is observed that the more the two components are coupled, the larger the vortex radii will be. This effect actually comes from the depletion originated by the vortex depletion which contributes to an increased vortex size. For both components, this behavior is qualitatively the same, suggesting that the different mass causes simply a shift between two curves.

Let us at this point address the question of how realistic the present predictions are from an experimental point of view. For example, a two species BEC with a tunable interspecies interaction has already been produced from the mixture of ^{87}Rb and ^{41}K, for which one has $M_{12} \approx 2.1$ (THALHAMMER et al., 2008). In that particular study, a Feshbach resonance around a magnetic field of $B \approx 79$G allows for tuning a_{12} from positive to negative values. For example, for 80.7G $a_{12} \approx -185a_0$ is reported, with a_0 the Bohr radius. This clearly opens up the possibility of obtaining the appropriate negative values of γ_{12} needed to experimentally observe the predicted vortex states. We also remark that, for a ^{87}Rb-^{85}Rb mixture, tunability of the interspecies interaction has already been used to probe various mean-field regimes such as spatial separation as well as the formation of long lived droplets (see Ref. (PAPP; PINO; WIEMAN, 2008)).

2.4.2 Vortex dimers and trimers in coherently coupled BECs

In this subsection, we consider the presence of an internal coherent coupling of the Rabi type between the different components. In order to do so, an extra term should be added to the energy density functional, as pointed out in Sec. 2.3. For a system with N_c components, the Rabi contribution in Eq. (2.9) can be rewritten in the form

$$-2\sum_{i}^{N_c}\sum_{j>i}^{N_c}\omega_{ij}|\psi_i||\psi_j|\cos(\theta_i-\theta_j).$$

If the signs of ω_{ij} coefficients are all positive, the ground state energy is achieved when all the phases θ_i are the same. Recalling that the phases fix the position of the vortices, this means that vortices of different components would overlap, featuring an attractive potential. On the other hand, by setting positive values for the contact coupling γ_{ij}, a repulsive inter-component vortex-vortex interaction emerges. The balance between these two types of interaction can lead to molecular conformations of vortices. Unlike the previous case, these bound states do not arise due to the mass difference between the components, but due to the competing interactions induced by the Rabi contribution. To illustrate the above argument, consider, for instance, the case with two components with equal masses $M_{1\alpha}=1$, with one vortex in each component.

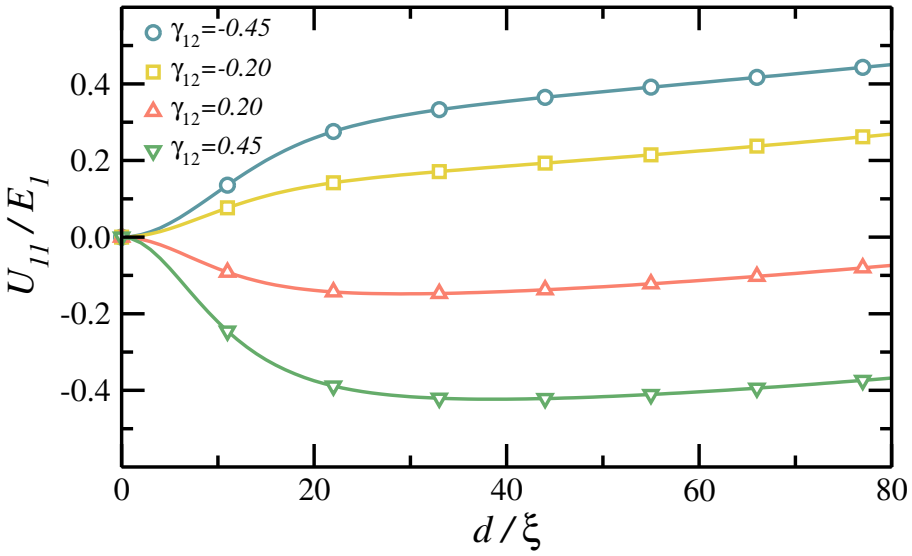

Figure 30 – Two-vortex inter-component interaction potential in the case of competing contact and Rabi coupling, $\omega = 2.1\times10^{-5}$ and $M_{12}=1$, for several values of γ_{12}.

As illustrated in Fig. 30, a vortex dimer may be formed in the case of a short range repulsive and long range attractive inter-component potential, as observed for positive values of γ_{ij}, where a minimum of interaction energy is found at finite inter-vortex distance due to a competition between two types of inter-component interaction. On the other hand, negative values of γ_{12} lead to an extended attractive interaction in the long range.

Let us now address the question of the formation of vortex trimers in a three-component condensate, i.e., bound states consisting of three vortices. In an attempt to reduce the excessive number of parameters, we shall consider the case with $\omega_{12} = \omega_{13} = \omega_{23} = \omega$ and $\gamma_{12} = \gamma_{13} = \gamma_{23} = \gamma$. This choice also helps in finding the minimum energy configuration, since in this case, for symmetry reasons, it is expected that the three vortices are arranged equidistantly. Thus, we manually placed the vortices at the vertices of an equilateral triangle of side d, whose loci then read $S_1 = (0, \sqrt{3}d/4)$, $S_2 = (-d/2, -\sqrt{3}d/4)$ and $S_3 = (d/2, -\sqrt{3}d/4)$. This is illustrated in Fig. 31, where contour plots of the densities of the three components are shown. Notice the presence of the depletion effect in this case as well. Subsequently, we investigated the minimum energy conformation as a function of d for several values of ω.

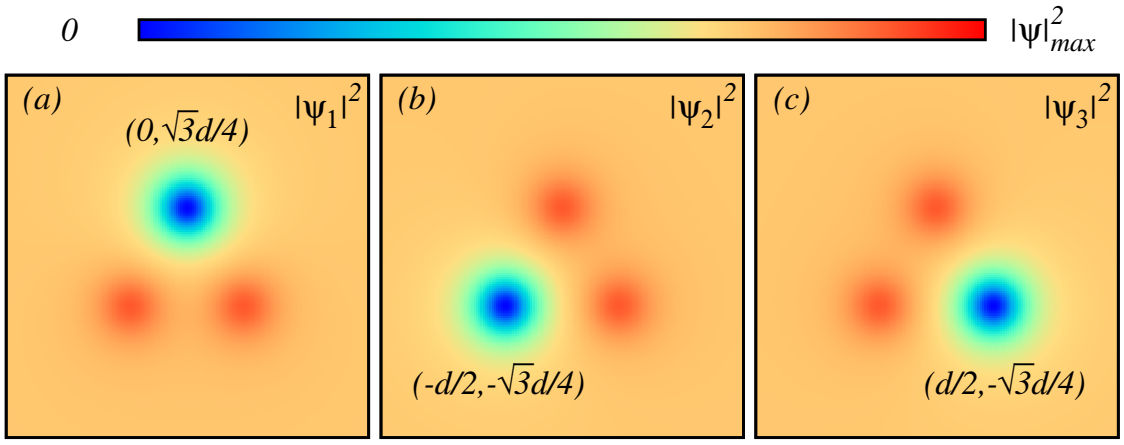

Figure 31 – The occupation number density contour plots of: (a) first component with a vortex positioned at $(0, \sqrt{3}d/4)$; (b) second component with a vortex positioned at $(-d/2, -\sqrt{3}d/4)$ and ; (c) third component with a vortex positioned at $(d/2, -\sqrt{3}d/4)$.

In Fig. 32(a), where we considered $\gamma = 0.45$, there is indeed a finite value d_{min} of the triangle side that minimizes the interaction energy U_{111}. Moreover, Fig. 32 (b) and (c) display power law dependencies of d_{min} in ω, for $\gamma = 0.45$ and $\gamma = 0.60$, respectively, which explains the vortex trimer configurations observed e.g. in Fig. 3 of Ref. (ETO; NITTA, 2012). Despite the fact that the exponents are quite similar in the two considered cases, they should depend on both γ and number of particles N. Indeed, considering the extreme case where γ vanishes, the inflection point of the vortex interaction should always be at $d = 0$ for any value of ω, leading to a vanishing exponent in the power law dependence $d_{min}(\gamma)$.

Since the geometry was imposed from the beginning by setting the vortices at the vertices of the equilateral triangle, the existence of a value d_{min} which minimizes the total energy does not guarantee that this configuration corresponds to the ground state.

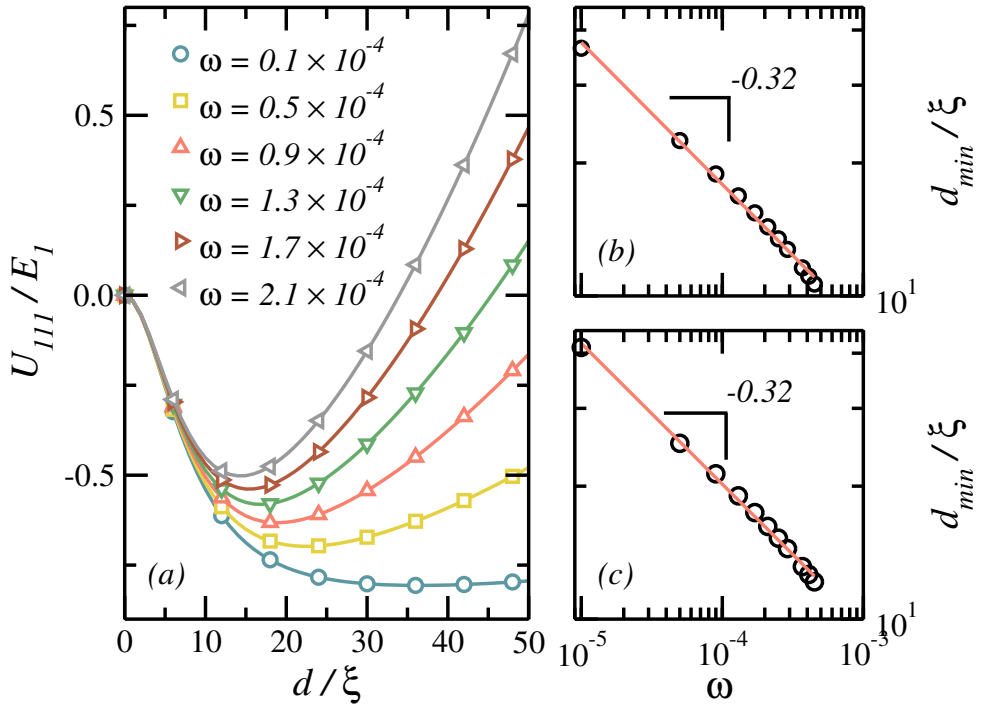

Figure 32 – (a) Total energy U_{111}, for the equilateral triangle vortex configuration as a function of the side d for $\gamma = 0.45$ and for several values of ω. (b) Plot of the optimal side of the equilateral vortex triangle against ω for $\gamma = 0.45$. The red line represents a power law with exponent -0.3214 and coefficient 0.9265. (c) Same as (b) but for $\gamma = 0.60$. The red line represents a power law with exponent -0.3186 and coefficient 1.0746.

In order to allow for different configurations and thereby check if the equilateral triangle is really a minimum of the energy, we have allowed for different positions of the vertex S_1, while keeping S_2 and S_3 fixed for $\omega = 1.7 \times 10^{-4}$ and $\gamma = 0.45$. As can be seen from Fig. 33, the equilateral triangle configuration turns out to be stable, corresponding to at least a local minimum of the interaction energy.

Although not very common, there are other ways to obtain bound vortex states which do not arise from a competition between different types of interaction. In fact, it is also possible to obtain dimers and trimers exclusively from Rabi coupling in condensates with at least three components. These vortex states arise from frustration between the phase locking tendencies. As it was mentioned previously, a set of positive Rabi frequencies $\omega_{12} = \omega_{13} = \omega_{23} = \omega > 0$ would lead to $\theta_1 = \theta_2 = \theta_3$ as a minimum of the energy, causing the same spatial occupation for all three vortices. However, by assuming, for example, $\omega_{12} = \omega_{13} = -\omega_{23} = \omega$, it is not possible to satisfy the minimization energy condition $\cos(\phi_1 - \phi_2) = \cos(\phi_1 - \phi_3) = 1$ and $\cos(\phi_2 - \phi_3) = -1$ simultaneously, which characterizes a frustrated system (ORLOVA et al., 2013; GARAUD2011; CARLSTRÖM; BABAEV, 2011; STANEV; TEŠANOVIĆ, 2010; LIN; HU, 2012).

Since the frustration phenomenon arises basically from the problem of min-

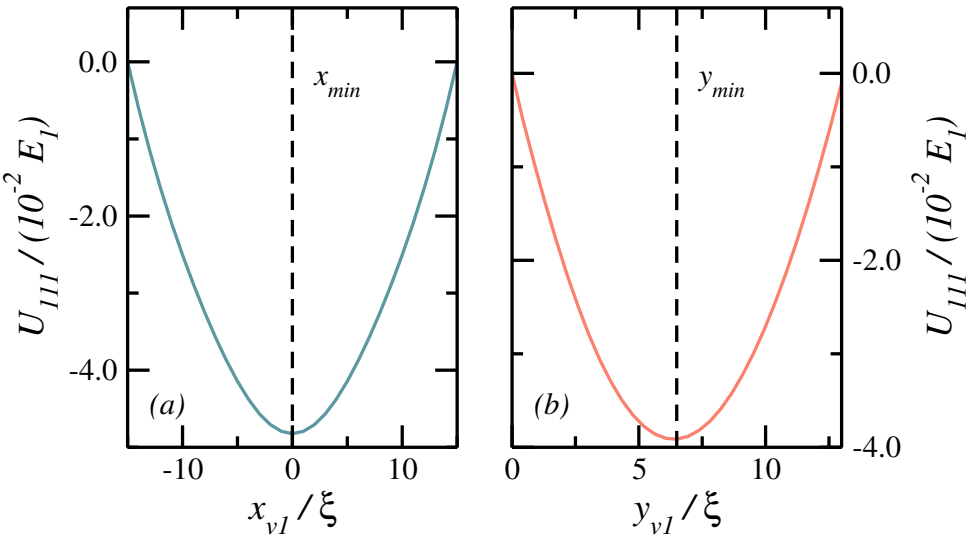

Figure 33 – (a) Total energy U_{111} as a function of the displacement of the first component vortex x_{v1} from S_1 position in the x direction. (b) Total energy U_{111} as a function of the displacement of the first component vortex y_{v1} from the origin in the y direction. For both cases, we have considered $\gamma = 0.45$ and $\omega = 1.7 \times 10^{-4}$. The vertical dashed line represents the coordinates of first component vortex for the minimum energy equilateral triangle configuration.

imizing the total energy with respect to the order parameter phases, we must redefine our ansatz, adding extra phases to our order parameters in order to account for the phase tendencies which minimize the energy. Thus, by assuming an ansatz of the form $\psi_n(x,y) = \sqrt{N}e^{i\theta_n}e^{-i\phi_n}f_n(x,y)$, the consequences of choosing Rabi frequencies which lead to a frustrated system were investigated for $\omega_{12} = \omega_{13} = -\omega_{23} = \omega$ and $\gamma_{12} = \gamma_{13} = \gamma_{23} = 0$, where we have considered $\phi_1 = \phi_2 = 0$ and several values for ϕ_3.

In Fig. 34(a), we pinned vortices of the first and second components on top of each other, in the center of the mesh and displaced the vortex of the third component at distance d from the origin. This procedure was made for different values of phase ϕ_3. The obtained results show a potential that suggests the formation of a bound vortex state, with the third component vortex outside the origin, for $\phi_3 = 0$, where the potential minimum is at $d \approx 4\xi$. This conformation arises from the competition between the attraction with the vortex of the first component and the repulsion with the vortex of the second component. By symmetry, the same result should also appear for $\phi = \pi$. This configuration has the lowest energy among the other investigated cases, however, we can not guarantee that this conformation is the ground state. Actually, finding the ground state conformation would require the variation of all three extra phases and also other vortices positions in the grid, which is very expensive computationally and is left for future investigation. Nevertheless, these results are sufficient to ensure that vortex molecules are stable states. In Fig. 34(b), we show that increasing the Rabi coupling makes the frustration effect even more robust and leads to a deeper minimum in the interaction potential.

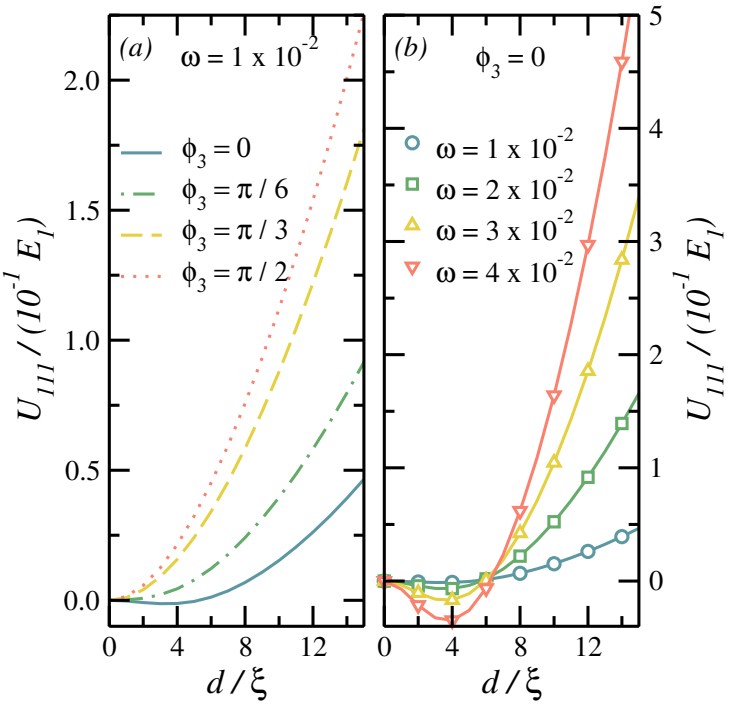

Figure 34 – (a) Total energy U_{111}, with vortices of the first and second components pinned in the center of the mesh, as a function of the third component vortex distance d from the origin, for different values of the third component extra phase ϕ_3: 0 (solid blue line), $\pi/6$ (green dashed dotted line), $\pi/3$ (yellow dashed line) and $\pi/2$ (red dotted line), with $\omega_{12} = \omega_{13} = -\omega_{23} = 1 \times 10^{-2}$. (b) Total energy U_{111} for the same conformation of (a), keeping $\phi_3 = 0$ and assuming different values of ω: $\omega = 1 \times 10^{-2}$ (blue circles), $\omega = 2 \times 10^{-2}$ (green squares), $\omega = 3 \times 10^{-2}$ (yellow upward triangles) and $\omega = 4 \times 10^{-2}$ (red downward triangles).

In view of the present predictions concerning Rabi coupled BECs, it becomes important to consider the possibilities of experimental realization of adequate samples. In that respect, we focus on the phenomena of interest, namely Rabi coupling and homogeneous confinement. They have both already been experimentally achieved with ^{87}Rb. Before we turn to the particular experimental setups, we recall that in our calculations the parameter governing the Rabi coupling is $\omega = w\bar{\rho}_1/\mathcal{E}_1$, where $w = \hbar\Omega$ relates the Rabi energy w to the Rabi oscillation frequency Ω.

We first consider a recent study in Ref. (CHOMAZ et al., 2015), demonstrating long-range coherence in quasi-two-dimensional Bose gases. There, two-dimensional densities of about a few hundred ^{87}Rb-atoms per square micrometer are achieved and combined with harmonic trapping in the third direction whose frequency ν_z ranges from 350 up to 1500 Hz. Moreover, for ^{87}Rb, the (three-dimensional) s-wave scattering length is $a_s \approx 100a_0$, with a_0 the Bohr radius. For the values of the Rabi couplings we turn to Ref. (MATTHEWS et al., 1999b), where Rabi oscillation frequencies of the order $2\pi \times 10^2 s^{-1}$ have been realized. We estimate the Rabi coupling parameter ω by calculating $E_1 = \xi^2\mathcal{E}_1$ for these values of

the particle density and Rabi frequencies, to arrive at $\omega = \frac{2m_1\Omega}{\hbar\bar{\rho}_1} = \frac{2}{a^2_{\mathrm{R}abi}\bar{\rho}_1} \approx 1.7 \times 10^{-2}$, where we have associated a length $a_{\mathrm{R}abi} = \sqrt{\hbar/m_1\Omega}$ with the Rabi oscillation. This value is already higher than ones needed for the effects discussed in this manuscript.

It is also possible to improve the estimates of the actual experimental values of the coherent coupling by including the effect of the transversal harmonic trapping, rendering the calculation more realistic. Indeed, in order to obtain typical values of ω in quasi-two-dimensional systems, one should correct the s-wave scattering parameter g for the freezing of the third dimension. This is done by dividing the three-dimensional $g_{3D} = 4\pi\hbar^2 a_s/m_1$ by $\sqrt{2\pi}a_z$, with a_z being the oscillator length in the third dimension (FISCHER, 2006). If one then associates the energy E_1 with the contact interaction energy $g\bar{\rho}_1$, a slightly different expression for the coherence parameter emerges $\omega = \frac{1}{a^2_{\mathrm{R}abi}\bar{\rho}_1}\frac{a_z}{\sqrt{8\pi}a_s} \approx 1 \times 10^{-1}$. Notice that, besides the fact that this value of ω is even higher in quasi-two-dimensional traps, this expression allows to identify the trap frequency in the third dimension, in addition to the Rabi oscillation frequency and the particle density, as tuning knobs for studying the effects of coherent coupling in multi-component BECs.

Part II

Superconductors

3 Vortex characterization in single- and two-gap superconducting bulk and films

The vortex structure is investigated for single-gap bulk superconductors outside the London regime. The order parameter phase fixing allow us to compute the magnetic and the Cooper pairs density profiles of isolated vortices for any set of parameters, including in type-I superconducting regime. With our approach, vortex and magnetic core sizes, as well as the magnetic field inside the vortex core, can be estimated as a function of system parameters. Signatures of type-I/type-II phase transition are observed and analytical expressions supposed to be valid only in London regime are used to describe the magnetic behavior of single-band superconductors. The approach is also extended to finite-thickness superconducting samples, where properties of vortices and giant-vortices were also investigated. Within the proper performed fitting functions we provide analytical expressions to describe the magnetic distribution and the Cooper pairs density of vortices and giant-vortices in films with different thickness. A comparison with bulk results is performed in the limit of very thin films, where the superconducting films are supposed to behave as bulk samples, but with an effective Ginzburg-Landau parameter, $\kappa_{eff} \sim \kappa^2/d$. On the opposite limit, we were also able to estimate the point at which all vortex features observed for bulks are recovered when the film is made thicker.

3.1 Introduction

A detailed understanding of any physical phenomenon requires the full characterization of its relevant composing elements. In this context, vortices play important role in many distinct physics topics, such as: Neutron stars (Baldo, M.; Saperstein, E. E.; Tolokonnikov, S. V., 2007), Bose-Einstein condensates (FETTER, 2009b), Graphene (BRITO; NAZARENO, 2012), superfluid liquid helium (YARMCHUK; GORDON; PACKARD, 1979), plasmas (BUNEMAN, 1958), turbulent classical fluids (TERHAAR; OBERLEITHNER; PASCHEREIT, 2015), ganular flow (FORTERRE; POULIQUEN, 2001) strongly interacting Fermi gases (ZWIERLEIN et al., 2005) and superconductors(ABRIKOSOV, 1957; ESSMANN; TRÄUBLE, 1967; ABRIKOSOV, 2004). As major components of both superfluidity and superconductivity, quantized vortices have been widely investigated since their first prediction in superfluid liquid helium (ONSAGER, 1949). Since then, most of efforts have focused on understanding the formation of vortex lattices (ABRIKOSOV, 1957; HARADA et al., 1992; SCHWEIGERT; PEETERS; DEO, 1998; ABRIKOSOV, 2004;

PALACIOS, 1998; MILOŠEVIĆ; PEETERS, 2003; CABRAL; BAELUS; PEETERS, 2004; KARAPETROV et al., 2006; KOMENDOVÁ; MILOŠEVIĆ; PEETERS, 2013; MENG et al., 2014) as well as their dynamics (HARADA et al., 1992; HARADA et al., 1996; WALLRAFF et al., 2003; PLOURDE et al., 2000; BUGOSLAVSKY et al., 2001), where the vortex-vortex interaction play an important role. Thus, even with the high interdisciplinarity, it is not surprising that some basic aspects such as the internal vortex structure have not been fully characterized nor understood. In fact, even for single-gap bulk superconductors, some vortex features are known only in very restricted regime, where the Ginzburg-Landau parameter κ is assumed to be extremely large and the finite size effect of the vortex core is neglected (TINKHAM, 1975; LONDON, 1937; CLEM, 1975). Moreover, even within this limit, only the asymptotic behavior of vortex properties can be derived analytically (TINKHAM, 1975).

Since Abrikosov's prediction of the mixed superconducting state(ABRIKOSOV, 1957), superconductors have been separated into two distinct classes, determined by the value of the Ginzburg-Landau parameter κ. In type-I superconductivity ($\kappa < 1/\sqrt{2}$), a bulk sample can not sustain a mixed state, since vortices attract each other, destroying the superconducting state abruptly. On the other hand, in type-II regime ($\kappa > 1/\sqrt{2}$), vortices repel each other, resulting in a triangular vortex lattice. However, such differentiation has proven to be only a limit of a more complex case, where the finite size of the sample is taken into account, as pointed out by Tinkham (TINKHAM, 1963; FETTER; HOHENBERG, 1967; TINKHAM, 1964). In fact, in superconducting films, even in type-I regime, where the vortex-vortex interaction is supposed to be monotonically attractive, vortices might experience a repulsive interaction due to the stray magnetic field interaction outside the sample (PEARL, 1964; IRZ; RYZHOV; TAREYEVA, 1995), resulting in a monotonically repulsive or even non-monotonic vortex-vortex interaction (BRANDT; DAS, 2011; DANTAS et al., a).

With the recent progress made in imaging techniques, vortex lattices, as well as the internal magnetic structure of vortices, have been widely investigated experimentally(KIRTLEY et al., 1996; ESKILDSEN et al., 2002; VOLODIN et al., 2002; VINNIKOV et al., 2003; HESS et al., 1990), also allowing the visualization of mixed states in Type-I finite-thickness superconducting samples (BRANDT; DAS, 2011; GE et al., 2013), where vortices with larger cores and carrying more than a quantum of flux can be observed. Theses giant-vortex states result from the overlaping of single-quantized vortices and are signatures of the non-monotonic vortex-vortex interaction. In this limit, where vortices are no longer governed by London equations, the ground-state phase diagram of vortex lattices is much richer than lattices found in bulk superconductors, with triangular, square and honeycomb lattices, as well as vortex stripes and giant-vortices(LASHER, 1967; SWEENEY; GELFAND, 2010; GLADILIN et al., 2015). Unfortunately, superconductors with finite thickness require the solution of three dimensional Ginzburg-Landau equations, which is

computationally very expensive. However, for very thin or thick samples, solutions can be achieved under the two-dimensional approximation, where the supercurrent is assumed to be uniform over the thickness direction. Yet, so far, vortex and giant-vortex structures have not been fully characterized even in these limits.

Also, the discovery of multi-band superconducting materials(BOUQUET et al., 2001; TEAGUE et al., 2011; KIM et al., 2011) has opened up even more this field, increasing the gap between experimental achievements and the theoretical knowledge. Indeed, such superconductors are far from being just a trivial extension of a single band superconductor case and there is still much information to be addressed concerning the vortex matter, like for example, their magnetic vortex structures and vortex core sizes, as well as their interactions and lattice conformations.

In the present work, by fixing the vortex phase, we have derived constrained Ginzburg-Landau equations, which allow us to control vortex winding numbers and positions. In this approach, no applied magnetic field is considered and all vortex singularities shall emerge naturally from the chosen condensate phase. This provide us the possibility of investigating isolated vortex features outside the London limit and in the absence of boundary effects and neighboring vortices. This method has been successfully used to describe the vortex-vortex interaction in single and double-gap superconductors and also explained vortex dimers and trimers conformations in multi-component Bose-Einstein condensates (CHAVES et al., 2011a; CHAVES et al., 2011b; DANTAS et al., 2015). Within this scheme, Cooper pairs density, magnetic profiles and current density distributions for a single isolated vortex are calculated for the single-gap and double-gap bulk superconductors without any imposed restriction in Ginzburg-Landau parameters spectrum. For both cases, finite thickness superconducting films are also considered, where the restrictions on the film thickness are extrapolated outside the range of the validity of uniform current density approximation in order to estimate, at least qualitatively, some vortex features for single-band superconducting films. As we shall see, all vortices features for bulk superconductors are recovered when the sample is made thicker. Since giant vortices are also predicted for superconductors with intermediate thickness, we also investigate vortices with winding number greater than unity.

3.2 Vortex structure

3.2.1 On bulk samples

3.2.1.1 Magnetic structure

Because Ginzburg-Landau equations are very difficult to solve analytically, approximations must be performed in order to qualitatively describe vortex structures. For instance, neglecting the vortex core and assuming an uniform and constant order

parameter reduces Ginzburg-Landau approach to

$$\frac{1}{\lambda^2}\vec{\nabla}\times\vec{\nabla}\times\vec{h}+\vec{h}=\Phi_0\delta(x)\delta(y)\hat{z}, \tag{3.1}$$

where the right side was artificially introduced in order to account for the presence of singularities in the condensate. The description lies in London's equation regime, supposed to be valid only when $\lambda >> \xi$. Losing information about the vortex core is a price to be paid when an analytical approach is required. Here, the consequences of London's approach are carefully reviewed for bulk samples. In order to do so, it is worth to notice that the gauge invariance is preserved and thus, physical properties might not change with the gauge choice. It is therefore appropriate to restrict ourselves to gauges that simplifies the equation, such as the London's one, $\vec{\nabla}\cdot\vec{A}=0$, where Eq. 3.1 becomes

$$\nabla^2\vec{h}-\frac{1}{\lambda^2}\vec{h}=-\frac{1}{\lambda^2}\Phi_0\delta(x)\delta(y)\hat{z}. \tag{3.2}$$

Taking advantage of vortex circular symmetry, this equation may be solved through Hankel's transform and its solution written as a function of zeroth order Hankel's function, K_0 ,

$$h(r)=\frac{\Phi_0}{2\pi\lambda^2}K_0\left(\frac{r}{\lambda}\right). \tag{3.3}$$

Except for the inner core space region $r\leq\xi$, the magnetic field must also obey

$$h(r)\approx\frac{\Phi_0}{2\pi\lambda^2}\left[\ln\left(\frac{\lambda}{r}\right)+0.12\right],\quad \text{for } \xi\ll r\ll\lambda \tag{3.4a}$$

$$h(r)\approx\frac{\Phi_0}{2\pi\lambda^2}\left(\frac{\pi}{2}\frac{\lambda}{r}\right)^{1/2}e^{-r/\lambda},\quad \text{for } r\to\infty \tag{3.4b}$$

as they perfectly fit the exact solution in their respective limits. In what follows, we may recall these functions in order to fit our numerical results obtained from the computational solution of the Ginzburg-Landau equation for single-vortex state.

3.2.1.2 Cooper pairs

Describing the Cooper pairs density distribution around the vortex core requires a different approach, where the first and second GL equation must be simultaneously satisfied. In general, the zero field approximation is taken into account and the solution assumed to be approximately described by $|\Psi|\propto\tanh(\nu r/\xi)$, where $\nu\approx 1$. However, the rigor of such assumption may be questionable for low values of GL parameter κ. Therefore, instead of restricting the Ginzburg-Landau parameter κ to extremely type-II materials, limits must be imposed in order to at least lead us to the expected asymptotic behavior. In such approach, the single vortex structure is modeled by the ansatz $\Psi(r)=e^{i\theta}f(r)$, which naturally fixes the gauge choice to,

$$\vec{A}(\vec{r})=\left[\frac{1}{r}\int_0^r r'h(r')dr'\right]\hat{\theta}. \tag{3.5}$$

Afterwards, GL equations are reduced to

$$f - f^3 - \xi^2 \left[\left(\frac{1}{r} - \frac{2\pi A}{\Phi_0} \right)^2 f - \frac{1}{r} \frac{d}{dr} \left(r \frac{df}{dr} \right) \right] = 0, \tag{3.6a}$$

$$J = -\frac{e^* \hbar}{m} \frac{\alpha}{\beta} f^2 \left(\frac{1}{r} - \frac{2\pi A}{\Phi_0} \right). \tag{3.6b}$$

Notice that, taking the curl of Eq. (3.6b) and then mixing it with the Maxwell equation, $\vec{\nabla} \times \vec{h} = 4\pi \vec{J}/c$, leads to London's equation for single-vortex structure. Unfortunately, this set of coupled equations can only be solved numerically. Still, it is possible to restrict ourselves to the core behavior, $r \to 0$ and find an approximate solution,

$$f \propto r \left[1 - \frac{r^2}{8\xi^2} \left(1 + \frac{h(0)}{H_{c2}} \right) \right]. \tag{3.7}$$

An sketch of the current density and the order parameter together with the magnetic field distribution of the vortex structure are respectively illustrated in Fig. 35 (a) and (b)

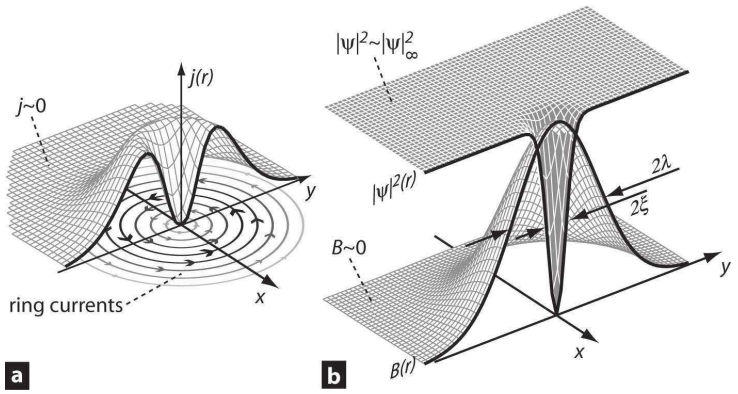

Figure 35 – (a) Sketch of the circulating current density distribution around the vortex core and (b) Cooper pair density and magnetic profiles of single quantized vortex. This figure was retrieved from (MOSHCHALKOV; FRITZSCHE, 2011).

3.2.2 On films

Properties of thin superconducting films highly contrast with those exhibited by bulk superconducting samples. In fact, theory of superconducting films represents an wide branch of superconductivity theory and has been investigated for more than half a century. Among the most important properties, the substantial increase of critical parameters, such as the critical magnetic field and critical density current makes thin films one of the best environments for commercial applications of superconductors. Also, it can be used to model high-temperature superconductors, as pointed out by Clem (CLEM, 1991).

The quantum confinement provided by finite size of superconducting sample has deep consequences on vortex structure. In fact, in such systems, screening current densities may be regarded as uniform along the outplane direction, so vortices can not bend as in normal superconducting sample. Because current densities are almost constant over the thickness, in the limit of extremely thin films, where the thickness δ is much smaller than the penetration depth λ, screening currents can be averaged over the thickness direction, so that the second GL equation for a single vortex structure becomes

$$\vec{\nabla} \times \vec{\nabla} \times \vec{A} = \delta \frac{\delta(z)}{\lambda^2} \left[\frac{\Phi_0}{2\pi r} \hat{\theta} - \vec{A} \right], \quad \text{for } |z| < \delta/2 \tag{3.8a}$$

$$\vec{\nabla} \times \vec{\nabla} \times \vec{A} = 0, \quad \text{for } |z| > \delta/2. \tag{3.8b}$$

This results in a larger effective penetration depth Λ, that may be approximated to $\Lambda \approx 2\lambda^2/\delta$. This is similar to redefine the two-dimensional density sheet of superconducting electrons as $n_{2D} = \delta n_{3D}$ (CLEM, 1991). Using the circular symmetry, $\vec{A}(r, \theta, z) = A_\theta(r, z)\hat{\theta}$, the solution may be achieved through a Hankel transform, (FETTER; HOHENBERG, 1967), yelding

$$A_\theta(r, z) = \frac{\Phi_0}{2\pi} \int_0^\infty dq \frac{J_1(qr)e^{-q|z|}}{1 + q\Lambda}, \tag{3.9}$$

where the symmetry over the outplane direction was implemented and J_1 represents the Bessel function. Replacing it on the density current expression, the result is summarized into

$$J_\theta(r) = c\frac{\Phi_0}{8\pi\Lambda^2} \left[H_1(r/\Lambda) - Y_1(r/\Lambda) - 2/\pi \right], \tag{3.10}$$

where H_1 in the Struve function, whereas Y_1 stands for Bessel function. The asymptotic behavior of current density is

$$j(r) = \frac{\Phi_0}{4\pi^2\Lambda} \frac{c}{r} \quad \text{for } \xi < r \ll \Lambda, \tag{3.11a}$$

$$j(r) = \frac{\Phi_0}{4\pi^2} \frac{c}{r^2} \quad \text{for } r \gg \Lambda. \tag{3.11b}$$

In order to calculate the associated magnetic field, it is useful to return to London's approach, since the curl of the vector potential given by Eq. 3.9 is not everywhere convergent when $z = 0$. Thus, neglecting the vortex core radius, the field may be derived from

$$\vec{h} + \frac{4\pi\lambda^2}{c} \vec{\nabla} \times \vec{J} = \Phi_0 \delta r \hat{z}. \tag{3.12}$$

At long-range approach, the solution is given by

$$h_z(\vec{r}) \approx \frac{\Phi_0}{2\pi} \frac{\Lambda}{r^3}. \tag{3.13}$$

These results greatly differ from those exhibited in Bulk samples and lead to remarkable behavior of the vortex-vortex interaction, which is derived from the current density

integration for a double vortex structure (PEARL, 1964; IRZ; RYZHOV; TAREYEVA, 1995). In fact, the energy associated with the double vortex structure is under the Maxwell-London equation, is given by

$$V_{12} = \frac{\Phi_0}{8\pi\Lambda}\left[H_0(r_{12}/\Lambda) - Y_0(r_{12}/\Lambda)\right], \tag{3.14}$$

which falls of as $1/r$ at the long-range limit, where $r \gg \Lambda$. As we shall see further in the next chapter, this long-range repulsive behavior makes richer the phase diagram of vortex lattices when compared to bulk samples. Before, however, we shall first examine the vortex inner structure in both bulk and film samples.

3.3 Theoretical Model

The superconducting state is well described within the Ginzburg-Landau phenomenological formalism extended from the Landau second-order phase transitions theory. In our approach, we start from the dimensionless GL energy functional for single-gap bulk superconductors

$$\begin{aligned} E = \frac{H_c^2}{4\pi}\int dV\Bigg[&\left|(\vec{\nabla} - i\vec{A})\Psi\right|^2 - \left(1 - \frac{T}{T_C}\right)|\Psi|^2 \\ &+\frac{1}{2}|\Psi|^4 + \kappa^2\left|\vec{\nabla}\times\vec{A}\right|^2\Bigg], \end{aligned} \tag{3.15}$$

where κ is the Ginzburg-Landau parameter. Here, distances are scaled to the coherence length $\xi = \hbar/\sqrt{-2m\alpha}$, order parameter to its convergence value $\sqrt{-\alpha/\beta}$, and magnetic field to H_{c2}.

In order to fix vortex position and winding number during the simulation, we properly set the vortex phase before minimizing the energy density. The pinning process for a single-vortex structure is achieved by considering the ansatz $\Psi = e^{in\theta}f(x,y)$, where $e^{in\theta}$ stands for the order parameter phase of single isolated vortex and $f(x,y)$ for the order parameter magnitude, which provide us the information about the local Cooper pairs density in the whole space. In order to keep the method as general as possible, we shall not restrict ourselves to cases where the system has circular symmetry. Therefore, Cartesian coordinates shall be used, where the order parameter phase is expressed as

$$e^{in\theta} = \left(\frac{x+iy}{x-iy}\right)^{n/2}. \tag{3.16}$$

Here, $\vec{r} = (x,y)$ is the in-plane position vector with origin at the vortex core. Minimizing the energy density functional with respect to $f(x,y)$ and $\vec{A}$ leads to the set of constrained Ginzburg-Landau equations for a single vortex conformation

$$\begin{aligned} \nabla^2 f - &\left[\overline{X}^2 + \overline{Y}^2 + 2\left(A_x\overline{Y} - A_y\overline{X}\right) + \vec{A}^2\right] f \\ &+ (\chi - f^2)f = 0. \end{aligned} \tag{3.17a}$$

$$-\kappa^2\vec{\nabla}\times\vec{\nabla}\times\vec{A}=\vec{j}=-\left[\vec{A}-\frac{n\hat{\theta}}{r}\right]f^2, \tag{3.17b}$$

where $\hat{\theta}$ is the angular unit vector, given by $\hat{\theta}=(-y/r,x/r,0)$ and

$$\overline{X}=\frac{nx}{r^2},\qquad \overline{Y}=\frac{ny}{r^2}.$$

For bulk superconductors, as long as vortices are assumed to be straight, all quantities remain constant over the $z-$direction and the system can be described under a two-dimensional approach, where equations are solved using an iterative relaxation method suitable for non-linear differential equations. Whenever the finite size of the thickness is taken into account, the system is no longer invariant over the outplane direction and therefore, a three dimensional solution is required. Unfortunately, solve CGL equations in three dimensions is computationally very expensive and challenging these days. Thus, we must reconcile ourselves to approximate methods to describe, at least from a qualitative point of view, the behavior observed experimentally. Here, we propose a way to work around this problem by using the fast Fourier transform suitable for two dimensional current density distributions (MILOŠEVIĆ; GEURTS, 2010). So, only Eq. (3.17a) is solved by the relaxation method, whereas the updated order parameter is used to estimate the current density in the whole space inside the sample. Within the updated order parameter, Eq. (3.17b) is solved by using the Fourier transform scheme, where an uniform density current distribution along the out-plane direction is assumed,

$$j(x,y,z)=j(x,y)\Pi(z,-\delta/2,\delta/2). \tag{3.18}$$

Here, $\Pi(z,-\delta/2,\delta/2)$ is the boxcar function, which is equal to 1 for $-\delta/2\leq z\leq\delta/2$ and 0 otherwise. This is a good approximation in both small and large thickness limits (MILOŠEVIĆ; GEURTS, 2010), where the inplane distribution accounts for averaged over the z-direction

$$j(x,y)=\frac{1}{d}\int_{-d/2}^{d/2}j(x,y,z)dz \tag{3.19}$$

Still, we shall extrapolate the range of validity of the method and also assume intermediate values of thickness δ (MILOŠEVIĆ; GEURTS, 2010).

3.3.1 Double-gap superconductors

When a double-gap superconductor is considered, two wave-functions are required to describe the superconducting state. The Ginzburg-Landau energy functional can be easily extended by superposing the energies of each condensate and adding up the Josephson term, which couples both condensates. Since vortices in the different bands are supposed to overlap each other in order to minimize the energy, the same phase is assumed

for both order parameters. The set of constrained Ginzburg-Landau are then obtained by assuming $\Psi_k = e^{in\theta} f_k(x,y)$ as the ansatz for the k-th band:

$$\begin{aligned}\nabla^2 f_1 - \left[\overline{X}^2 + \overline{Y}^2 + 2\left(A_x\overline{Y} - A_y\overline{X}\right) + \vec{A}^2\right] f_1 \\ + (\chi_1 - f_1^2) f_1 + \gamma f_2 = 0.\end{aligned} \tag{3.20a}$$

$$\begin{aligned}\nabla^2 f_2 - \left[\overline{X}^2 + \overline{Y}^2 + 2\left(A_x\overline{Y} - A_y\overline{X}\right) + \vec{A}^2\right] f_2 \\ + \alpha(\chi_2 - f_2^2) f_2 + \frac{\gamma\kappa_2^2}{\alpha\kappa_1^2} = 0.\end{aligned} \tag{3.20b}$$

$$-\kappa^2 \vec{\nabla} \times \vec{\nabla} \times \vec{A} = -\left[\vec{A} - \frac{n\hat{\theta}}{r}\right]\left(\frac{f_1^2}{\kappa_1^2} + \alpha\frac{f_2^2}{\kappa_2^2}\right). \tag{3.20c}$$

The parameters κ_1, κ_2, α and γ are not independent of each other and were determined within the correct microscopic framework described in Ref. (CHAVES et al., 2011a)

3.4 Results

3.4.1 Bulk

For bulk superconductors, it is well known that the vortex core radius R_v is of the order of the material coherence length ξ. In fact, this dependence was theoretically reported in Ref. (BRANDT, 2006) , where different values of Ginzburg-Landau parameter κ were assumed. In that case, the penetration depth was used as the system length scale, allowing the observation of the dependence between R_v and ξ. However, the relation between penetration depth λ and vortex core sizes is still not known. In what follows, we provide the effect of changing the Ginzburg-Landau parameter κ on both the vortex and magnetic field profiles, as illustrated in Figs. 36 (a) and (b), respectively. Here, ξ is the length scale and therefore, it remains fixed for any κ value. Thus, penetration depth values can be directly associated to the Ginzburg-Landau parameter. In Fig. 36 (a), vortex profiles are shown for different values of κ: 1.0 (blue solid line), 2.0 (green dotted-dashed line), 4.0 (yellow dashed line) and 8.0 (red dashed-dashed-dotted line). Remarkably, the core of the vortex also depends on the penetration depth of the material, with a wider radius for larger values of λ. However, this dependence is clear only in a very restrict range of low κ values, out of the London limit. In fact, for λ approximately greater than 4ξ the changes in vortex core becomes extremely soft, as illustrated in Fig. 36 (c) by gray circles. Similarly, larger values of λ also lead to more spread distributions of magnetic field around the vortex center, however, the increasing of the magnetic core is much more robust, as illustrated by red squares in Fig. 36 (c). The calculations of the core sizes presented in Fig. 36 (c) were performed by accounting for the distance between the center of the vortex up to half the maximum value of $|\Psi|^2$ and H. As a proof of validity of our approach, below the critical value $\kappa = 1/\sqrt{2}$, where vortices are known to attract each other, the vortex core is larger than the magnetic one, whereas, for approximately $\kappa = 1/\sqrt{2}$ (represented by the

vertical dashed line), this feature is reversed and the magnetic field distribution exceeds the vortex core profile. The choice of the mid-point value as a reference for the radius calculation proves to be quite convenient, since it is possible to associate the type-I/type-II transition point with the ratio R_v/R_H. If the R_v/R_H is greater than 1, vortices may attract each other, destroying the superconductivity abruptly. In contrast, if $R_v/R_H < 1$ the vortex-vortex interaction is repulsive, characterizing the type-II regime.

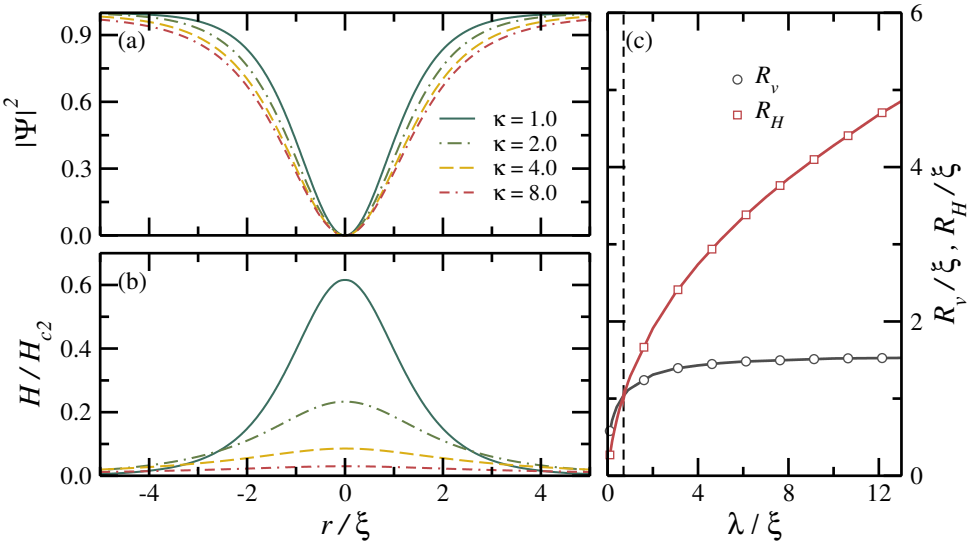

Figure 36 – Vortex and magnetic profiles for bulk superconductors in (a) and (b) respectively, for different values of Ginzburg-Landau parameter κ: 1.0 (blue solid line), 2.0 (green dotted-dashed line), 4.0 (yellow dashed line) and 8.0 (red dashed-dashed-dotted line). (c) Vortex and magnetic core represented by gray circles and red squares respectively. The vertical black dashed line represents the transition point $\kappa_c = 1/\sqrt{2}$ between type-I and type-II regimes.

Signatures of type-I/type-II transition may also be observed through the peak position of the angular current density or even through the peak value of the magnetic field, as pointed out in Ref. (WANG, 2015). The former is closely related to the definition of penetration depth λ. In fact, due to the magnetic field penetration, the angular current distribution shall increase with r until it reaches a maximum at $r \approx \lambda$; beyond this limit, the magnetic field becomes negligible and the density current shall decrease to zero. Such non-monotonic behavior of the angular current density is illustrated in Fig 37 (a), for different values of κ: 0.4 (blue solid line), 0.6 (green dotted-dashed line), 0.8 yellow (dashed line) and 1.0 (red dotted-dashed-dashed line). As expected, the higher the value of κ, the greater is the peak distance with respect to the vortex core. In Fig. 37 (b), the peak position as a function of the Ginzburg-Landau parameter κ is represented by red circles. The qualitative peak-position description proves to be inaccurate and even unsuitable specially for extremely type-II regime, where the dependence of κ becomes weaker. However, it still provides a good approximation near the transition point. Indeed,

on the threshold of type-I/type-II transition, one might expect to observe the peak at $r \approx 1/\sqrt{2}$, which is quite close to the value 0.76ξ, obtained by our approach. The behavior of the angular density current peak as a function of the Ginzburg-Landau parameter κ is well fitted by $a\kappa/(1+\kappa)$, as illustrated by the black solid line in Fig 37 (b).

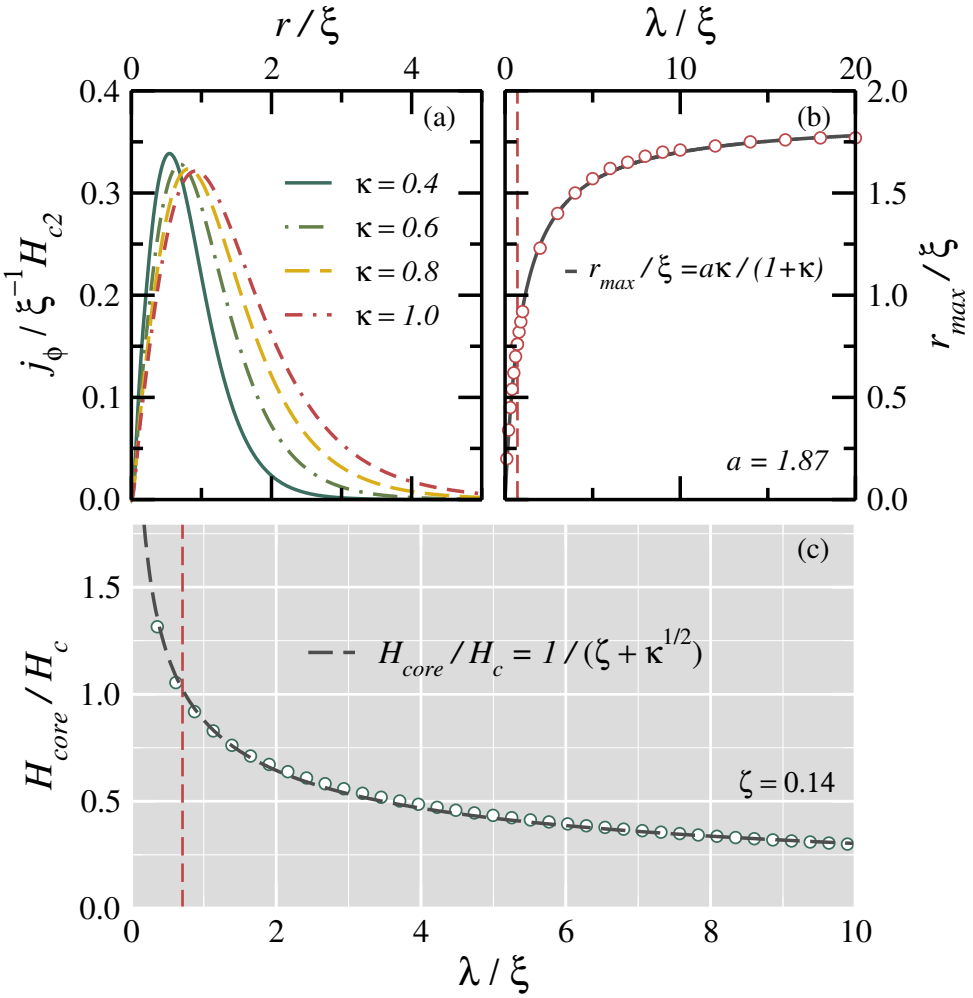

Figure 37 – (a) Angular current density for different κ values: 0.4 (blue solid line), 0.6 (green dotted-dashed line), 0.8 yellow (dashed line) and 1.0 (red dotted-dashed-dashed line). (b) Peak position of angular density current (red circles) as a function of κ, within an appropriate fitting function (solid gray line). (c) Magnetic field in vortex center as a function of κ. For $\kappa = 1/\sqrt{2}$, the magnetic field in the vortex center is exactly $H(0) = 1H_c$, which is the magnetic signature of type-I/type-II transition in single-band bulk superconductors.

The second transition signature arises due to the close link between vortex stability and the magnetic field inside its core, which allows its use as a new criterion for type-I/type-II superconductors classification. Through our method, the result obtained in Ref. (WANG, 2015) is revisited in order to emphasize the validity of our approach. In Fig. 37 (c), the magnetic field peak (blue circles) is plotted as a function of the Ginzburg-Landau parameter, where, exactly at $\kappa = 1/\sqrt{2}$ the magnetic field is observed to be

$H(0) = H_c = H_{c1} = H_{c2}$. This has been previously proposed as the magnetic signature of transition between type-I and type-II superconductors. At the core of the vortex, the magnetic field can be well described as a function of the Ginzburg-Landau parameter κ by the fitting function $H_{core}/H_c \approx 1/(\zeta + \sqrt{\kappa})$, with $\zeta \approx 0.14$. Therefore, more than just providing information concerning the superconductor type, this fitting function also enables one to estimate, based on experimental measurements of the magnetic field at the vortex core, the Ginzburg Landau parameter κ of the corresponding superconductor. This result holds as long as vortices remain far enough from each other, so that neighboring effects become negligible. The inter-vortex distances over which neighboring vortices might not disturb the magnetic field peak is illustrated for different values of κ: 0.4 (black circles), 0.5 (red squares), 0.6 (green triangles), 0.7 (blue diamonds), 0.8 (yellow downward triangles), and 1.0 (pink rightward triangles) in Fig. 38, where the magnetic field at the vortex core subtracted by the magnetic field under isolated conditions is illustrated as a function of inter-vortex distance d. Interestingly, vortex lattices in type-I materials would present smaller peaks than isolated vortices, whereas for type-II superconductors, this behavior is reversed. Particularly, for $\kappa \approx 1/\sqrt{2}$ (see blue diamonds in Fig. 38), the magnetic field peak might not experience significant changes, even at short-range inter-vortex distance scale.

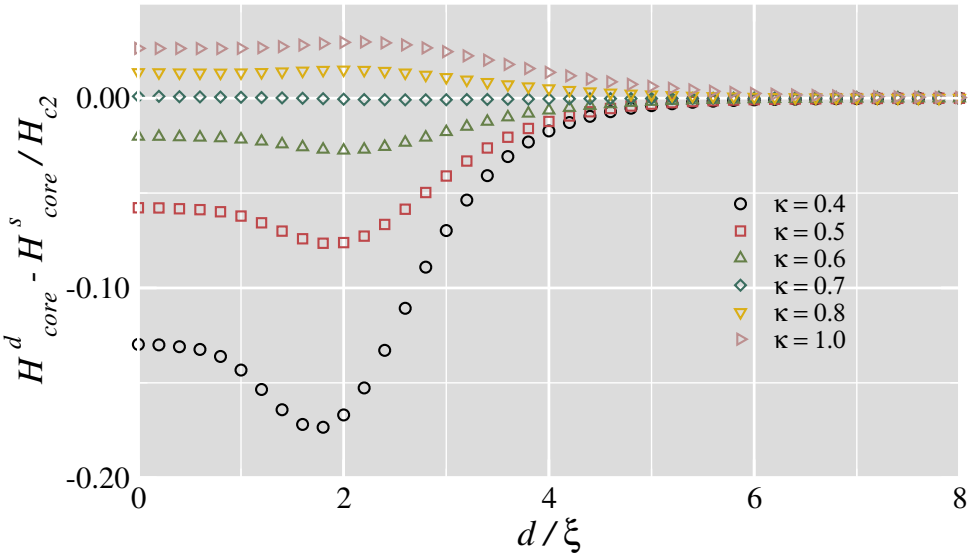

Figure 38 – Magnetic field difference at vortex core between double and single vortex conformations as a function of the inter-vortex distance d for different values of κ: 0.4 (black circles), 0.5 (red squares), 0.6 (green triangles), 0.7 (blue diamonds), 0.8 (yellow downward triangles), and 1.0 (pink rightward triangles).

From now on, we shall revisit the description of Cooper pairs density and magnetic profiles of vortices, in order to generalize and check the validity of well know expressions commonly used in literature. The Cooper pairs density distribution $|\Psi|^2$ in the presence of a single isolated vortex can be well fitted to the function $\tanh^2(\nu r/\xi)$, where ν

is the fitting parameter. This approximation was first suggested by Tinkham, who proposed a κ independent approximation, with $\nu \approx 1$. In Fig. 38, the validity of this approach can be observed for different κ regimes, including the hypothetical case where vortices are assumed to appear in a type-I superconductor. However, the fitting parameter values might depend on the Ginzburg-Landau parameter and differ from the unity, as illustrated in the inset of Fig. 39, where vortex profiles are represented by symbols, for different κ values: 0.2 (blue circles), 0.8 (yellow squares) and 8.0 (red triangles). The corresponding fitting functions are represented by dashed lines. In addition to the descriptive character, this approach might reduce the computational time of numerical methods which requires initial guess for the order parameter. Surprisingly, in the limit of very large κ, the fitting parameter ν approaches 1/1.87, which is exactly the inverse of density current peak position when κ goes to infinity.

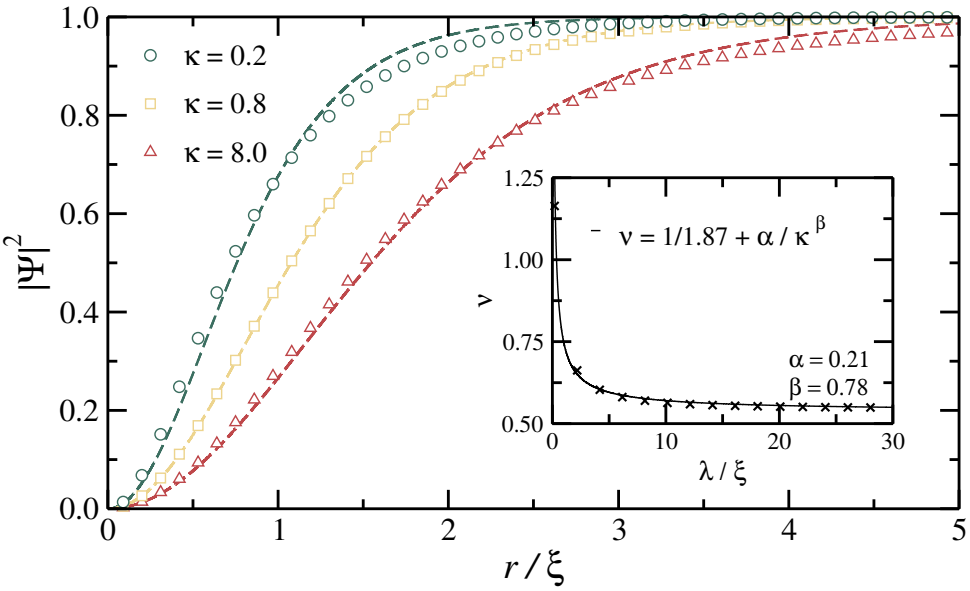

Figure 39 – Vortex profile in a superconducting bulk for different values of Ginzburg-Landau parameter κ: 0.2 (blue circles), 0.8 (yellow squares), 4.0 (yellow dashed line) and 8.0 (red triangles) and their respective fittings represented by dashed lines . The inset provide the fitting parameter ν as a function of the Ginzburg-Landau parameter κ.

In contrast, analytical expressions for the magnetic field distribution are obtainable only in the very restricted limit of extreme type-II superconductors, where κ is assumed to be very large and the finite size of the vortex core neglected. According to Tinkham, for extremely type-II superconductors, the magnetic profile of a vortex can be well approximated to

$$H(\vec{r}) \approx \frac{\Phi_0}{2\pi\lambda^2}\left(\frac{\pi}{2}\frac{\lambda}{r}\right)^{1/2} e^{-r/\lambda} \qquad r \to \infty, \tag{3.21a}$$

$$H(r) \approx \frac{\Phi_0}{2\pi\lambda^2}\left[\ln\frac{\lambda}{r} + 0.12\right] \qquad \xi \ll r \ll \lambda \tag{3.21b}$$

where Φ_0 is the quantum flux. In Fig. 39 (a-c), magnetic profiles for $\kappa = 2$, 4 and 8 are respectively illustrated by gray circles. Despite the restrictions imposed on Ginzburg-Landau equations, the solutions obtained by Tinkham provide accurate fittings far from vortex core, even for weakly type-II superconductors. The fitting functions used have the form $f(r) = \mu_> \sqrt{\lambda/r} e^{-r/\lambda}$ and are illustrated by red dashed lines. In Fig. 39 (d), represented by red circles, the fitting parameter $\mu_>$ is plotted as a function of the Ginzburg-Landau parameter κ in a log-log scale, where the expected power-law behavior is evidenced. The red dashed line stands for the power-law fit with exponent equal to -2. In general, the function expressed in Eq. (3.21a) provides good fitting even outside the limit $r \to \infty$ and also for low values of κ, like $\kappa = 2$. As κ increases, the vortex core increases and the dependence presented by Eq. (3.21b) becomes more evident. In Figs. 40 (b) and (c), fittings to the function $\mu_<[\ln(\mu_0\lambda/r) + 0.12]$ are presented by blue solid line. Again, despite the extrapolation of the limits of this solution, it is possible to observe in Fig. 40 (e) that, $\mu_<$ also obeys a power law behavior with exponent approximately equal to -1.9, which is almost the expected value obtained by the London theory.

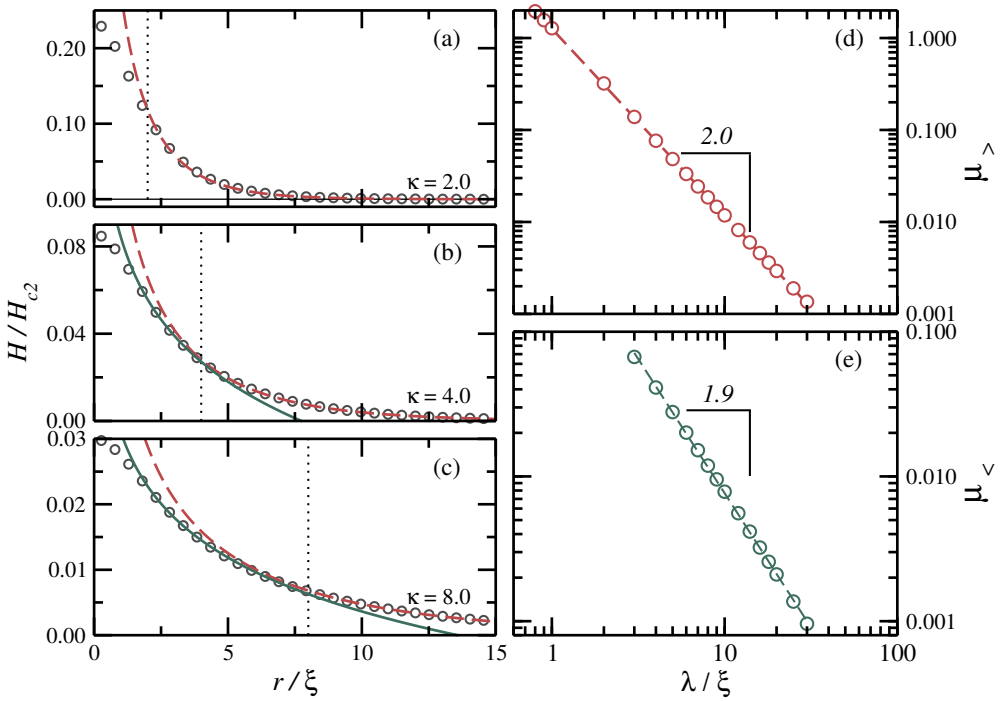

Figure 40 – (a-c) Magnetic profiles for superconducting bulk samples, with different values of Ginzburg-Landau parameter κ: 2.0, 4.0 and 8.0 respectively. Red dashed lines represent fittings made from $r \geq \lambda$ up to 80ξ using the function μ. Fitting parameters $\mu_>$ and $\mu_<$ as a function of the Ginzburg-Landau parameter in panels (d) and (e), respectively.

Notice that, for the short range behavior of the magnetic profile, another parameter μ_0 was also considered in order to fit the magnetic field properly. In expressions derived by Tinkham, this parameter is equal to the unity, which means that μ_0 should goes to unity as $\kappa \to \infty$. Here, we found a different convergence value, but still close to 1. This discrepancy might occur due to the negligence of the proper approach limits: $\xi \ll r \ll \lambda$. In fact, the fitting was performed in the range $[2\xi, 0.90\lambda]$, which, in some cases, leads to a small divergence when $r \approx 0.9\lambda$. Still, the parameter μ_0 illustrated in Fig. 41 leads one to a more general expression, valid in an wider interval of r if compared with the original one obtained from the formal asymptotic behaviors of the Hankel function.

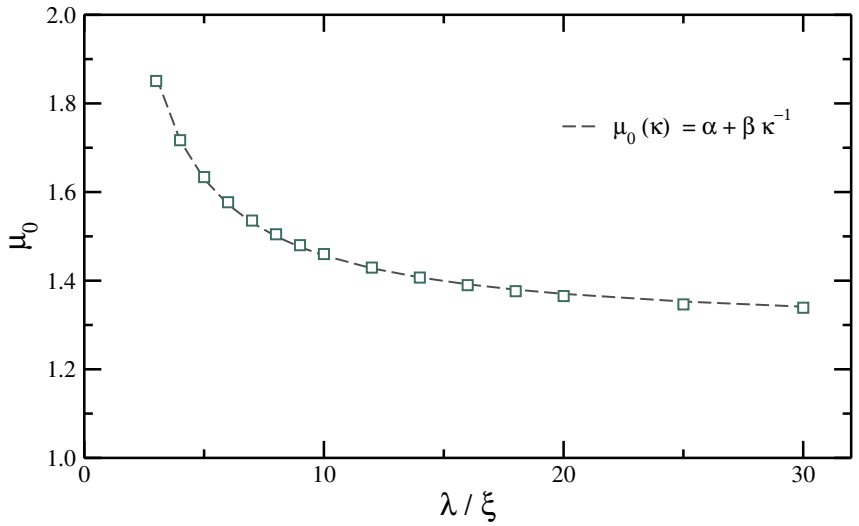

Figure 41 – The parameter μ_0 as a function of κ is represented by blue squares, whereas the gray dashed line stands for the fitting function $\alpha + \beta\kappa^{-1}$, with $\alpha = 1.28$ and $\beta = 1.73$

3.4.2 Films

3.4.2.1 Singly-quantized vortices

The sample dimensionality has strong influence on its superconducting properties. In fact, a thin superconducting film does not share same properties presented by a bulk sample of the same material. In general, these properties are investigated only in the extreme limits of ultra-thin films, where the sample thickness is approximated by a Dirac delta function, or in bulk limit, where the space is completely fulfilled by the sample and current density may be considered uniform along the applied field direction. According to Pearl approach (FETTER; HOHENBERG, 1967; PEARL, 1964), thin film and bulk properties may be correlated by an effective Ginzburg-Landau parameter $\kappa_{eff} \sim \kappa^2/d$, which characterizes films with Ginzburg-Landau parameter κ as they were bulk samples. Here, as a first proof of validity, we have explored this resemblance by comparing singly quantized vortex features in films and in its bulk analog. In Figs. 42 (a-f) a comparison

between Cooper pairs densities, angular current densities and magnetic profiles of films and their correspondent bulk materials are performed by considering $\kappa = 1.0$ and different values of thickness δ: 0.333ξ ($\kappa_{eff} \approx 3$), 0.250ξ ($\kappa_{eff} = 4$), 0.200ξ ($\kappa_{eff} = 5$), 0.125ξ ($\kappa_{eff} = 8$) 0.100ξ ($\kappa_{eff} = 10$) and 0.05ξ ($\kappa_{eff} = 20$). Here, film properties are represented by black symbols, whereas red lines stand for the bulk case. Notice that, while vortex profiles of bulk and films perfectly fit each other, current densities exhibit a disparity in the limit of $r/\xi > \kappa_{eff}$. In fact, according to Fetter *et al* (FETTER; HOHENBERG, 1967), the long-range behavior of angular current density in extremely thin films is given by

$$j_\theta^F = \frac{c\phi_0}{4\pi^2}\frac{1}{r^2}, \tag{3.22}$$

and it is expected to contrast with its analog in bulk samples,

$$j_\theta^B = \frac{c\phi_0}{8\pi^2}\frac{d}{\lambda^3}\left(\frac{\pi\lambda}{2r}\right)e^{-r/\lambda}. \tag{3.23}$$

Indeed, this divergence can only be observed in Figs. 42 (a-c), where the spatial range plotted is greater than the effective Ginzburg-Landau parameter value. On the other hand, despite share the same order of magnitude, magnetic profiles of bulk and films greatly differs from each other. In fact, there exist be two obvious reasons to explain it. It may be a consequence of long-range differences in current densities or even because magnetic fields in finite thickness samples spread up, contrasting with bulk case, where the field has null in-plane components.

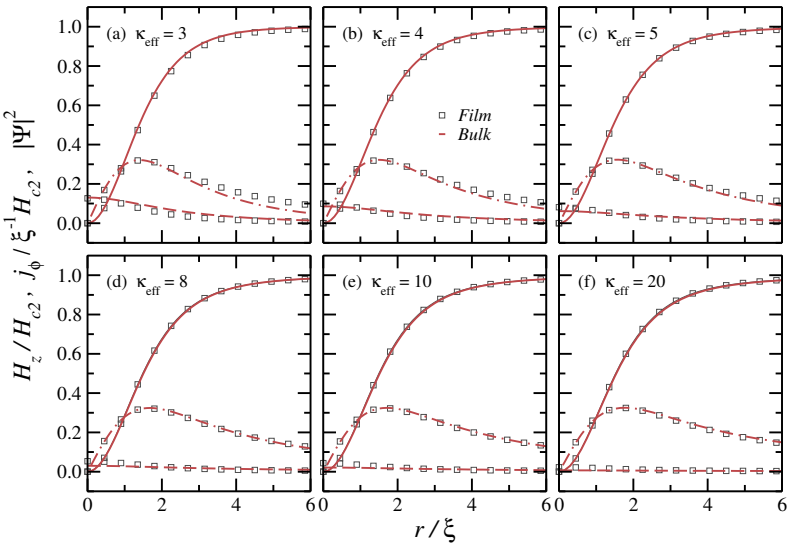

Figure 42 – Cooper pair density, angular current density and transverse component of the magnetic field for $\kappa = 1.0$ and for different values of sample thickness δ: 0.333 ξ ($\kappa_{eff} \approx 3$), 0.250 ξ ($\kappa_{eff} = 4$), 0.200 ξ ($\kappa_{eff} = 5$), 0.125 ξ ($\kappa_{eff} = 8$) 0.100 ξ ($\kappa_{eff} = 10$) and 0.05 ξ ($\kappa_{eff} = 20$), respectively illustrated in panels (a-f). Red lines account for bulk result with the corresponding effective Ginzburg-Landau parameter.

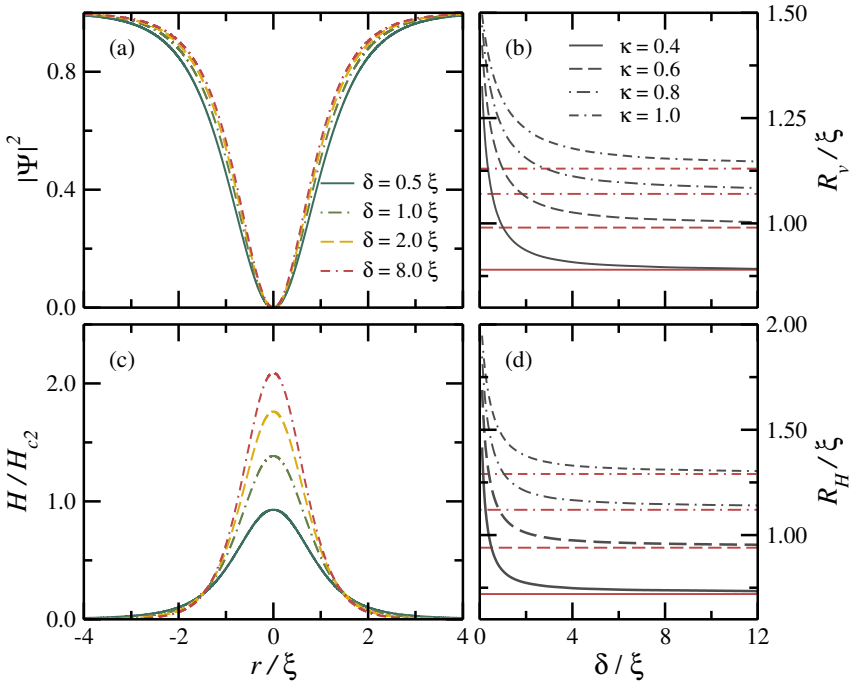

Figure 43 – (a-b)Vortex and magnetic field profiles are respectively illustrated for $\kappa = 0.4$ and different thickness sizes: 0.5 (blue solid line), 1.0 (green dotted-dashed line), 2.0 (yellow dashed line) and 8.0 (red dotted-dashed-dashed line). (c-d) Vortex and magnetic core radius as a function of thickness size δ for four different values of κ: 0.4 (solid line), 0.6 (dashed line), 0.8 (dotted-dashed line) and 1.0 (dotted-dashed-dashed line). The corresponding horizontal red lines stand for asymptotic behavior of each curve, which was obtained through the bulk case solution.

In what follows, in order to provide a more complete description, the effect of finite thickness on the vortex and magnetic field profiles was also investigated outside the thin film and bulk limits. In Figs. 43 (a) and (b), vortex and magnetic profiles were respectively plotted for $\kappa = 0.4$ and different thickness sizes δ: 0.5 (blue solid line), 1.0 (green dotted-dashed line), 2.0 (yellow dashed line) and 8.0 (red dotted-dashed-dashed line). The vortex and magnetic core radii as a function of the sample thickness are respectively illustrated in panels (c) and (d), for four different values of κ: 0.4 (solid line), 0.6 (dashed line), 0.8 (dotted-dashed line) and 1.0 (dotted-dashed-dashed line). In both cases, the core becomes smaller as the sample becomes thicker. This behavior is sustained until the recovery of the bulk features (designed by horizontal red lines), where the thickness dependence becomes negligible. For the corresponding κ values used here, bulk properties seems to be fully recovered at $\delta \approx 12\xi$, however, it is not possible to ensure the recovery of the type-I/type-II transition point, since most part of the energetic contribution to the vortex-vortex interaction comes from the repulsive magnetic field interaction outside the sample. Therefore, a negligible magnetic field outside the sample is also required. This also makes the usage of the ratio between the vortex and magnetic field core unsuitable,

since there is no competition between cores outside the sample, where most part of the repulsion comes from. Moreover, the magnetic field shown here is just the average one of an uniform current distribution and shall not represent exactly the magnetic field in the whole sample, which should change along the out-plane direction. However, it still provides a qualitative estimative of the magnetic field core of isolated vortices.

Still, as in the bulk case, vortex profiles can also be described by the function $\tanh^2(\nu r)$, where ν is a fitting parameter that depends on δ and κ. In Fig. 44 (a), the Cooper pairs density and the corresponding fittings are respectively represented by symbols and dashed lines for $\kappa = 0.4$ and different values of thickness δ. In Fig.44 (b), the fitting parameter ν is illustrated as a function of the sample thickness for four different values of κ.

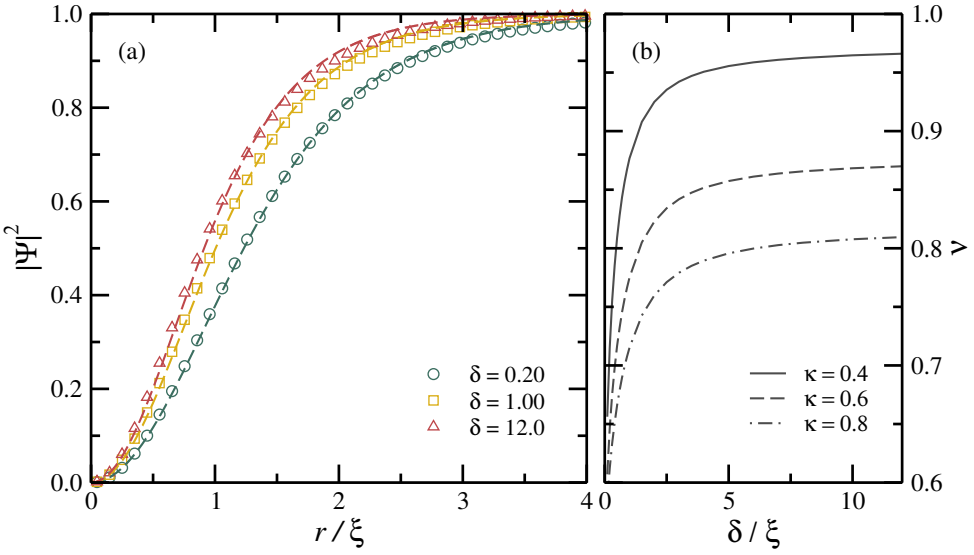

Figure 44 – (a) Cooper pairs density for $\kappa = 0.4$ and different values of thickness δ: 0.2 (blue circles), 1.0 (yellow squares) and 12.0 (red triangles). Dashed lines stand for the corresponding fitting functions. (b) The fitting parameter ν as a function of the sample thickness δ for different values of Ginzburg-Landau parameter κ: 0.4 (solid line), 0.6 (dashed line) and 0.8 (dotted-dashed line).

In contrast, expressions for the magnetic profile are analytically predicted only in the very restricted limit of coreless vortex structure and extremely thin samples, where the transverse component of the magnetic field at the long-range approximation might be expressed as the rapidly decaying function

$$H_z \sim \frac{\phi_0}{2\pi}\frac{\lambda_{eff}}{r^3}. \tag{3.24}$$

This, however, contrasts with the correct physical background, as it can be observed in Fig. 43 (b), where vortices are expected to exhibit wider cores than those usually observed in bulk materials and, therefore, it should not have their effects neglected. In fact, in

Fig. 45, by assuming $\kappa = 1.0$ and different values for the sample thickness, we show that the finite core size softens the magnetic field decay and, despite still obeys a power law behavior, the expected exponent is recovered only for $\delta = 2\xi$. Therefore, we may conclude that Pearl approach for the transverse component of magnetic field should be valid only in a very restricted range of sample thickness, which might not be too small so that vortex cores becomes extremely large and not too large so that the Dirac delta approximation remains valid. It also turns out that, the former approach should not be able to capture the magnetic behavior in a wide spatial range, since it is supposed to be valid only for $r > \lambda_{eff}$, which becomes larger as the thickness is made thinner. Therefore, the magnetic profile description of vortices in extremely thin films remains unknown for a wide and important range lying between vortex center and $r = \lambda_{eff}$.

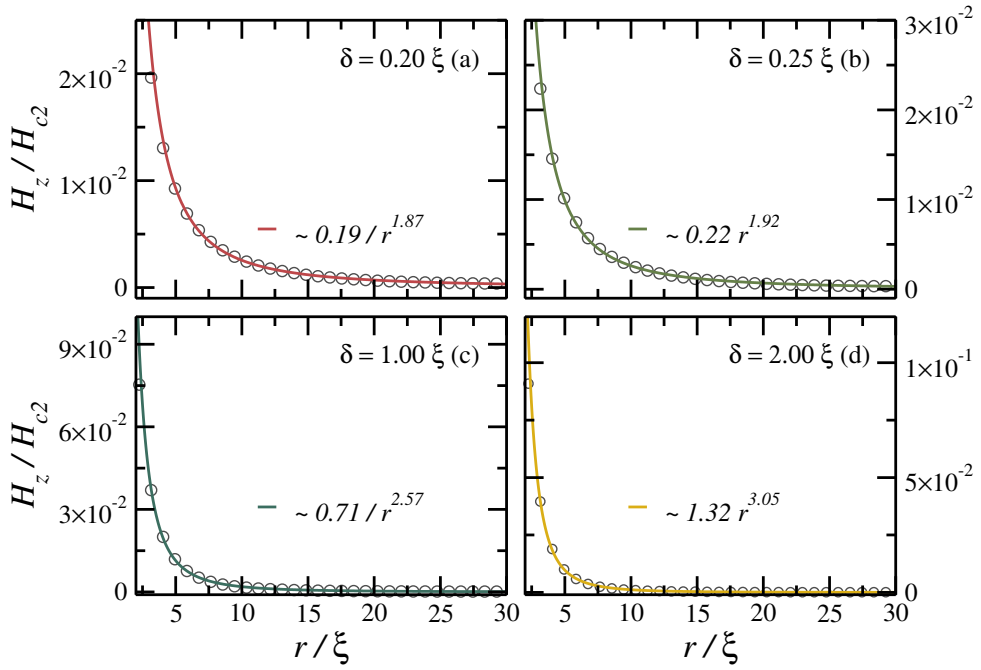

Figure 45 – Long-range magnetic profile for $\kappa = 1.0$ and different values of sample thickness δ: 0.20, 0.25, 1.0 and 2.0 respectively illustrated by circles in panels (a-d). Here, solid lines account for fitting functions that resembles Pearl's prediction for the magnetic field.

Within this context, we also propose here new expressions in order to describe the average transverse component of magnetic distribution for any spatial range, including also the vortex core. For this, we have subdivided the space into two different spatial ranges, the short range, where $r < R_H$, and the long-range defined by $r > R_H$. At short-range, we have found out that the magnetic distribution is well described by $H_z(0) - \mu_1 r^{\mu_2}$, whereas for the long-range, the bulk behavior, $\mu_3 \exp(-\mu_4 r)/\sqrt{r}$, remains as a good approach. In Figs. 46 (a-c), we respectively illustrate for thee different values of κ: 0.6, 0.8 and 1.0, the magnetic profiles and their corresponding fitting functions by considering three different thickness δ/ξ: 1.0 (circles), 2.0 (squares) and 8.0 (triangles). Here, the blue (red) line

accounts for the short(long)-range fitting function. Panels (d-g) of Fig. 46 respectively describe the fitting parameters μ_1, μ_2, μ_3 and μ_4 as a function of the sample thickness. Notice that, we have obtained slightly different parameters as the bulk limit is recovered. This is a consequence of using a different choice to define the short and long-range space interval, divided from the magnetic core instead of the effective penetration depth κ. This choice was made in order to better describe the profile at the vortex core without losing the concordance near the long-range regime. Moreover, the proper definition of effective κ is valid only in a very restricted regime of very thin samples, and therefore, using it as the reference point to delimit both regimes could lead to a methodological inconsistency for samples with intermediate thickness.

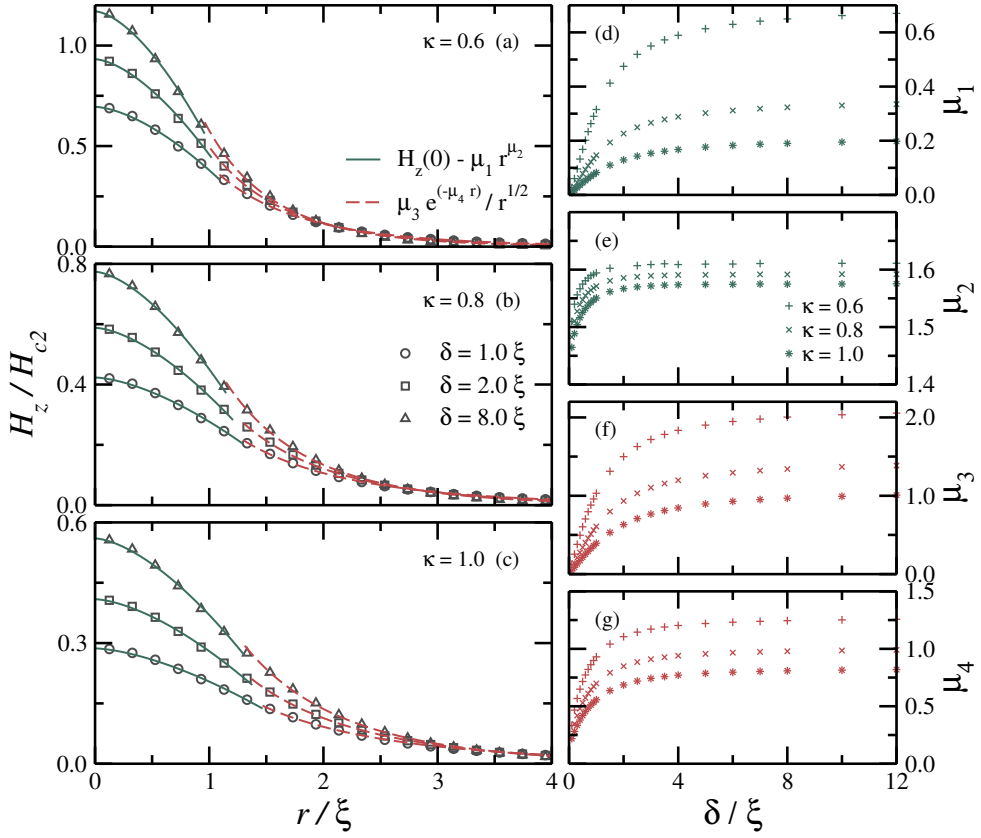

Figure 46 – (a-c) Magnetic profiles and their corresponding fitting functions respectively illustrated for three different values of $\kappa = 0.6$, 0.8 and 1.0. Three different values of sample thickness δ are considered in each panel: 1.0 (circles), 2.0 (squares) and 8.0 (triangles). Short(long)-range fitting functions are expressed by blue(red) solid(dashed) lines. (d-g) Fitting parameters are plotted as a function of sample thickness for three different values of κ: 0.6 (plus symbol), 0.8 (x symbol) and 1.0 (stars).

Notice that, in order to correctly account for the magnetic distribution near the vortex core, a previous knowledge of the average value of magnetic field at the vortex center, $H_z(r = 0)$, is required. Therefore, in what follows we show how to estimate $H_z(r = 0)$ from the bulk result by finding the proper function which describes the magnetic peak

as a function of sample thickness δ. The former result is presented in Fig. 47 (a), for different values of κ: 0.4 (blue circles), 0.6 (green squares), 0.8 (yellow triangles) and 1.0 (red squares), where solid lines account for the fitting functions, expressed in terms of H_{c2} as

$$H_z^{Film}(0) = H_z^{Bulk}(0) - \frac{\alpha_H}{\beta_H + \delta}. \tag{3.25}$$

In Fig. 47 (b), we also provide information about the peak value position of angular density current, which can also be achieved from the peak value position in bulk case by using the fitting function

$$r_{max}^{Film} = r_{max}^{Bulk} + \frac{\alpha_{rm}}{\beta_{rm} + \delta}. \tag{3.26}$$

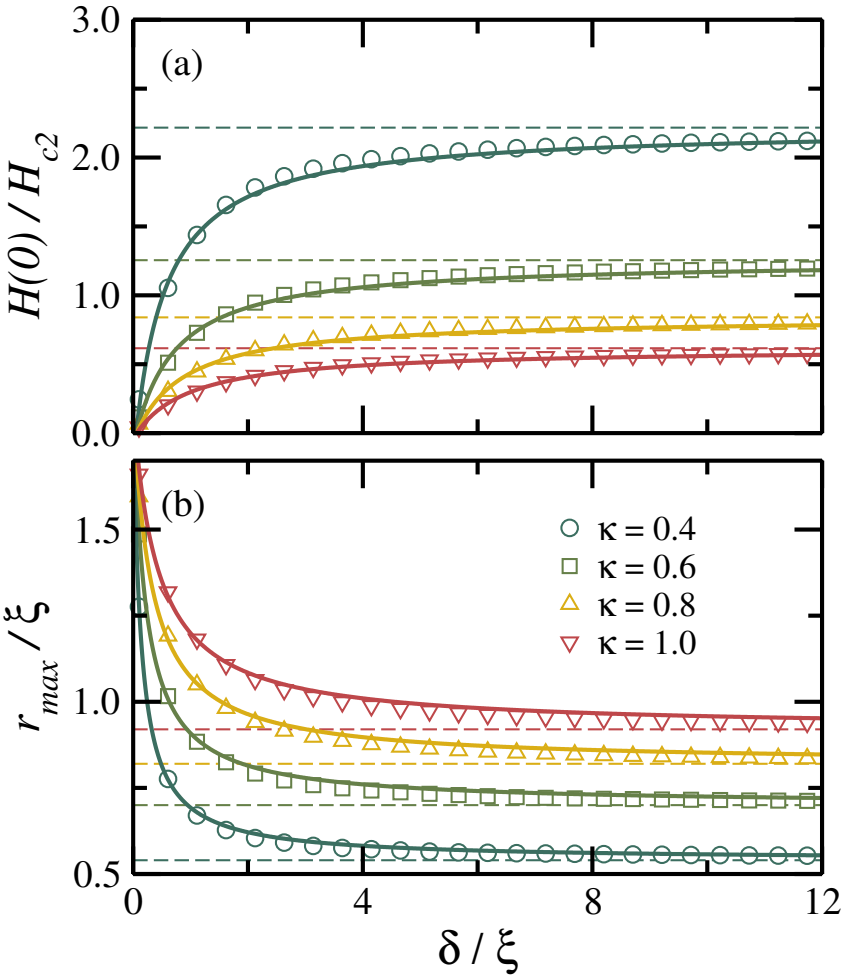

Figure 47 – Average transverse component of the magnetic field peak and the peak position of the angular density current as a function of sample thickness δ for different values of Ginzburg-Landau parameter κ: 0.4 (blue circles), 0.6 (green squares), 0.8 (yellow upward triangles) and 1.0 (red downward triangles) respectively illustrated in panels (a) and (b). Solid lines account for the fitting functions expressed in Eqs. 3.25 and 3.26 with parameters of Table 1.

Parameters α_H, β_H, α_{rm} and β_{rm} are presented in Table 1 for all κ values used in Fig.47.

κ	α_H	β_H	α_{rm}	β_{rm}
0.4	1.26	0.52	0.17	0.13
0.6	0.92	0.67	0.25	0.22
0.8	0.73	0.81	0.33	0.32
1.0	0.62	0.93	0.40	0.42

Table 1 – Table with fitting parameters for peak value of the magnetic field and peak position of angular current density filled with stuff for different values of κ.

3.4.2.2 Multi-quantized vortices

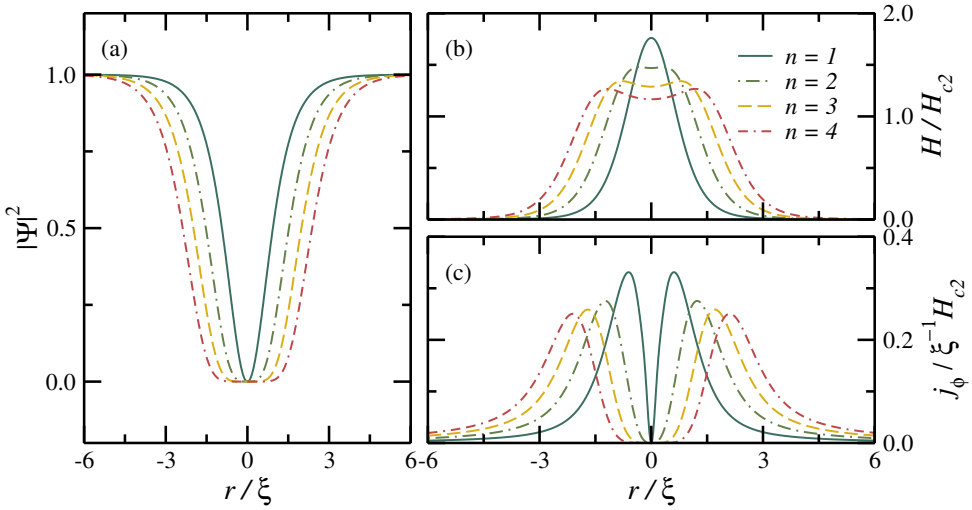

Figure 48 – (a) Single and multi-quanta vortex profiles for $\delta = 2.0$ and $\kappa = 0.4$.Corresponding magnetic fields and angular current densities profiles are illustrated in panels (b) and (c) respectively.

Because of the long-range repulsion of stray fields outside the sample, even a type-I superconductor behaves as a type-II if a sufficiently thin sample is considered. However, for an intermediate thickness, the vortex-vortex interaction behaves non-monotonically and giant-vortex states might be observed (DANTAS et al., a). Despite these states have already been exhaustively observed both theoretically and experimentally, to our knowledge, the internal structure of giant-vortices have never been described under isolated conditions. In Fig. 48 (a), we have calculated the effect of increasing winding number n on vortex profiles. As expected, larger n values lead to larger core sizes. In contrast, in Fig. 48 (b), where the averaged magnetic field distribution is plotted, the behavior is quite peculiar: instead of only larger magnetic cores, the finite thickness of a sample can also induce an off-centered peak distribution in the xy-plane for the giant-vortex magnetic field, which becomes clear for large values of vorticity n. This result is a consequence of a larger normal domain, which leads to a negligible and slow varying angular current density near the giant-vortex core, as observed in Fig. 48 (c). Therefore, in two dimensions, the magnetic peak will assume a ring shape distribution, in contrast to the centered one,

observed for vortices with winding number equal to unity. As we shall see further, this effect might emerge under very restricted conditions, making it difficult to be experimentally and theoretically observed. Moreover, whenever it appears as an stable conformation, the radius of the peak-ring distribution, as well as the difference between the peak and the magnetic field value in the core are very small and would require very high resolution equipments to be experimentally observed.

The off-center peak behavior of the magnetic field disappears for sufficiently thicker samples. In order to prove this, we have calculated the magnetic profiles of vortices with winding numbers $n = 1, 2, 3, 4$, assuming different values of film thickness δ. The results are shown in Figs. 49 (a-d), where $\kappa = 0.4$ was assumed. For all vorticities, the magnetic depletion is softened as the film becomes thicker, indicating the recovery of the centered magnetic peak profile for bulk samples, so that the visualization of off-centered peak is then restricted for low values of δ. This condition makes its experimental observation harder, since high-vorticity states might be unfavorable due to the strong repulsion of stray fields.

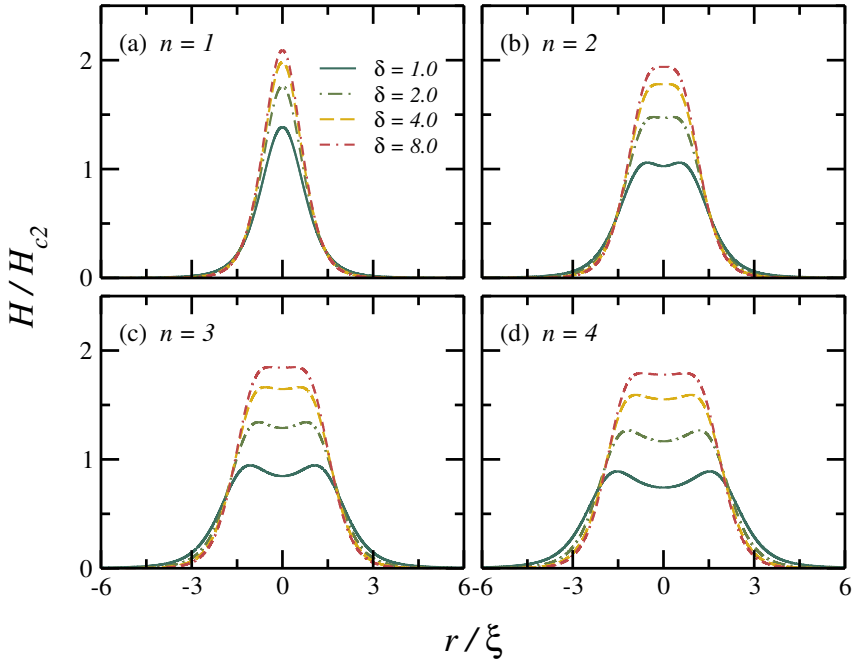

Figure 49 – Magnetic profiles of vortices with winding numbers $n = 1, 2, 3, 4$ are exhibited in panels (a-d) respectively, where $\kappa = 0.4$ and different film thickness were assumed: $\delta = 1.0$ (blue solid line), $\delta = 2.0$ (green dotted-dashed line), 4.0 (yellow dashed line) and 8.0 (dotted-dashed-dashed line).

In order to test the stability of the giant-vortex states presented in Figs. 49 (b-d), we have used the vortex-vortex interaction approach reported in Refs. (CHAVES et al., 2011a; CHAVES et al., 2011b). The short range interaction shall provide information concerning whether merging two vortices at the same position, forming a new vortex with higher vorticity, represents at least a local minimum energy conformation or not.

Interactions between a single vortex $n_1 = 1$ and vortices with vorticities $n_2 = 1, 2$ and 3 are respectively illustrated in Figs. 50 (a-c) for $\kappa = 0.4$ and different values of film thickness δ: 1.0 (blue solid line), 2.0 (green dashed line), 4.0 (yellow dashed line) and 8.0 (red dotted-dashed-dashed line). For $\delta = 1\xi$, where peak-depletions are more perceptible, giant-vortex states are clearly unstable. If larger thickness values are considered, the stability of the giant-vortex states is achieved and the depletion might be observed experimentally. However, increasing thickness sample in order to allow giant-vortices states to become the ground-state conformation might not be a good option, since the effect is more perceptible for lower values of δ and might become negligible for large values of δ. In fact, for a given n and κ, the off-centered peak field would be better visualized for vortices in the threshold of their stability with respect to δ.

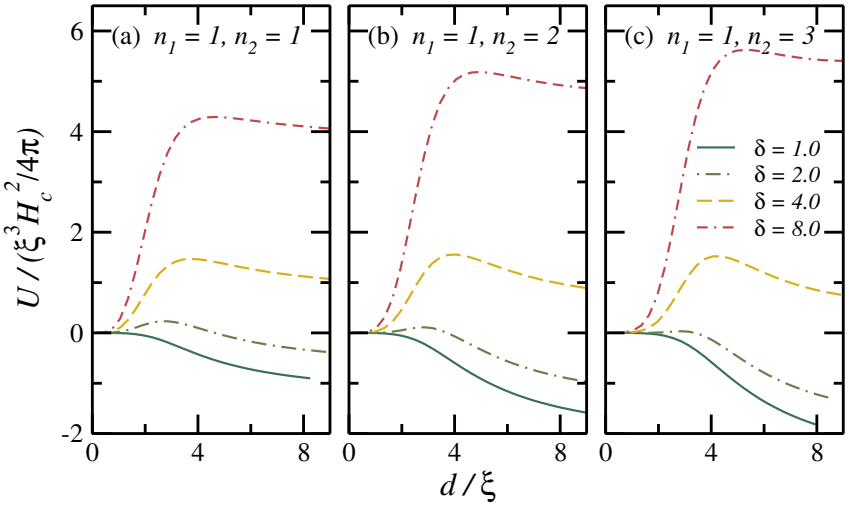

Figure 50 – Stability test of giant-vortex states with $n = 2, 3$ and 4 respectively illustrated in panels (a), (b) and (c) for different values of thickness δ: $\delta = 1.0$ (blue solid line), $\delta = 2.0$ (green dotted-dashed line), 4.0 (yellow dashed line) and 8.0 (dotted-dashed-dashed line).

In what follows, we have also considered giant-vortex states with $n = 3$ for $\delta = 2.0$ and different values of κ: 0.30 (blue solid lines), 0.35(yellow dashed-lines), 0.40 (red dashed-dotted lines). The magnetic profiles of such vortices are illustrated in Fig. 51 (a). Surprisingly, in the investigated regimes, the parameter κ barely affects the off-center peak behavior. The stability of giant-vortices with $n = 3$ are showed in Figs 51 (b) through the interactions of vortices with $n_1 = 1$ and $n_2 = 2$. From this result we can conclude that, using materials with lower values of Ginzburg-Landau parameter κ might be a better solution to experimentally probe giant-vortices with the off-centered peak profile of the magnetic field. In fact, the off-centered peak turns out to be a consequence of large vortex cores when compared to the sample thickness and, therefore, might experiment no significant influence of the Ginzburg-Landau parameter κ. However, this also leads to smaller radius of the depletion core, requiring a better experimental resolution.

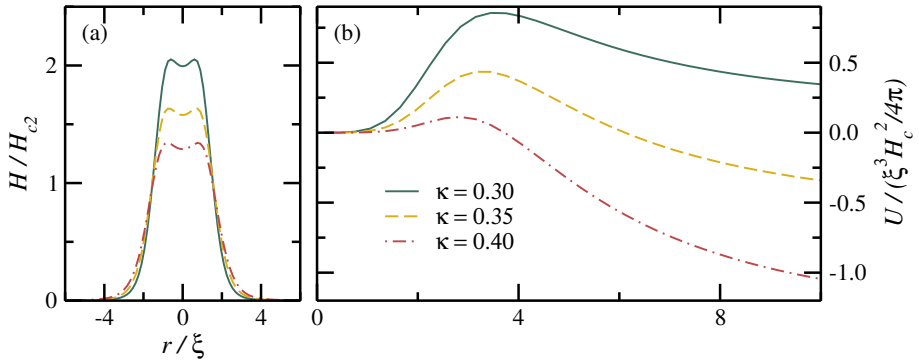

Figure 51 – (a) Magnetic profiles of giant-vortices ($n = 3$) for $\delta = 2.0\xi$ and different values of κ: 0.30 (blue solid lines), 0.35(yellow dashed-lines), 0.40 (red dashed-dotted lines). (b) Corresponding stability tests through the giant-vortex-vortex interaction calculation

In Figs. 52 (a-d), we illustrate for different values of vorticity $n = 1, 2, 3$ and 4, the orthogonal component of the magnetic field profile at the vortex core along the perpendicular direction z, by considering samples with different thickness δ: 1.0 (solid blue line), 2.0(yellow dashed line) and 4.0 (red dotted-dashed line). Here, vertical lines delimit the boundaries of the sample. Notice that, despite presenting weaker fields inside the superconducting sample, vortices with higher vorticity sustain these fields for longer distances in outside region. As a consequence, differently from what we have observed in former results, vortices with lower vorticities might not present higher magnetic fields at their cores if measured outside the sample.

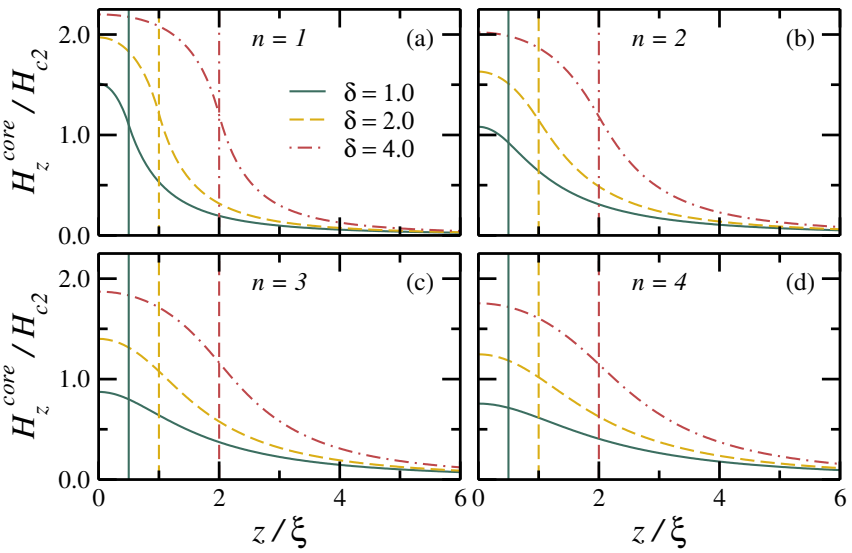

Figure 52 – Perpendicular component of magnetic field profile along z direction with vorticities $n = 1, 2, 3$ and 4 in panels (a-d), respectively. In each panel, three different sample thickness δ were considered $\delta = 1.0, 2.0$ and 4.0ξ

3.4.3 Double-gap bulk superconductors

As pointed out in Sec. 3.3, our approach can be easily extended to describe multi-band superconductors. Interestingly enough, the outcoming results are far from being a trivial extension of the single-gap case, as we will demonstrate in what follows. In fact, several features of the single band case are lost, among them, the monotonic behavior of the vortex-vortex interaction is one of the most remarkable. Naturally, it also becomes difficult to extend the magnetic-peak criterion in order to explain the possible interaction regimes exhibited in a double-gap superconductor. On the other hand, using vortices and magnetic core sizes still seems to be a reasonable way of recongnizing theses possible regimes. Indeed, this was already proposed in Ref. (BRANDT; ZHOU, 2009), in order to explain the non-monotonic nature of the vortex-vortex interaction observed in MgB_2 bulk samples. However, the validity of this approach was never discussed in greater details and the criteria of estimative of core sizes are still not well established. In order to test it, we have calculated core sizes of both magnetic and vortex profiles exhibited by a single votex conformation in a MgB_2 -like material. Here, we define a MgB_2-like material as a material which share same parameters with MgB_2, except for one. This is quite convenient, since two-gap superconductors have a large amount of parameters.

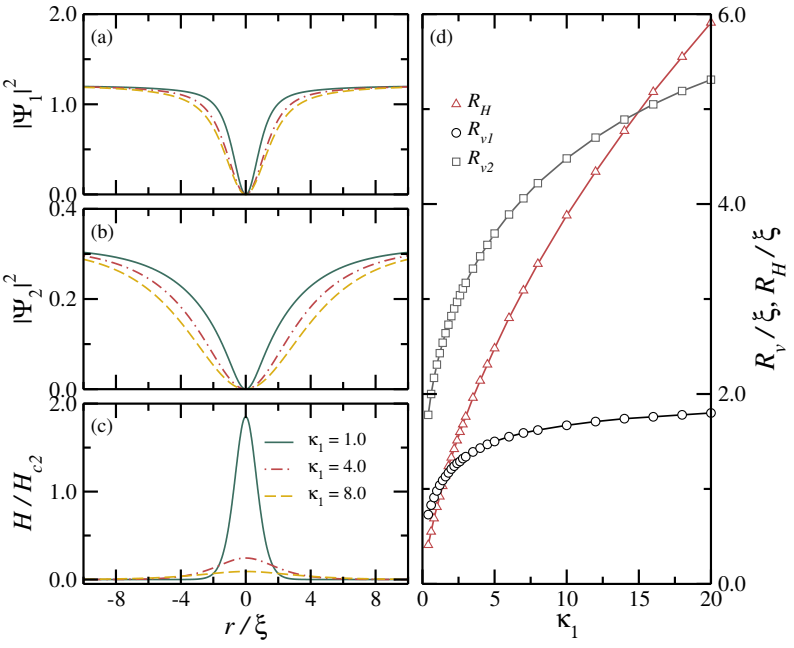

Figure 53 – Vortex profiles of σ- and π- bands respectively exhibited in panels (a) and (b) for a MgB_2-like material with different values of the σ-band Ginzburg-Landau parameter κ_1: 1.0 (blue solid line), 4.0 (red dotted-dashed line) and 8.0 (yellow dashed line) . The corresponding magnetic field profiles in (c). (d) The vortex and magnetic core radius as a function of κ_1 parameter in (d), where the vortex core of σ and π bands are respectively designed by black circles and gray squares, whereas red triangles stands for the magnetic field core.

Figs. 53 (a-c) illustrate the calculated Cooper pairs densities of both π and σ bands, as well as the corresponding magnetic field distribution for three different values of κ_1: 1.0 (blue solid line), 4.0 (red dashed-dashed-dotted line) and 8.0 (yellow dashed line). Both bands exhibits larger vortex cores for increasing κ_1. Notice that, both κ_1 and κ_2 are linearly dependent of each other, which explains the significant changes observed for the second band profile. As expected, the magnetic field profile also becomes more widespread for larger values of κ_1. In Fig. 53 (d), vortex and magnetic core sizes are estimated by using the same half-peak value approach used for single-band case. Three different regimes can be observed: (i) $R_{v2} > R_{v1} > R_H$ for $\kappa_1 \leq 1.57$;(ii) $R_{v2} > R_H > R_{v1}$ for $1.57 \geq \kappa_1 \leq 14.96$ and; (iii) $R_H > R_{v2} > R_{v1}$ for $\kappa_1 \geq 14.96$. This suggests a possible superconducting type change with an increasing κ_1. In fact, extending the argument used for single-band case, we should expect the vortex-vortex interaction to be attractive for $\kappa_1 \leq 1.57$, non-monotonic for $1.57 \geq \kappa_1 \leq 14.96$ and repulsive for $\kappa_1 \geq 14.96$.

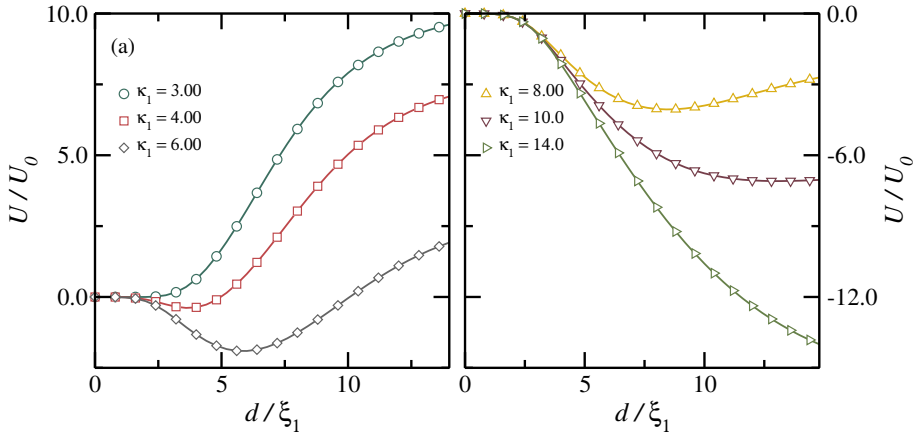

Figure 54 – Vortex-vortex interaction near transtion points. In panel (a) and (b), the transtions attractive/non-monotonic and non-monotonic/repulsive are respectively investigated by assuming different values of κ_1: 3.0 (blue circles), 4.0 (red squares), 6.0 (gray losangles), 8.0 (yellow upward triangles), 10.0 (violet downward triangles) and 14.0 (green rightward triangles).

In order to test the core size signature of the change of superconducting types, we provide, in Fig.54 (a) and (b), the vortex-vortex interaction near the supposed transition points with respect to κ_1: 3.0 (blue circles), 4.0 (red squares), 6.0 (gray losangles), 8.0 (yellow upward triangles), 10.0 (violet downward triangles) and 14.0 (green rightward triangles). Indeed, we have found all the regimes predicted from core size analysis, which suggest a correlation between them and the vortex-vortex interaction behavior. However, the approach which was sucessfully used to estimate core sizes for single band case seems to be inaccurate when extended to double-gap superconductors. In fact, as can be observed in Fig.54(a), the non-monotonic interaction appears only for $\kappa_1 > 3.0$. On the other hand, a fully repulsive behavior can be observed for $\kappa_1 > 10.0$. Even so, the core sizes approach can still be seen to provide reasonable estimates of the values where the transtion between

interaction regimes occur, while it is clearly possible to predict the kind of interaction when differences between core sizes, as defined here, are highly evident.

The effect of changing the partial density of states $n_{12} = n_1/n_2$ on vortex and magnetic profiles is illustrated in Figs. 55 (a-c) for different values of n_{12}: 0.30 (blue solid line), 0.60 (red dotted-dashed line) and 1.0 (yellow dashed line). The convergence values of both order parameters are reduced with the increasing of n_{12} (CHAVES et al., 2011a). Also, the vortex core seems to get larger as n_{12} increases, as a consequence of a more widespread magnetic field distribution, which can be observed in panel (c). Nevertheless, this behavior seems to saturate as n_{12} increases. In fact, differences between the cases $n_{12} = 1.0$ and $n_{12} = 0.6$ are clearly smaller than between the cases $n_{12} = 0.6$ and $n_{12} = 0.30$. This is also confirmed in panel (d), where the estimatives of core sizes are plotted as a function of n_{12}. For low values of n_{12}, all core sizes rapidly increase, however, for $n_{12} \approx 0.5$ both the magnetic core radius R_H, and the vortex core radius of first band R_{v1} become independent of n_{12}. On the other hand, the radius of the vortex core of the second band R_{v2} exhibits a non-monotonic behavior, decreasing instead of saturating, for n_{12} approximately greater than 0.5.

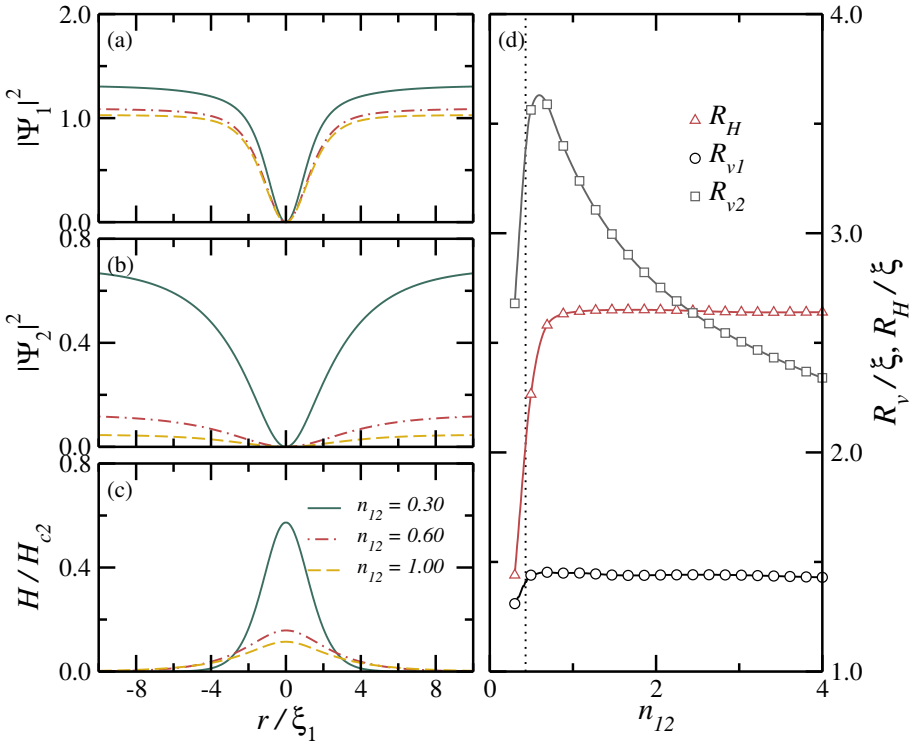

Figure 55 – Vortex profiles of σ- and π- bands respectively exhibited in panels (a) and (b) for a MgB_2-like material with different values of partial density of states n_{12}: 0.30 (blue solid line), 0.60 (red dotted-dashed line) and 1.00 (yellow dashed line). The corresponding magnetic field profiles in (c). The vortex and magnetic core radius as a function of n_{12} parameter in (d), where the vortex core of σ and π bands are respectively designed by black circles and gray squares, whereas red triangles stands for the magnetic field core.

4 Non-monotonic vortex-vortex interactions at the type-I to type-II transition of thin superconducting films

The vortex-vortex interaction potential in a thin superconducting film is calculated within the Ginzburg-Landau formalism. For superconductors with Ginzburg-Landau parameter $\kappa < 1/\sqrt{2}$, these interactions are verified to be monotonically attractive in the bulk and repulsive for a very thin film. However, considering moderate film thickness (of the order of few ξ), our results demonstrate that the vortex-vortex interaction potential is short-range attractive and long-range repulsive. This allows one to redefine the critical values of the GL parameter κ so that the well known critical value $1/\sqrt{2}$ appears just as a limiting case for large thickness of the film. The calculated potentials will enable understanding several vortex configurations at the type-I to type-II transition as the film thickness is reduced.

4.1 Introduction

Over the past years, bulk superconductors have been separated into two classes, (GINZBURG; LANDAU, 1950) according to their Ginzburg-Landau parameter κ: (i) type-I ($\kappa < 1/\sqrt{2}$), where the vortex-vortex interaction is attractive, and (ii) type-II ($\kappa > 1/\sqrt{2}$), where vortices repel each other. (CHAVES et al., 2011b; JACOBS; REBBI, 1979; KRAMER, 1971) However, it is widely accepted that in a sufficiently thin superconducting film, the vortex-vortex interaction is dominated by the repulsive interaction between the stray fields outside the film, (SWEENEY; GELFAND, 2010; BRANDT, 2009) so that even a type-I superconductor becomes effectively type-II, with an effective κ given by $2\lambda^2/\delta$, where λ is the penetration depth. Recent experimental results in MgB_2, which is a two-band superconductor, suggest the existence of a non-monotonic vortex-vortex interaction potential, (CHAVES et al., 2011a; MOSHCHALKOV et al., 2009) which is short range-repulsive and long-range attractive. Such a non-monotonic behavior of the interaction potential, although already theoretically predicted years before, (BABAEV; SPEIGHT, 2005) was surprising enough to (i) suggest the classification of MgB_2 into a third class for superconductors, coined as type-1.5, (ii) to create a huge debate about the possibility of observing attractive and repulsive behaviors due to different bands in this system, (BRANDT; DAS, 2011) and even (iii) about the validity of the results obtained by Ginzburg-Landau theory below T_C in the two-bands case. (KOGAN; SCHMALIAN, 2011; BABAEV; SILAEV, 2012) In this context, the discussion about how vortices interact in

superconductors has been re-opened and a new challenge of classifying possible interaction regimes emerged.

Although several theoretical simulations have confirmed the monotonic attraction (repulsion) of vortices in a type-I superconducting bulk (film), it is not clear how should the vortex-vortex interaction behave in a type-I film with a moderate value of thickness. One could presume that there are three possibilities for an attractive potential to become repulsive as an adjusting parameter (in this case, the film thickness δ) varies: for a moderate thickness, the potential could be (i) short-range attractive and long-range repulsive, so that the repulsive potential range increases and dominates the attractive part as the thickness decreases; or (ii) short-range repulsive and long-range attractive, which prevents the cores of the attractive vortices to overlap; or even (iii) practically zero, assuming that the attractive and repulsive contributions cancel out at a threshold thickness. Despite recent theoretical and experimental results on superconducting films of intermediate thickness have successively confirmed giant-vortex states as a possible stable conformation (GE et al., 2013; GLADILIN et al., 2015; CÓRDOBA-CAMACHO et al., 2016; PALONEN; JÄYKKÄ; PATURI, 2013), suggesting that the interaction between vortices may be non-monotonic, the role of the vortex-vortex interaction on these conformations have never been confirmed and critical parameters defining the cross-over between different phases was not yet proposed.

With constrained Ginzburg-Landau equations (CHAVES et al., 2011b) for a finite thickness superconducting film, we have calculated, in this chapter, the vortex-vortex interaction potential at the type-I regime. For sufficiently thin films, our results confirm the vortex-vortex monotonic repulsion widely known in the literature. However, assuming moderate values for the thickness, we demonstrate that the type-I to type-II transition occurs with a non-monotonic vortex-vortex interaction potential such as the one in the situation (i) described above, where vortices attract (repel) when they are close to (far from) each other. This result conclusively demonstrates that non-monotonic interactions are not an exclusive phenomenon to multi-band superconductors, but can also be observed and even controlled, by adjusting the film thickness, in single band type-I films.

4.2 Results

A typical resulting magnetic field profile is shown in Fig. 56. Figure 56(a) shows isosurfaces of the magnetic field distribution, considering two $n = 1$ vortices separated by a distance $d \approx 6\xi$ in a superconducting film with thickness $\delta = 4\xi$ and $\kappa = 0.4$. Inner (outter) surfaces represent regions with higher (lower) magnetic field. Magnetic peaks are observed in each vortex position, as expected, and they become more spread over the x, y-plane as z increases. Indeed, stray magnetic fields are supposed to merge far above (or below) the film. On the other hand, the magnetic field intensity decreases as z increases,

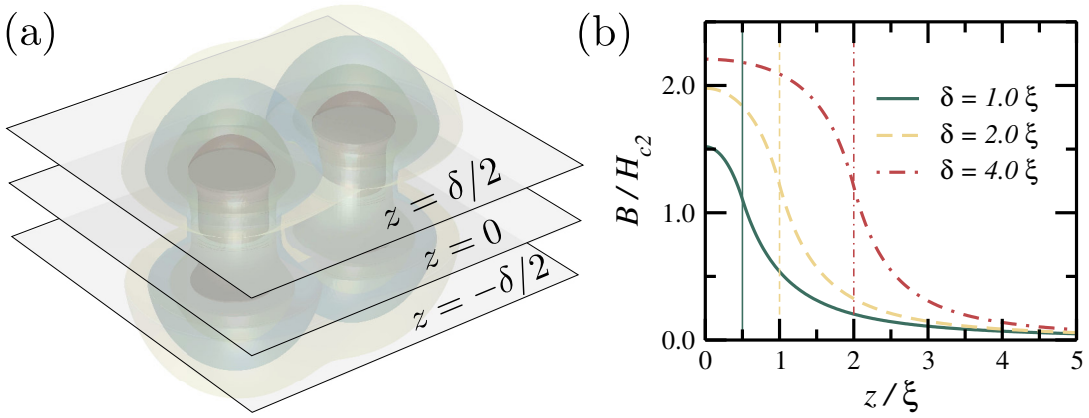

Figure 56 – (a) Isosurfaces of the magnetic field distribution, considering two $n = 1$ vortices separated by a distance $d \approx 6\xi$ in a superconducting film with thickness $\delta = 4\xi$ and $\kappa = 0.4$. Inner (outter) surfaces represent regions with higher (lower) magnetic field. (b) Magnetic field profile along the $z-$direction, calculated in one of the vortex cores, for film thickness $\delta = 1$ (blue solid line), 2 (yellow dashed line) and 4 ξ (red dotted-dashed line). The film limits in z in each case are illustrated by vertical lines.

specially outside the sample. Notice the magnetic field investigated here is not the external (applied) one, but only the one that comes from the contribution of the superconducting vortices, which is indeed expected to become weak far from the film surface. This is clearly observed in Fig. 56(b), where the curves represent the magnetic field amplitude along the z-direction in the core of one of the vortices, for three different values of sample thickness δ. This amplitude decreases with z, specially when $z > \delta/2$, i.e. beyond the film surface, which is represented by the vertical lines in Fig. 56(b) for each value of δ.

Figures 57 (a) and (b) show the energy of two singly quantized vortices as a function of their separation distance, i.e. the vortex-vortex interaction potential, for different values of the film thickness κ and δ respectively. In Fig. 57 (a) the sample thickness $\delta = 1.0$ is kept fixed and several values of GL parameters κ are considered, whereas in panel (b) the thickness effect is investigated for $\kappa = 0.4$. The zero energy level is assumed as the energy of the two vortices on top of each other (i.e. for $d = 0$, or, equivalently, for a $n = 2$ doubly quantized vortex). A repulsive potential when vortices are far from each other, due to the interaction between stray magnetic fields, is observed in all cases. On the other hand, the type-I character of these superconductors manifests itself as a short range attractive interaction. The former becomes stronger as the film thickness decreases. For instance, considering $\kappa = 0.4$, a film thickness of 4.0 ξ is enough to yield a strong short range interaction (see purple upward triangles in Fig. 57(b)), so that the overall vortex-vortex potential is predominantly attractive, as expected for a type-I superconductor. However, as the film thickness decreases, the stray fields repulsion enhances and the energy of two vortices on top of each other ($d = 0$) becomes just a

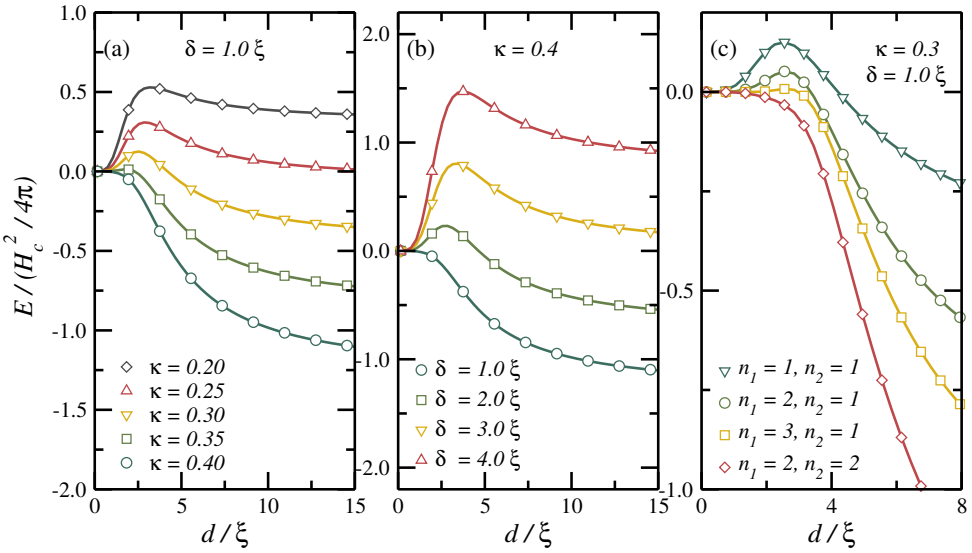

Figure 57 – Vortex-vortex interaction potential as a function of the vortex separation for $\delta = 1.0$ and different Ginzburg-Landau parameter κ in (a) and for $\kappa = 0.4$ and different film thickness δ in (b). In (c) Interaction potentials between a giant-vortices and vortices with vorticities n_1 and n_2 in the $\kappa = 0.3$ and $\delta = 1.0\xi$ case. The $n_1 = n_2 = 1$ case is shown again for comparison with the cases with different vorticities.

local minimum, as observed for $\delta = 2$ and $3\ \xi$. For even lower δ, the potential eventually becomes completely repulsive, as expected for any superconducting thin film. The nature of the interaction is then completely determined by the pair of parameters δ and κ where, for larger values (namely, less attractive) of κ, only thicker samples leads giant-vortex formation.

This conclusively shows that the monotonically repulsive or attractive vortex-vortex interaction potentials, expected for type-I and type-II bulk superconductors, respectively, are not the only possible cases for superconducting films. Actually, our results in Fig. 57 shows 3 situations: (i) pure repulsion, namely a type-II behavior, (ii) short range attraction and long range repulsion, with a local minimum at d=0, and (iii) a predominantly attractive potential with weak long range repulsion, namely a type-I-like potential. Case (ii) suggests that in type-I superconducting films with moderate thickness, a number of vortices might merge into a giant vortex or agglomerate very close to each other in a stable (although not the lowest energy) state. In order to understand the merging of vortices one-by-one, we have also calculated the interaction potential between a $n_2 = 1$ vortex and a giant vortex with winding number (vorticity) n_1. Such interaction is shown in Fig. 57(c) for n_1 ranging from 1 to 3 in a $\kappa = 0.3$ and $\delta = 1\xi$ superconducting film. Notice the $n_1 = n_2 = 1$ case is one of the curves in Fig. 57(a), which is replicated in (c) just for comparison with the curves for other values of n_1. Regarding the strong repulsive tail in the $n_1 = n_2 = 1$ potential curve, with just a shallow local minimum

around $d = 0$, one could imagine that just a few vortices could merge into this minimum. Indeed, as the vorticity of the giant vortex increases, the local minimum around $d = 0$ is smoothed out, but the potential never becomes monotonically repulsive - as a matter of fact, the energy of a giant vortex in a type-I superconductor decreases with the winding number, which compensates, to some extent, the repulsive contribution of the stray fields in the vortex-giant vortex interaction potential. Conversely, the giant vortex-giant vortex interaction potential is observed to be monotonically repulsive for any vorticity of the giant vortices - the specific case of $n_1 = n_2 = 2$ giant vortices is shown by the red diamonds curve in Fig. 57(c), as an example, where such repulsion is already observed. Thus, after merging into giant vortices, the agglomerations of vortices repel each other and might even form giant-vortex Abrikosov lattices. This scenario is compatible with the vortex conformations observed recently by solving GL equations in thin superconducting films (SWEENEY; GELFAND, 2010; PALONEN; JÄYKKÄ; PATURI, 2013). Besides, the agglomerates of vortices with high vorticity predicted here resemble the flux tubes experimentally observed in the intermediate state of type-I superconducting films (GE et al., 2013), illustrated in Fig. 58

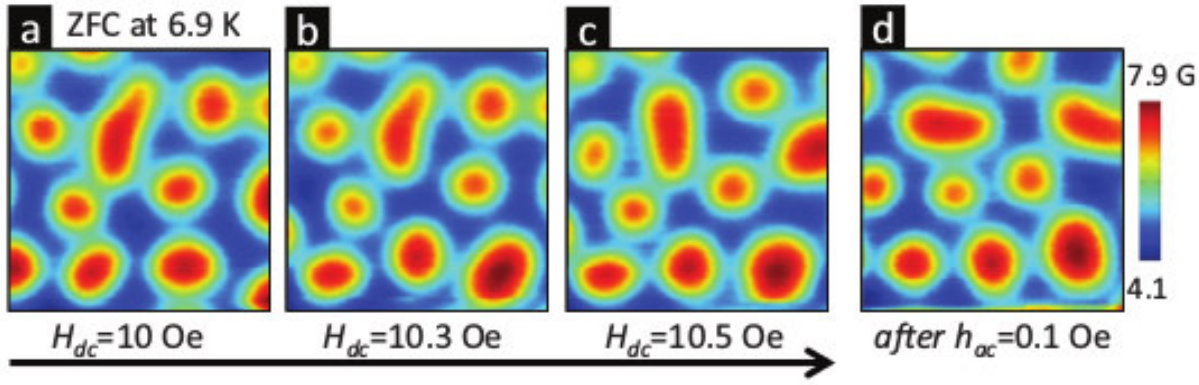

Figure 58 – Randomly nucleated giant vortices at 6.9 K after ZFC and then progressively increasing the magnetic field to (b) 10.3 Oe and (c) 10.5 Oe. (d) SHPM image taken after shaking the vortex pattern of (c) with $h_{ac} = 0.1$ Oe for 30 s. This figure was retrieved from Ref. (GE et al., 2013).

It is also worth to mention that, vortex-vortex interaction does not obey the superposition principle. In fact, if it does, in the presence of a giant vortex, a vortex should experience an interaction equivalent to twice the interaction of a single vortex, which does not occur (see in Fig. 57(c), the downward yellow triangles and blue circles). This restricts the utilization of molecular dynamics to cases where vortices may not overlap each other or to extremely type-II superconductors.

In order to estimate whether giant-vortex conformations are energetically favorable or not, we have constructed in Fig. 59 (a), a κ vs. δ phase diagram based on different regimes of interaction. The red background accounts for type-II behavior, where

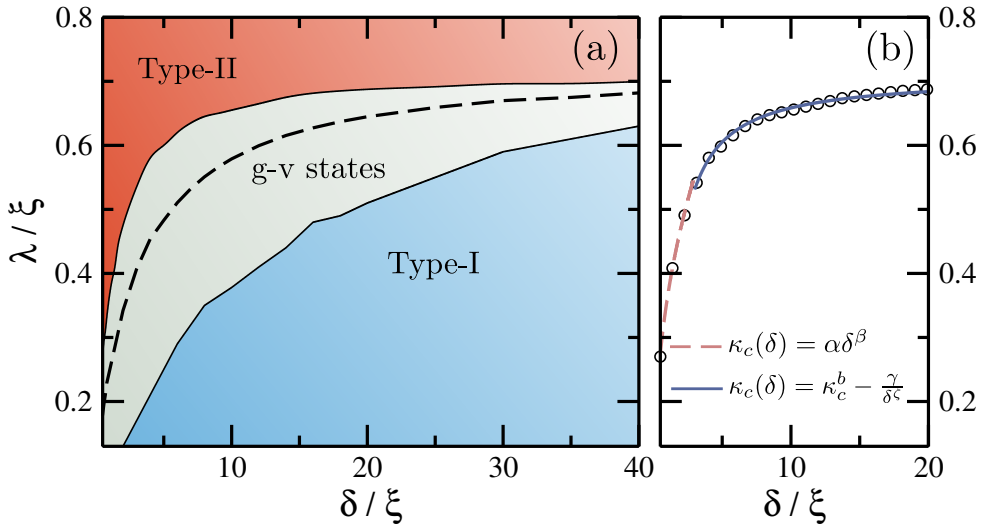

Figure 59 – (a) κ vs. δ phase diagram illustrating different types of regimes in superconducting films: type-II (red), giant-vortex state (gray) and type-I (blue). The black dashed line indicates whether the giant-vortex with $n = 2$ represents the ground state or not. (b) Redefined critical Ginzburg-Landau parameter (black circles), along with its corresponding fitting functions in both thin (red dashed line) and thick (blue solid line) limits, with $\alpha = 0.36$, $\beta = 0.39$, $\gamma = 0.57$ and $\zeta = 1.07$.

singly quantized vortices might repel each other. In the gray region, giant-vortex states are allowed by the presence of short-range attraction, however, not necessarily as the ground-state conformation. In fact, the minimum at the origin of interacting potential might be either a local or a global minimum. This distinction is represented for a giant-vortex with vorticity $n = 2$ by the black dashed line, under which the giant vortex conformation becomes energetically favorable. Vortices with higher vorticities, such as $n = 3, 4$, undergo this local/global transition for slightly lower(higher) values of κ (δ). On the other hand, the type-I behavior, illustrated by the blue background, is recovered whenever infinitely quantized vortices becomes the ground state conformation, exhibiting lower energy than an infinity number of separated singly quantized vortices. Notice that, the critical Ginzburg-Landau parameter dividing type-I/type-II regimes in bulk superconductors, $\kappa_c^b = 1/\sqrt{2}$, proves to be just a limiting case of a more general one, where the thickness of the sample is assumed to be extremely large when compared to the coherence length. Therefore, the GL parameter κ must be redefined in order to account for the phase transition in full range of sample thickness. Up to date, it is well established that extremely thin films share some bulk properties with an effective GL parameter $\kappa_{eff} = 2\kappa^2/\delta$. In Fig. 59 (b) we have performed fittings to the dividing line of repulsive and non-monotonic regimes. In contrast to the expected behavior at extremely thin film limit, we have found the critical GL parameter to obey $\kappa_c \approx 0.36\delta^{2/5}$ (red dashed line) instead of $0.59\sqrt{\delta}$. The difference is caused due to the energetic distributions in films, that, differently from bulk samples,

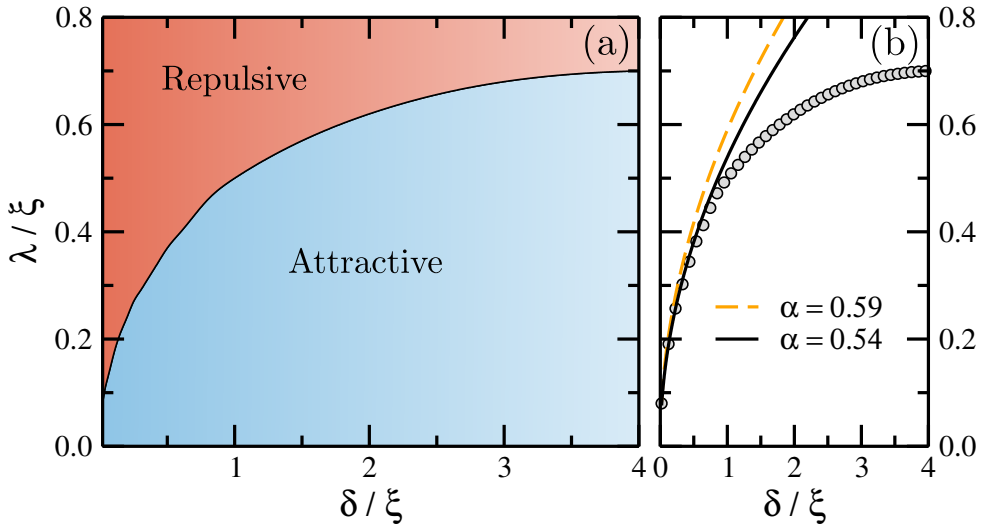

Figure 60 – (a) κ vs. δ phase diagram showing attractive (blue background) and repulsive (red background) interaction regimes according to the energetic contribution inside the sample and (b) dividing line between both regimes with its corresponding fitting function $\alpha\sqrt{\delta}$, for $\alpha = 0.54$ (black solid line) and the expected coefficient $\alpha = 0.59$ (orange dashed line).

are under influence of stray field outside the sample. In fact, once vortices share similar profiles to those of bulk samples with k_{eff}, the total energy calculated in the interaction potential could only be recovered if and only if the energetic contribution of stray fields outside the sample were disregarded. Indeed, by accounting only for internal contributions, we have obtained a slightly close relation to the expected one, $\kappa_c = 0.54\sqrt{\delta}$. The small discrepancy between coefficients lies in the fact that we have included values of thickness outside the extremely thin limit $\delta << \xi$ may even also be a consequence of the finite core structure, usually disregarded at literature. On the other limit, when the sample is made larger than 3ξ, we have found the critical GL parameter to obey $\kappa_c \approx \kappa_c^b - 0.57/\delta^{1.07}$.

In order to emphasize our approach validity, we also propose a different calculation that not only matches our previous result, but also provide the physical interpretation of transition between non-monotonic to repulsive vortex-vortex interaction regimes in terms of critical fields H_c and H_{c2}. In bulk superconductors the interaction is found to be either short-range attractive for $\kappa < 1/\sqrt{2}$ or short-range repulsive when $\kappa > 1/\sqrt{2}$. The behavioral change between these two regimes is characterized as the point where the upper H_{c2} and lower H_{c1} critical fields matches with H_c. In order to extend such criteria to samples with finite thickness, a tunable external magnetic field was added in an initially full superconducting sample and the critical field was defined as the field where the condensation energy becomes equal to the energy loss of expelling the magnetic field at the Meissner state, so that normal and superconducting states share the same energy, vanishing the Gibbs free energy. On the other hand, differently from H_c, the upper critical field H_{c2} do not change with the penetration depth and therefore, shall not depend

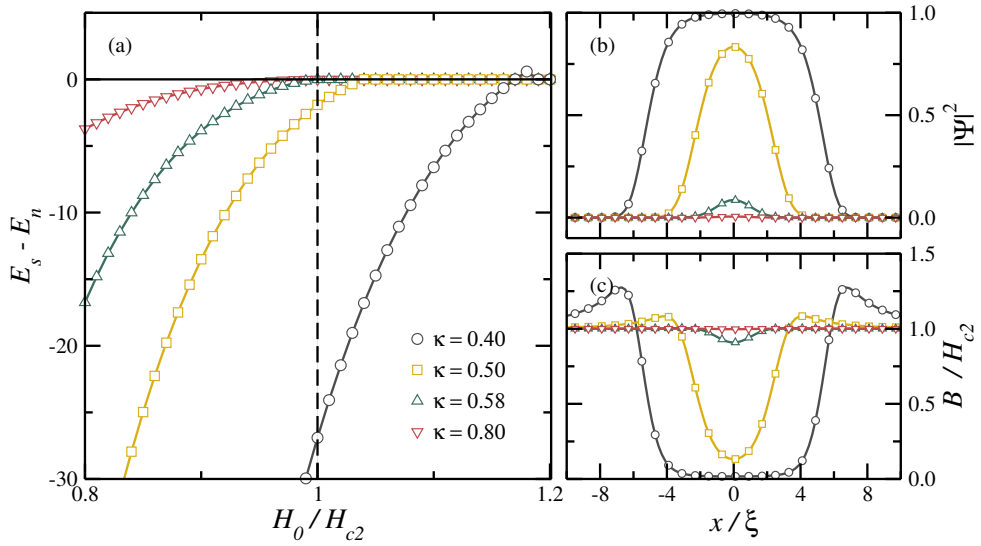

Figure 61 – (a) Energy difference between superconducting and normal domains as a function of the externally applied magnetic field for different values of κ. Order parameter and magnetic profiles at $H_0 = H_{c2}$, respectively illustrated in (b) and (c) for the same values of κ in (a).

significantly on the film thickness, preserving its definition used for bulk cases. Surprisingly, our obtained critical parameter κ_{eff}, defining the short-range transition also matches the point where $H_c = H_{c2}$. In Fig. 61, fixing the thickness $\delta = 4\xi$, the energy difference $E_s - E_n$ is shown for different values of Ginzburg-Landau parameter κ: 0.40 (gray circles), 0.50 (yellow squares), 0.58 (green upward triangles) and 0.80 (red downward triangles). Assuming low values of Ginzburg-Landau parameter, such as $\kappa = 0.4$ and 0.5, where the short-range interaction is attractive, H_c is greater than the upper critical field and the superconductor is fundamentally of type-I. This type-I behavior is, however, distorted by the presence of the long-range repulsion between stray fields, so that the full-range interaction becomes non-monotonic. As the Ginzburg-Landau parameter increases, however, H_c approaches H_{c2} and exactly over our redefined critical parameter, $\kappa = 0.58$, the free energy difference vanishes at exactly $H_0 = H_{c2}$, characterizing the transition between attractive and repulsive short-range regimes. In fact, whenever the material nature is of type-II, the Gibbs free energy should vanish at H_{c2}, since the superconducting state is completely destroyed, $|\Psi(x, y, z)| = 0$, and the magnetic field becomes the applied field. This behavior is shown in Fig. 61 for $\kappa = 0.8$ by red triangles.

In Fig. 62 (a), the critical field is shown as a function of the sample thickness for three different values of Ginzburg-Landau parameter κ: 0.3 (blue circles), 0.4 (gray squares) and 0.5 (red triangles). As the sample is made thicker, the ratio H_c/H_{c2} approaches their expected asymptotic values (dotted lines), analytically obtained from Ginzburg-Landau theory, $H_c^{bulk}/H_{c2} = 1/\sqrt{2}\kappa$. Because our approach convergence is greatly compromised when large values of thickness and small values of κ are assumed, fitting functions were

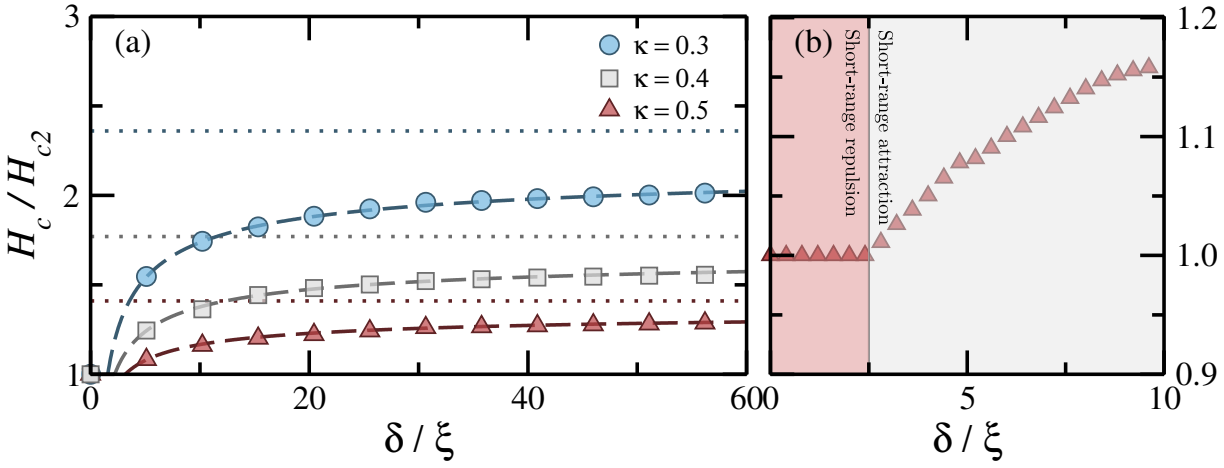

Figure 62 – (a) Critical field as a function of sample thickness δ for three different values of Ginzburg-Landau parameter κ: 0.30 (blue circles), 0.4 (gray squares) and 0.5 (red triangles); and their corresponding asymptotic values (dotted lines). Fitting functions $H_c/H_{c2} = \alpha_\kappa[1 - \sqrt{(\beta_\kappa/\delta)}]$ are represented by dashed lines, with fitting parameters $(\alpha_{0.3}, \beta_{0.3}) = (0.22, 0.47)$, $(\alpha_{0.4}, \beta_{0.4}) = (1.71, 0.38)$ and $(\alpha_{0.5}, \beta_{0.5}) = (1.38, 0.24)$. (b) Critical field near the film limit for $\kappa = 0.5$. Red and gray backgrounds account for the short-range repulsion and short-range attractive regimes.

used in order to speculate the critical field behavior when δ/ξ goes to infinity. According to Ref. (HARPER; TINKHAM, 1968), the critical field of a film approximately obeys

$$\frac{H_c}{H_{c2}} = \frac{1}{\sqrt{2}\kappa}\left[1 - \left(\frac{\Delta}{\delta}\right)^{1/2}\right], \tag{4.1}$$

where Δ is a length associated with the energy at the interface between normal and superconducting domains. Notice that, in the limit where $\delta/\xi \to \infty$, the bulk result is indeed recovered, $H_c/H_{c2} \to 1/\sqrt{2}\kappa$. Here, however, $1/\sqrt{2}\kappa$ and Δ were respectively replaced by fitting parameters α_κ and β_κ. Performed fittings are illustrated by dashed lines in Fig. 62 (a), with $(\alpha_{0.3}, \beta_{0.3}) = (0.22, 0.47)$, $(\alpha_{0.4}, \beta_{0.4}) = (1.71, 0.38)$ and $(\alpha_{0.5}, \beta_{0.5}) = (1.38, 0.24)$. In fact, asymptotic values provided by fitting functions, α_k, are very close to the theoretical predictions, $1/\sqrt{2}\kappa$, with errors of the order of 5.0%, 3.5% and 2.7%, respectively.

On the other hand, as the sample is made thinner its critical field decreases until it reaches the transition point, characterized by $H_c = H_{c2}$. Below this point, the Gibbs free energy should always vanish at H_{c2}, when the full normal state is achieved. This behavior is shown at Fig. 62 (b) for $\kappa = 0.5$, where the red and gray backgrounds represent the repulsive and non-monotonic vortex-vortex interaction regimes, respectively. The dividing line between both regimes was extracted from vortex-vortex interaction phase diagram shown in Fig. 59 (a).

The dividing line separating repulsive and non-monotonic regimes is only slightly affected by the many-body effect. In fact, in Fig. 63 (a) , considering a triple

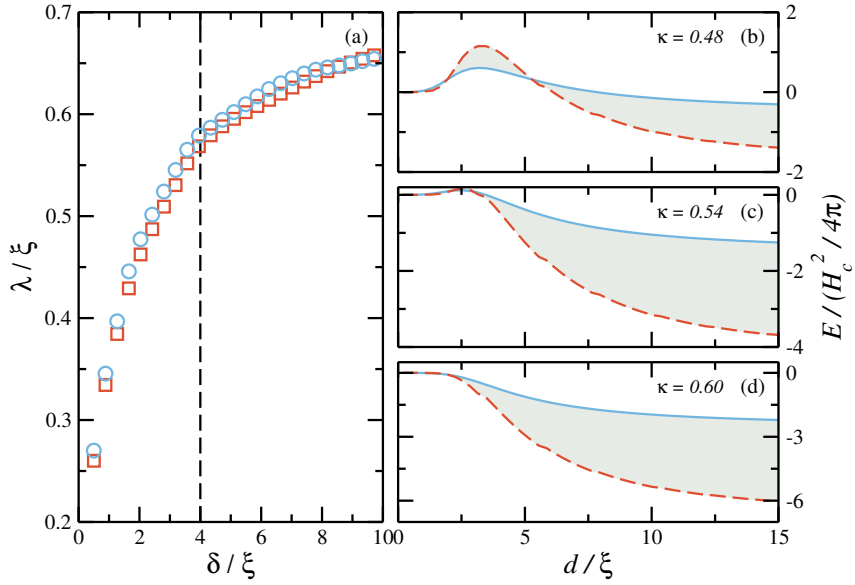

Figure 63 – (a) Dividing line between short-range attractive and short-range repulsive regimes for double- (blue circles) and triple- (red squares) vortex structures. (b-d) Total energy E as a function of inter-vortex distance d for double- (blue solid line) and triple- (red dashed line) vortex structures with $\kappa = 0.48$, 0.54 and 0.60, respectively.

vortex structure, where vortices are sited at vertices of an equilateral triangle of lateral size d, the dividing line separating short-range attraction and short-range repulsion is shown by blue circles. For comparison, the result obtained with the double-vortex structure was replicated (red squares). In Figs. 63 (b-d), the total energy is shown as a function of the inter-vortex distances d for the double- (blue solid line) and triple- (red dashed line) vortex structures, where $\delta = 4\xi$ and different values of κ were assumed. In all these three situations, many-body effect has small influence on the nature of the short-range interaction. Indeed, relevant differences are observed only when vortex cores do not overlap with each other.

5 Conclusions

Overall, the vortex pinning approach provides a powerful tool, allowing us to investigate from the most basic and simplest properties exhibited in their internal structure, to their dynamical properties governed by the vortex-vortex interaction (DANTAS et al., a; DANTAS et al., b). Our approach proved to be general enough, describing vortex properties under different backgrounds, such as single- and multi- component Bose-Einstein condensates as well as bulk and film superconductors. Nevertheless, there is still room for improvements. In fact, the method can be extended in order to cover Bose-Einstein condensates with different kinds of particle-particle interaction or even superconductors with more than one superconducting band. Anyway, restricting ourselves to the cases covered in this thesis, we have presented a method for calculating pairwise vortex-vortex interaction potentials in multi-component Bose-Einstein condensates, capable of revealing the underlying reasons for the unusual vortex configurations, such as different lattice geometries and few-vortex clusters. We have applied our theory in specific examples and could thereby clarify the formation of a lattice of dimers in rotating two-component BECs as well as the dimer/trimer state in a coherently coupled two/three-component BEC by pointing out the role of the non-monotonic interaction potential with respect to the inter-vortex distance in both cases. Our analysis of the present day experimental capabilities, combined with simple estimates of relevant parameters, indicates that considered effects are on the verge of being directly observed in the lab. We remark that the present theory can be straightforwardly adapted to any number of condensate components, providing a tool to anticipate different aspects of vortex physics in Bose-Einstein condensates. As a matter of fact, even for one-component BECs featuring the anisotropic and long-range dipolar interaction, vortex phases such as bubbles and stripes have been foreseen (COOPER; REZAYI; SIMON, 2005; ZHANG; ZHAI, 2005; KUMAR; MURUGANANDAM, 2014), for which a thorough understanding of the role of vortex-vortex interaction is still lacking.

Taking advantage of the control of number of vortices in the superconducting sample, we have investigated, under the zero-field approximation, the inner structure of a single and isolated vortex, as well as some of their properties, such as the magnetic field, current density and order parameter profile. Some of these features were known only under the London's approach or in very restricted spatial regimes. Within the advent of our approach, we have extended some expression known in literature, covering, for any value of Ginzburg-Landau parameter κ, vortex properties over full spatial range. For bulk samples, we have found that type-I/type-II transition is closely related to the ratio between vortex and magnetic core sizes. Actually, with the mean-value definition for core sizes, the threshold of interaction regimes lies exactly over the point where the

vortex and the magnetic profiles have exactly the same core size. This argument was used to explain non-monotonic vortex-vortex interactions in two-band superconductors. Here, however, despite it shows a close relation with their sizes, the threshold of interaction regime transitions are not well defined under our definitions of core sizes.

Subsequently, extending up the formalism in order to account for superconducting samples with finite thickness, we have described the vortex and magnetic core sizes as a function of the film thickness. Our results shows that both cores become larger as the thickness becomes smaller and shall recover the bulk value for samples with 12ξ. Interestingly, for giant-vortex states, magnetic profiles might present off-centered peak as a consequence of the large core radius when compared to the film thickness. In general, magnetic fields produced by giant-vortex inside the sample are weaker than those produced by single vortices, however this behavior might be reverted outside the sample, which makes giant-vortices more easily detectable far from the sample. In contrast, we have also find out that signatures of phase transition between different regimes of vortex-vortex interaction may not be extended to describe vortex states in samples with finite thickness due to the magnetic contribution of stray fields outside the sample region.

Finally, we have calculated the vortex-vortex interaction potential in a type-I superconducting film by solving constrained GL equations. Our results demonstrate that the repulsion between stray fields in films with a thickness of a few ξ lead to a non-monotonic vortex-vortex interaction potential that is short range attractive and long range repulsive, which differs even from the recently observed non-monotonic potential in two-band superconductors, where vortices attract (repel) when placed far away from (close to) each other. By analyzing the obtained potential profiles, one can have a deeper understanding of the vortex conformations in these films. The critical value for which the vortex-vortex interaction becomes repulsive and vortices are suppose to form ordinary Abrikosov lattices, which has been assumed as $\kappa_c^b = 1/\sqrt{2}$ for bulk superconductors, is demonstrated to be a limiting case for a more general $\kappa_c(\delta)$ as the film thickness δ increases. The redefined $\kappa_c(\delta)$ satisfies $\kappa_c(\delta) = \alpha\delta^\beta$ in the $\delta \to 0$ limit, with $\alpha \approx 0.36$ and $\beta \approx 0.4$. This result contrasts with the well know definition of effective Ginzburg-Landau parameter, which should lead to $\kappa_c \approx 0.59\sqrt{\delta}$. On the other hand, if the film is made thicker, the critical parameter must satisfy $\kappa_c \approx \kappa_c^b - 0.57/\delta^{1.07}$, rapidly recovering the bulk transition point.

Bibliography

ABO-SHAEER, J. R. et al. Observation of vortex lattices in Bose-Einstein condensates. *Science*, American Association for the Advancement of Science, v. 292, n. 5516, p. 476–479, 2001. ISSN 0036-8075. Disponível em: <http://science.sciencemag.org/content/292/5516/476>. Cited 5 times in pages 13, 42, 43, 76, and 80.

ABRIKOSOV, A. A. Magnetic properties of superconductors of the second group. *Soviet Physics JETP*, v. 5, p. 1174, 1957. Cited 3 times in pages 66, 97, and 98.

ABRIKOSOV, A. A. Nobel lecture: Type-II superconductors and the vortex lattice*. *Rev. Mod. Phys.*, American Physical Society, v. 76, p. 975–979, Dec 2004. Disponível em: <http://link.aps.org/doi/10.1103/RevModPhys.76.975>. Cited 2 times in pages 97 and 98.

AFTALION, A.; DANAILA, I. Giant vortices in combined harmonic and quartic traps. *Phys. Rev. A*, American Physical Society, v. 69, p. 033608, Mar 2004. Disponível em: <http://link.aps.org/doi/10.1103/PhysRevA.69.033608>. Cited in page 86.

AFTALION, A.; MASON, P.; WEI, J. Vortex-peak interaction and lattice shape in rotating two-component Bose-Einstein condensates. *Phys. Rev. A*, American Physical Society, v. 85, p. 033614, Mar 2012. Disponível em: <http://link.aps.org/doi/10.1103/PhysRevA.85.033614>. Cited 2 times in pages 43 and 77.

AIKAWA, K. et al. Bose-Einstein condensation of erbium. *Phys. Rev. Lett.*, American Physical Society, v. 108, p. 210401, May 2012. Disponível em: <http://link.aps.org/doi/10.1103/PhysRevLett.108.210401>. Cited in page 77.

ALLEN, A. D. M. J. F. Viscosity of liquid helium below the λ-point. *Nature*, Nature, v. 142, p. 643–644, Oct 1938. Disponível em: <http://www-nature-com.ez11.periodicos.capes.gov.br/nature/journal/v142/n3597/abs/142643a0.html>. Cited in page 32.

ANDERSON, M. H. et al. Observation of Bose-Einstein condensation in a dilute atomic vapor. *Science*, American Association for the Advancement of Science, v. 269, n. 5221, p. 198–201, 1995. ISSN 0036-8075. Disponível em: <http://science.sciencemag.org/content/269/5221/198>. Cited 2 times in pages 33 and 76.

ANNETT, J. *Superconductivity, Superfluids and Condensates*. OUP Oxford, 2004. (Oxford Master Series in Physics). ISBN 9780198507567. Disponível em: <https://books.google.com.br/books?id=WZcXmBrZIc8C>. Cited 2 times in pages 28 and 35.

BABAEV, E.; SILAEV, M. Comment on "Ginzburg-Landau theory of two-band superconductors: Absence of type-1.5 superconductivity". *Phys. Rev. B*, American Physical Society, v. 86, p. 016501, Jul 2012. Disponível em: <http://link.aps.org/doi/10.1103/PhysRevB.86.016501>. Cited in page 125.

BABAEV, E.; SPEIGHT, M. Semi-Meissner state and neither type-I nor type-II superconductivity in multicomponent superconductors. *Phys. Rev. B*, American Physical Society, v. 72, p. 180502, Nov 2005. Disponível em: <http://link.aps.org/doi/10.1103/PhysRevB.72.180502>. Cited in page 125.

Baldo, M.; Saperstein, E. E.; Tolokonnikov, S. V. A realistic model of superfluidity in the neutron star inner crust. *Eur. Phys. J. A*, v. 32, n. 1, p. 97–108, 2007. Disponível em: <http://dx.doi.org/10.1140/epja/i2006-10356-5>. Cited in page 97.

BARDEEN, J.; COOPER, L. N.; SCHRIEFFER, J. R. Theory of superconductivity. *Phys. Rev.*, American Physical Society, v. 108, p. 1175–1204, Dec 1957. Disponível em: <http://link.aps.org/doi/10.1103/PhysRev.108.1175>. Cited 2 times in pages 32 and 49.

BEDNORZ, J. G.; MÜLLER, K. A. Possible high-Tc superconductivity in the Ba-La-Cu-O system. *Zeitschrift für Physik B Condensed Matter*, v. 64, n. 2, p. 189–193, 1986. Disponível em: <http://dx.doi.org/10.1007/BF01303701>. Cited in page 49.

BERDIYOROV, G. R.; MILOŠEVIĆ, M. V.; PEETERS, F. M. Vortex configurations and critical parameters in superconducting thin films containing antidot arrays: Nonlinear Ginzburg-Landau theory. *Phys. Rev. B*, American Physical Society, v. 74, p. 174512, Nov 2006. Disponível em: <https://link.aps.org/doi/10.1103/PhysRevB.74.174512>. Cited in page 50.

BOGOLIUBOV, N. On the theory of superfluidity. *J. Phys. USSR*, v. 11, p. 23, 1947. Cited in page 39.

BOLLE, C. A. et al. Observation of a commensurate array of flux chains in tilted flux lattices in Bi-Sr-Ca-Cu-o single crystals. *Phys. Rev. Lett.*, American Physical Society, v. 66, p. 112–115, Jan 1991. Disponível em: <http://link.aps.org/doi/10.1103/PhysRevLett.66.112>. Cited in page 67.

BOSE, S. N. Plancks gesetz und lichtquantenhypothese. *Zeitschrift für Physik*, v. 26, n. 1, p. 178–181, 1924. ISSN 0044-3328. Disponível em: <http://dx.doi.org/10.1007/BF01327326>. Cited in page 25.

BOTELHO, S. S.; MELO, C. A. R. Sá de. Vortex-antivortex lattice in ultracold fermionic gases. *Phys. Rev. Lett.*, American Physical Society, v. 96, p. 040404, Feb 2006. Disponível em: <http://link.aps.org/doi/10.1103/PhysRevLett.96.040404>. Cited in page 77.

BOUQUET, F. et al. Specific heat of $Mg^{11}B_2$: Evidence for a second energy gap. *Phys. Rev. Lett.*, American Physical Society, v. 87, p. 047001, Jul 2001. Disponível em: <http://link.aps.org/doi/10.1103/PhysRevLett.87.047001>. Cited 2 times in pages 49 and 99.

BRADLEY, C. C.; SACKETT, C. A.; HULET, R. G. Bose-Einstein condensation of lithium: Observation of limited condensate number. *Phys. Rev. Lett.*, American Physical Society, v. 78, p. 985–989, Feb 1997. Disponível em: <http://link.aps.org/doi/10.1103/PhysRevLett.78.985>. Cited 2 times in pages 33 and 34.

BRADLEY, C. C. et al. Evidence of Bose-Einstein condensation in an atomic gas with attractive interactions. *Phys. Rev. Lett.*, American Physical Society, v. 75, p. 1687–1690, Aug 1995. Disponível em: <http://link.aps.org/doi/10.1103/PhysRevLett.75.1687>. Cited 3 times in pages 33, 34, and 76.

BRANDT, E. H. Vortices in superconducting bulk, films and squids. *Pramana*, v. 66, n. 1, p. 67–81, 2006. ISSN 0973-7111. Disponível em: <http://dx.doi.org/10.1007/BF02704938>. Cited in page 105.

BRANDT, E. H. Vortex-vortex interaction in thin superconducting films. *Phys. Rev. B*, American Physical Society, v. 79, p. 134526, Apr 2009. Disponível em: <http://link.aps.org/doi/10.1103/PhysRevB.79.134526>. Cited in page 125.

BRANDT, E. H.; DAS, M. P. Attractive vortex interaction and the intermediate-mixed state of superconductors. *Journal of Superconductivity and Novel Magnetism*, v. 24, n. 1, p. 57–67, 2011. ISSN 1557-1947. Disponível em: <http://dx.doi.org/10.1007/s10948-010-1046-8>. Cited 3 times in pages 65, 98, and 125.

BRANDT, E. H.; INDENBOM, M. V.; FORKL, A. Type-II superconducting strip in perpendicular magnetic field. *EPL (Europhysics Letters)*, v. 22, n. 9, p. 735, 1993. Disponível em: <http://stacks.iop.org/0295-5075/22/i=9/a=017>. Cited in page 50.

BRANDT, E. H.; ZHOU, S. P. Attractive vortices. *Physics*, v. 2, p. 22, 2009. Cited in page 122.

BRITO, P. de; NAZARENO, H. Wave packets in graphene under external fields: Vortices formation. *Physica B: Condensed Matter*, v. 407, n. 7, p. 1068 – 1074, 2012. ISSN 0921-4526. Disponível em: <http://www.sciencedirect.com/science/article/pii/S0921452611013147>. Cited in page 97.

BROGLIE, L. de. Xxxv. a tentative theory of light quanta. *Philosophical Magazine Series 6*, v. 47, n. 278, p. 446–458, 1924. Disponível em: <http://dx.doi.org/10.1080/14786442408634378>. Cited in page 26.

BUCKEL, W.; KLEINER, R. *Superconductivity: Fundamentals and Applications*. Wiley, 2008. (Physics textbook). ISBN 9783527618514. Disponível em: <https://books.google.com.br/books?id=v_k3EyDe40IC>. Cited in page 50.

BUGOSLAVSKY, Y. et al. Vortex dynamics in superconducting MgB_2 and prospects for applications. *Nature*, Macmillian Magazines Ltd., v. 410, p. 563 – 565, 2001. Cited in page 98.

BUNEMAN, O. Transverse plasma waves and plasma vortices. *Phys. Rev.*, American Physical Society, v. 112, p. 1504–1512, Dec 1958. Disponível em: <http://link.aps.org/doi/10.1103/PhysRev.112.1504>. Cited in page 97.

BURNETT MARK EDWARDS, C. W. C. K. The theory of Bose-Einstein condensation of dilute gases. *Physics Today*, AIP Publishing LLC, v. 52, p. 37–42, Jan 2008. Cited in page 32.

BUTTS, D. A.; ROKHSAR, D. S. Predicted signatures of rotating Bose-Einstein condensates. *Nature*, Nature Publishing Group, v. 397, p. 327–329, Jan 1999. Disponível em: <http://dx.doi.org/10.1038/16865>. Cited in page 81.

CABRAL, L. R. E.; BAELUS, B. J.; PEETERS, F. M. From vortex molecules to the Abrikosov lattice in thin mesoscopic superconducting disks. *Phys. Rev. B*, American Physical Society, v. 70, p. 144523, Oct 2004. Disponível em: <http://link.aps.org/doi/10.1103/PhysRevB.70.144523>. Cited 2 times in pages 97 and 98.

CALLEN, H. *Thermodynamics: an introduction to the physical theories of equilibrium thermostatics and irreversible thermodynamics*. [S.l.]: Wiley, 1960. Cited in page 25.

CHAUDHARI, R. D. Critical magnetic fields in superconducting films of indium. *Phys. Rev.*, American Physical Society, v. 151, p. 96–100, Nov 1966. Disponível em: <http://link.aps.org/doi/10.1103/PhysRev.151.96>. Cited in page 50.

CHAVES, A. et al. Conditions for nonmonotonic vortex interaction in two-band superconductors. *Phys. Rev. B*, American Physical Society, v. 83, p. 214523, Jun 2011. Disponível em: <http://link.aps.org/doi/10.1103/PhysRevB.83.214523>. Cited 8 times in pages 49, 77, 84, 99, 105, 119, 124, and 125.

CHAVES, A. et al. Vortex-vortex interaction in bulk superconductors: Ginzburg-Landau theory. *Phys. Rev. B*, American Physical Society, v. 83, p. 054516, Feb 2011. Disponível em: <http://link.aps.org/doi/10.1103/PhysRevB.83.054516>. Cited 6 times in pages 77, 84, 99, 119, 125, and 126.

CHIN, C. et al. Feshbach resonances in ultracold gases. *Rev. Mod. Phys.*, American Physical Society, v. 82, p. 1225–1286, Apr 2010. Disponível em: <http://link.aps.org/doi/10.1103/RevModPhys.82.1225>. Cited in page 34.

CHOMAZ, L. et al. Emergence of coherence via transverse condensation in a uniform quasi-two-dimensional Bose gas. *Nat Commun*, Nature Publishin Group, v. 6, p. 6162, May 2015. Cited 2 times in pages 77 and 94.

CHU, S. Nobel lecture: The manipulation of neutral particles. *Rev. Mod. Phys.*, American Physical Society, v. 70, p. 685–706, Jul 1998. Disponível em: <http://link.aps.org/doi/10.1103/RevModPhys.70.685>. Cited in page 32.

CIPRIANI, M.; NITTA, M. Crossover between integer and fractional vortex lattices in coherently coupled two-component Bose-Einstein condensates. *Phys. Rev. Lett.*, American Physical Society, v. 111, p. 170401, Oct 2013. Disponível em: <http://link.aps.org/doi/10.1103/PhysRevLett.111.170401>. Cited 2 times in pages 43 and 77.

CLEM, J. R. Simple model for the vortex core in a type II superconductor. *Journal of Low Temperature Physics*, v. 18, n. 5, p. 427–434, 1975. ISSN 1573-7357. Disponível em: <http://dx.doi.org/10.1007/BF00116134>. Cited in page 98.

CLEM, J. R. Two-dimensional vortices in a stack of thin superconducting films: A model for high-temperature superconducting multilayers. *Phys. Rev. B*, American Physical Society, v. 43, p. 7837–7846, Apr 1991. Disponível em: <http://link.aps.org/doi/10.1103/PhysRevB.43.7837>. Cited 2 times in pages 101 and 102.

COHEN-TANNOUDJI, C.; DIU, B.; LALOE, F. *Quantum Mechanics*. Wiley, 1991. (Quantum Mechanics, v. 1). ISBN 9780471164333. Disponível em: <https://books.google.be/books?id=iHcpAQAAMAAJ>. Cited 2 times in pages 25 and 48.

COHEN-TANNOUDJI, C. N. Nobel lecture: Manipulating atoms with photons. *Rev. Mod. Phys.*, American Physical Society, v. 70, p. 707–719, Jul 1998. Disponível em: <http://link.aps.org/doi/10.1103/RevModPhys.70.707>. Cited in page 32.

COOPER, N. Rapidly rotating atomic gases. *Advances in Physics*, v. 57, n. 6, p. 539–616, 2008. Disponível em: <http://dx.doi.org/10.1080/00018730802564122>. Cited in page 76.

COOPER, N. R.; REZAYI, E. H.; SIMON, S. H. Vortex lattices in rotating atomic Bose gases with dipolar interactions. *Phys. Rev. Lett.*, American Physical Society, v. 95, p. 200402, Nov 2005. Disponível em: <http://link.aps.org/doi/10.1103/PhysRevLett.95.200402>. Cited 2 times in pages 76 and 135.

CÓRDOBA-CAMACHO, W. Y. et al. Between types I and II: Intertype flux exotic states in thin superconductors. *Phys. Rev. B*, American Physical Society, v. 94, p. 054511, Aug 2016. Disponível em: <http://link.aps.org/doi/10.1103/PhysRevB.94.054511>. Cited in page 126.

CORNISH, S. L. et al. Stable ^{85}Rb Bose-Einstein condensates with widely tunable interactions. *Phys. Rev. Lett.*, American Physical Society, v. 85, p. 1795–1798, Aug 2000. Disponível em: <http://link.aps.org/doi/10.1103/PhysRevLett.85.1795>. Cited 2 times in pages 33 and 34.

CREN, T. et al. Vortex fusion and giant vortex states in confined superconducting condensates. *Phys. Rev. Lett.*, American Physical Society, v. 107, p. 097202, Aug 2011. Disponível em: <http://link.aps.org/doi/10.1103/PhysRevLett.107.097202>. Cited in page 86.

CUCOLO, A. M. et al. Visualizing vortex dynamics in py/nb thin film hybrids by low temperature magnetic force microscopy. *Journal of Superconductivity and Novel Magnetism*, v. 25, n. 7, p. 2167–2171, 2012. Disponível em: <http://dx.doi.org/10.1007/s10948-012-1644-8>. Cited in page 50.

DALFOVO, F. et al. Theory of Bose-Einstein condensation in trapped gases. *Rev. Mod. Phys.*, American Physical Society, v. 71, p. 463–512, Apr 1999. Disponível em: <http://link.aps.org/doi/10.1103/RevModPhys.71.463>. Cited in page 26.

DANAILA, I. Three-dimensional vortex structure of a fast rotating Bose-Einstein condensate with harmonic-plus-quartic confinement. *Phys. Rev. A*, American Physical Society, v. 72, p. 013605, Jul 2005. Disponível em: <http://link.aps.org/doi/10.1103/PhysRevA.72.013605>. Cited in page 86.

DANTAS, D. S. et al. Non-monotonic vortex-vortex interactions at the type-I to type-II transition of thin superconducting films. To be published. Cited 3 times in pages 98, 118, and 135.

DANTAS, D. S. et al. Vortex characterization in single-gap superconducting bulk and films. To be published. Cited in page 135.

DANTAS, D. S. et al. Bound vortex states and exotic lattices in multicomponent Bose-Einstein condensates: The role of vortex-vortex interaction. *Physical Review A*, APS, v. 91, n. 2, p. 023630, 2015. Cited 2 times in pages 77 and 99.

DAVIS, K. B. et al. Bose-Einstein condensation in a gas of sodium atoms. *Phys. Rev. Lett.*, American Physical Society, v. 75, p. 3969–3973, Nov 1995. Disponível em: <http://link.aps.org/doi/10.1103/PhysRevLett.75.3969>. Cited 2 times in pages 33 and 76.

DEAVER, B.; RUVALDS, J.; DIVISION, N. A. T. O. S. A. *Advances in Superconductivity*. Plenum Press, 1983. (NATO ASI Series: Physics). ISBN 9780306413889. Disponível em: <https://books.google.com.br/books?id=nk23AAAAIAAJ>. Cited in page 52.

DEAVER, B. S.; FAIRBANK, W. M. Experimental evidence for quantized flux in superconducting cylinders. *Phys. Rev. Lett.*, American Physical Society, v. 7, p. 43–46, Jul 1961. Disponível em: <http://link.aps.org/doi/10.1103/PhysRevLett.7.43>. Cited in page 57.

DELBRUCK, M. Was Bose-Einstein statistics arrived at by serendipity? *Journal of Chemical Education*, v. 57, n. 7, p. 467, 1980. Disponível em: <http://dx.doi.org/10.1021/ed057p467>. Cited in page 27.

DEO, P. S. et al. Magnetization of mesoscopic superconducting disks. *Phys. Rev. Lett.*, American Physical Society, v. 79, p. 4653–4656, Dec 1997. Disponível em: <http://link.aps.org/doi/10.1103/PhysRevLett.79.4653>. Cited in page 61.

DOLL, R.; NÄBAUER, M. Experimental proof of magnetic flux quantization in a superconducting ring. *Phys. Rev. Lett.*, American Physical Society, v. 7, p. 51–52, Jul 1961. Disponível em: <http://link.aps.org/doi/10.1103/PhysRevLett.7.51>. Cited in page 57.

DURFEE, D. S.; KETTERLE, W. Experimental studies of Bose-Einstein condensation. *Opt. Express*, OSA, v. 2, n. 8, p. 299–313, Apr 1998. Disponível em: <http://www.opticsexpress.org/abstract.cfm?URI=oe-2-8-299>. Cited 2 times in pages 12 and 33.

EINSTEIN, A. Quantentheorie des einatomigen idealen gases. *Sitzungsbericht der Preussichen Akademie der Wissenschaften, Physikalisch-mathematische Klasse*, p. 3, 1925. Cited in page 25.

ESCOBAR, Y. N. M. de et al. Bose-Einstein condensation of ^{84}Sr. *Phys. Rev. Lett.*, American Physical Society, v. 103, p. 200402, Nov 2009. Disponível em: <http://link.aps.org/doi/10.1103/PhysRevLett.103.200402>. Cited 2 times in pages 33 and 34.

ESKILDSEN, M. R. et al. Vortex imaging in the π band of magnesium diboride. *Phys. Rev. Lett.*, American Physical Society, v. 89, p. 187003, Oct 2002. Disponível em: <http://link.aps.org/doi/10.1103/PhysRevLett.89.187003>. Cited in page 98.

ESSMANN, U.; TRÄUBLE, H. The direct observation of individual flux lines in type II superconductors. *Physics Letters A*, v. 24, n. 10, p. 526 – 527, 1967. ISSN 0375-9601. Disponível em: <http://www.sciencedirect.com/science/article/pii/0375960167908195>. Cited 4 times in pages 13, 67, 68, and 97.

ETO, M. et al. Interaction of half-quantized vortices in two-component Bose-Einstein condensates. *Phys. Rev. A*, American Physical Society, v. 83, p. 063603, Jun 2011. Disponível em: <http://link.aps.org/doi/10.1103/PhysRevA.83.063603>. Cited 2 times in pages 43 and 77.

ETO, M.; NITTA, M. Vortex trimer in three-component Bose-Einstein condensates. *Phys. Rev. A*, American Physical Society, v. 85, p. 053645, May 2012. Disponível em: <http://link.aps.org/doi/10.1103/PhysRevA.85.053645>. Cited 5 times in pages 14, 43, 77, 81, and 91.

FERRARI, G. et al. Collisional properties of ultracold k-rb mixtures. *Phys. Rev. Lett.*, American Physical Society, v. 89, p. 053202, Jul 2002. Disponível em: <http://link.aps.org/doi/10.1103/PhysRevLett.89.053202>. Cited in page 35.

FETTER, A. L. Rotating trapped Bose-Einstein condensates. *Rev. Mod. Phys.*, American Physical Society, v. 81, p. 647–691, May 2009. Disponível em: <http://link.aps.org/doi/10.1103/RevModPhys.81.647>. Cited in page 26.

FETTER, A. L. Rotating trapped Bose-Einstein condensates. *Rev. Mod. Phys.*, American Physical Society, v. 81, p. 647–691, May 2009. Disponível em: <http://link.aps.org/doi/10.1103/RevModPhys.81.647>. Cited 2 times in pages 76 and 97.

FETTER, A. L.; HOHENBERG, P. C. The mixed state of thin superconducting films in perpendicular fields. *Phys. Rev.*, American Physical Society, v. 159, p. 330–343, Jul 1967. Disponível em: <http://link.aps.org/doi/10.1103/PhysRev.159.330>. Cited 5 times in pages 50, 98, 102, 111, and 112.

FETTER, A. L.; JACKSON, B.; STRINGARI, S. Rapid rotation of a Bose-Einstein condensate in a harmonic plus quartic trap. *Phys. Rev. A*, American Physical Society, v. 71, p. 013605, Jan 2005. Disponível em: <http://link.aps.org/doi/10.1103/PhysRevA.71.013605>. Cited in page 86.

FEYNMAN, R. Chapter {II} application of quantum mechanics to liquid helium. In: GORTER, C. (Ed.). *Progress in low temperature physics*. Elsevier, 1955, (Progress in Low Temperature Physics, v. 1). p. 17 – 53. Disponível em: <http://www.sciencedirect.com/science/article/pii/S0079641708600773>. Cited 3 times in pages 42, 81, and 86.

FEYNMAN, R. *Statistical Mechanics: A Set Of Lectures*. Westview Press, 1998. (Advanced Books Classics). ISBN 9780813346106. Disponível em: <https://books.google.com.br/books?id=Ou4ltPYiXPgC>. Cited in page 41.

FEYNMAN, R. P. Superfluidity and superconductivity. *Rev. Mod. Phys.*, American Physical Society, v. 29, p. 205–212, Apr 1957. Disponível em: <http://link.aps.org/doi/10.1103/RevModPhys.29.205>. Cited 2 times in pages 29 and 32.

FISCHER, U. R. Stability of quasi-two-dimensional Bose-Einstein condensates with dominant dipole-dipole interactions. *Phys. Rev. A*, American Physical Society, v. 73, p. 031602, Mar 2006. Disponível em: <http://link.aps.org/doi/10.1103/PhysRevA.73.031602>. Cited in page 95.

FORTERRE, Y.; POULIQUEN, O. Longitudinal vortices in granular flows. *Phys. Rev. Lett.*, American Physical Society, v. 86, p. 5886–5889, Jun 2001. Disponível em: <http://link.aps.org/doi/10.1103/PhysRevLett.86.5886>. Cited in page 97.

FRÖHLICH, H. Theory of the superconducting state. i. the ground state at the absolute zero of temperature. *Phys. Rev.*, American Physical Society, v. 79, p. 845–856, Sep 1950. Disponível em: <http://link.aps.org/doi/10.1103/PhysRev.79.845>. Cited 2 times in pages 68 and 70.

GAMMEL, P. L. et al. Observation of hexagonally correlated flux quanta in $yba_2cu_3o_7$. *Phys. Rev. Lett.*, American Physical Society, v. 59, p. 2592–2595, Nov 1987. Disponível em: <http://link.aps.org/doi/10.1103/PhysRevLett.59.2592>. Cited in page 67.

GARAUD2011, J.; CARLSTRÖM, J.; BABAEV, E. Topological solitons in three-band superconductors with broken time reversal symmetry. *Phys. Rev. Lett.*, American Physical Society, v. 107, p. 197001, Nov 2011. Disponível em: <http://link.aps.org/doi/10.1103/PhysRevLett.107.197001>. Cited in page 92.

GAUNT, A. L. et al. Bose-Einstein condensation of atoms in a uniform potential. *Phys. Rev. Lett.*, American Physical Society, v. 110, p. 200406, May 2013. Disponível em: <http://link.aps.org/doi/10.1103/PhysRevLett.110.200406>. Cited in page 77.

GE, J. et al. Flux pattern transitions in the intermediate state of a type-I superconductor driven by an ac field. *New Journal of Physics*, v. 15, n. 3, p. 033013, 2013. Disponível em: <http://stacks.iop.org/1367-2630/15/i=3/a=033013>. Cited 4 times in pages 19, 98, 126, and 129.

GENNES, P. D. *Superconductivity of Metals and Alloys*. Benjamin, 1966. (Frontiers in physics). Disponível em: <https://books.google.com.au/books?id=KtJEAAAAIAAJ>. Cited in page 62.

GEURTS, R.; MILOŠEVIĆ, M. V.; PEETERS, F. M. Topologically trapped vortex molecules in Bose-Einstein condensates. *Phys. Rev. A*, American Physical Society, v. 78, p. 053610, Nov 2008. Disponível em: <http://link.aps.org/doi/10.1103/PhysRevA.78.053610>. Cited in page 86.

GINZBURG, V. *On Superconductivity and Superfluidity: A Scientific Autobiography*. Springer Berlin Heidelberg, 2008. ISBN 9783540680086. Disponível em: <https://books.google.com.br/books?id=ufC9Ar8iuDcC>. Cited 2 times in pages 58 and 61.

GINZBURG, V. L. On the theory of superconductivity. *Nuovo Cimento*, v. 2, p. 1234, 1955. Cited in page 58.

GINZBURG, V. L.; LANDAU, L. D. To the theory of superconductivity. *Eskp. Teor. Fiz.*, v. 20, p. 1064, 1950. Cited 2 times in pages 58 and 125.

GLADILIN, V. N. et al. Vortices in a wedge made of a type-I superconductor. *New Journal of Physics*, v. 17, n. 6, p. 063032, 2015. Disponível em: <http://stacks.iop.org/1367-2630/17/i=6/a=063032>. Cited 2 times in pages 98 and 126.

GOR'KOV, L. P. Microscopic derivation of Ginzburg-Landau equations in the theory of superconductivity. *Soviet Phys.- JETP*, v. 9, p. 1364, Dec 1959. Cited in page 74.

GORTER, C. J.; CASIMIR, H. G. B. On supraconductivity i. *Physica*, v. 1, p. 305, 1934. Cited in page 53.

GRIESMAIER, A. et al. Bose-Einstein condensation of chromium. *Phys. Rev. Lett.*, American Physical Society, v. 94, p. 160401, Apr 2005. Disponível em: <http://link.aps.org/doi/10.1103/PhysRevLett.94.160401>. Cited 2 times in pages 33 and 34.

GROSS, E. P. Structure of a quantized vortex in boson systems. *Il Nuovo Cimento (1955-1965)*, v. 20, n. 3, p. 454–477, 1961. ISSN 1827-6121. Disponível em: <http://dx.doi.org/10.1007/BF02731494>. Cited in page 43.

GROSS, E. P. Hydrodynamics of a superfluid condensate. *Journal of Mathematical Physics*, v. 4, n. 2, p. 195–207, 1963. Disponível em: <http://scitation.aip.org/content/aip/journal/jmp/4/2/10.1063/1.1703944;jsessionid=rfKElL3uaOwyeGYtw0Ys6Qm_.x-aip-live-06>. Cited in page 43.

GUTIERREZ, J. et al. Vortex dynamics in thin films of $yba_2cu_3o_{7-x}$ with three-dimensional nanoscale patterns. *Phys. Rev. B*, American Physical Society, v. 79, p. 064526, Feb 2009. Disponível em: <http://link.aps.org/doi/10.1103/PhysRevB.79.064526>. Cited in page 50.

HALL, D. S. et al. Dynamics of component separation in a binary mixture of Bose-Einstein condensates. *Phys. Rev. Lett.*, American Physical Society, v. 81, p. 1539–1542, Aug 1998. Disponível em: <http://link.aps.org/doi/10.1103/PhysRevLett.81.1539>. Cited in page 35.

HARADA, K. et al. Direct observation of vortex dynamics in superconducting films with regular arrays of defects. *Science*, American Association for the Advancement of Science, v. 274, n. 5290, p. 1167–1170, 1996. ISSN 0036-8075. Disponível em: <http://science.sciencemag.org/content/274/5290/1167>. Cited in page 98.

HARADA, K. et al. Real-time observation of vortex lattices in a superconductor by electron microscopy. *Nature*, Nature Publishing Group, v. 360, p. 51, 1992. Disponível em: <http://link.aps.org/doi/10.1103/PhysRevLett.66.112>. Cited 3 times in pages 67, 97, and 98.

HARPER, F. E.; TINKHAM, M. The mixed state in superconducting thin films. *Phys. Rev.*, American Physical Society, v. 172, p. 441–450, Aug 1968. Disponível em: <http://link.aps.org/doi/10.1103/PhysRev.172.441>. Cited in page 133.

HENN, E. A. L. et al. Emergence of turbulence in an oscillating Bose-Einstein condensate. *Phys. Rev. Lett.*, American Physical Society, v. 103, p. 045301, Jul 2009. Disponível em: <http://link.aps.org/doi/10.1103/PhysRevLett.103.045301>. Cited in page 76.

HESS, H. F. et al. Scanning-tunneling-microscope observation of the Abrikosov flux lattice and the density of states near and inside a fluxoid. *Phys. Rev. Lett.*, American Physical Society, v. 62, p. 214–216, Jan 1989. Disponível em: <http://link.aps.org/doi/10.1103/PhysRevLett.62.214>. Cited in page 67.

HESS, H. F. et al. Spectroscopic and spatial characterization of superconducting vortex core states with a scanning tunneling microscope. *Journal of Vacuum Science & Technology A*, v. 8, n. 1, p. 450–454, 1990. Disponível em: <http://scitation.aip.org/content/avs/journal/jvsta/8/1/10.1116/1.577016>. Cited in page 98.

HILLMER, F. et al. Vortex dynamics in bi2sr2cacu2o8-thin films in the presence of columnar defects. *Journal of Low Temperature Physics*, v. 105, n. 5, p. 1153–1158, 1996. ISSN 1573-7357. Disponível em: <http://dx.doi.org/10.1007/BF00753855>. Cited in page 50.

HUANG, K. *Statistical Mechanics*. Wiley, 1963. Disponível em: <https://books.google.be/books?id=MolRAAAAMAAJ>. Cited 3 times in pages 25, 27, and 28.

HUANG, K.; YANG, C. N. Quantum-mechanical many-body problem with hard-sphere interaction. *Phys. Rev.*, American Physical Society, v. 105, p. 767–775, Feb 1957. Disponível em: <http://link.aps.org/doi/10.1103/PhysRev.105.767>. Cited in page 34.

INGUSCIO, M. et al. *Bose-Einstein Condensation in Atomic Gases: Proceedings of the International School of Physics "Enrico Fermi", Varenna on Lake Como, Villa Monastero, 7-17 July 1998*. IOS Press, 1999. (Bose-Einstein Condensation in Atomic Gases). ISBN 9780967335551. Disponível em: <https://books.google.com.br/books?id=OJH1SU0n4dgC>. Cited in page 28.

INOUYE, S. et al. Observation of Feshbach resonances in a Bose-Einstein condensate. *Nature*, Nature, v. 392, p. 151–154, March 1998. Cited in page 34.

IRZ, D.; RYZHOV, V.; TAREYEVA, E. Vortex-vortex interaction in a superconducting film of finite thickness. *Physics Letters A*, v. 207, n. 6, p. 374 – 378, 1995. ISSN 0375-9601. Disponível em: <http://www.sciencedirect.com/science/article/pii/037596019500694X>. Cited 2 times in pages 98 and 103.

JACOBS, L.; REBBI, C. Interaction energy of superconducting vortices. *Phys. Rev. B*, American Physical Society, v. 19, p. 4486–4494, May 1979. Disponível em: <http://link.aps.org/doi/10.1103/PhysRevB.19.4486>. Cited in page 125.

KAMERLINGH-ONNES, H. The superconductivity of mercury. *Comm. Phys. Lab. Univ. Leiden*, v. 120b, 122b, 124c, 1911. Cited 4 times in pages 12, 48, 50, and 51.

KAPITSZA, P. Viscosity of liquid helium below the λ-point. *Nature*, Nature, v. 141, p. 74–74, Jan 1938. Disponível em: <http://www-nature-com.ez11.periodicos.capes.gov.br/nature/journal/v141/n3558/abs/141074a0.html>. Cited in page 32.

KARAPETROV, G. et al. Direct observation of vortex lattice transitions in mesoscopic superconducting single crystals using {STM}. *Physica C: Superconductivity and its Applications*, v. 437-438, p. 127 – 131, 2006. ISSN 0921-4534. Proceedings of the Fourth International Conference on Vortex Matter in Nanostructured Superconductors {VORTEX} {IVProceedings} of the Fourth European Conference on Vortex Matter in Nanostructured Superconductors (VORTEX IV). Disponível em: <http://www.sciencedirect.com/science/article/pii/S0921453405008439>. Cited 2 times in pages 97 and 98.

KASAMATSU, K.; TSUBOTA, M. Dynamical vortex phases in a Bose-Einstein condensate driven by a rotating optical lattice. *Phys. Rev. Lett.*, American Physical Society, v. 97, p. 240404, Dec 2006. Disponível em: <http://link.aps.org/doi/10.1103/PhysRevLett.97.240404>. Cited in page 86.

KASAMATSU, K.; TSUBOTA, M.; UEDA, M. Vortex molecules in coherently coupled two-component Bose-Einstein condensates. *Phys. Rev. Lett.*, American Physical Society, v. 93, p. 250406, Dec 2004. Disponível em: <http://link.aps.org/doi/10.1103/PhysRevLett.93.250406>. Cited 2 times in pages 43 and 77.

KETTERLE, W. Nobel lecture: When atoms behave as waves: Bose-Einstein condensation and the atom laser. *Rev. Mod. Phys.*, American Physical Society, v. 74, p. 1131–1151, Nov 2002. Disponível em: <http://link.aps.org/doi/10.1103/RevModPhys.74.1131>. Cited in page 33.

KETTERLE, W. Bose-Einstein condensation: Identity crisis for indistinguishable particles. In: _____. *Quantum Mechanics at the Crossroads: New Perspectives from History, Philosophy and Physics*. Berlin, Heidelberg: Springer Berlin Heidelberg, 2007. p. 159–182. ISBN 978-3-540-32665-6. Disponível em: <http://dx.doi.org/10.1007/978-3-540-32665-6_9>. Cited 2 times in pages 25 and 26.

KETTERLE, W.; DRUTEN, N. J. van. Evaporative cooling of atoms. *Adv. At. Mol. Opt. Phys.*, v. 37, p. 181, 1996. Cited in page 32.

KIM, H. et al. Nodeless two-gap superconducting state in single crystals of the stoichiometric iron pnictide lifeas. *Phys. Rev. B*, American Physical Society, v. 83, p. 100502, Mar 2011. Disponível em: <http://link.aps.org/doi/10.1103/PhysRevB.83.100502>. Cited 2 times in pages 49 and 99.

KIRTLEY, J. R. et al. Direct imaging of integer and half-integer Josephson vortices in high- T_c grain boundaries. *Phys. Rev. Lett.*, American Physical Society, v. 76, p. 1336–1339, Feb 1996. Disponível em: <http://link.aps.org/doi/10.1103/PhysRevLett.76.1336>. Cited 2 times in pages 67 and 98.

KOGAN, V. G.; SCHMALIAN, J. Ginzburg-Landau theory of two-band superconductors: Absence of type-1.5 superconductivity. *Phys. Rev. B*, American Physical Society, v. 83, p. 054515, Feb 2011. Disponível em: <http://link.aps.org/doi/10.1103/PhysRevB.83.054515>. Cited in page 125.

KOMENDOVÁ, L.; MILOŠEVIĆ, M. V.; PEETERS, F. M. Soft vortex matter in a type-I/type-II superconducting bilayer. *Phys. Rev. B*, American Physical Society, v. 88, p. 094515, Sep 2013. Disponível em: <http://link.aps.org/doi/10.1103/PhysRevB.88.094515>. Cited 2 times in pages 97 and 98.

KRAFT, S. et al. Bose-Einstein condensation of alkaline earth atoms: ^{40}Ca. *Phys. Rev. Lett.*, American Physical Society, v. 103, p. 130401, Sep 2009. Disponível em: <http://link.aps.org/doi/10.1103/PhysRevLett.103.130401>. Cited 2 times in pages 33 and 34.

KRAMER, L. Thermodynamic behavior of type-II superconductors with small κ near the lower critical field. *Phys. Rev. B*, American Physical Society, v. 3, p. 3821–3825, Jun 1971. Disponível em: <http://link.aps.org/doi/10.1103/PhysRevB.3.3821>. Cited in page 125.

KREMEN, A. et al. Mechanical control of individual superconducting vortices. *Nano Letters*, v. 16, n. 3, p. 1626–1630, 2016. PMID: 26836018. Disponível em: <http://dx.doi.org/10.1021/acs.nanolett.5b04444>. Cited in page 50.

KUMAR, K. R.; MURUGANANDAM, P. Effect of optical lattice potentials on the vortices in rotating dipolar Bose-Einstein condensates. *The European Physical Journal D*, v. 68, n. 10, p. 1–9, 2014. ISSN 1434-6079. Disponível em: <http://dx.doi.org/10.1140/epjd/e2014-40787-1>. Cited in page 135.

KUOPANPORTTI, P.; HUHTAMÄKI, J. A. M.; MÖTTÖNEN, M. Exotic vortex lattices in two-species Bose-Einstein condensates. *Phys. Rev. A*, American Physical Society, v. 85, p. 043613, Apr 2012. Disponível em: <http://link.aps.org/doi/10.1103/PhysRevA.85.043613>. Cited 7 times in pages 14, 43, 77, 80, 81, 84, and 88.

LANCASTER, T.; BLUNDELL, S.; BLUNDELL, S. *Quantum Field Theory for the Gifted Amateur*. OUP Oxford, 2014. ISBN 9780199699339. Disponível em: <https://books.google.com.br/books?id=Y-0kAwAAQBAJ>. Cited in page 39.

LANDAU, L.; LIFSHITZ, E.; PITAEVSKII, L. *Statistical Physics*. Pergamon Press, 1980. (Course of theoretical physics, pt. 2). ISBN 9780750626361. Disponível em: <https://books.google.be/books?id=NaB7oAkon9MC>. Cited in page 25.

LANDAU, L. D. The theory of superfluidity of helium ii. *J. Phys. USSR*, v. 5, p. 71–100, 1941. Cited in page 41.

LASHER, G. Mixed state of type-I superconducting films in a perpendicular magnetic field. *Phys. Rev.*, American Physical Society, v. 154, p. 345–348, Feb 1967. Disponível em: <http://link.aps.org/doi/10.1103/PhysRev.154.345>. Cited 2 times in pages 50 and 98.

LEE, T. D.; HUANG, K.; YANG, C. N. Eigenvalues and eigenfunctions of a Bose system of hard spheres and its low-temperature properties. *Phys. Rev.*, American Physical Society, v. 106, p. 1135–1145, Jun 1957. Disponível em: <http://link.aps.org/doi/10.1103/PhysRev.106.1135>. Cited in page 34.

LEGGETT, A. J. Interpretation of recent results on He^3 below 3 mK: A new liquid phase? *Phys. Rev. Lett.*, American Physical Society, v. 29, p. 1227–1230, Oct 1972. Disponível em: <http://link.aps.org/doi/10.1103/PhysRevLett.29.1227>. Cited in page 32.

LEINAAS, J. M.; MYRHEIM, J. On the theory of identical particles. *Il Nuovo Cimento B (1971-1996)*, v. 37, n. 1, p. 1–23, 1977. ISSN 1826-9877. Disponível em: <http://dx.doi.org/10.1007/BF02727953>. Cited in page 27.

LIMA, A. R. P.; PELSTER, A. Beyond mean-field low-lying excitations of dipolar Bose gases. *Phys. Rev. A*, American Physical Society, v. 86, p. 063609, Dec 2012. Disponível em: <http://link.aps.org/doi/10.1103/PhysRevA.86.063609>. Cited in page 77.

LIN, S.-Z.; HU, X. Massless Leggett mode in three-band superconductors with time-reversal-symmetry breaking. *Phys. Rev. Lett.*, American Physical Society, v. 108, p. 177005, Apr 2012. Disponível em: <http://link.aps.org/doi/10.1103/PhysRevLett.108.177005>. Cited in page 92.

LIN, Y.-J.; JIMENEZ-GARCIA, K.; SPIELMAN, I. B. Spin-orbit-coupled Bose-Einstein condensates. *Nature*, American Physical Society, v. 471, p. 83–86, Aug 2011. Disponível em: <http://dx.doi.org/10.1038/nature09887>. Cited in page 34.

LINN, M.; FETTER, A. L. Stability of a vortex in a small trapped Bose-Einstein condensate. *Phys. Rev. A*, American Physical Society, v. 60, p. 4910–4917, Dec 1999. Disponível em: <http://link.aps.org/doi/10.1103/PhysRevA.60.4910>. Cited in page 81.

LIU, C. F. et al. Crystallized and amorphous vortices in rotating atomic-molecular Bose-Einstein condensates. *Sci. Rep.*, Nature, v. 4, p. 4224, Feb 2014. Disponível em: <http://www.nature.com/articles/srep04224>. Cited 2 times in pages 43 and 77.

LONDON, F. A new conception for supraconductivity. *Nature*, Nature Publishing Group, v. 140, n. 866, p. 793–796, 1937. Disponível em: <http://www-nature-com.ez11.periodicos.capes.gov.br/nature/journal/v140/n3549/abs/140793a0.html>. Cited 2 times in pages 54 and 98.

LONDON, F. On the Bose-Einstein condensation. *Phys. Rev.*, American Physical Society, v. 54, p. 947–954, Dec 1938. Disponível em: <http://link.aps.org/doi/10.1103/PhysRev.54.947>. Cited 2 times in pages 32 and 54.

LONDON, F. On the problem of the molecular theory of superconductivity. *Phys. Rev.*, American Physical Society, v. 74, p. 562–573, Sep 1948. Disponível em: <http://link.aps.org/doi/10.1103/PhysRev.74.562>. Cited in page 54.

LONDON, F. *Superfluids*. Wiley, 1950. (Structure of matter series, v. 1). Disponível em: <https://books.google.com.br/books?id=DtvvAAAAMAAJ>. Cited 4 times in pages 51, 53, 54, and 56.

LONDON, F.; LONDON, H. The electromagnetic equations of the supraconductor. *Proceedings of the Royal Society of London A: Mathematical, Physical and Engineering Sciences*, The Royal Society, v. 149, n. 866, p. 71–88, 1935. ISSN 0080-4630. Disponível em: <http://rspa.royalsocietypublishing.org/content/149/866/71>. Cited in page 54.

LU, M. et al. Strongly dipolar Bose-Einstein condensate of dysprosium. *Phys. Rev. Lett.*, American Physical Society, v. 107, p. 190401, Oct 2011. Disponível em: <http://link.aps.org/doi/10.1103/PhysRevLett.107.190401>. Cited 3 times in pages 33, 34, and 77.

LUNDQVIST, B. et al. Vortex dynamics in a thin film of tl2ba2cuo6. *Journal of Low Temperature Physics*, v. 117, n. 5, p. 1441–1445, 1999. Cited in page 50.

MADISON, K. W. et al. Vortex formation in a stirred Bose-Einstein condensate. *Phys. Rev. Lett.*, American Physical Society, v. 84, p. 806–809, Jan 2000. Disponível em: <http://link.aps.org/doi/10.1103/PhysRevLett.84.806>. Cited 5 times in pages 13, 42, 43, 76, and 78.

MADISON, K. W. et al. Vortices in a stirred Bose-Einstein condensate. *Journal of Modern Optics*, v. 47, n. 14-15, p. 2715–2723, 2000. Disponível em: <http://www.tandfonline.com/doi/abs/10.1080/09500340008232191>. Cited 2 times in pages 76 and 78.

MATTHEWS, M. R. et al. Vortices in a Bose-Einstein condensate. *Phys. Rev. Lett.*, American Physical Society, v. 83, p. 2498–2501, Sep 1999. Disponível em: <http://link.aps.org/doi/10.1103/PhysRevLett.83.2498>. Cited in page 43.

MATTHEWS, M. R. et al. Watching a superfluid untwist itself: Recurrence of Rabi oscillations in a Bose-Einstein condensate. *Phys. Rev. Lett.*, American Physical Society, v. 83, p. 3358–3361, Oct 1999. Disponível em: <http://link.aps.org/doi/10.1103/PhysRevLett.83.3358>. Cited 3 times in pages 46, 82, and 94.

MEISSNER, W.; OCHSENFELD, R. Ein neuer effekt bei eintritt der supraleitfähigkeit. *W. Meissner and R. Ochsenfeld*, v. 21, p. 787, Nov 1933. Cited in page 53.

MENG, Q. et al. Honeycomb, square, and kagome vortex lattices in superconducting systems with multiscale intervortex interactions. *Phys. Rev. B*, American Physical Society, v. 90, p. 020509, Jul 2014. Disponível em: <http://link.aps.org/doi/10.1103/PhysRevB.90.020509>. Cited 2 times in pages 97 and 98.

MERZBACHER, E. *Quantum Mechanics*. Wiley, 1998. ISBN 9780471887027. Disponível em: <https://books.google.com.br/books?id=6Ja_QgAACAAJ>. Cited in page 35.

MICKELSON, P. G. et al. Bose-Einstein condensation of ^{88}Sr through sympathetic cooling with ^{87}Sr. *Phys. Rev. A*, American Physical Society, v. 81, p. 051601, May 2010. Disponível em: <http://link.aps.org/doi/10.1103/PhysRevA.81.051601>. Cited 2 times in pages 33 and 34.

MILOŠEVIĆ, M.; GEURTS, R. The Ginzburg-Landau theory in application. *Physica C: Superconductivity*, v. 470, n. 19, p. 791 – 795, 2010. ISSN 0921-4534. Vortex Matter in Nanostructured Superconductors. Disponível em: <http://www.sciencedirect.com/science/article/pii/S0921453410001632>. Cited in page 104.

MILOŠEVIĆ, M. V.; PEETERS, F. M. Superconducting Wigner vortex molecule near a magnetic disk. *Phys. Rev. B*, American Physical Society, v. 68, p. 024509, Jul 2003. Disponível em: <http://link.aps.org/doi/10.1103/PhysRevB.68.024509>. Cited 2 times in pages 97 and 98.

MODUGNO, G. et al. Two atomic species superfluid. *Phys. Rev. Lett.*, American Physical Society, v. 89, p. 190404, Oct 2002. Disponível em: <http://link.aps.org/doi/10.1103/PhysRevLett.89.190404>. Cited in page 35.

MOSER, A. et al. Observation of single vortices condensed into a vortex-glass phase by magnetic force microscopy. *Phys. Rev. Lett.*, American Physical Society, v. 74, p. 1847–1850, Mar 1995. Disponível em: <http://link.aps.org/doi/10.1103/PhysRevLett.74.1847>. Cited in page 67.

MOSHCHALKOV, V.; FRITZSCHE, J. *Nanostructured Superconductors*. World Scientific, 2011. ISBN 9789814343916. Disponível em: <https://books.google.com.br/books?id=WquWFTw00F4C>. Cited 4 times in pages 13, 15, 67, and 101.

MOSHCHALKOV, V. et al. Type-1.5 superconductivity. *Phys. Rev. Lett.*, American Physical Society, v. 102, p. 117001, Mar 2009. Disponível em: <http://link.aps.org/doi/10.1103/PhysRevLett.102.117001>. Cited in page 125.

MYATT, C. J. et al. Production of two overlapping Bose-Einstein condensates by sympathetic cooling. *Phys. Rev. Lett.*, American Physical Society, v. 78, p. 586–589, Jan 1997. Disponível em: <http://link.aps.org/doi/10.1103/PhysRevLett.78.586>. Cited in page 35.

ONNES, H. K.; TUYN, W. *Proc. Acad. Sci. Amsterdam*, v. 26, p. 443, 1923. Cited in page 51.

ONORI, S.; ROGANI, A. Critical magnetic fields in tin superconducting films. *Physica B+C*, v. 100, n. 1, p. 93 – 96, 1980. ISSN 0378-4363. Disponível em: <http://www.sciencedirect.com/science/article/pii/0378436380900637>. Cited in page 50.

ONSAGER, L. Statistical hydrodynamics. *Il Nuovo Cimento (1943-1954)*, v. 6, n. 2, p. 279–287, 1949. ISSN 1827-6121. Disponível em: <http://dx.doi.org/10.1007/BF02780991>. Cited 2 times in pages 42 and 97.

ORLOVA, N. V. et al. Ginzburg-Landau theory for multiband superconductors: Microscopic derivation. *Phys. Rev. B*, American Physical Society, v. 87, p. 134510, Apr 2013. Disponível em: <http://link.aps.org/doi/10.1103/PhysRevB.87.134510>. Cited 2 times in pages 49 and 92.

OSBORN, J. C.; DORSEY, A. T. Surface tension and kinetic coefficient for the normal/superconducting interface: Numerical results versus asymptotic analysis. *Phys. Rev. B*, American Physical Society, v. 50, p. 15961–15966, Dec 1994. Disponível em: <http://link.aps.org/doi/10.1103/PhysRevB.50.15961>. Cited in page 65.

OSHEROFF, D. D. et al. New magnetic phenomena in liquid He^3 below 3 mk. *Phys. Rev. Lett.*, American Physical Society, v. 29, p. 920–923, Oct 1972. Disponível em: <http://link.aps.org/doi/10.1103/PhysRevLett.29.920>. Cited in page 32.

OSHEROFF, D. D.; RICHARDSON, R. C.; LEE, D. M. Evidence for a new phase of solid He^3. *Phys. Rev. Lett.*, American Physical Society, v. 28, p. 885–888, Apr 1972. Disponível em: <http://link.aps.org/doi/10.1103/PhysRevLett.28.885>. Cited in page 32.

PALACIOS, J. J. Vortex matter in superconducting mesoscopic disks: Structure, magnetization, and phase transitions. *Phys. Rev. B*, American Physical Society, v. 58, p. R5948–R5951, Sep 1998. Disponível em: <http://link.aps.org/doi/10.1103/PhysRevB.58.R5948>. Cited 2 times in pages 97 and 98.

PALONEN, H.; JÄYKKÄ, J.; PATURI, P. Giant vortex states in type I superconductors simulated by Ginzburg-Landau equations. *Journal of Physics: Condensed Matter*, v. 25, n. 38, p. 385702, 2013. Disponível em: <http://stacks.iop.org/0953-8984/25/i=38/a=385702>. Cited 2 times in pages 126 and 129.

PAPP, S. B.; PINO, J. M.; WIEMAN, C. E. Tunable miscibility in a dual-species Bose-Einstein condensate. *Phys. Rev. Lett.*, American Physical Society, v. 101, p. 040402, Jul 2008. Disponível em: <http://link.aps.org/doi/10.1103/PhysRevLett.101.040402>. Cited 2 times in pages 35 and 89.

PARKS, R. D. Quantized magnetic flux in superconductors. *Science*, American Association for the Advancement of Science, v. 146, n. 3650, p. 1429–1435, 1964. ISSN 0036-8075. Disponível em: <http://science.sciencemag.org/content/146/3650/1429>. Cited in page 57.

PATHRIA, R. K. *Statistical Mechanics*. Butterworth-Heinemann Limited, 1995. ISBN 9780080372297. Disponível em: <https://books.google.be/books?id=jSDmPQAACAAJ>. Cited 2 times in pages 25 and 28.

PEARL, J. Current distribution in superconducting films carrying quantized fluxoids. *Applied Physics Letters*, v. 5, n. 4, p. 65–66, 1964. Disponível em: <http://scitation.aip.org/content/aip/journal/apl/5/4/10.1063/1.1754056>. Cited 4 times in pages 50, 98, 103, and 111.

PENROSE, O.; ONSAGER, L. Bose-Einstein condensation and liquid helium. *Phys. Rev.*, American Physical Society, v. 104, p. 576–584, Nov 1956. Disponível em: <http://link.aps.org/doi/10.1103/PhysRev.104.576>. Cited in page 40.

PETHICK, C.; SMITH, H. *Bose-Einstein Condensation in Dilute Gases*. Cambridge University Press, 2002. ISBN 9780521665803. Disponível em: <https://books.google.com.br/books?id=iBk0G3_5iIQC>. Cited 2 times in pages 26 and 34.

PHILLIPS, W. D. Nobel lecture: Laser cooling and trapping of neutral atoms. *Rev. Mod. Phys.*, American Physical Society, v. 70, p. 721–741, Jul 1998. Disponível em: <http://link.aps.org/doi/10.1103/RevModPhys.70.721>. Cited in page 32.

PITAEVSKII, L. P. Vortex lines in an imperfect Bose gas. *Soviet Physics JETP*, v. 13, p. 451–454, 1961. Cited in page 43.

PLOURDE, B. et al. Vortex dynamics in thin superconducting strips observed by scanning squid microscopy. *Physica C: Superconductivity*, v. 341, p. 1023 – 1026, 2000. ISSN 0921-4534. Disponível em: <http://www.sciencedirect.com/science/article/pii/S0921453400007681>. Cited in page 98.

POSEN, S. et al. Shielding superconductors with thin films as applied to rf cavities for particle accelerators. *Phys. Rev. Applied*, American Physical Society, v. 4, p. 044019, Oct 2015. Disponível em: <http://link.aps.org/doi/10.1103/PhysRevApplied.4.044019>. Cited in page 50.

POZA, M. et al. Nanosized superconducting constrictions. *Phys. Rev. B*, American Physical Society, v. 58, p. 11173–11176, Nov 1998. Disponível em: <http://link.aps.org/doi/10.1103/PhysRevB.58.11173>. Cited in page 50.

PROZOROV, R. Equilibrium topology of the intermediate state in type-I superconductors of different shapes. *Phys. Rev. Lett.*, American Physical Society, v. 98, p. 257001, Jun 2007. Disponível em: <http://link.aps.org/doi/10.1103/PhysRevLett.98.257001>. Cited in page 65.

RADIĆ, J. et al. Vortices in spin-orbit-coupled Bose-Einstein condensates. *Phys. Rev. A*, American Physical Society, v. 84, p. 063604, Dec 2011. Disponível em: <http://link.aps.org/doi/10.1103/PhysRevA.84.063604>. Cited in page 76.

REIF, F. *Fundamentals of statistical and thermal physics*. McGraw-Hill, 1965. (McGraw-Hill series in fundamentals of physics). Disponível em: <https://books.google.com.br/books?id=3ApRAAAAMAAJ>. Cited in page 28.

RJABININ, J. N.; SHUBNIKOW, L. W. Magnetic properties and critical currents of supra-conducting alloys. *Nature*, Nature Publishing Group, v. 135, p. 581, April 1935. Cited in page 53.

ROBERT, A. et al. A Bose-Einstein condensate of metastable atoms. *Science*, American Association for the Advancement of Science, v. 292, n. 5516, p. 461–464, 2001. ISSN 0036-8075. Disponível em: <http://science.sciencemag.org/content/292/5516/461>. Cited 2 times in pages 33 and 34.

ROBERTSON, B. Introduction to field operators in quantum mechanics. *American Journal of Physics*, v. 41, n. 5, p. 678–690, 1973. Disponível em: <http://scitation.aip.org/content/aapt/journal/ajp/41/5/10.1119/1.1987330>. Cited 2 times in pages 35 and 38.

SABARI, S. et al. Dynamical stability of dipolar Bose-Einstein condensates with temporal modulation of the *s*-wave scattering length. *Phys. Rev. E*, American Physical Society, v. 92, p. 032905, Sep 2015. Disponível em: <http://link.aps.org/doi/10.1103/PhysRevE.92.032905>. Cited in page 34.

SAKURAI, J.; NAPOLITANO, J. *Modern Quantum Mechanics*. Addison-Wesley, 2011. ISBN 9780805382914. Disponível em: <https://books.google.com.br/books?id=N4I-AQAACAAJ>. Cited 3 times in pages 25, 27, and 35.

SCHMIDT, V.; MÜLLER, P.; USTINOV, A. *The Physics of Superconductors: Introduction to Fundamentals and Applications*. Springer, 1997. ISBN 9783540612438. Disponível em: <https://books.google.com.br/books?id=8O8svNo_tWoC>. Cited in page 51.

SCHWEIGERT, V. A.; PEETERS, F. M.; DEO, P. S. Vortex phase diagram for mesoscopic superconducting disks. *Phys. Rev. Lett.*, American Physical Society, v. 81, p. 2783–2786, Sep 1998. Disponível em: <http://link.aps.org/doi/10.1103/PhysRevLett.81.2783>. Cited 3 times in pages 86, 97, and 98.

SCOTTO, P.; PESCH, W. On the theory of critical fields of superconducting films. *Journal of Low Temperature Physics*, v. 84, n. 5, p. 301–320, 1991. ISSN 1573-7357. Disponível em: <http://dx.doi.org/10.1007/BF00683523>. Cited in page 50.

SENAPATI, K. et al. Normal-state transport and vortex dynamics in thin films of two structural polymorphs of superconducting nbn. *Phys. Rev. B*, American Physical Society, v. 74, p. 104514, Sep 2006. Disponível em: <http://link.aps.org/doi/10.1103/PhysRevB.74.104514>. Cited in page 50.

SEYFARTH, G. et al. Multiband superconductivity in the heavy fermion compound $PrOs_4Sb_{12}$. *Phys. Rev. Lett.*, American Physical Society, v. 95, p. 107004, Sep 2005. Disponível em: <http://link.aps.org/doi/10.1103/PhysRevLett.95.107004>. Cited in page 49.

SILHANEK, A. V. et al. Optimization of superconducting critical parameters by tuning the size and magnetization of arrays of magnetic dots. *Phys. Rev. B*, American Physical Society, v. 76, p. 100502, Sep 2007. Disponível em: <http://link.aps.org/doi/10.1103/PhysRevB.76.100502>. Cited in page 50.

SILVA, C. C. d. S. et al. Probing the low-frequency vortex dynamics in a nanostructured superconducting strip. *Phys. Rev. B*, American Physical Society, v. 94, p. 024516, Jul 2016. Disponível em: <http://link.aps.org/doi/10.1103/PhysRevB.94.024516>. Cited in page 50.

SILVA, R. M. da et al. Giant paramagnetic Meissner effect in multiband superconductors. *Sci. Rep.*, Nature Publishing Group, v. 5, p. 12695, Aug 2015. Disponível em: <http://www.ncbi.nlm.nih.gov/pmc/articles/PMC4525483/>. Cited in page 49.

STANEV, V.; TEŠANOVIĆ, Z. Three-band superconductivity and the order parameter that breaks time-reversal symmetry. *Phys. Rev. B*, American Physical Society, v. 81, p. 134522, Apr 2010. Disponível em: <http://link.aps.org/doi/10.1103/PhysRevB.81.134522>. Cited in page 92.

STELLMER, S. et al. Bose-Einstein condensation of ^{86}Sr. *Phys. Rev. A*, American Physical Society, v. 82, p. 041602, Oct 2010. Disponível em: <http://link.aps.org/doi/10.1103/PhysRevA.82.041602>. Cited 2 times in pages 33 and 34.

STELLMER, S. et al. Bose-Einstein condensation of strontium. *Phys. Rev. Lett.*, American Physical Society, v. 103, p. 200401, Nov 2009. Disponível em: <http://link.aps.org/doi/10.1103/PhysRevLett.103.200401>. Cited 2 times in pages 33 and 34.

SUDEROW, H. et al. Imaging superconducting vortex cores and lattices with a scanning tunneling microscope. *Superconductor Science and Technology*, v. 27, n. 6, p. 063001, 2014. Disponível em: <http://stacks.iop.org/0953-2048/27/i=6/a=063001>. Cited in page 49.

SUHL, H.; MATTHIAS, B. T.; WALKER, L. R. Bardeen-Cooper-Schrieffer theory of superconductivity in the case of overlapping bands. *Phys. Rev. Lett.*, American Physical Society, v. 3, p. 552–554, Dec 1959. Disponível em: <http://link.aps.org/doi/10.1103/PhysRevLett.3.552>. Cited in page 49.

SWEENEY, M. C.; GELFAND, M. P. Simple vortex states in films of type-I Ginzburg-Landau superconductor. *Phys. Rev. B*, American Physical Society, v. 82, p. 214508, Dec 2010. Disponível em: <http://link.aps.org/doi/10.1103/PhysRevB.82.214508>. Cited 3 times in pages 98, 125, and 129.

SZABÓ, P. et al. Evidence for two superconducting energy gaps in MgB_2 by point-contact spectroscopy. *Phys. Rev. Lett.*, American Physical Society, v. 87, p. 137005, Sep 2001. Disponível em: <http://link.aps.org/doi/10.1103/PhysRevLett.87.137005>. Cited in page 49.

TAKASU, Y. et al. Spin-singlet Bose-Einstein condensation of two-electron atoms. *Phys. Rev. Lett.*, American Physical Society, v. 91, p. 040404, Jul 2003. Disponível em: <http://link.aps.org/doi/10.1103/PhysRevLett.91.040404>. Cited 2 times in pages 33 and 34.

TANAKA, Y. Multicomponent superconductivity based on multiband superconductors. *Superconductor Science and Technology*, v. 28, n. 3, p. 034002, 2015. Disponível em: <http://stacks.iop.org/0953-2048/28/i=3/a=034002>. Cited in page 49.

TEAGUE, M. L. et al. Measurement of a sign-changing two-gap superconducting phase in electron-doped $Ba(Fe_{1-x}Co_x)_2As_2$ single crystals using scanning tunneling spectroscopy. *Phys. Rev. Lett.*, American Physical Society, v. 106, p. 087004, Feb 2011. Disponível em: <http://link.aps.org/doi/10.1103/PhysRevLett.106.087004>. Cited 2 times in pages 49 and 99.

TELES, R. P. et al. Free expansion of Bose-Einstein condensates with a multicharged vortex. *Phys. Rev. A*, American Physical Society, v. 87, p. 033622, Mar 2013. Disponível em: <http://link.aps.org/doi/10.1103/PhysRevA.87.033622>. Cited in page 77.

TERHAAR, S.; OBERLEITHNER, K.; PASCHEREIT, C. Key parameters governing the precessing vortex core in reacting flows: An experimental and analytical study. *Proceedings of the Combustion Institute*, v. 35, n. 3, p. 3347 – 3354, 2015. ISSN 1540-7489. Disponível em: <http://www.sciencedirect.com/science/article/pii/S1540748914003459>. Cited in page 97.

THALHAMMER, G. et al. Double species Bose-Einstein condensate with tunable interspecies interactions. *Phys. Rev. Lett.*, American Physical Society, v. 100, p. 210402, May 2008. Disponível em: <http://link.aps.org/doi/10.1103/PhysRevLett.100.210402>. Cited 2 times in pages 35 and 89.

TINKHAM, M. Effect of fluxoid quantization on transitions of superconducting films. *Phys. Rev.*, American Physical Society, v. 129, p. 2413–2422, Mar 1963. Disponível em: <http://link.aps.org/doi/10.1103/PhysRev.129.2413>. Cited 2 times in pages 50 and 98.

TINKHAM, M. Consequences of fluxoid quantization in the transitions of superconducting films. *Rev. Mod. Phys.*, American Physical Society, v. 36, p. 268–276, Jan 1964. Disponível em: <http://link.aps.org/doi/10.1103/RevModPhys.36.268>. Cited in page 98.

TINKHAM, M. *Introduction to superconductivity*. McGraw-Hill, 1975. (International series in pure and applied physics). ISBN 9780070648777. Disponível em: <https://books.google.com.br/books?id=sbrvAAAAMAAJ>. Cited 3 times in pages 49, 51, and 98.

TOXEN, A. M. Critical fields of thin superconducting films. I. Thickness effects. *Phys. Rev.*, American Physical Society, v. 127, p. 382–386, Jul 1962. Disponível em: <http://link.aps.org/doi/10.1103/PhysRev.127.382>. Cited in page 50.

VAGOV, A. et al. Superconductivity between standard types: Multiband versus single-band materials. *Phys. Rev. B*, American Physical Society, v. 93, p. 174503, May 2016. Disponível em: <http://link.aps.org/doi/10.1103/PhysRevB.93.174503>. Cited in page 49.

VINNIKOV, L. Y. et al. Vortex structure in MgB_2 single crystals observed by the bitter decoration technique. *Phys. Rev. B*, American Physical Society, v. 67, p. 092512, Mar 2003. Disponível em: <http://link.aps.org/doi/10.1103/PhysRevB.67.092512>. Cited in page 98.

VOLODIN, A. et al. Magnetic-force microscopy of vortices in thin niobium films: Correlation between the vortex distribution and the thickness-dependent film morphology. *EPL (Europhysics Letters)*, v. 58, n. 4, p. 582, 2002. Disponível em: <http://stacks.iop.org/0295-5075/58/i=4/a=582>. Cited in page 98.

WALLRAFF, A. et al. Quantum dynamics of a single vortex. *Nature*, Nature Publishing Group, v. 425, p. 155 – 158, 2003. Cited in page 98.

WANG, J.-P. Magnetic field at the center of a vortex: A new criterion for the classification of the superconductors. *Physics Letters A*, v. 379, n. 22-23, p. 1472 – 1474, 2015. ISSN 0375-9601. Disponível em: <http://www.sciencedirect.com/science/article/pii/S0375960115002686>. Cited 3 times in pages 49, 106, and 107.

WEBER, T. et al. Bose-Einstein condensation of cesium. *Science*, American Association for the Advancement of Science, v. 299, n. 5604, p. 232–235, 2003. ISSN 0036-8075. Disponível em: <http://science.sciencemag.org/content/299/5604/232>. Cited 2 times in pages 33 and 34.

XU, B. et al. Formation of multiple-flux-quantum vortices in mesoscopic superconductors from simulations of calorimetric, magnetic, and transport properties. *Phys. Rev.*

Lett., American Physical Society, v. 107, p. 057002, Jul 2011. Disponível em: <http://link.aps.org/doi/10.1103/PhysRevLett.107.057002>. Cited in page 86.

YANAGISAWA, T. et al. Vortices and chirality in multi-band superconductors. *Journal of the Physical Society of Japan*, v. 81, n. 2, p. 024712, 2012. Disponível em: <http://dx.doi.org/10.1143/JPSJ.81.024712>. Cited in page 49.

YARMCHUK, E. J.; GORDON, M. J. V.; PACKARD, R. E. Observation of stationary vortex arrays in rotating superfluid helium. *Phys. Rev. Lett.*, American Physical Society, v. 43, p. 214–217, Jul 1979. Disponível em: <http://link.aps.org/doi/10.1103/PhysRevLett.43.214>. Cited 3 times in pages 42, 76, and 97.

ZAVARITSKII, N. N. *Dokl. Akad. Nauk SSSR*, v. 86, p. 501, 1952. Cited in page 66.

ZHANG, J.; ZHAI, H. Vortex lattices in planar Bose-Einstein condensates with dipolar interactions. *Phys. Rev. Lett.*, American Physical Society, v. 95, p. 200403, Nov 2005. Disponível em: <http://link.aps.org/doi/10.1103/PhysRevLett.95.200403>. Cited 2 times in pages 76 and 135.

ZWIERLEIN, M. W. et al. Vortices and superfluidity in a strongly interacting Fermi gas. *Nature*, Nature Publishing Group, v. 435, p. 1047–1051, Jun 2005. Disponível em: <http://dx.doi.org/10.1038/nature03858>. Cited in page 97.